AUTHOR: KOPSIDA, M.

TITLE: Targeting histone deacetylase (HDACs) enzymes with novel bisnaphthalimidopropyl derivatives (BNIPs) as alternative breast cancer therapies.

YEAR: 2018

Targeting histone deacetylase (HDACs) enzymes with novel bisnaphthalimidopropyl derivatives (BNIPs) as alternative breast cancer therapies.

Maria Kopsida

School of Pharmacy and Life Sciences,

Robert Gordon University, Aberdeen

A Thesis submitted in partial fulfilment of the requirements of The Robert Gordon University for the degree of Doctor of Philosophy

March 2018

DECLARATION

This thesis has been composed by myself and has not been submitted in any previous application for a higher degree. The work that is documented was carried out by myself, sources of information are referenced and any help provided by other people have been specifically acknowledged.

Maria Kopsida

ACKNOWLEDGEMENTS

Firstly, I would like to express my most sincere gratitude to my principal supervisor Dr Marie Goua for the unlimited support, encouragement, patience and guidance over the last four years. Marie, thank you so much for all your help and for being you!

Many thanks to my secondary supervisors Prof Paul Kong, Dr Giovanna Bermano and Dr Gemma Barron for providing their help and advice.

I would also like to thank Dr Craig McKenzie, Mr John Wood, Mrs Kirstin Scott, Mrs Moira Middleton, Mrs Lauren Wilson, Mrs Emily Hunter, Mr Ian Tough and Mr Chris Fletcher for providing their invaluable help, advice and company in the labs and Dr Rachel Knott, Dr Andrew Lamb, Dr Anita Weidman, Prof Susan Duthie, Dr Colin Thomson and Mrs Andrea MacMillan for their advice and support during my Ph.D.

Many thanks are also going to Dr Konstantinos Minas for his unlimited support, advice and friendship over the last four years. Κώστα, σ' ευχαριστώ!

I would also like to thank Dr Sarah Walsh, Dr Emma Hector and Dr Karen Skene for their friendship, support and company in and out RGU. Ladies, thank you!

A special thanks to Mrs Anna Lindahl, Mrs Wendy Deegan (D.D!), and Dr Elena Lendoiro for having the opportunity to work together and have an amazing time in the lab!

And now… many thanks to some great people I had the chance to meet during my Ph.D. Garifalia (the καμάρι), Zoi (the γατόφιδο), Dean (and Holly: the Rosemount gang), Steve (the Priory buddy), Camille (la shenille), Floriane (Floflo), Thomas (the "caracol" teacher), Muayad (the habibi), Olivia (the cat "kidnapper"), Charlene (or Sally, once in Paris), Elise (the secret keeper), Ana and Pedro (the portuguese gang), Alice (the sirtaki master), Yuan (the Ph.D sister), Kheira (the artist), Clarisse (the dreamer), Camille (the gold fork), Mathieu (the twin), Justine (the data analyst), Josef (the traveller), Maria (the halloumi specialist), Stephen and Lee (the Presidents), Stephen and Sandie (the guardians), thank you for all the beautiful moments!

Many thanks to Robert Gordon University for funding my Ph.D and my "trips"!

To my students/friends from the Greek Classes and my friends from the Scottish Hellenic Society of Aberdeen for the great moments,the Greek Easters, the music, dance and company over the last years!

To my Queen Vic gang for our "endless scientific converstations"!

To my teacher and my "classmates" at the North East Scotland College for the great time we had during our French lessons: Merci beacoup!

To my Sensei and my "classmates" at RGU Karate Club: Oss!

To kasetophono and its playlists, for keeping me great company during the lab, reading and writing of my thesis!

A HUGE thank you to my FAMILY, my beloved father, mother and brother, who are my strength and my treasure. Χρήστο, Χρυσούλα και Δημήτρη, σας ευχαριστώ! To my grandparents, γιαγιά Σταυρούλα and παππού Γιώργο, for their unlimited love. And to my cousins, uncles and aunts, who complete my big, greek family… σας αγαπώ!

A HUGE thank you to my FRIENDS. According to Pythagoras, "friends are as companions on a journey, who ought to aid each other to persevere in the road to a happier life". I am convinced he was right and grateful that you have proved him right. THANK YOU for having you in my life… you know who you are!

A HUGE thank you to my teachers, lecturers and supervisors, for teaching me that "educating the mind without educating the heart, is no education at all".

And finally, my DEEPEST thanks to Supie, my academic mum.

Cette thèse est dédiée à toi!!!

ABSTRACT

Breast cancer is the most commonly occurring cancer in women, with incidence rates approaching 1.38 million cases per year worldwide. Over the last few decades, there have been numerous attempts to develop, synthesise and advance into the clinic novel and selective breast cancer therapies. Research work has shown that bisnaphthalimidopropyl diaminodicyclohexylmethane (BNIPDaCHM) exerts potent *in vitro* anti-cancer activities and strong DNA binding properties. The aim of this thesis was to synthetise novel bisnaphthalimidopropyl derivatives (BNIPs) and investigate their subsequent modes of action within two human metastatic breast cancer cell lines, MDA-MB-231 and SKBR-3. A series of novel BNIPs, bisnaphthalimidopropyl-piperidylpropane (BNIPPiProp), bisnaphthalimidopropyl- ethylenedipiperidine (BNIPPiEth) and (*trans(trans*))-4,4'-methylenebis-cyclohexylamine *(trans,trans*-BNIPDaCHM) were synthesised, characterised and studied in comparison to BNIPDaCHM for their DNA binding and anti-cancer activities against MDA-MB-231 and SKBR-3 cells. Thermal denaturation studies have shown that BNIPs can intercalate and stabilize the double helix of *Calf Thymus*, each BNIP can competitively displace EtBr from DNA in a dose dependent manner and by UV binding studies, high affinity was found for the three novel BNIPs. After 24 hours treatment, all novel BNIPs, exhibited strong cytotoxicity with IC_{50} values ranging from 1.4 μM to 3.3 μM in MDA-MB-231 cells and 0.2 - 0.7 μM in SKBR-3 cells, confirming the importance of bisnaphthalimidopropyl functionality. BNIPs were also found to increase intracellular ROS levels after 8 hours treatment and induce a significant increase in DNA strand breaks compared to endogenous levels, after 24 hour treatment in both cell lines. After cell synchronisation, cell cycle distribution was studied, revealing that *trans,trans*-BNIPDaCHM induces sub-G1 cell population arrest in

MDA-MB-231 and SKBR-3 cells, after 24 hours treatment. In addition, BNIPs induced apoptotic phosphatidylserine exposure, after 0.5 hours treatment, inhibited Caspase-3 activity and increased autophagy, after 24 hour treatment in MDA-MB-231 and SKBR-3 cells. Moreover, BNIPs inhibited histone deacetylases (HDAC) activity after 24 hours treatment in MDA-MB-231 and SKBR-3 cells and BNIPDaCHM was identified as a potential SIRT2 inhibitor, in SKBR-3 cells. According to Proteome Profiler Arrays, BNIPDaCHM and BNIPPiEth altered the expression of cell stress-related proteins in a cell dependent manner and bioinformatic analysis revealed two novel, putative pathways for BNIP-induced oxidative stress-mediated cell death in MDA-MB-231 and SKBR-3 cells. The above findings indicate that BNIPs represent promising candidates for future breast cancer studies and cancer treatment.

Keywords: Bisnaphthalimidopropyl, DNA binding, DNA damage, Apoptosis, Autophagy, HDAC inhibition, Bioinformatics.

CONTENTS

List of Figures

CHAPTER 1

CHAPTER 2

CHAPTER 3

CHAPTER 4

CHAPTER 5

CHAPTER 6

CHAPTER 7

List of Tables and Schemes

CHAPTER 1

CHAPTER 2

CHAPTER 3

CHAPTER 4

CHAPTER 6

Abbreviations

AAD	Aminoactinomycin D
ADAMTS1	ADAM Metallopeptidase with Thrombospondin Type 1 Motif 1
ADP	Adenosine Diphosphate
ATP	Adenosine Triphosphate
Bad	Bcl-2 Associated Agonist of Cell Death
Bak	Bcl-2 Antagonist/Killer
Bax	Bcl-2 Associated X
BC	Betweenness Centrality
BCA	Bicinchoninic acid
Bcl-Xs	Bcl-2 Like 1
Bid	BH3 Interacting Domain Death Agonist
BNIPDaCHM	Bisnaphthalimidopropyl diaminodicyclohexylmethane
BNIPPiEth	Bisnaphthalimidopropyl- ethylenedipiperidine dihydrobromide
BNIPPiProp	Bisnaphthalimidopropyl-piperidylpropane
BNIPPs	Bisnaphthalimidopropyl polyamine derivatives
BNIPs	Bisnaphthalimidopropyl derivatives
BRAF	B-Raf Proto-Oncogene
BSA	Bovine Serum Albumin
C6	Glioma cells
CAIX	Carbonic Anhydrase
CC	Closeness Centrality
CD95	Caspase 8
$CDCl_3$	Chloroform-D
CDK	Cyclin/cyclin dependent kinase
CDKI	Cyclin/cyclin dependent kinase inhibitor

CDKN2A	Cyclin Dependent Kinase Inhibitor 2 Alpha
CH_3CO_2H	Acetic acid
Cited-2	Cbp/P300 Interacting Transactivator with Glu/Asp Rich Carboxy-Terminal Domain 2
CM-H_2DCFDA	Chloromethyl derivative of 2′,7′-Dichlorodihydrofluorescein diacetate
COX-2	Cytochrome c Oxidase Subunit 2
Cs_2CO_3	Caesium carbonate
DAPI	4',6-Diamidino-2-Phenylindole, Dihydrochloride
DCM	Dichloromethane
DISC	Death-inducing signalling complex
Dkk-4	Dickkopf WNT Signaling Pathway Inhibitor 4
DMF	Dimethylformamide
DMSO	Dimethyl sulfoxide
DNA	Deoxyribonucleic Acid
DNBC	Double Negative Breast Cancer
ds	Doubled Stranded
ER-	Oestrogen Independent
ER+	Oestrogen Dependent
EtBr	Ethidium Bromide
FABP-1	Fatty Acid-Binding Protein 1
FBS	Fetal Bovine Serum
FITC	Fluorescein Isothiocyanate
G0	State of quiescence
G1	Gap Phase 1
G2	Gap Phase 2

H	Hydrogen
H_2O_2	Hydrogen peroxide
HBr	Hydrogen bromide
HDAC	Histone Deacetylase
HeLa	Human cervical cancer cells
HER2-	Human Epidermal growth factor Receptor 2 negative
HER2+	Human Epidermal growth factor Receptor 2 positive
HIF-1a	Hypoxia Inducible Factor 1 Alpha Subunit
HIF-2a	Hypoxia Inducible Factor 2 Alpha Subunit
HOCl	Hypochloride
HRP	Horseradish Peroxidase
HSP60	Heat Shock Protein Family D (Hsp60)
HSP70	Heat Shock Protein Family A (Hsp70) Member 1 Alpha
IBC	Inflammatory breast cancer
IDC	Invasive ductal carcinoma
IDO	Indoleamine 2,3-Dioxygenase 1
INT	2-(4-Iodophenyl)-3-(4-nitrophenyl)-5-phenyl-2H-tetrazolium chloride
JNK Pan	c-Jun N-terminal kinases Pan
KRAS	KRAS Proto-Oncogene
LDH	Lactate dehydrogenase
M	Mitosis
MCLA	2-methyl-6-[p-methoxyphenyll-3,7dihydroimidazo-1,2-alpyrazin-3-one
MDA-MB-231	Human metastatic breast cancer cells
MP	Melting Points

MS	Mass Spectroscopy
MTS	3-(4,5-dimethylthiazol-2-yl)-5-(3-carboxymethoxyphenyl)-2-(4-sulfophenyl)-2H-tetrazolium
Mts-Cl	2-mesitylenesulfonyl chloride
MTT	3-(4, 5-dimethyl-2-thiazolyl)-2, 5-diphenyl-2H-tetrazolium bromide
N_2O_2	Dinitrogen dioxide
Na_2HPO_4	Disodium phosphate
NAD	Nicotinamide adenine dinucleotide
NAD^+	Nicotinamide adenine dinucleotide
NADH	Nicotinamide adenine dinucleotide proton
NADPH	Nicotinamide adenine dinucleotide phosphate
NBT	2,2′-bis(4-Nitrophenyl)-5,5′-diphenyl-3,3′-(3,3′-dimethoxy-4,4′-diphenylene)ditetrazolium chloride 3,3′-(3,3′-Dimethoxy-4,4′-biphenylene)bis[2-(4-nitrophenyl)-5-phenyl-2H-tetrazolium chloride]
NFkB1	Nuclear factor NF-kappa-Beta 1
NH_2	Amide
NMR	Nuclear Magnetic Resonance
$NO^{\bullet}$	Nitric oxide
NO_2	Nitrogen Dioxide
NO_2^+	Nitronium
NOS	Nitric Oxide Synthase
$^{\bullet}OH$	Hydroxyl radical
$^1O_2$	Singlet oxygen
$O=NOOCO_2^-$	Nitrosoperoxycarbonate anion

$O_2^{\bullet-}$	Superoxide
$O_2NOCO_2^-$	Nitrocarbonate anion
O_3	Ozone/Trioxygen
ONO^-	Peroxynitrite
p21	Cyclin-dependent kinase inhibitor 1
p27	Cyclin-dependent kinase inhibitor 1 Beta
p38a	P38 mitogen-activated protein kinase Alpha
p53	Phosphoprotein 53
PAT	Polyamine Transporter
PBS	Phosphate Buffered Saline
Phospho-HSP27	Phosphorylated Heat Shock Protein Family A (Hsp70) Member 1 Alpha
Phospho-JNK Pan (T183/Y185)	Mitogen-Activated Protein Kinase 8
PI	Propidium Iodide
pNA	p-Nitroaniline
PON1	Paraoxonase 1
PON2	Paraoxonase 2
PON3	Paraoxonase 3
PPI	Protein-protein Interaction
PR-	Progesterone receptor negative
PR+	Progesterone receptor positive
PS	Phosphatidylserine
PVDF	Polyvinylidene fluoride
$R^{\bullet}$	Organic radicals
$RO^{\bullet}$	Alkoxyl radicals

ROO•	Peroxyl radicals
ROOH	Organic hydroperoxides
ROS	Reactive Oxygen Species
ROS•	Sulfonyl radicals
RS•	Thiyl radicals
RSOO•	Thiyl peroxyl radicals
RSSR	Disulfides
S	DNA Synthesis
SDS	Sodium dodecyl sulphate
Sir2	Silent information regulator 2
SIRT	Sirtuin
SIRT2	Sirtuin 2
SKBR-3	Human metastatic breast cancer cells
SOD2	Superoxide dismutase 2
SSB	Singe-strand Break
SSC	Saline Sodium Citrate
TBS/T	Tris-buffered saline, 0.1% Tween 20
TEMED	Tetramethylethylenediamine
THF	Tetrahydrofuran
TLC	Thin Layer Chromatography
Tm	The melting temperature
TNBC	Triple Negative Breast Cancer
TNFα	Tumour Necrosis Factor Alpha
trans,trans-BNIPDaCHM	*trans,trans*-4,4'-methylenebis-cyclohexylamine bisnaphthalimidopropyl diaminodicyclohexylmethane

Ts-Cl	*p*-toluenesulfonyl chloride
TXN	Thioredoxin-1
UV	Ultraviolet
WRN	Werner syndrome helicase
XTT	2,3-bis-(2-methoxy-4-nitro-5-sulfophenyl)-2H-tetrazolium-5-carboxanilide
Zn^{2+}	Zinc ion

CHAPTER 1

Introduction

1.1 Cancer: an overview

Cancer remains a leading cause of death worldwide. Nowadays, more than 200 different types of cancer that affect humans have been identified, with incidence and mortality rates increasing: 25 million of people are diagnosed with cancer worldwide and 7 million cancer patients die on an annual basis (Popat *et al*, 2013). More specifically, an estimated 3.45 million new cases of cancer (excluding non-melanoma skin cancer) and 1.75 million deaths from cancer were reported in Europe in 2012 (Ferlay *et al*, 2013). Incidence rates by age and sex are reported in Figure 1.1, according to different areas and countrys in Europe (Ferlay *et al*, 2013).

According to the GLOBOCAN project 2012 statistics, female breast (464,000 cases), followed by colorectal (447,000), prostate (417,000) and lung cancer (410,000) were the four most common cancer cases, representing half of the overall burden of all cancer in Europe (Ferlay *et al,* 2013). Mortality rates revealed that the most common causes of death from the disease, were from cancers of the lung (353,000 deaths), followed by colorectal (215,000), breast (131,000) and stomach cancers (107,000) (Ferlay *et al,* 2013). The estimated numbers of cancer cases in Europe were approximately 1.4 million in males and 1.2 million in females in 2012, while 707,000 men and 555,000 women died from cancer in the same year (Ferlay *et al*, 2013). The increased incidence rates over the last few decades are related to the current life-span extension and living standards in developed countries (João, 2013).

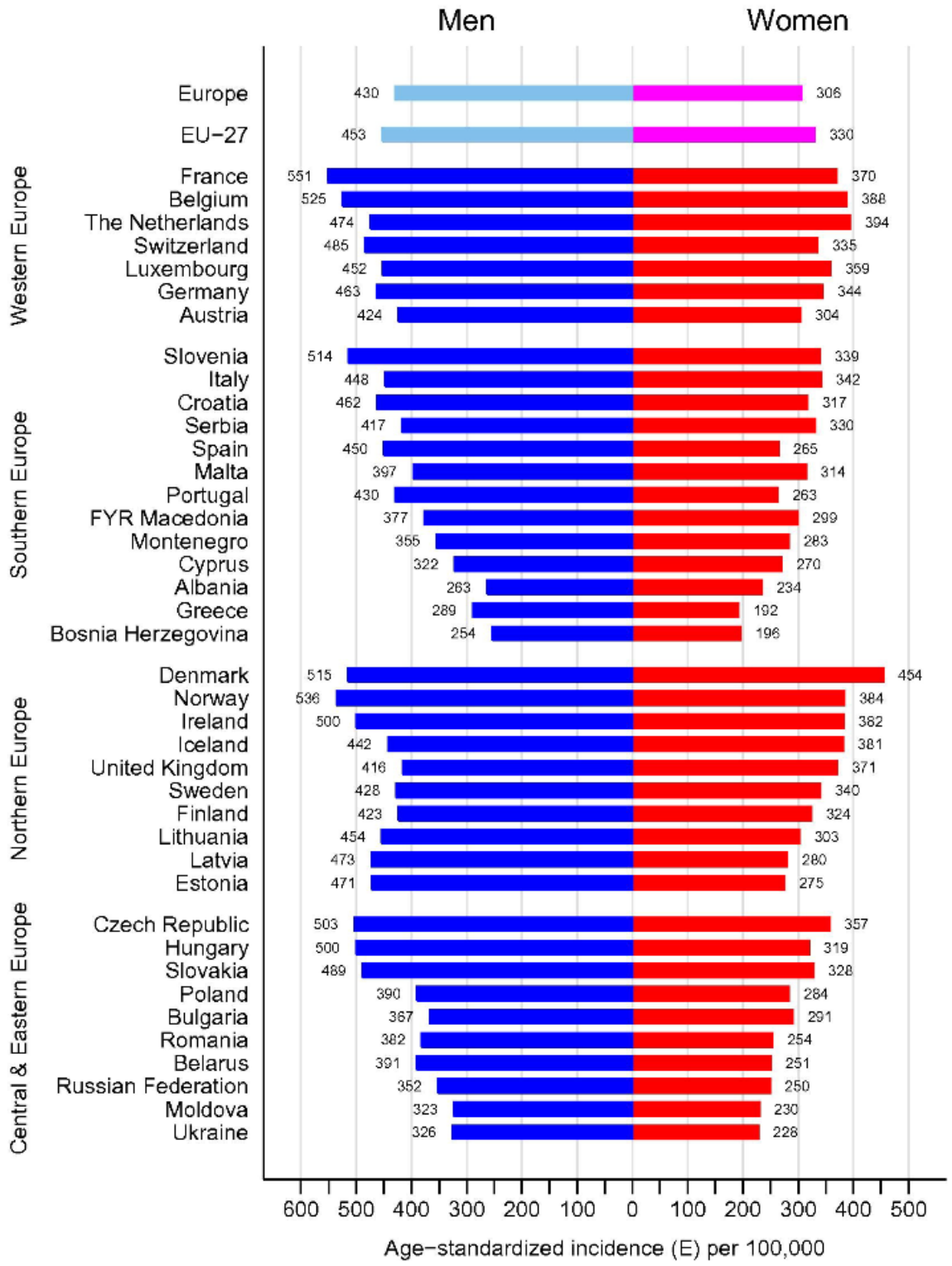

Figure 1.1.: Age-standardised incidence rates by sex, area and country in Europe 2012: all cancers excluding non-melanoma skin cancers (From: Fenley *et al,* 2013).

Cancer is a class of diseases, associated with uncontrolled cell growth that leads to a build-up of abnormal cells due, to irregular cell proliferation. Therefore, cancer impairs a cell's functionality and affects an organism's ability to maintain homeostasis (Bertoli *et al*, 2013). The fundamental abnormality resulting in irregular cell proliferation is due to changes in cell cycle regulation (Burcham, 2014). Cell cycle checkpoints are biological stoplights, able to interrupt the cell cycle in order to avoid the progression or production of dysfunctional cells. However, there are cells that do not obey the rules of the cell cycle: they overcome the multiple checkpoint machinery and begin to divide in an uncontrolled manner, forming masses of tissue or "lumps", known as tumours (Burcham, 2014).

Tumours or neoplasms are divided into two basic categories: the benign (non-cancerous) and the malignant (cancerous) (Lawrence *et al*, 2014). Most of the time, a benign tumour grows in a non-aggressive way and remains in a particular part of the body without spreading to nearby tissues or forming new abnormal growths (neoplasia). On the other hand, a malignant tumour grows in an uncontrolled, aggressive way that results in cells invading surrounding tissues and spreading to other sites of the body, affecting healthy organs (Lawrence *et al*, 2014). This cancer spreading process from a primary to a secondary cancer site is called metastasis and it can occur through the blood circulation or the lymphatic system (Lee *et al*, 2014).

The main differences between benign and malignant tumours are that benign tumours are not invasive, do not metastasise and after being removed by surgery, rarely redevelop (Mangham and Kindblom, 2014). There is however a higher risk for a malignant tumour to reoccur after surgery. Cancer mortality is indeed mainly associated with the development and metastasis of malignant tumours (Ward *et al*, 2014).

Although benign tumours are non-cancerous, they can produce excess hormones (e.g. steroid hormones, such as aldosterone) and cause 10% of cancer deaths (Feldman *et al*, 2016).

Both benign and malignant tumours share similar traits, known as the hallmarks of cancer, which were reported by Douglas Hanahan and Robert Weinberg in 2000 (Hanahan and Weinberg, 2000). Hanahan and Weindberg described for the first time the six biological capabilities acquired during the development of all human tumours and in 2011, they proposed four additional hallmarks (Hanahan and Weinberg, 2011), which are the following:

1. Cancer cells stimulate their own growth.

2. They resist inhibitory signals that might otherwise stop their growth.

3. They resist their programmed cell death.

4. They can multiply indefinitely.

5. They stimulate the growth of blood vessels to supply nutrients to tumours.

6. They invade local tissue and spread to distant sites.

7. They use abnormal metabolic pathways to generate energy.

8. They are characterised by genomic instability.

9. They evade the immune system.

10. They promote inflammation.

The hallmarks of cancer have proved influential in the understanding of cancer's common traits, the mechanisms that underlie the ability of cancers to kill the patients and have helped the research community to gain insights into therapeutic

targets. In the recent years, researchers have revisited the hallmarks of cancer, suggesting the inclusion\exclusion of specific hallmarks (eg. invasion and metastasis are not shared by both benign and malignant growths, as mentioned above) (Lazebnik, 2000), which will emphasise the fact that cancer is not a single disease and that many hallmarks are variable among different tumour types (Fouad and Aanei, 2017).

1.1.1 Breast cancer

Breast cancer is the most common malignancy in women and according to 2008 GLOBOCAN estimates, incidence approached 1.38 million cases per year worldwide (Ma and Ahmedin, 2013). In the United Kingdom, almost 54,833 women and 389 men were diagnosed with breast cancer in 2014 (Cancer Research UK, 2014). Despite improvements in overall survival rates over the past 10 years, breast cancer still causes the most deaths after lung and colorectal cancers. Moreover, Western Europe has the highest incidence rates of breast cancer, which has been associated with lifestyle and environmental changes that occurred in the last decades, such as diet, smoking or radiation exposures (Munsell *et al*, 2014).

An adult (female) breast consists of three main types of tissue: adipose tissue (fat), gland tissue (lobules) and connective tissue (Figure 1.1.1). During lactation, the lobules produce milk that is transferred to the nipples *via* a number of tubes, called lactiferous ducts and released from the aerola (Chinyama, 2014).

A wide range of sex hormones (oestrogen, progesterone, prolactin and oxytocin) have an important impact on breast development and other major biological functions, like breast cell proliferation, division or milk production stimulation (Munsell *et al*, 2014). Breast growth and development are mainly promoted by

oestrogen, the levels of which are increased, during puberty and pregnancy. In men, the levels of oestrogen remain low, which explains why the male breast enlargement is limited (Munsell *et al*, 2014). Having said that, there are cases of breast enlargement in males, however it is rare (Cancer Research UK, 2016). This abnormal condition is called gynecomastia and can occur due to hormone imbalances (lower levels of testosterone), aging or malnutrition (Sandoval *et al*, 2014).

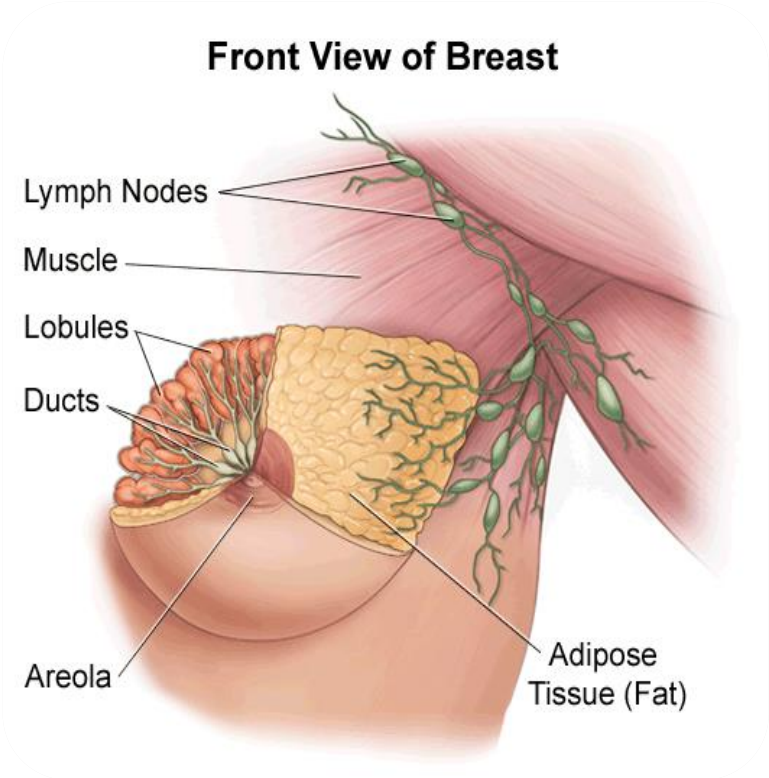

Figure 1.1.1.: Anatomy of the breast and its compartments (From: Wexner Medical Center).

1.1.2 Different types of breast cancer

According to Cancer Research UK statistics, there are about 100 different types and subtypes of breast cancer (Cancer Research UK, 2016). Ducts and lobules are the two parts of the breast that are mainly affected by cancer and as a result, these types of cancer are called ductal carcinoma or lobular carcinoma, respectively (Cancer Research UK, 2016). Almost 80% of breast cancer cases are ductal, 8% lobular and the rest a combination of the two (Hida *et al*, 2012). Cancer of the nipple (known as Paget's disease of the breast) is the least common type and was first characterised in 1874, by Sir James Paget (Hida *et al*, 2012).

In parallel, breast cancer, depending on its potential of spreading to nearby tissues, can also be characterised as non-invasive, invasive or inflammatory. In non-invasive breast cancer, the cancer cells remain restricted to the lobules or ducts and do not spread (Fernandez *et al*, 2013). Invasive ductal carcinoma (IDC) is the predominant breast cancer type, which begins in the ducts and then spreads to other parts of the breast or body. If the spread occurs in an aggressive way and blocks the lymph system of the breast, it is characterised as an inflammatory breast cancer (IBC). IBC can metastasise to the lymph nodes, lungs, liver, brain and bones (Fernandez *et al*, 2013).

1.2 Risk factors

Several studies have shown that breast cancer is a multifactorial disease, however its full aetiology remains unknown (Brinton *et al*, 2013). The most common risk factors that have been associated with the development of breast cancer are divided in two groups: the first group includes inherent factors such as age, sex,

genetics/heredity and race, while the second group includes extrinsic factors, such as lifestyle, diet and environment (Yang *et al*, 2011).

Age is the first basic factor to be considered in the aetiology of the disease, as women around menopause develop breast cancer more frequently compared to women below 45 years of age (Kaminska *et al*, 2015). In addition, reproductive factors, such as younger age at menarche, older age at first birth, older age at menopause and hormonal factors, such as oestrogen receptor overexpression or hormone replacement therapy (HRT) *(*eg. oral contraceptives), have been also associated with the development of breast cancer (Kaminska *et al*, 2015).

In relation to sex, it can be firmly stated that women are predominantly diagnosed with breast cancer (Gnerlich *et al*, 2011). Incidental occurrence in men is rare and mainly linked to excessive obesity and longer life expectancy (Gnerlich *et al*, 2011).

An additional intrinsic factor elevating the risk of breast cancer development are genetic/heredity factors. Almost 10% of breast cancers arise from hereditary mutations in breast cancer susceptibility genes (Yang *et al*, 2010). The majority of them are tumour suppressor genes and as a result, loss or reduction in their function leads to cancer progression. The most common mutations have been reported on Breast Cancer 1 (BRCA1), Breast Cancer 2 (BRCA2), followed by Phosphatase and tensin homolog (PTEN) and Tumour suppressor p53 (p53) genes (Figure 1.2) (Yang *et al*, 2010). Additional genes that have been added to the category of breast cancer susceptibility genes are ATM serine/threonine kinase (ATM), Checkpoint kinsase 2 (CHEK2), BRCA1 interacting protein C-terminal helicase 1 (BRIP1) and partner and localizer of BRCA2 gene (PALB2) (Figure 1.2).

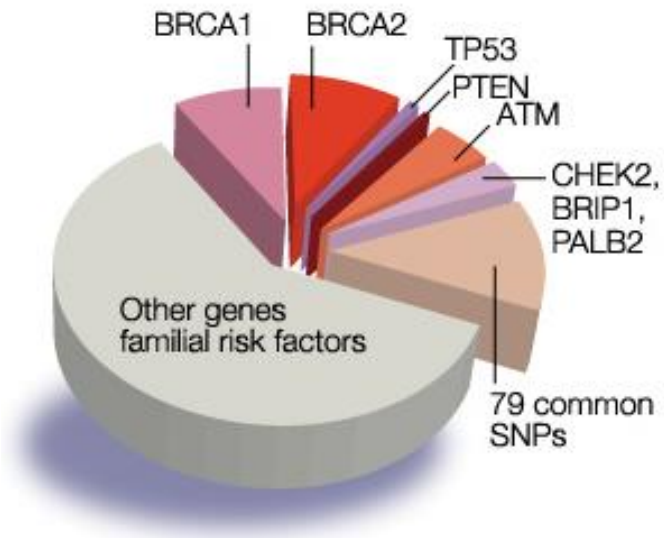

Figure 1.2.: Hereditary mutations in breast cancer susceptibility genes (From: Yang *et al*, 2011).

The above genes are involved in transcriptional regulation, control of cell cycle and induction of cell death and as a result, mutations in these genes are associated with high risk of hereditary breast cancer development (Yang *et al*, 2011). Patients who are positive for these mutations have an 80% risk in developing breast cancer, compared to individuals with the corresponding wild-type genes (Yang *et al*, 2011). However, gene mutations are only responsible for a small percentage (10%) of breast cancer development compared to the total number of breast cancers, which supports the existing evidence that breast cancer is a multifactorial disease (Abdulkareem, 2013).

Race is another risk factor associated to breast cancer. More specifically, African American, Hispanic, and Asian women are less likely to develop breast cancer compared to white women, suggesting the impact of extrinsic factors, such as lifestyle, environment and diet, to the development of the disease (Kaminska *et al*, 2015). In addition, cases of breast cancer are higher in developed countries, due to dietary habits that often lead to excess weight or obesity (Kaminska *et al*,

2015). Further studies have revealed that several polymorphisms in breast cancer susceptibility genes in combination with exogenous factors that generate free radicals, such as pollution, alcohol consumption, or endogenous factors (oestrogen levels), increase the risk for breast cancer pathogenesis (Abdulkareem, 2013).

1.2.1 Reactive Oxygen Species

Increased generation of oxygen radicals, ions and molecules, known as Reactive Oxygen Species (ROS), within cells results in deoxyribonucleic acid (DNA) damage, tumour development and progression. ROS are mainly produced as inevitable by-products during mitochondrial electron transport of oxidative phosphorylation (Ray *et al,* 2012). Recent studies have revealed a dual role of ROS, depending on their intracellular levels (Figure 1.2.1) (Ramis *et al,* 2015). Physiological levels of ROS are responsible for cellular stress responses that promote cell survival, while high levels of ROS can cause oxidative damage to important macromolecules, such as DNA, proteins and lipids, changing their structure and functions (Ramis *et al*, 2015). These changes contribute to the progression of cancer, as well as to a wide range of inflammatory diseases, ischemic diseases and neurological disorders (Ramis *et al*, 2015). In addition, ROS can act as both intra- and inter-cellular messenger and play an important role in cell signalling, activating cell death processes such as apoptosis (Sena and Chandel, 2012).

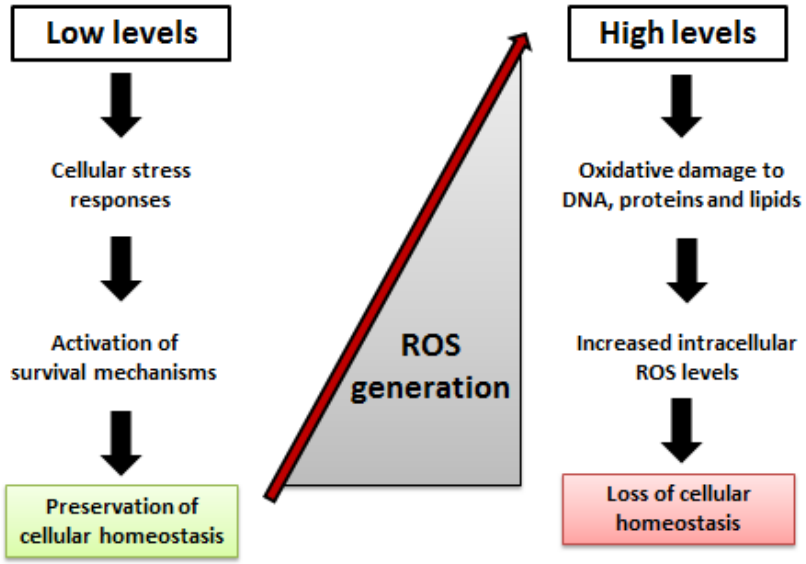

Figure 1.2.1.: Dual role of ROS levels (Adapted from: Ramis *et al,* 2015).

In almost all cancers, elevated ROS levels have been detected and appear to promote tumour development and progression, by altering redox balance and deregulating redox signalling due to genetic, metabolic and microenvironment-associated alterations (Liou *et al*, 2010, Panieri and Santoro, 2016). However, tumour cells tend to express increased levels of antioxidant enzymes or molecules, such as catalase, glutathione peroxidase (GPX) and peroxiredoxins (Prx), to detoxify ROS by reducing them to water (Liou *et al*, 2010, Liou and Storz, 2014), suggesting a dual role of ROS. Thus, it has been suggested that cancer cell function can be maintained only *via* a delicate balance of intracellular ROS levels, similar to the one maintained in healthy cells (Trachootham *et al*, 2008). Changes in cellular function are dependentent on the type of the radical that is generated, the location of its generation and its concentration (Bayr, 2005). However, high levels of ROS in cancer cells are mainly produced due to increased metabolic activity, mitochondrial dysfunction, oncogene activity, peroxisome activity, increased cellular receptor signalling or increased activity of oxidases (Liou *et al*,

2010). In addition, macrophages induce the generation of ROS within tumour cells through secretion of various molecules, such as TNFα (Sena and Chandel, 2012). Within tumour cells, NADPH oxidase initiates the formation of superoxide that later on leads to the production of hydrogen peroxide and apoptotic cell death. This is the typical cellular response to stress: to leave the cell cycle and enter into G0 (cells enter into a quiescent state, neither dividing nor preparing to divide) (Duronio and Xiong, 2013). In other words, continuous exposure to and/or high levels of ROS, can trigger apoptotic mechanisms. Therefore, novel anti-cancer therapeutic strategies are focusing on the development of drugs to promote ROS-induced apoptotic signalling in cancer cells and ensure the fine tuning of intracellular ROS levels after treatment (Vurusaner *et al*, 2012).

1.2.2 ROS-mediated signalling pathways

ROS-mediated signalling pathways are elevated in many types of cancer and seem to affect cell growth and proliferation, glucose metabolism and cell inflammation (Liou and Storz, 2014). Currently, three ROS-mediated signalling pathways have been reported: the mitogen-activated protein (MAP) kinase/ extracellular signal-regulated kinase (Erk) cascade, the phosphoinositide-3-kinase (PI3K)/ Protein kinase B (Akt)-regulated signalling cascade and the IκB kinase (IKK)/nuclear factor κ-B (NF-κB)-activating pathway (Liou and Storz, 2014).

The activation of the MAPK (mitogen-activated protein kinase)/Erk1/2 (extracellular-regulated kinase 1/2) pathway in cancer is mediated through ras and growth factors, such as epidermal growth factor receptor (EGFR) (Khavari and Rinn, 2007, Roberts and Der, 2007). In breast cancer cells, Erk1/2 is activated by hydrogen peroxide that is generated as a by-product during oestrogen

metabolism, increasing cell proliferation (Reddy and Glaros, 2007). On the other hand, Akt (protein kinase B) mediates cell survival through phosphorylation and inactivation of pro-apoptotic proteins (Bad, Bax, Bim) and transcription factors (FOXO) (Xin *et al,* 2005, Qi *et al*, 2006). In breast cancer, ROS generation has been found to activate the PI3K/Akt signaling pathway (Park *et al*, 2009). NF-κB, which is a redox-regulated sensor for oxidative stress, is mainly activated by low doses of hydrogen peroxide that activate the NF-κB-inducing kinase (NIK) and the IκB kinase (IKK) complex (Li and Karin, 1999). IKK is phosphorylated on serine residues, enabling its ubiquitination and degradation. Upon IKK degradation, NF-κB is translocated to the nucleus (Karin, 2008). Then, NF-κB acts as a transcription factor, inducing the expression of anti-apoptotic and anti-inflammatory genes (Karin, 2008).

The above pathways indicate the involvement of ROS in cancer development, by affecting all characters of cancer cell behaviour, including cell cycle progression, proliferation, DNA damage and cell death (Liou and Storz, 2014), suggesting the need for more detailed understanding of ROS-mediated signalling, in order to develop new strategies for ROS-based therapeutics against cancer cells.

1.3 Epigenetics and cancer

Epigenetics is defined as the study of heritable changes in gene activities that occur without changes in the DNA sequence (Schemies *et al*, 2009). Epigenetic modifications, like DNA methylation or histone acetylation and deacetylation, alter the gene function and can cause mutations, responsible for the development of diseases (Dawson and Kouzarides, 2013). In 1983, cancer was the first disease to be associated with epigenetics, when researchers found that there was loss of DNA

methylation in the diseased tissue of colorectal cancer patients, compared to the healthy tissue (Feinberg and Vogelstein, 1983).

Epigenetic information is stored in DNA/protein complexes, known as chromatins. The fundamental unit of chromatins is the nucleosome, which consists of an octamer of four core histones (H3, H4, H2A, H2B) (Rivera and Bennett, 2010). Histones are positively charged proteins that structure DNA into nucleosomes, by interacting with its negatively charged phosphate groups. Histones are predominantly globular; however, their N-terminal tails are unstructured and susceptible to a large number and type of modifications (Rivera and Bennett, 2010). Histones recruit several enzyme complexes in order to manipulate DNA. Thus, histone modifications have a direct effect on fundamental biological processes, such as gene transcription, DNA replication and DNA repair, which can be epigenetically inherited (Biswas and Rao, 2017).

More specifically, eight different classes of histone modifications have been reported (Table 1.3.1) and seem to disrupt the levels of histones, deregulate the control of chromatin-based processes and ultimately lead to oncogenic transformation and the development of cancer (Kouzarides, 2007).

The majority of these modifications are the result of reversible acetylation of lysine residues, which are clustered at the basic amino-terminal domains of histones (Kouzarides, 2007). Consequently, these residues interact ionically with the negatively charged phosphates of the DNA backbone, resulting in charge neutralization and separation of histones from the DNA (Kouzarides, 2007).

Table 1.3.1.: Different classes of modification identified on histones and function that they regulate (Adapted from: Kouzarides, 2007).

Chromatin Modifications	Residue Modification	Functions Regulated
Acetylation	K-ac	Transcription, Repair, Replication, Condensation
Methylation (lysines)	K-me1 K-me2 K-me3	Transcription, Repair
Methylation (arginines)	R-me1 R-me2a R-me2s	Transcription
Phosphorylation	S-ph T-ph	Transcription, Repair, Condensation
Ubiquitylation	K-ub	Transcription, Repair
Sumoylation	K-su	Transcription
ADP ribosylation	E-ar	Transcription
Deimination	R > Cit	Transcription
Proline Isomerization	P-cis > P-trans	Transcription

Abbreviations: ac=Acetylation, me=Methylation, ph=Phosphorylation, ub=Ubiquitylation, su=Sumoylation, ar=ADP ribosylation, K=Lysine, R=Arginine, S=Serine, T=Threonine, E=Glutamic acid.

The level of histone acetylation is controlled by two families of enzymes, histone acetyltransferases (HATs) and histone deacetylases (HDACs). Histone acetylation is catalysed by HATs that neutralise the charge of histone proteins, leading to DNA loosening (Bannister and Kouzarides, 2011). Histone acetylation is associated with DNA repair and proliferation, as well as with chromosomal organisation (Bannister and Kouzarides, 2011). On the other hand, HDACs are enzymes divided into four classes that enhance the ability of histones to wrap tightly around the DNA (Bannister and Kouzarides, 2011). HDAC overexpression can decrease the levels of histone acetylation and compact DNA/histone complex, in a way that gene transcription and differentiation can be blocked (Woan *et al*, 2011).

The activity of HDACs can highly modify the chromatin structure and their functional importance is highlighted by the fact that their deregulation has been linked to the progression of cancers, such as leukaemia, colorectal and breast cancer (Toh *et al*, 2017). Therefore, identification of therapeutic targets which involves the ability of potential agents to inhibit HDAC activity has received much attention.

1.3.1 HDAC inhibitors in cancer treatment

Over the last few years, HDAC inhibitors have been considered as potential anti-cancer therapeutic agents and nowadays, several derivatives (see Table 1.3.1.1), such as Vorinostat (cutaneous T cell lymphoma) and Belinostat (peripheral T cell lymphoma) have been approved and licensed for cancer treatment, as they were found to inhibit HDAC activity (Ceccacci and Minucci, 2016, Seidel *et al*, 2014).

HDACs are classified based on their functional and phylogenetic criteria (Marks, 2010). More specifically, HDACs are divided into Zn^{2+}-dependent (Class I, II and IV) and Zn^{2+}-independent, NAD-dependent (class III - sirtuins) enzymes. Currently, the majority of inhibitors being developed target class I, II and IV enzymes (Seidel *et al,* 2014).

However, new evidence has shown that the class III HDACs, which are homologous related to yeast Silent information regulator 2 (Sir2) protein family and are well distributed in several cellular locations (nucleus, cytoplasm and mitochondria), are critical transcriptional regulators (Tang, 2016).

Table 1.3.1.1: HDAC inhibitors classified according to status of clinical advancement, targeted HDACs and chemical class (Adapted from: Valente and Mai, 2014).

Compound	Target	Class	Highest phase trial
Panobinostat (LBH-589)	Pan-HDAC inhibitor	Hydroxamic acids	Approved in 2015 for multiple myeloma
Belinostat (PXD101)	Pan-HDAC inhibitor	Hydroxamic acids	Approved in 2014 for PTCL
Romidepsin (desipeptide-FK228)	Pan-HDAC inhibitor	Cyclic tetrapeptides	Approved in 2009 for CTCL
SAHA(Vorinostat, Zolinza)	Pan-HDAC inhibitor	Hydroxamic acids	Approved in 2006 for CTCL

Abbreviations: CTCL=cutaneous T-cell lymphoma, PTCL=peripheral T-cell lymphoma.

The function of HDACs and their potential as therapeutic targets has become an area of intense investigation in cancer treatment. With regards to breast cancer, the first clinical study evaluating the co-administration of an HDAC inhibitor (vorinostat) with an anti-estrogen (tamoxifen) in advanced breast cancer patients was reported in 2015 (Raha *et al*, 2015). For the very first time, there was a 40% clinical benefit (19% objective response and 21% stable disease for more than 6

months) in patients who did not respond to earlier anti-estrogen therapies and chemotherapy (Raha *et al*, 2015). The same study demonstrated that another HDAC inhibitor, entinostat, can reverse hormone therapy resistance when combined with the aromatase inhibitor exemestane. Therefore, although the understanding of the mechanism that underlies HDAC effectiveness is still unknown, HDACs are currently among the most promising therapeutic targets for cancer treatment.

1.4 Cancer therapeutics: use and limitations of chemotherapy

Radiotherapy, hormone therapy, surgery and chemotherapy are existing treatments used for breast cancer therapy. More specifically, chemotherapy is used to treat different types of cancer, based on the use of anti-cancer compounds that are able to recognise and attack fast-dividing cells. In breast cancer, the drugs are provided to patients in tablet form (e.g. Cyclophosfamide) or intravenously (e.g. Adriamycin), depending on the dosage and application (Siden and Wolf, 2013). As cancer diagnosis has increased, not only due to the rise of cancer incidence, but also due to the improved diagnostic technologies (e.g. Mammograms, Magnetic Resonance Imaging, Elastograms), researchers aim to develop novel anti-cancer compounds and study their effects on cancer cells (Leong *et al*, 2013), in order to overcome existing limitations (i.e. chemoresistance) in current treatments.

More specifically, breast cancer, depending on whether or not it develops in response to the hormone oestrogen, is divided in two categories: oestrogen dependent (ER+) and oestrogen independent (ER-) cancer (Redmond *et al*, 2015). ER+ breast cancers respond better to anti-oestrogen (endocrine) therapies, such as tamoxifen and exemestane, by inhibiting the effect of oestrogen and decreasing

the uncontrolled proliferation of breast cancer cells (Redmond *et al*, 2015). On the other hand, ER- breast cancers are more invasive and less responsive to current standard of care treatment regimes, such as Adrucil (fluorouracil), Ellence (epirubicin) and Adriamycin (doxorubicin), which do not selectively target breast cancer cells hence leading to severe side effects, especially when they are used in combination (Becorpi *et al*, 2014). Therefore, researchers have focused on the development and clinical application of novel cancer-specific therapies that will act on potential molecular targets. Nucleic acids are such an example of molecular targets, that could potentially increase the selectivity against breast cancer cells, reduce treatment resistance and/or adverse severe side effects (Lehmann and Pietenpol, 2013).

1.4.1 DNA binding properties of compounds with therapeutic potential

Over the last few decades, studies in cancer chemotherapy have focused on derivatives being able to interact directly with nucleic acids and specifically with deoxyribonucleic acid (DNA) (Palchaudhuri and Hergenrother, 2005). A variety of small molecules, often referred to as ligands (e.g. ifosfamide), have been classified into three categories: compounds that bind covalently to cell DNA, such as alkylating agents, compounds that cause breakage of the DNA molecule (e.g. bleomycins), or compounds that bind to DNA either by intercalating among the base pairs of its double strand or by external binding to its major/minor groove (e.g. netropsin) (Figure 1.4.1) (Ali and Bhattacharya, 2014).

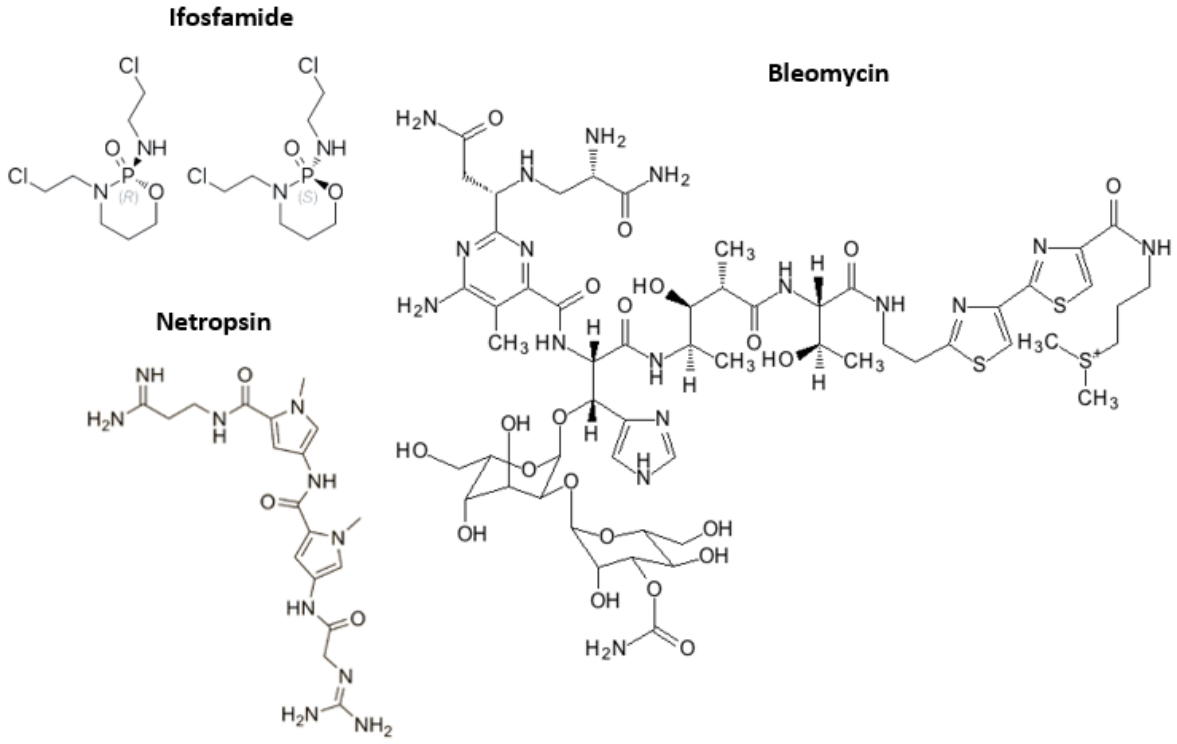

Figure 1.4.1.: Chemical structures of agents that interact with DNA.

1.4.2 Synthesis of mononaphthalimide and bisnaphthalimide derivatives

Naphthalimido compounds were first synthesised in 1970's (Chen *et al*, 1993). A naphthalimido compound consists of three fused 6-membered rings with a basic terminal group in one of its side chains, which is critical for its cytotoxic activity (Porter *et al*, 1985). The first series of naphthalimides had variations not only on side chains, but ring substituents, too. More specifically, when the nitrogen atom in the basic side chain was separated from the ring nitrogen atom by methylene units, maximum growth inhibition in HeLa cervical cancer and KB epidermal carcinoma of the mouth cells was obtained (Brana and Ramos, 2001; Brana *et al*, 2001). This showed that naphthalimido compounds were found to be highly active against cancer cell lines *in vitro*, however once clinical trials were undertaken, they induced multiple side effects, such as myelosupression and dementia (Llombart *et al*, 1992; Brana *et al*, 2001, 2004), probably due to high dose toxicity, resulting in considerable mortality (Lyman, 2009).

However, the increased anti-cancer activity of naphthalimido derivatives had led Brana and others to design and synthetise novel symmetrical compounds, the bisnaphthalimides (Brana *et al*, 2001, Dance *et al*, 2005). The main characteristic of bisnaphthalimido compounds was a linker sequence that would join the two naphthalimido units together, in order to improve the therapeutic properties of precursor mononaphthalimides (Brana *et al,* 2001). Indeed, the use of polyamine linker sequences were found to improve the *in vivo* and *in vitro* activity of bisnaphthalimides and their DNA intercalating properties (Brana *et al*, 2001). Intercalating agents are able to insert themselves between DNA base pairs (reversible inclusion) and interfere with DNA transcription and replication. In addition, Brana and Ramos (2001) also proved that different pharmacophore substitutions (NO_2 > H > NH_2 > CH_3CONH) and the length of linker chain could

improve compound cytotoxicity. However, the aqueous insolubility of bisnaphthalimides was a main disadvantage for their potential use as chemotherapeutic agents, even if there was strong evidence that bisnaphthalimides could be further developed to be suitable anti-cancer drugs.

1.4.3 Synthesis of novel bisnaphthalimidopropyl polyamine derivatives

In order to overcome the insolubility issues of bisnaphthalimides, Kong Thoo Lin and Pavlov designed and synthesised in 2000, a number of bisnaphthalimidopropyl derivatives (BNIPs), by incorporating natural polyamines in the bisnaphthalimide linker chain. Polyamines were previously proved to be promising carriers in delivering cytotoxic drugs into cancer cells, thus a promising target for therapeutic intervention in cancer research. The addition of two or more amide (NH_2) groups in the aliphatic chain improved their aqueous solubility, as well as their biological activity. Cancer cells have higher polyamine levels compared to normal cells due to an active polyamine transporter (PAT) (Phanstiel *et al*, 2007). Synthesis of naturally occurring polyamine analogues (with a polyamine linker) that inhibit the polyamine synthesis metabolic pathway by targeting PAT on cancer cells could lead to targeted drug delivery. Kong Thoo Lin and Pavlov (2000) combined both the characteristics of naphthalimides and polyamines, forming the bisnaphthalimidopropyl polyamine derivatives (BNIPPs): Bis-naphthalimidopropyl putrescine (BNIPPut), spermidine (BNIPSpd), spermine (BNIPSpm) and oxa-putrescine (BNIPOPut) were tested for their cytotoxicity and proved to be highly toxic anti-cancer agents (Figure 1.4.3) (Kong Thoo Lin and Pavlov, 2000).

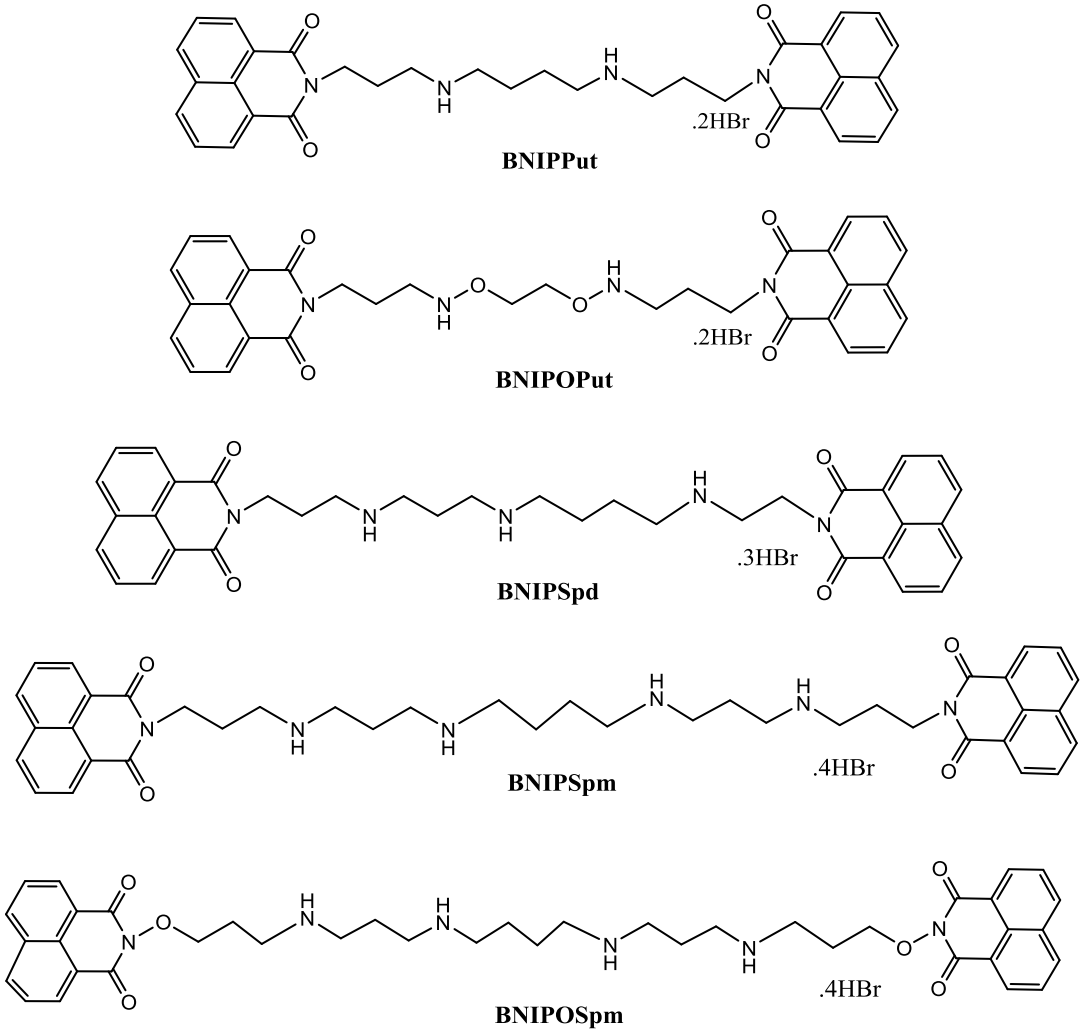

Figure 1.4.3.: Chemical structures of bisnaphthalimidopropyl polyamine derivatives: BNIPPut, BNIPOPut, BNIPSpd, BNIPSpm and BNIPOSpm.

Interestingly, the main outcome of the above studies was that the shorter the linker chain, the higher the cytotoxicity of the compound is and the presence of more heteroatoms, the better the solubility.

In 2005, Brana *et al* determined that symmetry in the structure was also an important factor for cytotoxicity and, according to these studies, non-symmetrical BNIPPs were less toxic than symmetrical BNIPPs.

Research focused on the synthesis of BNIPPs was continued by Dance *et al.* (2005), who introduced oxygen atoms into the α-position of the naphthalimido

ring, enhancing the solubility of previously synthesised derivatives, but decreasing their cytotoxicity. Oliveira *et al*. (2007) showed that depending on the nature of the polyamine linker chain and increasing length, its aqueous solubility was increased. Barron *et al*. (2010) demonstrated how modification in the central linker chain of BNIPs, either by removing nitrogen atoms or by substituting with cyclohexane rings, can result in higher cytotoxicity levels.

However, there were still important questions about BNIPs: whether structural isomers possess different cytotoxic and DNA-binding properties and which modifications could further improve BNIP solubility, cytotoxicity and DNA intercalation. This has lead to the design and synthesis of more effective novel BNIPs which will be tested in this thesis in the context of cancer treatment in different *in vitro* models of breast cancer.

1.5 Aims and thesis layout

The aims of this project were to investigate the mode of action of newly synthetised BNIPs in an *in vitro* cell system, which could be used as new chemotherapeutic drugs for breat cancer treatment.

Based on previous findings (Kong Thoo Lin and Pavlov, 2000, Pavlov *et al*, 2001, Dance *et al*, 2005, Ralton 2006, Oliveira *et al*, 2007, Ralton *et al*, 2009, Barron *et al*, 2010), where either BNIPPs or BNIPs were found to possess cytotoxicity against several types of cancer cells, such as MCF-7 (breast cancer), CaCO-2 (colon cancer) or HL-60 (human leukaemia), the aim was to synthesise three novel BNIPs that would possess higher cytotoxicity towards breast cancer cells compared to previously synthetised BNIPs and/or anticancer drugs that are currently used in the clinic. After trying various chemical structure modifications on the parental compound Bisnaphthalimidopropyl diaminodicyclohexylmethane (BNIPDaCHM), questioning whether cytotoxicity differs among structural isomers, whether the length of the linker chain, the ring structure position or the existence of stereoisomers affects the cytotoxicity, the Bisnaphthalimidopropyl-piperidylpropane (BNIPPiProp), bisnaphthalimidopropyl- ethylenedipiperidine dihydrobromide (BNIPPiEth) and *trans,trans*-4,4'-methylenebis-cyclohexylamine bisnaphthalimidopropyl diaminodicyclohexylmethane (*trans,trans*-BNIPDaCHM) were synthetised, characterised (Chapter 2) and tested for their DNA binding affinities through a number of studies, including thermal denaturation of DNA, EtBr displacement and UV binding studies (Chapter 3).

Human MDA-MB-231 and SKBR-3, two highly metastatic breast cancer cell lines that do not respond to current chemotherapy treatments (Denkert *et al*, 2016, Loi *et al*, 2016), were used to test BNIPDaCHM, BNIPPiProp, BNIPPiEth and *trans,trans*-BNIPDaCHM with regards to theirs cytotoxicity, production of

intracellular ROS and DNA damage, confirming or not the importance of bisnaphthalimido moiety for biological activity (Chapter 4) and also to extend the knowledge on BNIP derivative cytotoxicity against different breast cancer cell types and their mode of action.

Furthermore, investigations into the mode of cell death were undertaken, by examining the cell cycle distribution and induction of early apoptosis or autophagy, by treating human MDA-MB-231 and SKBR-3 cells with BNIPDaCHM, BNIPPiProp, BNIPPiEth and *trans,trans*-BNIPDaCHM (Chapter 5).

Finally, the effect of BNIPs on HDAC activity, with emphasis on SIRT2 and cell stress-related proteins were studied and protein-protein interaction (PPI) network analysis and bioinformatic analysis were undertaken to link the proteins of interest for further research and validation towards the delineation of the mode/mechanisms of BNIPs action in breast cancer (Chapter 6). The full thesis layout is presented on Figure 1.5.

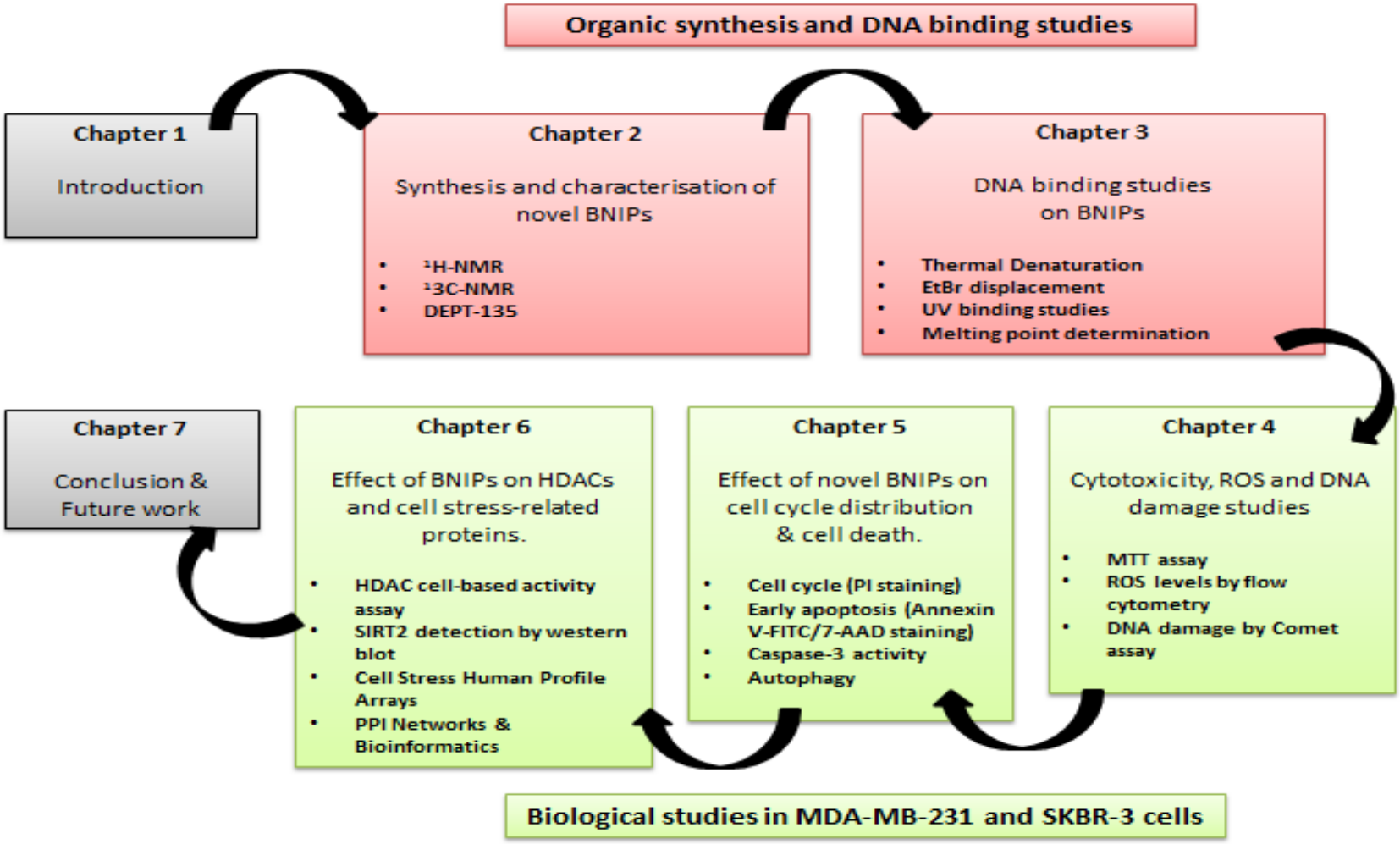

Figure 1.5.: Layout of thesis.

CHAPTER 2

Synthesis and characterisation of novel bisnaphthalimidopropyl derivatives

2.1 Introduction

2.1.1 Aims

The aim of the presented experimental work in Chapter 2 was the synthesis of three novel BNIPs that would possess higher cytotoxicity towards breast cancer cells. Various chemical structure modifications of the BNIPs have been tried and the synthesis was based on previous methods that have been used within Robert Gordon University by Kong Thoo Lin and Pavlov (2000) and Barron *et al* (2010). The three BNIPs that were synthesised and characterised are bisnaphthalimidopropyl-piperidylpropane (BNIPPiProp), bisnaphthalimidopropyl-ethylenedipiperidine dihydrobromide (BNIPPiEth) and *trans*,*trans*-4,4'-methylenebis-cyclohexylamine bisnaphthalimidopropyl diaminodicyclohexylmethane (*trans,trans*-BNIPDaCHM) (Figure 2.1.1). The first BNIP, BNIPPiProp is a structural isomer of BNIPDaCHM that consists of only one species (enantiopure). The aim of synthesising BNIPPiProp was to investigate whether cytotoxicity and DNA binding properties differ amongst structural isomers and how the position of the saturated ring structure in the linker chain affects cytotoxicity in breast cancer cells. The second BNIP, BNIPPiEth, consists of one carbon less between the two piperidine ring structures, compared to BNIPPiProp and was synthesised in order to assess the effect of a shorter linker chain on cytotoxicity and DNA binding properties. In parallel, it is still unknown whether the cytotoxicity of BNIPDaCHM is associated with the existence of the three isomers in its structure, therefore (*trans(trans*))-4,4'-Methylenebis (cyclohexylamine), the only commercially available stereoisomer precursor required to synthesise *trans,trans*-BNIPDaCHM the latter being, the third BNIP used in this study. The synthesis of *trans,trans*-BNIPDaCHM lead to the investigation into the importance of this stereoisomer compared to the mixture

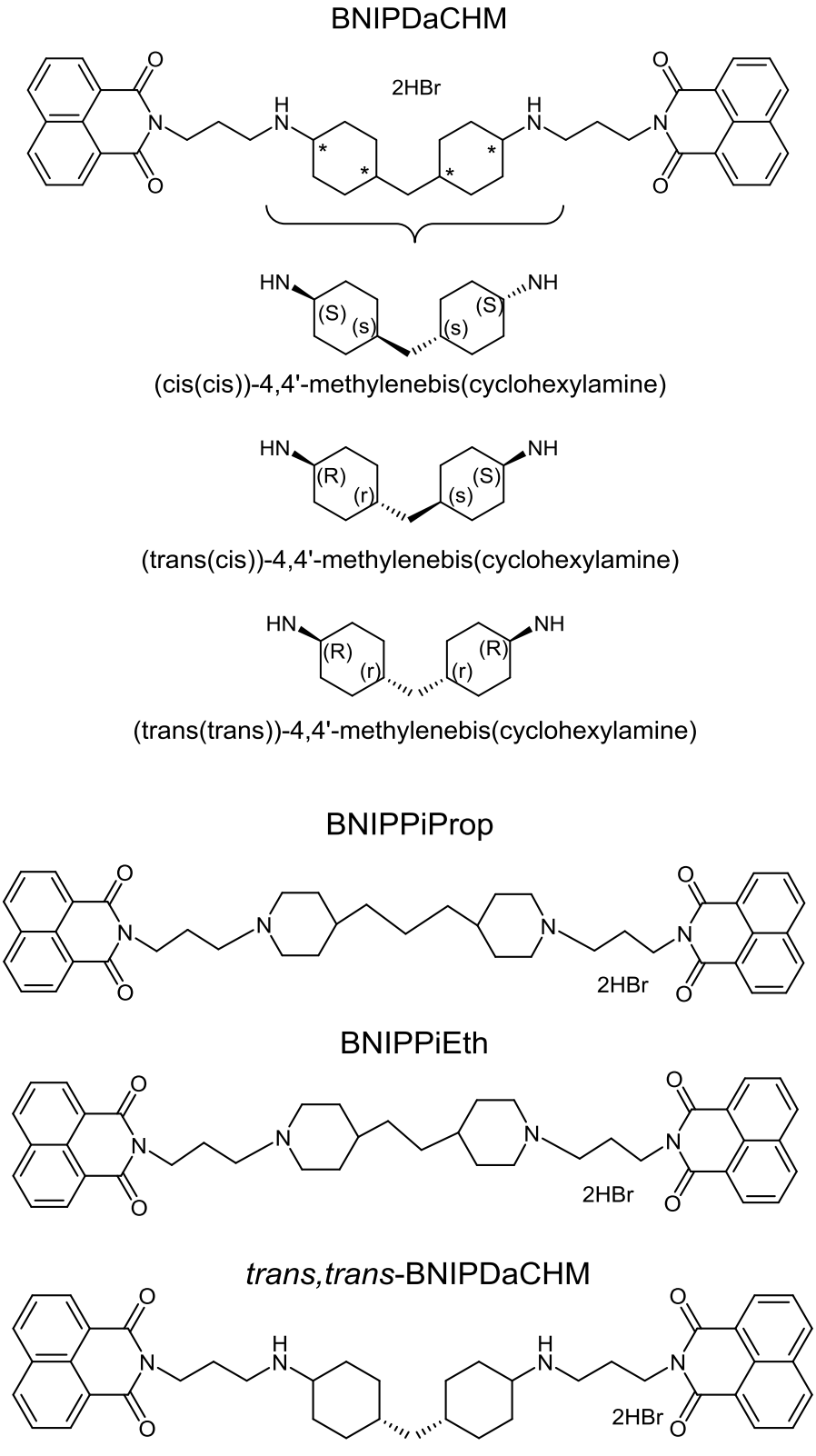

Figure 2.1.1.: Chemical structures of BNIPs: BNIPDaCHM with its three stereo isomers, bisnaphthalimidopropyl-piperidylpropane (BNIPPiProp), bisnaphthalimidopropyl- ethylenedipiperidine (BNIPPiEth) and *trans,trans*-4,4'Methylenebis(cyclohexylamine) bisnaphthalimidopropyl diaminodicyclohexylmethane (*trans,trans*-BNIPDaCHM).

of three stereoisomers of unknown relative proportion present in BNIPDaCHM in relation to DNA binding affinities, cytotoxicity in breast cancer cell lines and the possible mode of cell death.

2.1.2 Synthetic method of bisnapthalimidopropyl derivatives.

The first BNIPPs were synthesised by Kong Thoo Lin and Pavlov (2000) and the synthetic strategy they proposed was also used for the synthesis of BNIPPiProp, BNIPPiEth and *trans,trans*-BNIPDaCHM (Kopsida *et al*, 2016).

The synthesis of the three novel BNIPs consisted of two step reactions: firstly, the synthesis of the common precursor *N*-(3-hydroxypropyl)naphthalimide, prepared from the reaction of 1,8-naphthalic anhydride with 3-amino-1-propanol (Figure 2.1.2a[1]) and secondly, the synthesis of toluenesulfonyloxypropylnaphthalimide, prepared from *N*-(3-hydroxypropyl)naphthalimide with p-toluenesulfonyl chloride in pyridine (Figure 2.1.2a[2]).

BNIPPiProp was obtained from the reaction between 1,3-bis-(4-piperidyl)propane and toluenesulfonyloxypropylnaphtalamide in tetrahydrofuran (THF) at 50 ^{o}C for 15 minutes, fitted with a reflux condenser and in the presence of caesium carbonate (Cs_2CO_3) (Figure 2.1.2b). Synthesis of BNIPPiProp dihudrobromide salt was obtained upon dissolution of BNIPPiProp base in dichloromethane (DCM) and treatment with hydrogen bromide (HBr)/acetic acid (CH_3CO_2H) at room temperature for 2 hours to yield a precipitate. The latter was filtered off by vacuum filtration and washed with DCM and ether.

BNIPPiEth was prepared upon the reaction of 4,4 Ethylenedipiperidine with toluenesulfonyloxypropylnaphthalimide, in the presence of caesium carbonate in THF overnight at 60 °C (Figure 2.1.2b). Synthesis of BNIPPiEth dihydrochloride salt was completed upon reaction with concentrated HCl in DCM at room temperature for 60 minutes (Figure 2.1.2b).

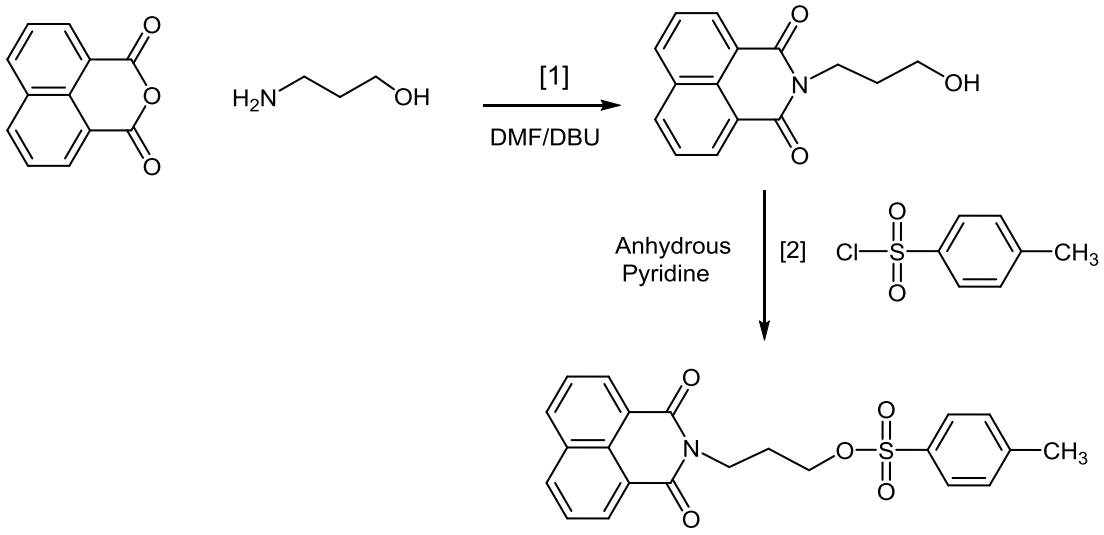

Figure 2.1.2a.: General synthetic method for the synthesis of BNIPPs: [1] 3-amino-1-propanol, DMF/DBU, 85°C, 5 hours [2] p-toluenesulfonyl chloride (Ts-Cl), anhydrous pyridine, 4 °C, 12 hours.

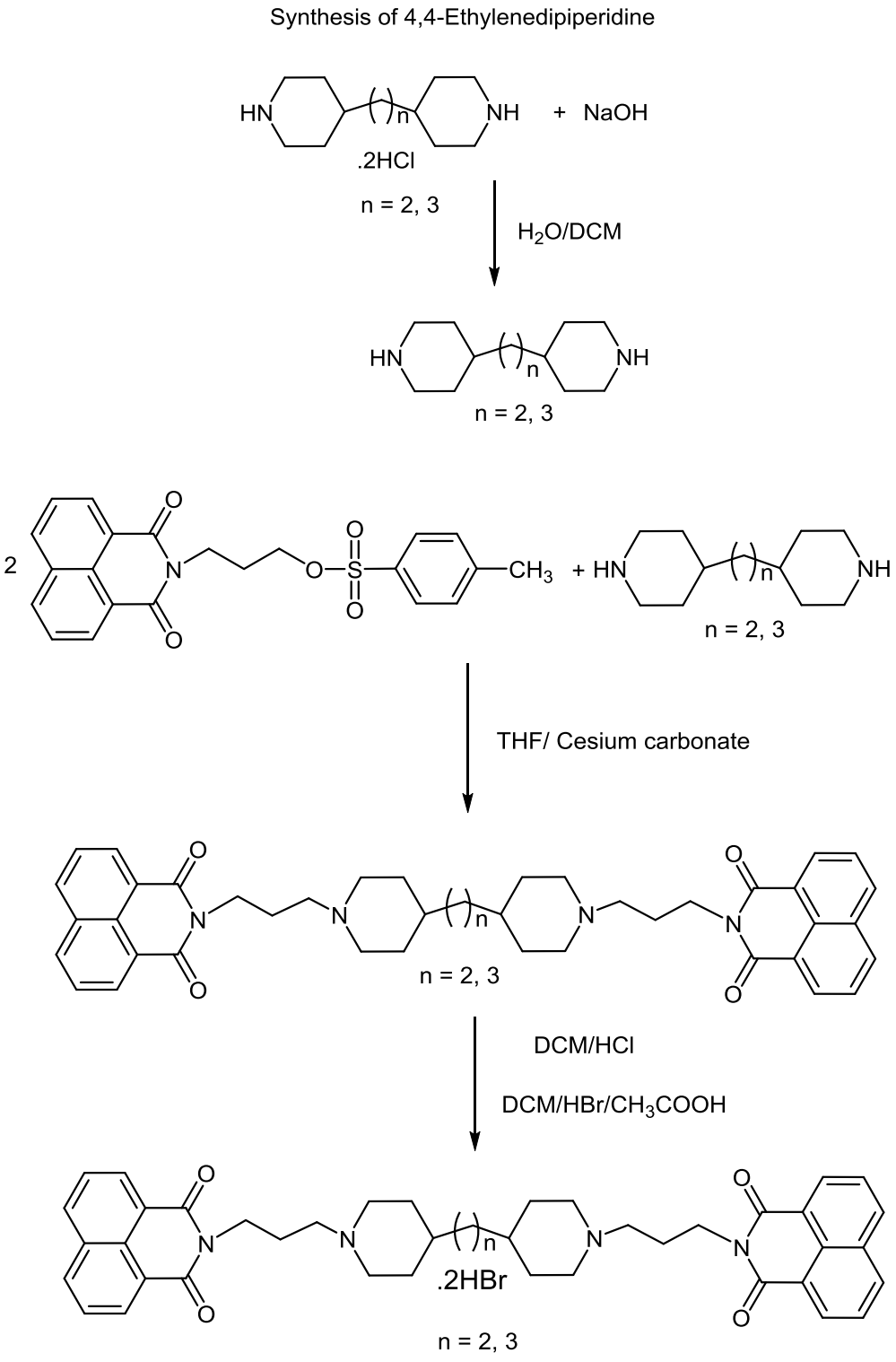

Figure 2.1.2b.: Synthetic pathway of bisnaphthalimidopropyl-piperidylpropane (BNIPPiProp) and bisnaphthalimidopropyl- ethylenedipiperidine dihydrobromide (BNIPPiEth).

The synthesis of *trans,trans*-BNIPDaCHM was based on methods previously developed in our group for the synthesis of BNIPDaCHM (Kong Thoo Lin and Pavlov, 2000, Barron *et al*, 2010). Here the single isomer *(trans(trans))*-4,4'-methylenebis-cyclohexylamine was used as the starting material. The synthesis of *trans,trans*-N^4,N^4-dimesityl-dicyclohexylmethane was carried out by reacting *(trans(trans))*-4,4'-methylenebis-cyclohexylamine with 2-mesitylenesulfonyl chloride (Mts-Cl) in anhydrous pyridine (Figure 2.1.2c). *N*-Alkylation was performed by reacting *trans,trans*-N^4,N^4-dimesityl-dicyclohexylmethane with toluenesulfonyloxypropylnaphthalimide in dimethylformamide (DMF). For the final step, *trans,trans*-bisnaphthalimido-dimesityl-dicyclohexylmethane was dissolved in DCM, followed by treatment with hydrobromic acid/glacial acetic acid (HBr/g.CH_3CO_2H) (Figure 2.1.2c) to obtain the novel BNIP *trans,trans*-BNIPDaCHM.

Synthesis of trans,trans-N^4N^4-dimesityl-dicyclohexylmethane

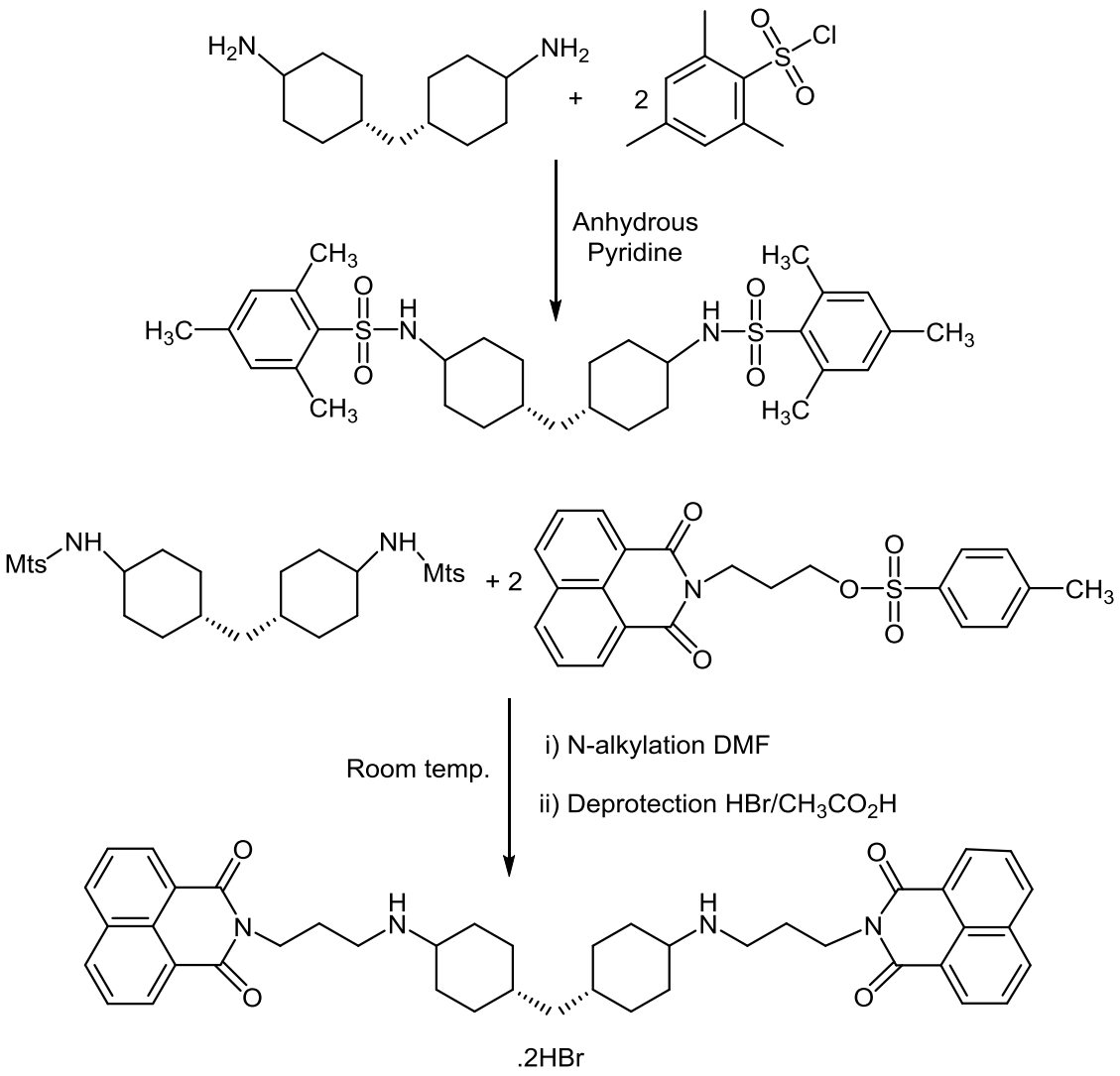

Figure 2.1.2c.: Synthetic pathway of *trans,trans*-4,4'-methylenebis(cyclohexylamine) bisnaphthalimidopropyl diaminodicyclohexylmethane (*trans,trans*-BNIPDaCHM).

2.1.3 Separation, identification and characterisation of BNIPs.

Thin Layer Chromatography (TLC), Nuclear Magnetic Resonance (NMR) and Mass Spectrometry (MS) were the three analytical techniques that were applied for the characterisation of the three novel BNIPs.

TLC is a method used for separating compounds of a mixture and determining the number of co-existing components in the mixture, the purity and identity of the final compound (Geiss, 1987). During the synthesis of all the compounds, TLC was used to observe the appearance or disappearance of reactants, while monitoring the progress of a chemical reaction.

TLC is a sensitive, quick and low cost technique that consists of three basic steps: spotting, development and visualisation. The first step requires the sample to be dissolved in volatile solvent (5% v/v solution). By using a micro pipette, a small amount of this solution is transferred to one end of a TLC plate (silica gel aluminium plate). Once the spotting solvent evaporates, a small spot of material appears on the TLC plate (Stoddard *et al*, 2007). The next step is to place the bottom of the TLC place in a TLC development tank with a solvent, which moves upwards due to capillary action. Between the silica gel plate and the development solvent, there is a competition where the silica gel (polar) tries to keep the spot in its original place whilst the solvent moves further up the TLC plate. Once the solvent has almost moved to the other side of the plate, the plate is removed, the solvent front is marked and the TLC plate is left to dry (Figure 2.1.3). The spots of coloured compounds can be directly observed after the development step. However, most of the compounds are colourless and a visualisation method is required to observe the movement of material along the plate. The most common detection method is to observe the TLC plate under ultraviolet (UV) light, as the silica gel plates are permeated with fluorescent material so that every material

appears as a dark spot. The quantification of the material movement is expressed by the R_f value, which is equal to the distance of the substance divided by the distance of the solvent.

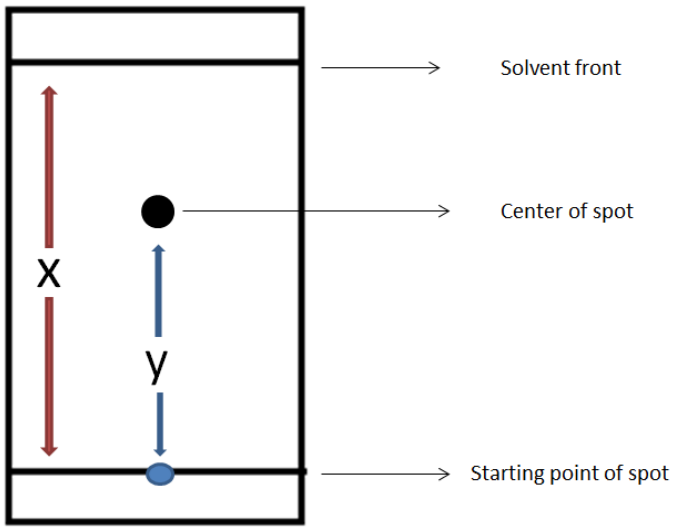

Figure 2.1.3.: Silica gel plate and calculation of R_f value, where R_f=y/x (always ≤1).

NMR is an analytical tool used for determining and characterising the complete chemical structure of an organic compound. Compared to other spectroscopic methods, NMR is the only technique that can provide a complete elucidation of an unknown compound from only a few milligrams of the sample. The samples are prepared in NMR tubes, by dissolving the compound in deuterated solvents, such as chloroform-D ($CDCl_3$). Afterwards, samples are introduced into the NMR instrument and processed by Bruker Topspin Software which produces the NMR spectrum.

The main principle of this analytical tool is the ability to capture a phenomenon occurring once specific atomic nuclei (usually proton and carbon-13 nuclei) are in

a static magnetic field: if the nuclei possess a property called nuclear spin, then it is exposed to a second oscillating magnetic field (Koutcher and Burt, 1984). ^{1}H-NMR and ^{13}C-NMR detect the signals of protons and carbons respectively and DEPT-135 NMR, which is another ^{13}C-NMR experiment, can supply further information on the different type of carbons present within a compound, such as the $-CH_3$ and –CH signals which appear above the baseline, whilst the $-CH_2$ signals appear inverted and quaternary carbons signals disappear. ^{1}H-NMR (400.1 MHz), ^{13}C-NMR (100.6 MHz) and DEPT-135 NMR (100.6 MHz) are observed at different frequencies, as the proton nucleus processes faster than the carbon nucleus, requiring higher frequency radiation.

Although NMR spectroscopy can provide important information about the entire chemical structure of a compound, Mass Spectrometry (MS) is an appropriate analytical tool that can determine and confirm the purity and molecular mass of the final compound (Yurek *et al*, 2002). For all the BNIPs that were synthesised in this project, MS was used to confirm their full characterisation.

Mass spectrometers consist of three fundamental parts: the ionisation source, the analyser and the detector. Once the sample is introduced into the ionisation source, sample molecules are ionised and extracted into the analyser region. At that point, the charged molecules are separated according to their mass (m) to charge (z) ratios (m/z) (Smith *et al*, 1991).

2.2 Materials

A list of the reagents that were used during the synthesis and characterisation of the novel BNIPs are presented below. All the reagents were manipulated according to the COSHH standards.

1,8-naphthalic anhydride	Sigma-Aldrich, UK
3-amino-1-propanol	Sigma-Aldrich, UK
1,8-diazabicylo[5.4.0]undec-7-ene (DBU)	Sigma-Aldrich, UK
Dimethylformamide (DMF)	Fisher Scientific, UK
Pyridine (anhydrous)	Sigma-Aldrich, UK
p-toluenesulfonyl chloride (Ts-Cl)	Sigma-Aldrich, UK
4,4'-methylenebis(cyclohexylamine)	TCI, Japan
2-mesitylenesulfonyl chloride (Mts)	Sigma-Aldrich, UK
Caesium carbonate	Alfa Aescar, UK
Hydrobromic acid/glacial acetic acid	Sigma-Aldrich, UK
Dichloromethane (DCM)	Fisher Scientific, UK
1,3-bis-(4-piperidyl)propane	Sigma-Aldrich, UK
Tetrahydrofuran (THF)	Sigma-Aldrich, UK
4,4-Ethylenedipiperidine dihydrochloride	Sigma-Aldrich, UK
Sodium hydroxide	Sigma-Aldrich, UK
Diethyl ether	Fisher Scientific, UK
Ethanol	Acros Organics, Belgium

Hydrochloric acid	Sigma-Aldrich, UK
Methanol	Acros Organics, Belgium
Chloroform-D	Cambridge Isotope, USA
Dimethylsulfoxide-d_6	Cambridge Isotope, USA

2.3 Instrumentation

Thin Layer Chromatography (TLC) assays were carried out to verify the completion and purity of the products. TLCs were performed on 2cm×5cm silica gel 60 F254 aluminium plates (Merck, Germany). One % (v/v) methanol in dichloromethane solution was used as mobile phase and the spots were visualized under UV light (254nm-375nm).

Nuclear Magnetic Resonance (NMR) spectroscopy was performed on a Bruker 400 Ultrashield spectrometer, using chloroform-D ($CDCl_3$) or dimethyl-sulfoxide (DMSO-D_6).

Mass spectral analysis was undertaken at the Engineering and Physical Sciences Research Council National Mass Spectrometry Centre at Swansea University, Swansea, UK.

Thermal melting points (MP) were defined by using the standard operating procedure of Griffin Melting Point Apparatus (Fisher Scientific, UK).

2.4 Results and Discussion: Synthesis of bisnaphthalimidopropyl-diaminodicyclohexylmethane (BNIPDaCHM)

2.4.1 Synthesis of N-(3-hydropropyl) naphthalimide

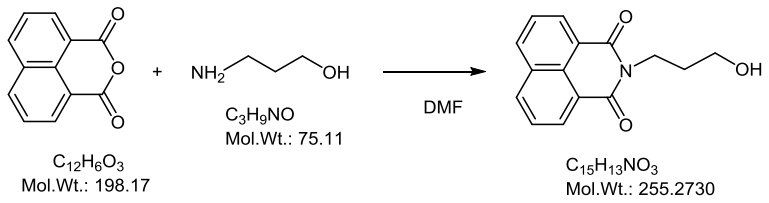

Figure 2.4.1a.: Synthesis of N-(3-hydropropyl)naphthalimide.

In a round bottom flask (250cm^3), 1,8-naphthalic anhydride (Molecular mass (M) = 198.17 g mol^{-1}, Number of moles (n) = 0.050 mol, 10 g) was dissolved in dimethylformamide (DMF) (140 mL) (Figure 2.4.1a). Once the 1,8-naphthalic anhydride was totally dissolved, 3-amino-1-propanol (M = 75.11 g mol^{-1}, n = 0.050 mol, 3.75 g) and 1,8-diazabicylo[5.4.0]undec-7-ene (DBU) (13 mL) were added. The reaction was left to stir for 5 hours at 85 °C. Reaction completion was monitored with TLC and once completed, the solution was poured into icy water (200 mL) while stirring with a glass rod to allow formation of a white precipitate. The precipitate was filtered off by vacuum filtration, followed by several water washes, and dried in a vacuum oven set at 45 °C overnight. The pure product was characterised using ^{1}H-NMR. Yield was calculated as: 53.9%

N-(3-hydroxypropyl) naphthalimide ^{1}H-NMR ($CDCl_3$): δ_H 8.66 – 8.63 (2H, aromatic H, doublet, J=7.2 Hz), 8.29 – 8.25 (2H, aromatic H, doublet, J=8.4 Hz), 7.83 – 7.78 (2H, aromatic H, doublet, J=8.0 Hz), 4.41-4.38 (3H, triplet, J=5.6 Hz), 3.64-

3.59 (2H, CH_2, multiplet) 3.23 (OH, singlet) and 2.06–2.00 (2H, CH_2 multiplet) parts per million (ppm).

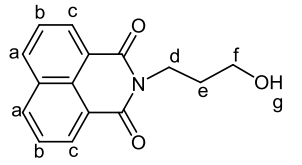

N-(3-hydroxypropyl)naphthalimide

Figure 1.4.1b.: Equivalent protons of N-(3-hydroxypropyl)naphthalimide.

Chemical shifts corresponding to protons situated at the aromatic carbons c, a, and b of the naphthalimido group resonated at 8.66-8.63 ppm, 8.29, 8.25 ppm and 7.83-7.778 ppm respectively (Figure 2.4.1b). Integration analysis within the aromatic region of the spectrum showed that the signals correspond to six hydrogens, hence were assigned to protons a, b and c. The chemical shift of the solvent signal was observed at 7.26 ppm (chloroform-d). At 4.41-4.38 ppm, aliphatic peaks resonated for protons d, due to the deshielding effect from nitrogen and oxygen atoms. Signal for protons at carbon f occurred upfield, at 3.64-3.59 ppm, for protons on carbon e at 2.06–2.00 ppm and the chemical shift corresponding to proton of the OH group (g) resonated at 3.23ppm.

2.4.2 Synthesis of toluenesulfonyloxypropylnaphthalimide

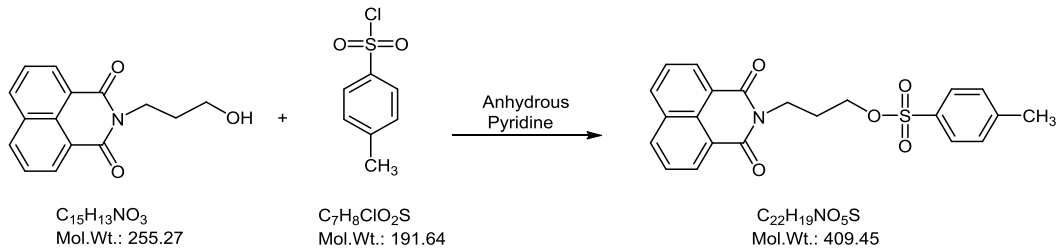

Figure 2.4.2a.: Synthesis of toluenesulfonyloxypropylnaphthalimide.

In a round bottom flask (150cm^3), *N*-(3-hydropropyl)naphthalimide (M = 255.27 g mol^{-1}, n = 0.0196 mol, 5.0 g) was dissolved in anhydrous pyridine (70 mL), whilst stirring on ice. Once the *N*-(3-hydropropyl)naphthalimide was completely dissolved, *p*-toluenesulfonyl chloride (Ts-Cl) (M = 190.65 g mol^{-1}, n = 0.0394 mol, 7.51 g, 2.01 excess) was slowly added to the reaction (Figure 2.4.2a). The reaction was left at 4 °C overnight. It was monitored using TLC and once it was complete, the solution was poured into icy water (200 mL) and stirred with a glass rod until a precipitate was formed. After vacuum filtration and several washes with water, the final product was left to dry under negative pressure in a vacuum oven at 45°C for 3 hours. The product was recrystallised from ethanol and characterised by ^{1}H-NMR. Yield was calculated as: 68.2%

Toluenesulfonyloxypropylnaphthalimide ^{1}H-NMR ($CDCl_3$): δ_H 8.59 – 8.57 (2H, aromatic H, doublet, 8.2 Hz), 8.25 – 8.23 (2H, aromatic H, triplet, 7.2 Hz), 7.81–7.76 (2H, multiplet), 7.30 (2H, aromatic H, doublet, 1.2 Hz), 4.27-4.20 (2H, CH_2, multiplet), 2.44 (3H, CH_3 , singlet) and 2.19–2.12 (2H, CH_2, multiplet) ppm.

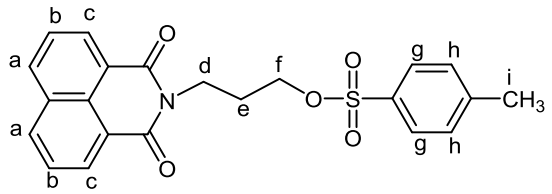

Toluenesulfonyloxypropylnaphthalimide

Figure 2.4.2b.: Equivalent hydrogens of toluenesulfonyloxypropyl-naphthalimide.

Chemical shifts corresponding to protons situated at carbons c, a and b of the naphthalimido group resonated at 8.59–8.57 ppm, 8.25–8.23 ppm and 7.81–7.78 ppm respectively (Figure 2.4.2b). Integration analysis within the aromatic region showed that the signals correspond to six hydrogens, hence were assigned to protons a, b and c respectively. The chemical shift of the solvent signal was observed at 7.26 ppm (chloroform-d). At 4.27-4.20 ppm, aliphatic peaks resonated for CH_2 protons f and downfield when compared with d, since nitrogen atom is less electronegative (3.0) than the oxygen atom (3.5). Signal for proton i was detected at 2.44 ppm and the chemical shift corresponding to proton e resonated at 2.19-2.12 ppm. Chemical shifts for g and h resonated downfield at 7.81–7.76 ppm, between protons a and b.

2.4.3 Synthesis of *N⁴,N⁴*-dimesityl-dicyclohexylmethane

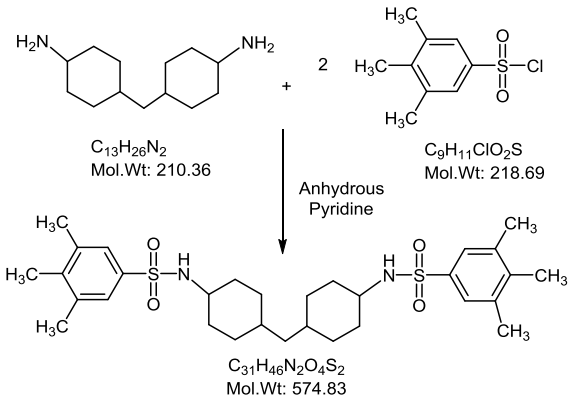

Figure 2.4.3a.: Synthesis of *N⁴,N⁴*-dimesityl-dicyclohexylmethane.

In a round bottom flask (50cm^3), 4,4'-methylenebis(cyclohexylamine) (M = 210.36 g mol^{-1}, n= 4.75x10^{-3} mol, 1.0 g) was added in anhydrous pyridine (10 mL) and left to stir for 15 minutes. After dissolution, 2-mesitylenesulfonyl chloride (Mts) (M = 218.70 g mol^{-1}; n = 9.56x10^{-3} mol; 2.1 g) was added (Figure 2.4.3a). The reaction was left to stir overnight at room temperature and TLC confirmed reaction completion. The solution was poured into icy water (150 mL) and stirred with a glass rode until the formation of a precipitate. The product was filtered off by vacuum filtration, left to dry in a vacuum oven set at 45 °C for 24 hours. The product was afterwards characterised by ^{1}H-NMR. Yield of the reaction was calculated as: 43.3%.

N⁴,N⁴-dimesityl-dicyclohexylmethane ^{1}H-NMR ($CDCl_3$): δ_H 7.30 (NH), 6.97 (4H, CH aromatic protons), 2.99 (4H, CH protons), 2.67-2.66 (6H, CH_3-Mts protons) and 1.73-1.49 (CH_2 and cyclohexane protons) ppm.

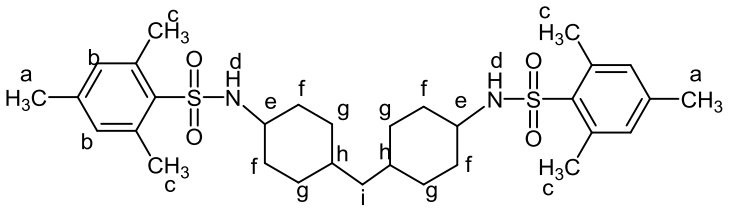

Figure 2.4.3b.: Equivalent hydrogens of *N*^{4},*N*^{4}-dimesityl-dicyclohexylmethane.

The NMR signal for the NH proton d resonated at 7.30 ppm, due to the deshielding effect of the electronegative sulfonamide group (Figure 2.4.3b). Chemical shifts corresponding to aromatic proton b resonated at 6.97 ppm and the signal for the methane proton e observed further upfield at 2.99 ppm. Chemical shifts corresponding to methyl groups on the aromatic ring resonated at 2.67-2.66 ppm and 2.21 ppm respectively. Signals for protons at carbons f, g and h of the cyclohexane ring were detected upfield between 1.75-1.43 ppm. Chemical shift corresponding to methylene group i resonated further upfield at 1.04 ppm. Due to signals overlapping and the co-existance of three isomers in the above compound, the assignment of the rest signals was difficult to assign.

2.4.4 *N*-alkylation reaction

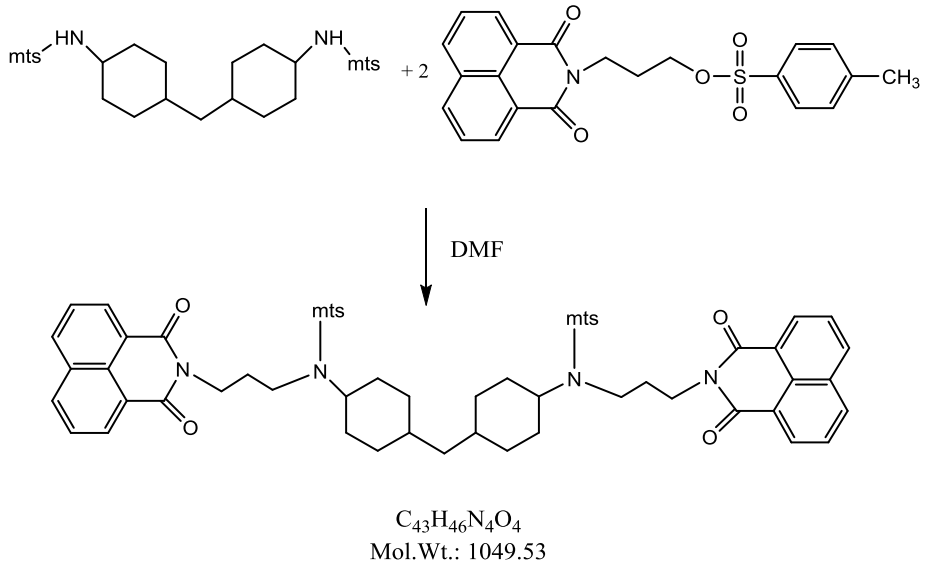

Figure 2.4.4a.: Synthesis of protected bisnaphthalimidopropyl-dimesityl-dicyclohexylmethane.

In a round bottom flask (50cm^3), *N*^{4},*N*^{4}-dimesityl-dicyclohexylmethane (M = 574.83 g mol^{-1}, n = 6.968x10^{-4} mol, 0.4 g) and toluenesulfonyloxypropylnaphthalimide (M = 409.46 g mol^{-1}; n = 1.400x10^{-3} mol, 0.57 g, 2.01 excess) were dissolved in DMF (8 mL). Afterwards, excess of caesium carbonate (M = 325.82 g mol^{-1}, n = 3.5x10^{-3} mol, 1.13 g, 2.5 excess) was added slowly (Figure 2.4.4a).

The reaction was left to stir for 48 hours at 60 °C. After TLC confirmed the reaction was complete, the solution was poured into icy water (150 mL) to form a precipitate. After vacuum filtration and several washes with water, the product was left to dry under negative filtration in a vacuum oven at 45 °C for 3 hours. The product was recrystallised with pure ethanol and characterised by ^{1}H-NMR. Yield was calculated as: 92.2%.

Protected bisnaphthalimido-dimesityl-dicyclohexylmethane ^{1}H-NMR ($CDCl_3$): δ_H 8.50–8.47 (2H, aromatic H), 8.18–8.15 (2H, aromatic H), 7.72–7.67 (2H, aromatic H), 6.87 (2H, CH-Mts H), 6.55–6.53 (2H, CH-Mts H), 3.94–3.92 (2H, CH_2), 3.12–3.10 (2H, CH_2), 2.87-2.80 (2H, CH_2), 2.35-2.32 (3H, CH_3), 2.05-2.04 (3H, CH_3), 1.61-1.58 (H, CH), 1.61 (2H,CH_2) 1.49-1.37 (2H, CH) and 1.04 (2H, CH_2) ppm.

^{13}C-NMR ($CDCl_3$): δ_H 163.87-162.76 (C=O), 134.36 (C aromatic), 131.40-130.74 (C aromatic), 127.75 (C aromatic), 35.75 (CH_2), 30.41 (CH_2), 21.97 (CH_3) and 20.32 (CH_3) ppm.

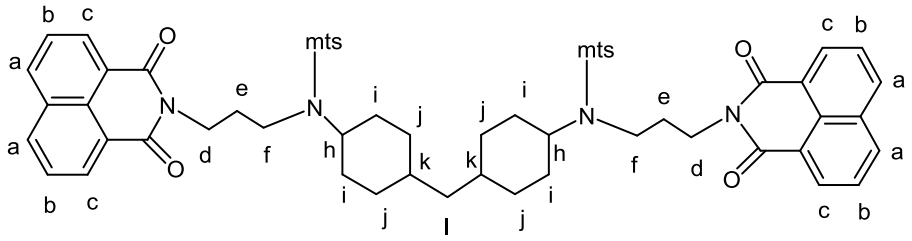

Bisnaphthalimido-dimesityl-dicyclohexylmethane

Figure 2.4.4b.: Equivalent proton and carbons of bisnaphthalimido-dimesityl-dicyclohexylmethane.

Chemical shifts corresponding to protons situated at carbons a, b and c of the naphthalimide rings resonated at 8.50-7.67 ppm (Figure 2.4.4b). Integration analysis within the aromatic region showed that the signals correspond to six hydrogens, hence were assigned to protons a, b and c respectively. The chemical shift of the solvent signal was observed at 7.26 ppm (chloroform-d). At 6.87 ppm and 6.55-6.53 ppm, chemical shifts corresponded to protons that were situated on the *N*^{4},*N*^{4}-dimesityl-dicyclohexylmethane methyl groups were detected. Signal for proton d was detected next upfield, due to the deshielding effect from nitrogen and oxygen atoms, the signal for proton f and h were observed upfield at 3.12–3.10 ppm and 2.87-2.80 ppm, respectively. Chemical shifts corresponding to

protons of the methyl groups on the N^4,N^4-dimesityl-dicyclohexylmethane aromatic ring resonated at 2.35-2.04 ppm. Further upfield, the proton signal for carbon e was detected at 1.61-1.58 ppm and for i and j at 1.61 ppm, respectively. Chemical shifts corresponding to protons situated at k resonated at 1.49-1.37 ppm and for i at 1.04 ppm.

For the ^{13}C spectrum, chemical shifts corresponding to the amide carbon of the naphthalimido ring resonated at 163.87-162.76 ppm and for a, b and c at 134.36-127.17 ppm. At 35.75 ppm, the chemical shift corresponded to i and j of the cyclohexane ring and further upfield, the chemical shift for k resonated at 30.41 ppm. The next upfield, chemical shifts corresponded to the methyl groups of *N^4,N^4*-dimesityl-dicyclohexylmethane were detected at 21.97 and 20.32 ppm, respectively.

2.4.5 Deprotection reaction

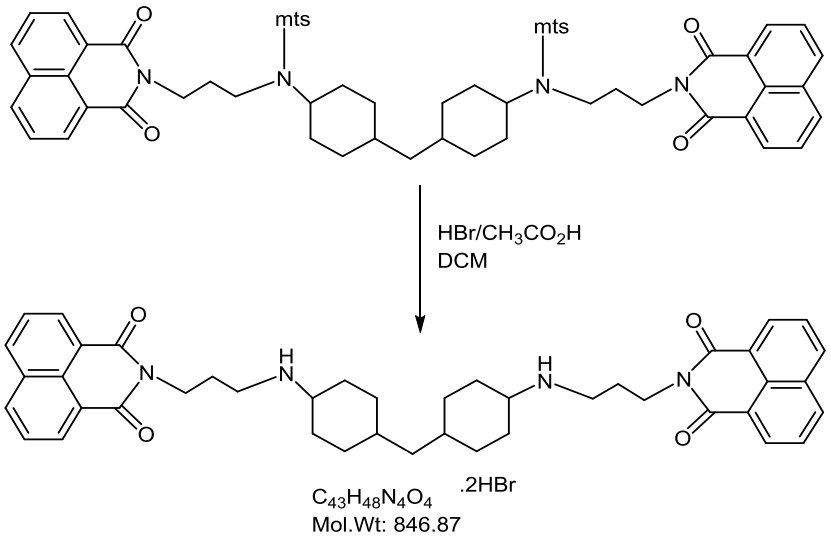

Figure 2.4.5a.: Synthesis of bisnaphthalimidopropyl-diamino-dicyclohexyl-methane dihydro-bromide salt (BNIPDaCHM).

In a round bottom flask (50cm^3), bisnaphthalimido-dimesityl-dicyclohexylmethane (M = 1049.53 g mol^{-1}, n = 3.813x10^{-4} mol, 0.4 g) was dissolved in dichloromethane (DCM) (8 mL). Afterwards, hydrobromic acid/glacial acetic acid (HBr/CH_3CO_2H) (1 mL) was added drop wise (Figure 2.4.5a). The reaction was stirred overnight at room temperature. TLC was used to confirm that the reaction was complete. The precipitate formed, was filtered off by vacuum filtration and washed with DCM (15 mL) and ether (5 mL). The final product was dried under negative pressure in a vacuum oven set at 45 °C for 3 hours. Once dry, the final product was characterised by ^{1}H-NMR (Figure 2.4.5b), ^{13}C-NMR (Figure 2.4.5c) and DEPT-135 NMR. Yield was calculated as 37.5% and the relative molecular mass of bisnaphthalimidopropyl-diamino-dicyclohexylmethane (BNIPDaCHM) was confirmed by mass spectral analysis (Figure 2.4.5e).

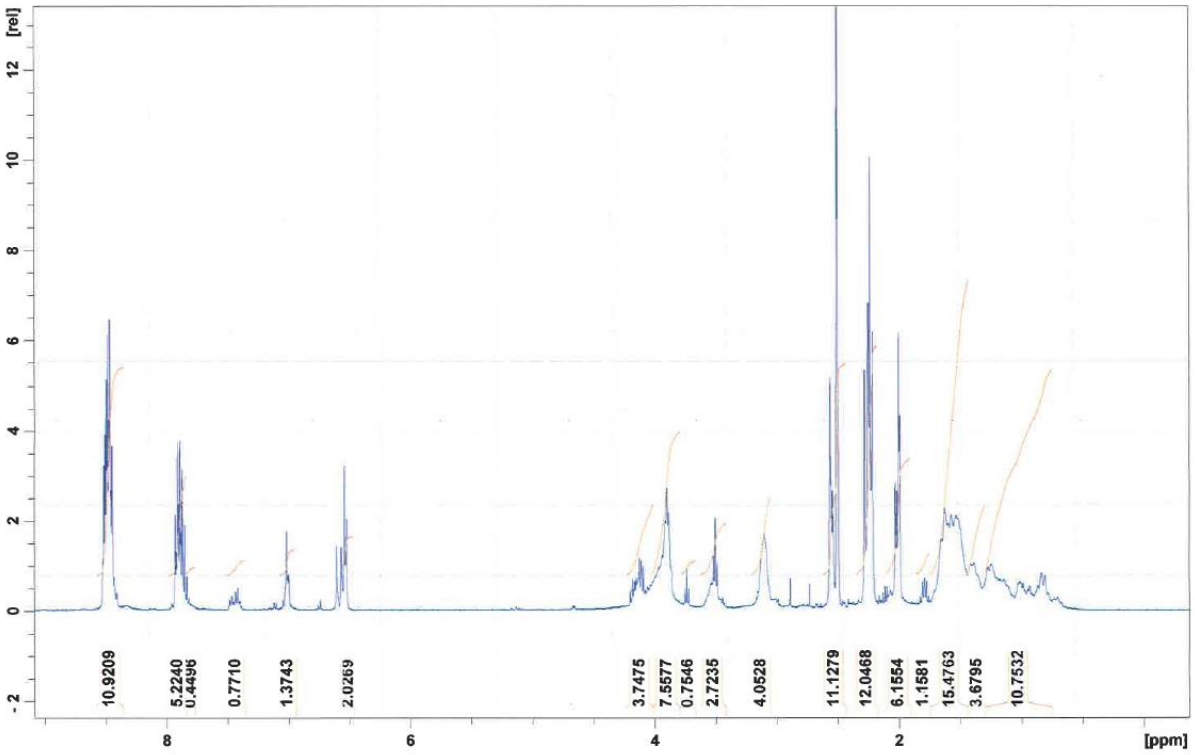

Figure 2.4.5b.: ^{1}H-NMR spectrum for BNIPDaCHM.

Bisnaphthalimidopropyl-diamino-dicyclohexylmethane dihydro-bromide salt ^{1}H-NMR ($CDCl_3$) (Figure 2.4.5b): δ_H 8.32–8.25 (2H, aromatic Hs), 7.73–7.65 (2H, aromatic Hs), 3.70–3.64 (2H, CH_2 protons), 3.13 (2H, CH_2 protons), 2.90-2.30 (3H, CH_3 protons), 2.09-2.02 (3H, CH_3 protons), 1.83-1.80 (H, CH proton), 1.43-1.33 (2H, CH_2 protons) ppm.

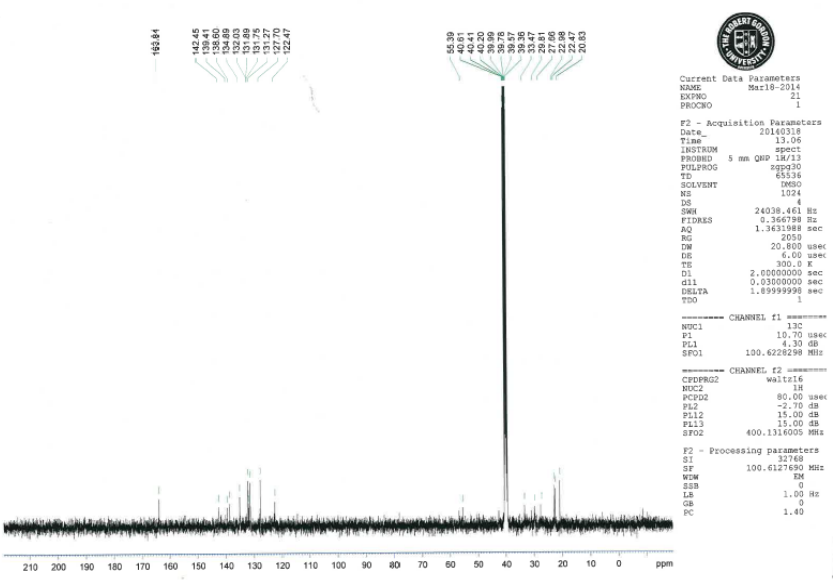

Figure 2.4.5c.: ^{13}C-NMR spectrum for BNIPDaCHM.

^{13}C-NMR ($CDCl_3$) (Figure 2.4.5c): δ 163.87-162.76 (C=O), 134.36 (C aromatic), 131.40-130.74 (C aromatic), 127.75 (C aromatic), 35.75 (CH_2) and 30.41 (CH_2) ppm.

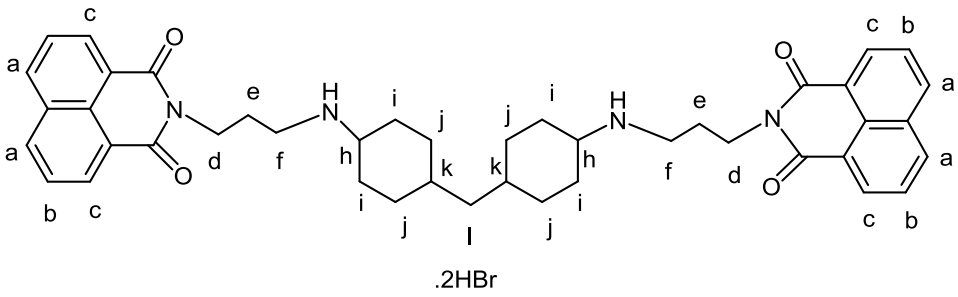

Bisnaphthalimidopropyl-diamino-dicyclohexylmethane dihydro-bromide salt

Figure 2.4.5d.: Equivalent protons and carbons of bisnaphthalimidopropyl-diamino-dicyclohexylmethane dihydro-bromide salt (BNIPDaCHM).

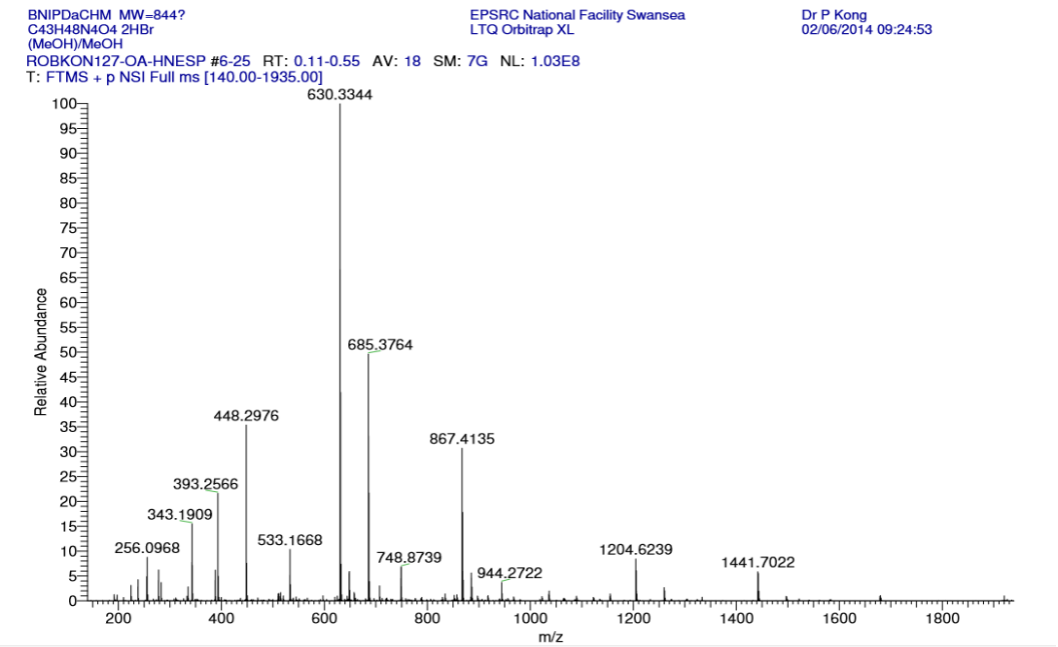

Figure 2.4.5e.: High resolution mass spectrum of BNIPDaCHM: $M^{+=}$630.3344.

The chemical shifts for the final product BNIPDaCHM resonated on a similar way, as for bisnaphthalimido-dimesityl-dicyclohexylmethane (Section 2.4.5b). The absence of resonance signals corresponding to protons which were present from the methyl groups of N^4,N^4-dimesityl-dicyclohexylmethane confirmed that the reaction was complete and that BNIPDaCHM was formed. However, the aromatic rings could not be assigned accurately, due to the mixture of isomers (*cis,cis* or *trans,trans*, or *trans,cis*) that makes the assignment of peaks more complex.

2.5 Results and Discussion: Synthesis of bisnaphthalimidopropyl-piperidylpropane (BNIPPiProp)

2.5.1 Synthesis of bisnaphthalimidopropyl-dipiperidyl-propane base

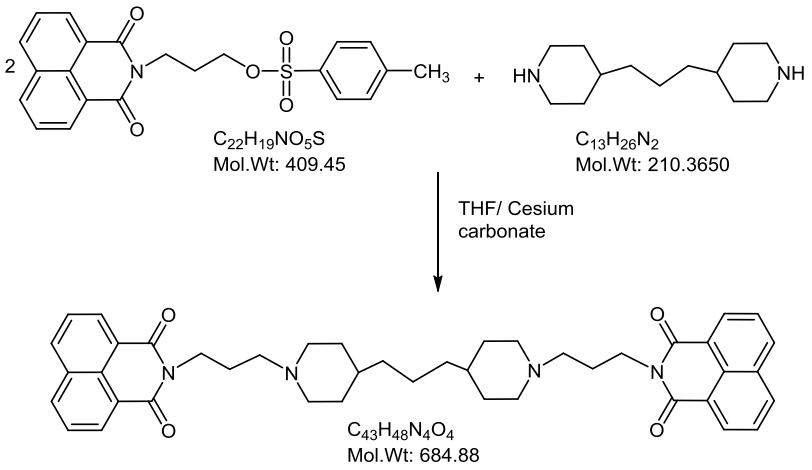

Figure 2.5.1a.: Synthesis of BNIPPiProp free base.

In a round bottom flask (50cm^3), 1,3-bis-(4-piperidyl)propane (M = 210.36g/mol, n = 1.19 x10^{-3}mol, 0.25g) and toluenesulfonyloxypropylnaphtalamide (M = 409.46 g mol^{-1}, n = 2.39 x10^{-3}mol, 0.98g) were dissolved in tetrahydrofuran (THF)(6 mL). Using a reflux condenser, the reaction was stirred at 50^{o}C for 15 minutes and after the addition of caesium carbonate (M = 325.82 g mol^{-1}, n = 3.069 x10^{-3} mol, 1 g), the reaction was left to stir overnight at 50 ^{o}C (Figure 2.5.1a). The reaction was monitored with TLC and once complete, the solution was poured into icy water (100 mL). A precipitate was formed and after vacuum filtration, the product was dried in a vacuum oven at 45 ^{o}C overnight. The crude product (base of BNIPPiProp) was recrystallised in ethanol and the pure product was characterised by ^{1}H-NMR. Yield was calculated as: 64.8%.

^{1}H-NMR : δ_H 8.53–8.51 (2H, CH aromatic protons), 8.14–8.12 (2H, CH aromatic protons), 7.70–7.66 (2H, CH aromatic protons), 4.17–4.14 (2, CH_2 protons),

2.84–2.82 (2H, CH_2 protons), 2.41–2.37 (2H, CH_2 protons), 1.91-1.83 (2H, CH_2 protons), 1.79-1.74 (2H, CH_2 protons), 1.51-1.48 (2H, CH_2 protons), 1.71-1.09 (H, CH protons) ppm.

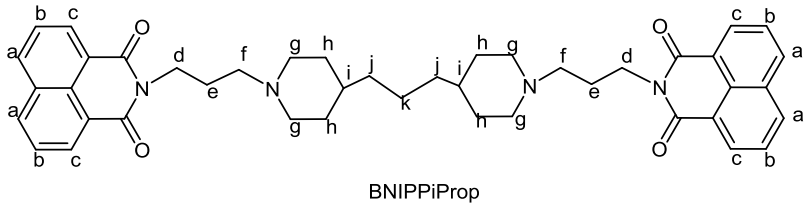

Figure 2.5.1b.: Equivalent hydrogen of BNIPPiProp base.

As expected, chemical shifts which corresponded to protons of naphthalimido rings, at carbons a, b and c resonated between 8.53-7.66 ppm (Figure 2.5.1b). Integration analysis within the aromatic region of the spectrum showed that the signals correspond to six hydrogens, hence were assigned to protons a, b and c, respectively. The chemical shift of the solvent signal was observed at 7.26 ppm (chloroform). At 4.17-4.14 ppm, aliphatic peaks resonated as a triplet for d, due to the existence of two adjacent protons on carbon e. The signal for proton e was detected upfield, due to the deshielding effect from nitrogen atoms and next to them, the chemical shifts corresponding to protons situated at carbons r, h, i, j and k were resonated.

2.5.2 Synthesis of BNIPPiProp salt

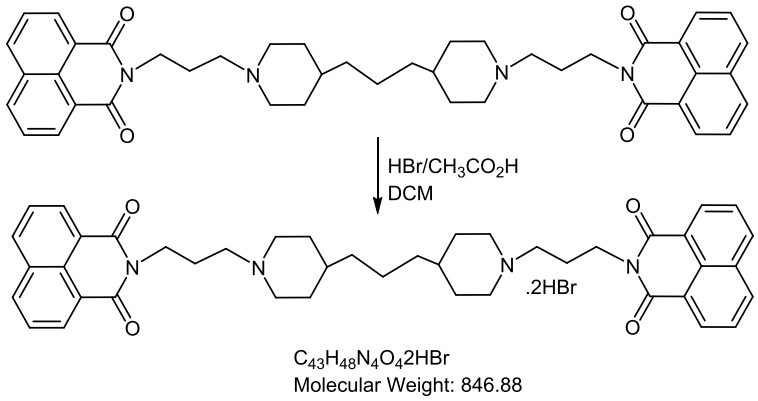

Figure 2.5.2a.: Synthesis of BNIPPiProp salt.

In a round bottom flask (50cm^3), the base of BNIPPiProp (M = 685.05 g mol^{-1}, n = 1.459 x10^{-3} mol, 1 g) was dissolved in DCM (20mL) and HBr/CH_3CO_2H (2 mL) was added slowly (Figure 2.5.2a). The reaction was stirred for 2 hours at room temperature and reaction completion was monitored by TLC yielding a precipitate.

The precipitate was filtered off by vacuum filtration and washed with DCM (30 mL) and ether (10 mL). The BNIPPiProp salt was dried under negative pressure in a vacuum oven set at 45 ^oC for 2 hours and the pure product was characterised by ^{1}H-NMR (Figure 2.5.2b), ^{13}C-NMR (Figure 2.5.2c) and DEPT-135 NMR. Yield was calculated as 72.3%. The relative molecular mass of bisnaphthalimidopropyl-piperidylpropane was confirmed by mass spectral analysis (Figure 2.5.2e).

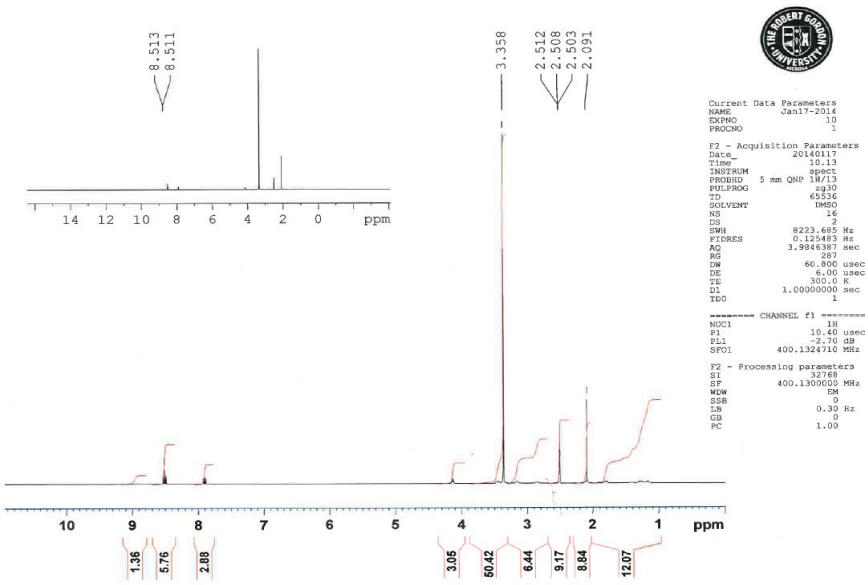

Figure 2.5.2b.: ^{1}H-NMR spectrum for BNIPPiProp.

^{1}H-NMR ($CDCl_3$) (Figure 2.5.2b): δ_H 8.53–8.51 (2H, CH aromatic protons), 8.14–8.12 (2H, CH aromatic protons), 7.70–7.66 (2H, CH aromatic protons), 4.69 (2H, CH_2 protons), 4.17–4.14 (2H, CH_2 protons), 2.84–2.82 (2H, CH_2 protons), 2.41–2.37 (2H, CH_2 protons), 1.91-1.83 (2H, CH_2 protons), 1.79-1.74 (2H, CH_2 protons), 1.51-1.48 (2H, CH_2 protons), 1.71-1.09 (H, CH proton) ppm.

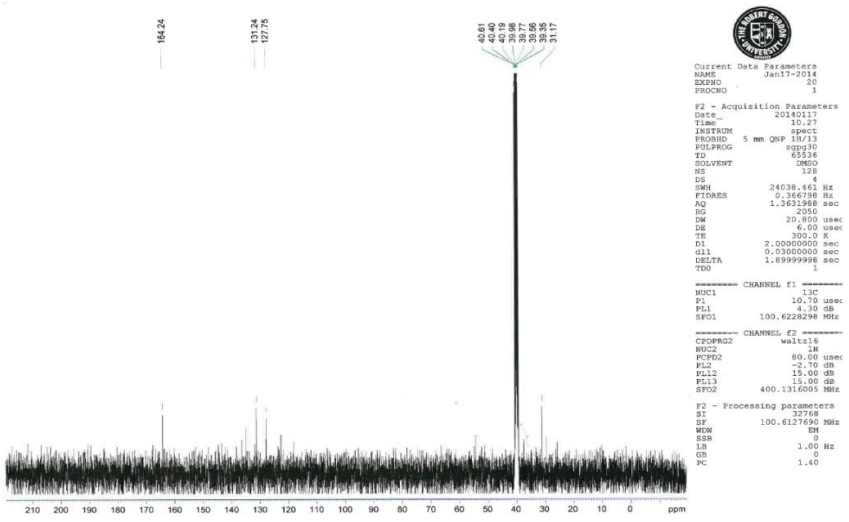

Figure 2.5.2c.: ^{13}C-NMR spectrum for BNIPPiProp.

^{13}C-NMR ($CDCl_3$) (Figure 2.5.2c): δ_H 164.24 (C=O), 131.87 (CH aromatic), 131.60 (C aromatic), 131.24 (CH aromatic), 127.75 (C aromatic), 126.94 (CH aromatic), 122.80 (C aromatic), 56.58 (CH_2), 54.03 (CH_2), 39.10 (CH_2 aromatic), 36.77-35.69 (CH), 32.34 (CH_2), 25.33 (CH_2) and 23.76 (CH_2) ppm.

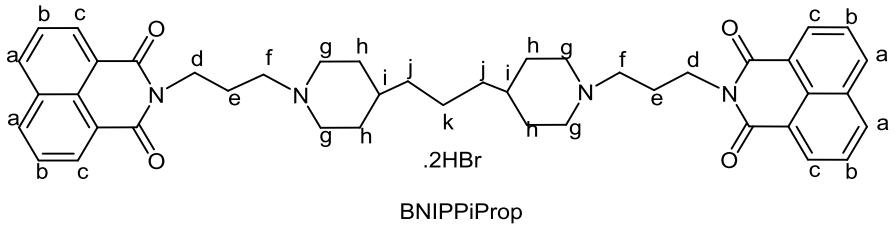

BNIPPiProp

Figure 2.5.2d.: Equivalent protons and carbons of BNIPPiProp salt.

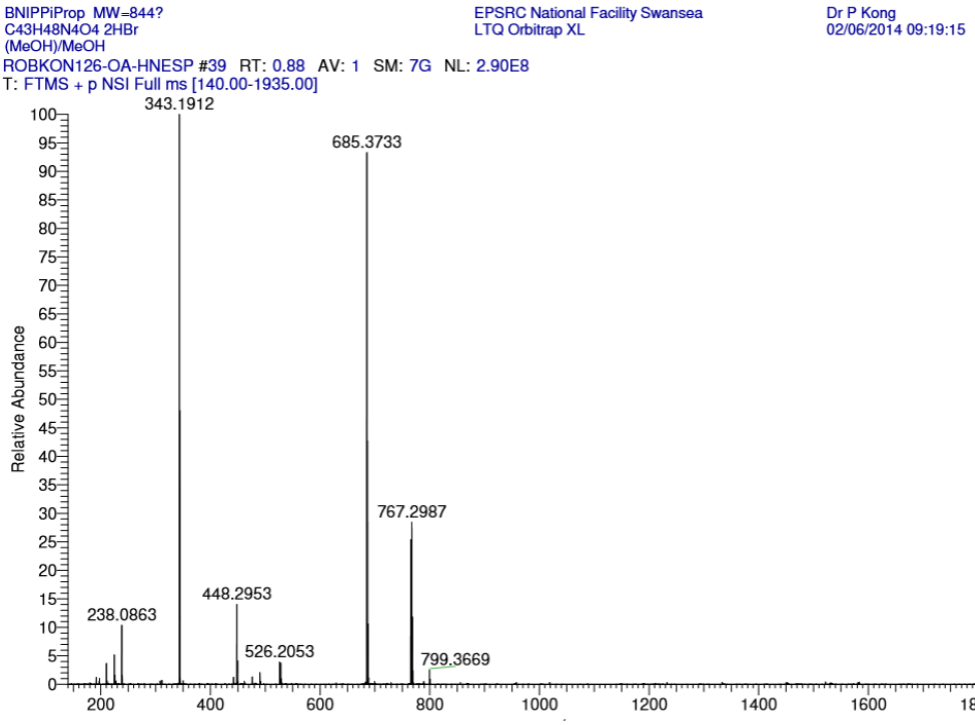

Figure 2.5.2e.: High resolution mass spectrum of BNIPPiProp: $M^{+=}$685.3733.

For the BNIPPiProp salt, chemical shifts resonated on a similar way, as for the BNIPPiProp free base, as they are structurally similar compounds. However, in its ^{13}C spectrum, the chemical shifts of the aliphatic carbons were weak and difficult to assign (Figure 2.5.2c).

2.6 Results and Discussion: Synthesis of bisnaphthalimidopropyl-ethylenedipiperidine (BNIPPiEth)

2.6.1 Synthesis of 4,4-Ethylenedipiperidine

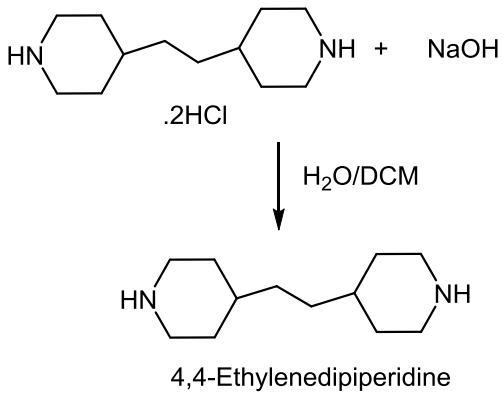

Figure 2.6.1.: Synthesis of 4,4-Ethylenedipiperidine

In a round bottom flask (50cm^3), 4,4-Ethylenedipiperidine dihydrochloride (M = 269.25 g mol^{-1}, n = 7.428x10^{-4} mol, 0.2 g) was dissolved in distilled water (2 mL), Sodium hydroxide (2M, 1mL) was added until the pH of the solution was 14, resulting in the formation of a precipitate (Figure 2.6.1). The. The resulting solution was transferred into a separating funnel (100 mL) followed by extraction with DCM (300 mL). The organic layer was collected, dried with sodium sulfate and filtered. The solvent was evaporated off by a rotary film evaporator. The final white solid product was left to dry under negative pressure in a vacuum oven at 45 °C for 30 minutes. The synthesis of the free base was confirmed by ^{1}H-NMR. Yield was calculated as 90.6%.

^{1}H-NMR ($CDCl_3$): δ 2.98–2.95 (2H, CH_2 protons), 2.52–2.45 (2H, CH_2 protons), 1.8 (NH), 1.60–1.57 (2H, CH_2 protons), 1.25–1.21 (H, CH protons) and 1.19–1.16 (2H, CH_2 protons) ppm.

2.6.2 Synthesis of BNIPPiEth base

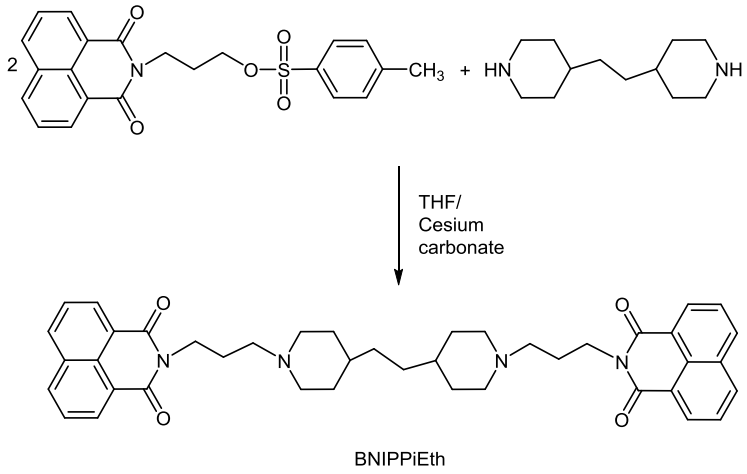

Figure 2.6.2a.: Synthesis of BNIPPiEth base.

In a round bottom flask (50cm^3), 4,4 Ethylenedipiperidine (M = 198.25 g/mol, n = 5.044 x10^{-4} mol, 0.1 g) was reacted with toluenesulfonyloxypropyl-naphthalamide (M = 409.46 g mol^{-1}, n = 1.001 x10^{-3} mol, 0.41 g, 2.01 excess) (Figure 2.6.2a). Caesium carbonate (M = 325.82 g mol^{-1}, n = 3.069 x10^{-3} mol, 1 g) was added in the reaction. All the reagents were dissolved in THF (6 mL) and the solution refluxed overnight at 60 °C. The reaction was monitored using TLC. Once the reaction was complete, the solution was poured into icy water (100 mL), which resulting in the formation of a precipitate. The precipitate was filtered using a Buchner funnel and the product was left to dry under negative pressure in a vacuum oven at 45 °C for 60 minutes. The crude product was recrystallised from ethanol and the pure product was characterised by ^{1}H-NMR. The yield of the reaction was calculated as 72.3%.

^{1}H-NMR ($CDCl_3$): δ_H 8.52–8.50 (2H, CH aromatic protons), 8.13–8.11 (2H, CH aromatic protons), 7,69–7.65 (2H, CH aromatic protons), 4.18–4.14 (2H, CH_2 protons), 2.83–2.80 (2H, CH_2 protons), 2.40–2.36 (2H, CH_2 protons), 1.90-1.83

(2H, CH_2 protons), 1.79-1.71 (2H, CH_2 protons), 1.48 (2H, CH_2 protons), 1.2(H, CH protons) and 1.00-0.80 (2H, CH_2 protons) ppm.

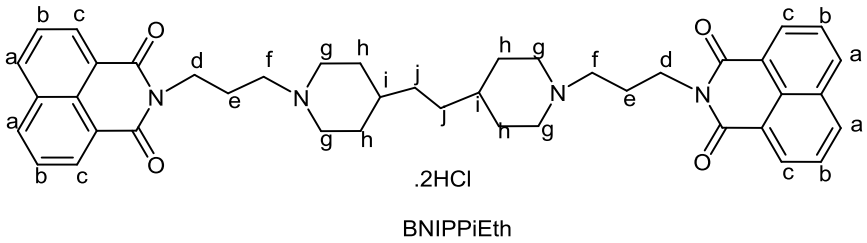

BNIPPiEth

Figure 2.6.2b.: Equivalent protons for BNIPPiEth.

The chemical shifts corresponding to protons situated at carbons a, b and c of the naphthalimido rings resonated at 8.52-7.65 ppm (Figure 2.6.2b). Integration analysis within the aromatic region of the spectrum allowed identification between the signals a, b and c, respectively. At 4.18-4.14 ppm, aliphatic peaks resonated as a triplet for d, due to the existence of two adjacent protons. Signal for e was detected next, due to the shielding from nitrogen atoms and furthest upfield chemical shifts were the peaks protons at positions for h, i and j, respectively.

2.6.3 Synthesis of BNIPPiEth salt

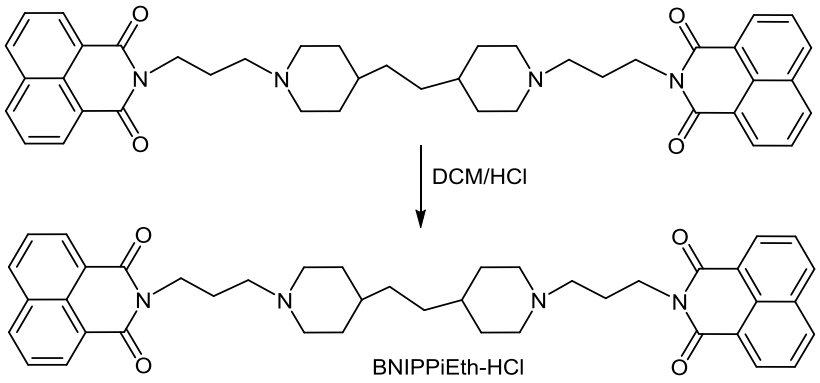

Figure 2.6.3.a: Synthesis of BNIPPiEth salt.

In a round bottom flask (50cm^3), BNIPPiEth (0.1g) was dissolved in DCM (20 mL). Then, HCl (1.5 mL) was added to the flask and the solution stirred at room temperature for 60 minutes, which resulted in the formation of a pale, blue precipitate (Figure 2.6.3a). The precipitate was filtered and washed with ether (50 mL) and afterwards with ethanol (50 mL). The product was left under negative pressure in a vacuum oven at 45 °C for 60 minutes. The final product of BNIPPiEth was characterised by ^{1}H-NMR, ^{13}C-NMR and DEPT-135 NMR. Yield was calculated as 29.5%. The relative molecular mass of BNIPPiEth was confirmed by mass spectral analysis (Figure 2.6.3e).

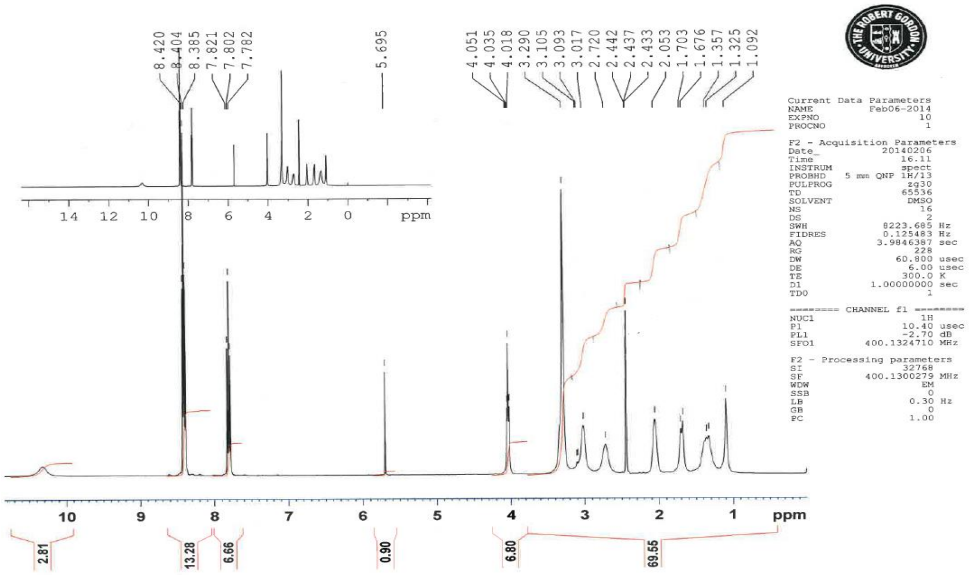

Figure 2.6.3b.: ^{1}H-NMR spectrum for BNIPPiEth

^{1} H-NMR ($CDCl_3$) (Figure 2.6.3b): δ_H 8.42–8.38 (2H, CH aromatic protons), 7,82–7.78 (2H, CH aromatic protons), 4.05–4.01 (2H, CH_2 protons), 2.7 (2H, CH_2 protons), 2.44 – 2.43 (2H, CH_2 protons), 2.05 (2H, CH_2 protons), 1.70-1.67 (2H, CH_2 protons), 1.35-1.32 (H, CH protons) and 1.090 (2H, CH_2 protons) ppm.

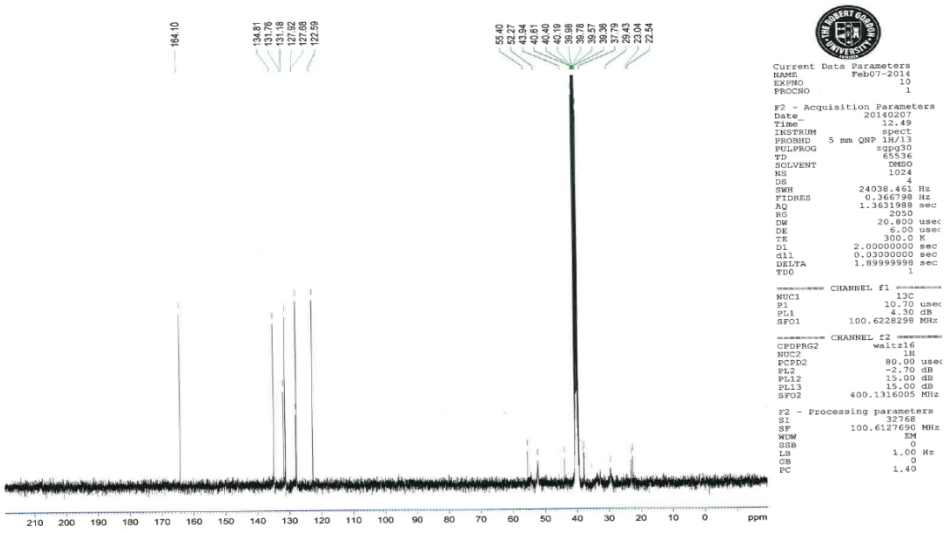

Figure 2.6.3c.: ^{13}C-NMR spectrum for BNIPPiEth.

^{13}C-NMR ($CDCl_3$) (Figure 2.6.3c): δ_H 164.10 (C=O), 134.81 (CH aromatic), 131.76 (C aromatic), 131.18 (CH aromatic), 127.92 (C aromatic), 127.68 (CH aromatic), 122.59 (C aromatic), 55.40 (CH_2), 52.27 (CH_2), 37.79 (CH), 29.43 (CH_2) 23.04 (CH_2) and 22.54 (CH_2) ppm.

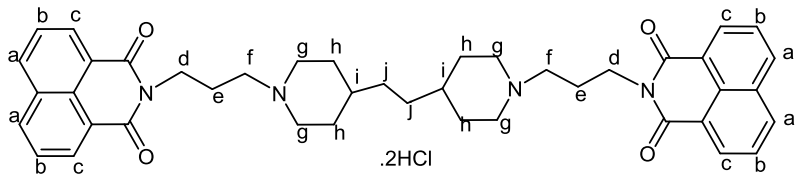

BNIPPiEth-2HCl

Figure 2.6.3d.: Equivalent protons and carbons for BNIPPiEth salt.

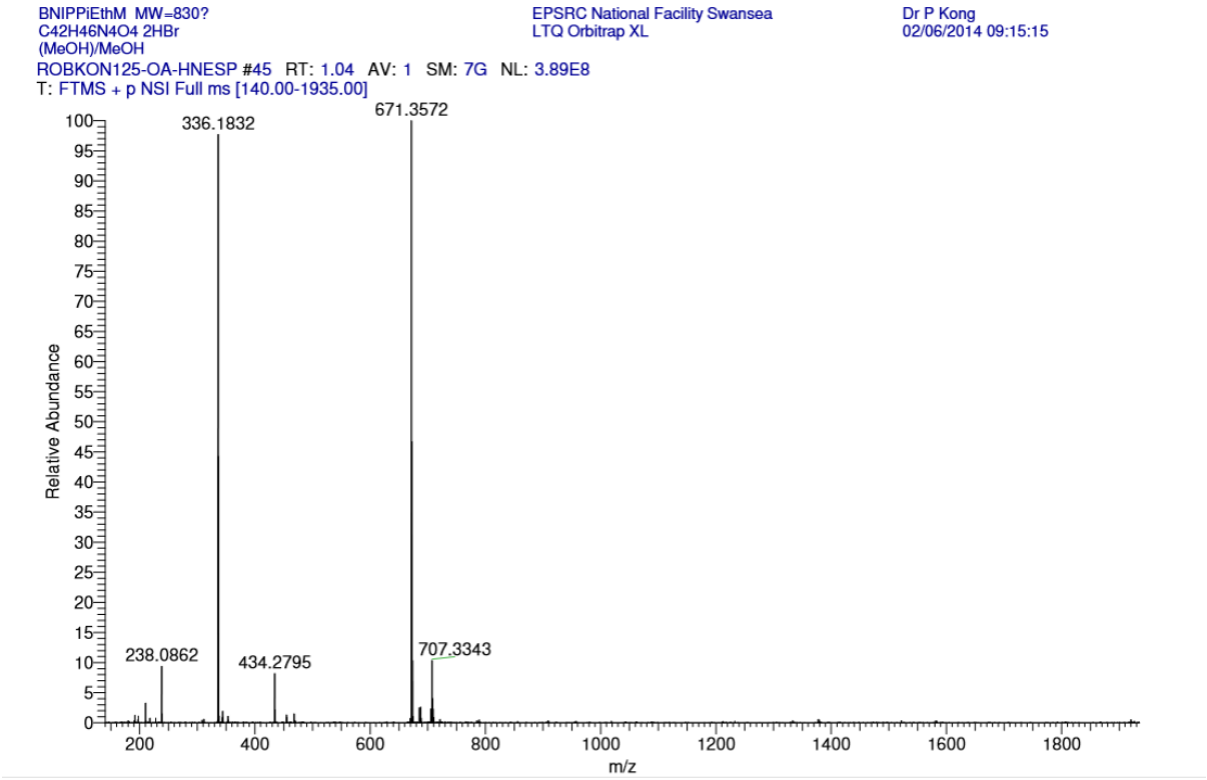

Figure 2.6.3e.: High resolution mass spectrum of BNIPPiEth: $M^{+=}$671.3572.

For the BNIPPiEth salt, chemical shifts are resonated in a similar way, as that for BNIPPiEth free base. However, for the ^{13}C spectrum, the aliphatic chemical shifts were weak and hard to be assigned, as observed with the analysis of BNIPPiProp salt.

2.7 Results and Discussion: Synthesis of *trans,trans*-bisnaphthalimidopropyl diaminodicyclohexylmethane (*trans,trans*-BNIPDaCHM)

2.7.1 Synthesis of *trans,trans*-N^4,N^4-dimesityl-dicyclohexylmethane

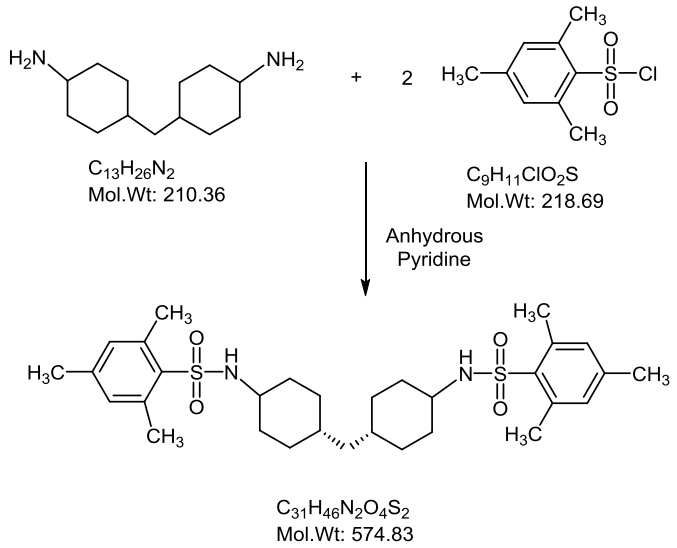

Figure 2.7.1a.: Synthesis of *trans,trans*-N^4,N^4-dimesityl-dicyclohexylmethane.

In a round bottom flask (25cm^3), *trans,trans*-4,4'-methylenebis(cyclohexylamine) (M = 210.37 g mol^{-1}, n= 2.38x10^{-4} mol, 0.05 g) was added in anhydrous pyridine (1.5 mL) and left to stir for 15 minutes with warming. After dissolution, 2-mesitylenesulfonyl chloride (Mts) (M = 218.70 g mol^{-1}; n = 4.76x10^{-4} mol; 0.10 g) was added (Figure 2.7.1a). The reaction was left to stir overnight at room temperature and TLC confirmed reaction completion. The solution was poured into icy water (10 mL) and stirred with a glass rod until the formation of a precipitate. The suspension was centrifuged and was washed 3 times with distilled water and the precipitate was left to dry under negative pressure in a vacuum oven set at 45 °C for overnight. The product was afterwards characterised by ^{1}H-NMR. Yield was calculated as: 21%.

N^4,N^4-dimesityl-dicyclohexylmethane ^{1}H-NMR ($CDCl_3$): δ_H 7.31 (NH), 6.98 (4H, CH aromatic protons), 3.87 (4H, CH protons), 2.67 (6H, CH_3-Mts protons), 2.33 (3H, CH_3-Mts protons), 1.84-1.82 (CH_2-cyclohexane ring), 1.65-1.62 (CH_2-cyclohexane ring), 1.16-1-10 (CH-cyclohexane ring) and 0.99-0.95 (CH_2 cyclohexane protons) ppm.

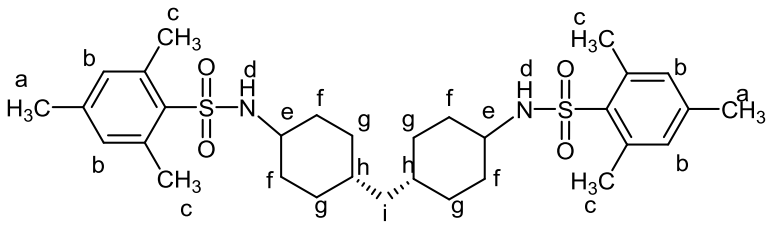

Figure 2.7.1b.: Equivalent hydrogen atoms of *trans, trans*-N4,N4-dimesityl-dicyclohexylmethane.

The NMR signal for proton d resonated at 7.31 ppm, due to the deshielding effect of the electronegative sulfur dioxide group (Figure 2.7.1b). Chemical shifts corresponding to aromatic proton b resonated at 6.98 ppm and the signal for e observed further upfield at 3.87 ppm. Chemical shifts corresponding to methyl protons situated at carbon c and a of the aromatic ring resonated at 2.67 ppm and 2.33 ppm respectively. Signals for protons at carbons f, g and h of the cyclohexane ring were detected upfield, at 1.84-1.82 ppm, 1.65-1.62 ppm and 1.16-1.10 ppm. Chemical shift corresponding to i resonated further upfield at 0.99-0.95 ppm.

2.7.2 *N*-alkylation reaction

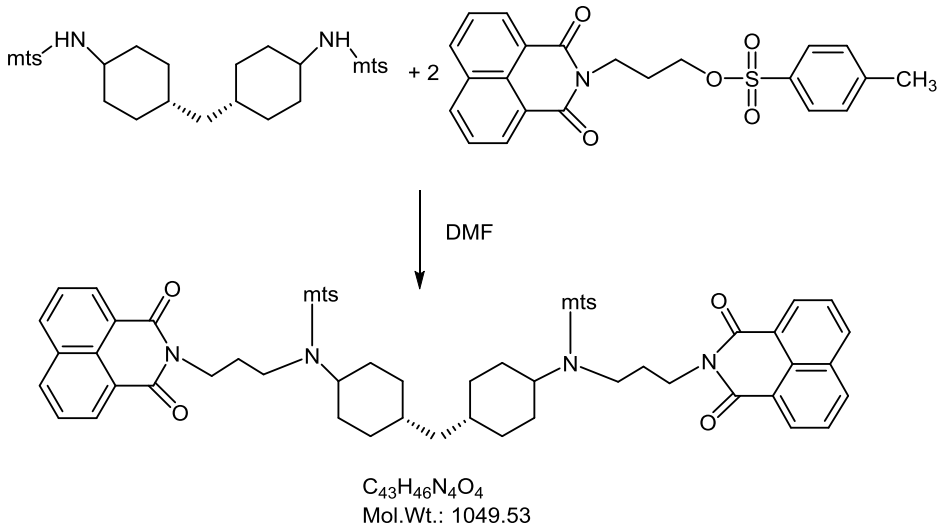

Figure 2.7.2a.: Synthesis of protected *trans,trans*-bisnaphthalimidopropyl-dimesityl-dicyclohexylmethane.

In a round bottom flask (25cm^3), *trans, trans*-N^4,N^4-dimesityl-dicyclohexylmethane (M = 574.83 g/mol, n = 6.44x10^{-5} mol, 0.037 g) and toluenesulfonyloxypropylnaphthalimide (M = 409.46 g mol^{-1}; n = 1.29x10^{-4} mol, 0.053 g, 2.01 excess) (synthesis of toluenesulfonyloxypropylnaphthalimide has been detailed in Section 2.4.2) were dissolved in DMF (1 mL). Afterwards, excess of caesium carbonate (M = 325.82 g mol^{-1}, n = 3.07x10^{-4} mol, 0.1 g, 5.0 excess) was added slowly (Figure 2.7.2a).

The reaction was left to stir for 48 hours at 60 °C. After TLC confirmed the reaction was complete, the solution was poured into icy water (10 mL) to form a precipitate. The suspension was applied to centrifugation and was washed twice with distilled water. The product was left to dry under negative filtration in a vacuum oven at 45 °C for 24 hours. The crude product (59 mg, 88%) was purified using column chromatography and the final product (25 mg) was characterised by ^{1}H-NMR. Yield was calculated as: 37%.

Protected bisnaphthalimido-dimesityl-dicyclohexylmethane ^{1}H-NMR ($CDCl_3$): δ_H 8.65–8.59 (2H, CH aromatic protons), 8.30–8.25 (2H, CH aromatic protons), 7.84–7.78 (2H, CH aromatic protons), 6.65–6.60 (4H, CH-Mts protons), 4.41–4.38 (2H, CH_2 protons), 4.06–4.04 (2H, CH_2 protons), 3.71-3.68 (2H, CH_2 protons), 2.68 (3H, CH_3 protons), 2.46-2.44 (3H, CH_3 protons), 2.34 (H, CH protons), 2.16-2.15 (2H,CH_2 protons) 1.84 (2H, CH protons) and 1.73-1.71 (2H, CH_2 protons) ppm.

^{13}C-NMR ($CDCl_3$): δ_H 141.93(C=O), 138.76 (C aromatic), 135.17 (C aromatic), 131.95 (C aromatic), 43.72 (CH2), 33.93-31.99 (CH_2), 23.02 (CH_3) and 20.97 (CH_3) ppm.

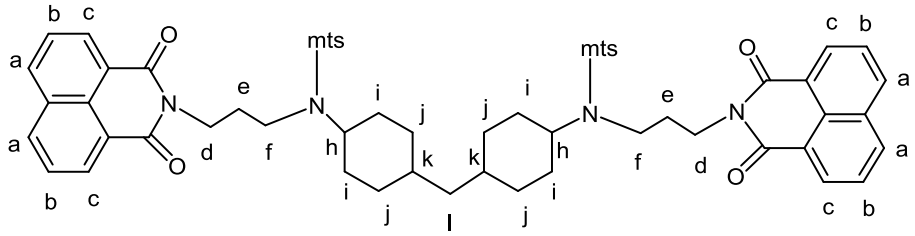

trans,trans-bisnaphthalimido-dimesityl-dicyclohexylmethane

Figure 2.7.2b.: Equivalent proton and carbons of *trans,trans*-bisnaphthalimido-dimesityl-dicyclohexylmethane.

Chemical shifts corresponding to protons situated at carbons a, b and c of the naphthalimide rings resonated at 8.65-7.78 ppm (Figure 2.7.2b). Integration analysis within the aromatic region showed that the signals correspond to six hydrogens, hence were assigned to protons a, b and c respectively. The chemical shift of the solvent signal was observed at 7.30 ppm (chloroform). At 6.65 ppm, chemical shifts corresponded to protons that were situated on the *trans,trans*-N^4,N^4-dimesityl-dicyclohexylmethane methyl groups were detected. Signal for proton d was detected next upfield at 4.41-4.38 ppm, due to the deshielding effect

from nitrogen and oxygen atoms, the signal for proton f and h were observed upfield at 4.06-4.04 ppm and 3.71-3.68 ppm, respectively. Chemical shifts corresponding to protons of the methyl groups on the N^4,N^4-dimesityl-dicyclohexylmethane aromatic ring resonated at 2.68 ppm and 2.46-2.44 ppm. Further upfield, the proton signal for carbon e was detected at 2.34 ppm and for i and j at 2.16-2.15 ppm, respectively. Chemical shifts corresponding to protons situated at k resonated at 1.84 ppm and for l at 1.73-1.71 ppm.

From the ^{13}C spectrum, chemical shifts corresponding to the amide carbon of the naphthalimido ring resonated at 141.93 ppm and for a, b and c at 138.76-131.95 ppm. At 43.72 ppm, the chemical shift corresponded to i and j of the aromatic ring and further upfield, the chemical shift for k resonated at 33.93-31.99 ppm. The next upfield, chemical shifts corresponded to the methyl groups of *trans,trans-N4,N4*-dimesityl-dicyclohexylmethane were detected at 23.02 ppm and 20.97 ppm, respectively.

2.7.3 Deprotection reaction

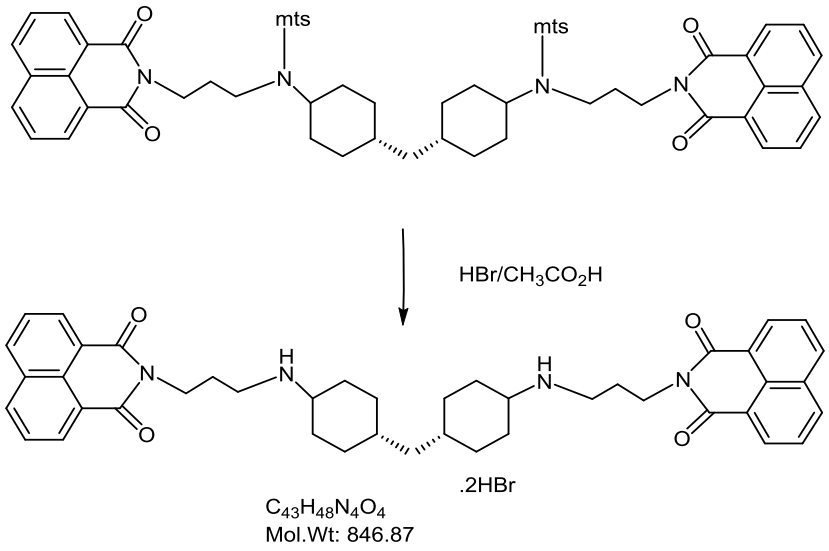

Figure 2.7.3a.: Synthesis of *trans,trans*-bisnaphthalimidopropyl-diamino-dicyclohexylmethane dihydro-bromide salt (*trans,trans*-BNIPDaCHM).

In a round bottom flask (10cm^3), *trans,trans*-bisnaphthalimido-dimesityl-dicyclohexylmethane (M = 1049.53 g mol^{-1}, n = 2.38x10^{-5} mol, 25mg) was dissolved in dichloromethane (DCM) (1.0 mL). Afterwards, hydrobromic acid/glacial acetic acid (HBr/CH_3CO_2H) (0.2 mL) was added slowly (Figure 2.7.3a). The reaction was stirred overnight at room temperature. TLC was used to confirm that the reaction was complete. The suspension formed was transferred to Eppendorf tubes and centrifuged, washed with DCM (1.0 mL) and ether (1.0 mL). The final product was dried under negative pressure in a vacuum oven set at 45 °C for 3 hours to give the product as a white solid (8.3 mg). Once dry, the final product was characterised by ^{1}H-NMR, ^{13}C-NMR and DEPT-135 NMR. Yield was calculated as 41% and the relative molecular mass of *trans,trans*-bisnaphthalimidopropyl-diamino-dicyclohexylmethane (*trans,trans*-BNIPDaCHM) was confirmed by mass spectral analysis (Figure 2.7.3e).

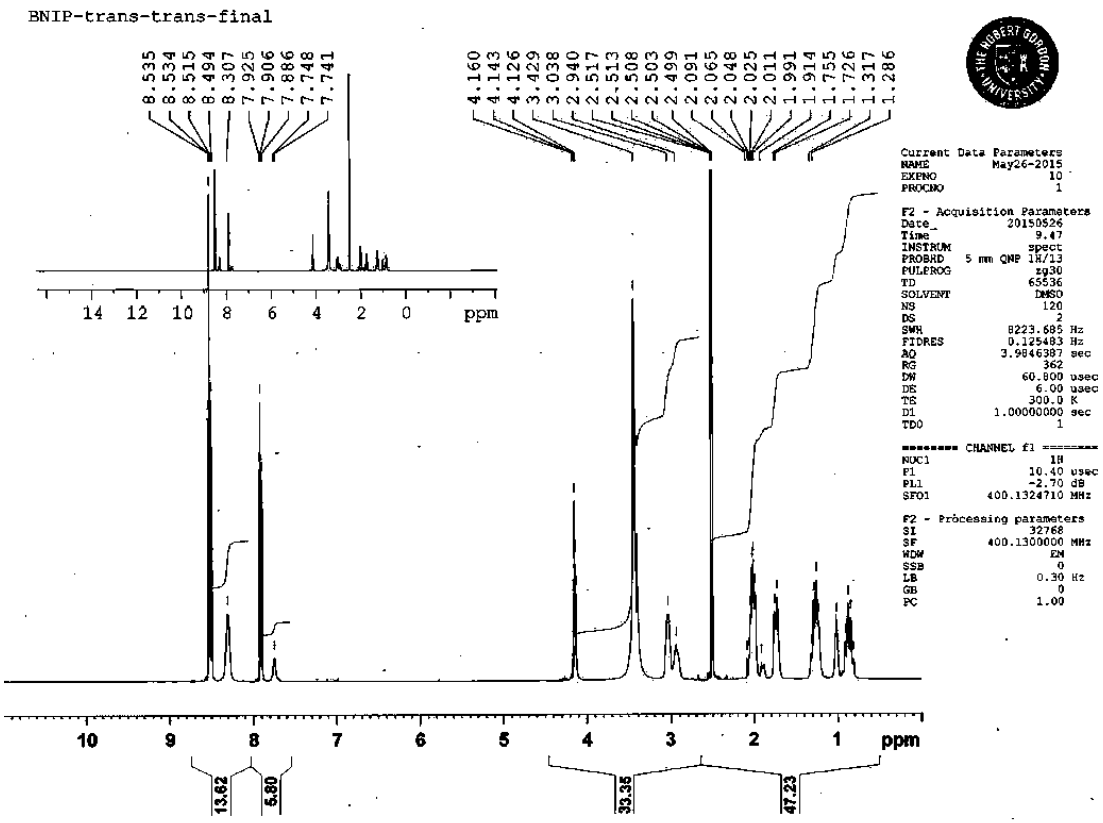

Figure 2.7.3b.: ^{1}H-NMR (DMSO-d_6 solvent) spectrum for *trans,trans*-BNIPDaCHM.

Bisnaphthalimidopropyl-diamino-dicyclohexylmethane dihydro-bromide salt ^{1}H-NMR ($CDCl_3$) (Figure 2.7.3b): δ 8.53–8.49 (2H, CH aromatic protons), 4.16–4.12 (2H, CH aromatic protons), 3.42 (2H, CH aromatic protons) 3.04 (2H, CH_2 protons), 2.94 (2H, CH_2 protons), 2.51-2.49 (3H, CH_3 protons), 2.09-1.99 (3H, CH_3 protons), 1.75-1.72 (H, CH proton), 1.31-1.28 (2H,CH_2 protons) ppm.

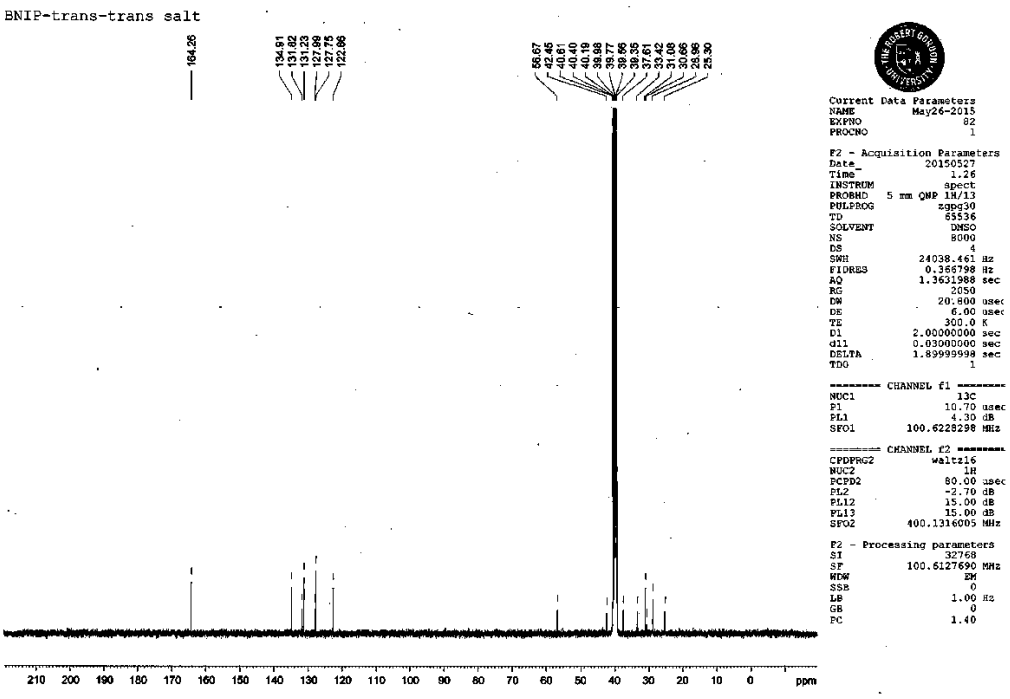

Figure 2.7.3c.: ^{13}C-NMR spectrum for *trans,trans*-BNIPDaCHM.

^{13}C-NMR ($CDCl_3$) (Figure 2.7.3c): δ 164.26 (C=O), 131.82-131.23 (C aromatic), 127.99-127.75 (C aromatic), 122.66 (C aromatic), 42.45 (CH_2) and 40.61-37.61 (CH_2) ppm.

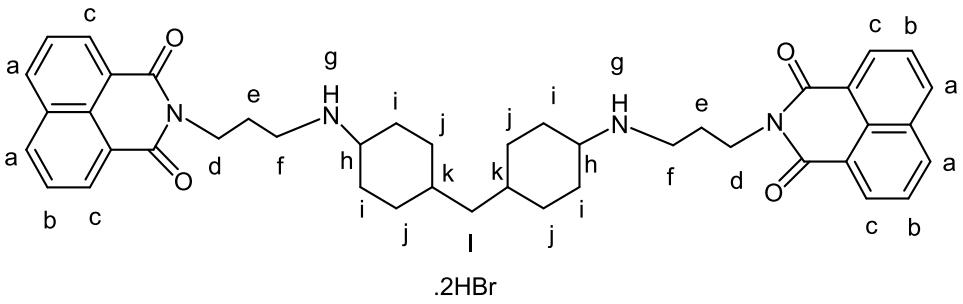

trans,trans-bisnaphthalimidopropyl-diamino-dicyclohexylmethane dihydro-bromide salt

Figure 2.7.3d.: Equivalent protons and carbons of *trans,trans*-bisnaphthalimidopropyl-diamino-dicyclohexylmethane dihydro-bromide salt (*trans,trans*-BNIPDaCHM).

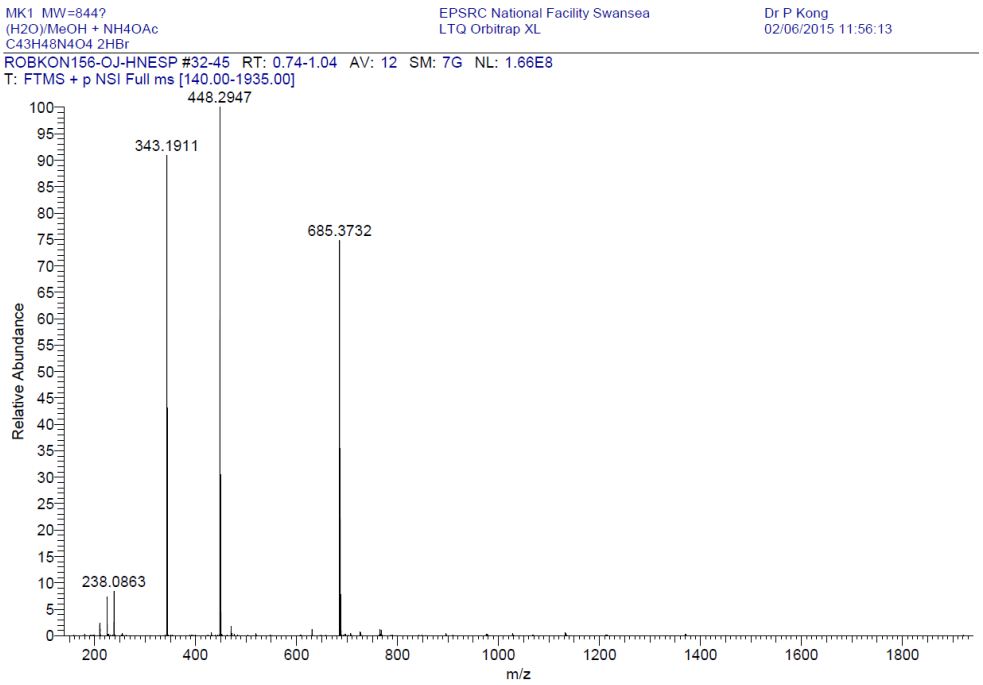

Figure 2.7.3e.: High resolution mass spectrum of *trans,trans*-BNIPDaCHM: $M^{+=}$685.3732.

The chemical shifts for BNIPDaCHM resonated on a similar way, as for bisnaphthalimido-dimesityl-dicyclohexylmethane (Section 2.4.7). The absence of chemical shifts corresponding to protons which were present on the methyl groups of N^4,N^4-dimesityl-dicyclohexylmethane confirmed that the reaction was complete and that *trans,trans*-BNIPDaCHM was formed.

2.8 Melting point determination

Melting point (MP) determination is one of the analytical techniques applied to the characterisation of pharmaceutical drugs. A Griffin melting point apparatus (Fisher Scientific, UK) was switched on and allowed to heat to 10 °C below starting point. A compatible capillary (10 cm length, 0.8 mm internal diameter and 0.2 mm wall thickness), containing a small amount of each compound (4 mg: maximum weight that can be tested), was placed in the heating block's closed end first and left there until the melting point could be identified. Each capillary tube contained a sufficient amount of dry powder in order to form a column (2-4 mm high): the powder was well packed at the bottom, after tapping the tube on a solid surface.

For every experiment, the use of variable heat was kept constant (heat constant: 7). Important step of the procedure was to ensure that the capillary was placed on the heating block 10 °C below a compound's expected MP. At the end of the melt, MP range was recorded. For this method, the onset and the clear point of the melt were measured.

In order to investigate the physical properties of BNIPDaCHM, BNIPPiProp, BNIPPiEth and *trans,trans*-BNIPDaCHM, measurements of their melting points were carried out. Table 2.8 shows the onset and clear melting point of the four BNIP derivatives. The derivative with the highest melting points was BNIPPiProp. The onset melting point for BNIPPiProp was measured at 160 °C and clear melting point at 170 °C. Lower melting points were determined for BNIPPiEth and *trans,trans*-BNIPDaCHM. BNIPPiEth started its melting process at 125 °C and reached its liquid phase at 130 °C and *trans,trans*-BNIPDaCHM at 120 °C and 125 °C, respectively. The onset melting point for BNIPDaCHM was measured at 105 °C and clear melting point at 130 °C.

Previous studies have shown that MP depends on the chemical structure of a compound, its properties and its purity. In addition, sharp and characteristic melting points cannot be determined for compounds with impurities and their melting point range is increased, compared to compounds with less impurity (Lipinski *et al*, 2012). According to the above results, BNIPDaCHM has the widest melting point range amongst the four BNIP derivatives. The wide range could be explained by the fact that BNIPDaCHM is a mixture of isomers and as a result, the least pure compound. This hypothesis can be also supported by the fact that *trans,trans*-BNIPDaCHM, that consists of only one isomer, has a sharper melting point range, in comparison to BNIPDaCHM.

Table 2.8.: Melting points of BNIPDaCHM, BNIPPiProp, BNIPPiEth and *trans,trans*-BNIPDaCHM (use of variable heat: 7).

BNIPs	Melting Point (°C)
BNIPDaCHM	105-130
BNIPPiProp	160-170
BNIPPiEth	125-130
trans,trans-BNIPDaCHM	120-125

On the other hand, BNIPPiProp which is an enantiopure compound exhibited higher melting point temperatures than BNIPDaCHM. This outcome may be because BNIPPiProp does not consist of more than one isomer (thus better purity), together with the fact that it is a larger molecule with two extra carbons in the linker chain when compared to BNIPDaCHM. In parallel, it is an important indication that may

the position of the ring structure on the linker chain affects the stability of a compound and its DNA binding properties that will be examined later on. Similarly, BNIPPiEth consists of one carbon less between the two ring structures, compared to BNIPPiProp, showing that smaller molecules tend to melt in lower temperatures, due to less surface area for hydrophobic interactions.

2.9 Conclusion

Three novel BNIPs, BNIPPiProp, BNIPPiEth and *trans,trans*-BNIPDaCHM were successfully synthesised and characterised. The *N*-alkylation reaction that has been used previously for the synthesis of other BNIPs in this series has been proved a suitable synthetic process to produce the above compounds, as apart from high yields, it resulted in formation of compounds without by-products (Lima *et al*, 2013).

In addition, melting point determination revealed that BNIPs have stable structures due to the carbons that support their linker chains and the two naphthalimide rings that protect their two ending points, results that are in agreement with previous studies of Banerjee *et al*. (2013). Consequently, the three above derivatives were further examined, with regards to their DNA binding and biological affinities, structure-activity relationship and mode of action.

CHAPTER 3

DNA binding studies on bisnaphthalimidopropyl derivatives.

3.1 Introduction

3.1.1 Naphthalimides, bisnaphthalimides and DNA intercalation

In 1970's, researchers synthesised the first naphthalimide compounds, based on the fact that DNA is a fundamental biochemical target in the design of anti-cancer therapeutics (Huang *et al*, 2009). A naphthalimide compound consists of three fused 6-membered rings with a basic terminal group in one of its side chains. Naphthalimido compounds were found to be highly active against cervical cancer and leukaemia cells *in vitro* (Llombart *et al*, 1992, Brana *et al,* 2001), mainly due to the existence of nitrogen atoms. As a result, the next objective was to design and synthesise bisnaphthalimide compounds, by using a linker sequence that would join the two naphthalimide units together, in order to improve the therapeutic properties of their precursor form mononaphthalimides. Later on, polyamine linker sequences were incorporated into their structure, improving their stability and DNA intercalating properties. The existence of a flexible aminoalkyl linker chain that consisted of different numbers of amino groups was found to be the major parameter that bisnaphthalimide could exhibit strong DNA binding affinities (Brana *et al,* 1993, 2001).

More specifically, it has been suggested that the mechanism of action of those bisnaphthalimides involves intercalation or bis-intercalation of the chromophore units between the DNA base pairs (Pavlov *et al*, 2001, Dance *et al*, 2005). Therefore, synthesis of novel bisnaphthalimides and further investigation on their DNA binding properties could lead to more effective and selective cancer treatment.

3.1.2 Assessment of DNA binding interactions

Over the last decade, studies on DNA-small molecule interactions have been the focus of medicinal chemistry and is of importance, as these interactions are the basis of therapeutic, antitumour or antivirus properties of novel compounds and have great significance for medicine design (Wilson and Kool, 1990). The interaction mode between DNA and molecules can be developed *via* binding interactions with the minor and/or major grooves of DNA double helix, intercalation between DNA adjacent base pairs or electrostatic interactions with the sugar phosphate backbone (Strekowski and Wilson, 2007).

Several methods have been developed and used for the assessment of DNA-small molecule interactions, such as DNA thermal denaturation, competitive displacement of DNA bound Ethidium Bromide (EtBr), circular dichroism, NMR spectroscopy and UV binding studies (Rajesh *et al*, 2012).

In this study, the methods that were used to determine the physical interactions of the novel BNIPs and DNA were DNA thermal denaturation, competitive displacement of DNA bound EtBr and UV binding studies. Biological mechanisms of DNA, such as replication and transcription require separation of the DNA double helix, which is called denaturation and can be partial or total. DNA denaturation depends on several factors, such as DNA polymer geometry, DNA sequence composition and temperature (Benham, 1979, 1990, 1996).

In DNA thermal denaturation studies, double stranded DNA (in the presence or absence of derivatives, i.e. BNIPs) is gradually heated, resulting in double strand separation (denaturation) (Figure 3.1.2.1) (Martinez and Chacon-Garcia, 2005). As a derivative stabilises DNA, the temperature at which denaturation takes place increases.

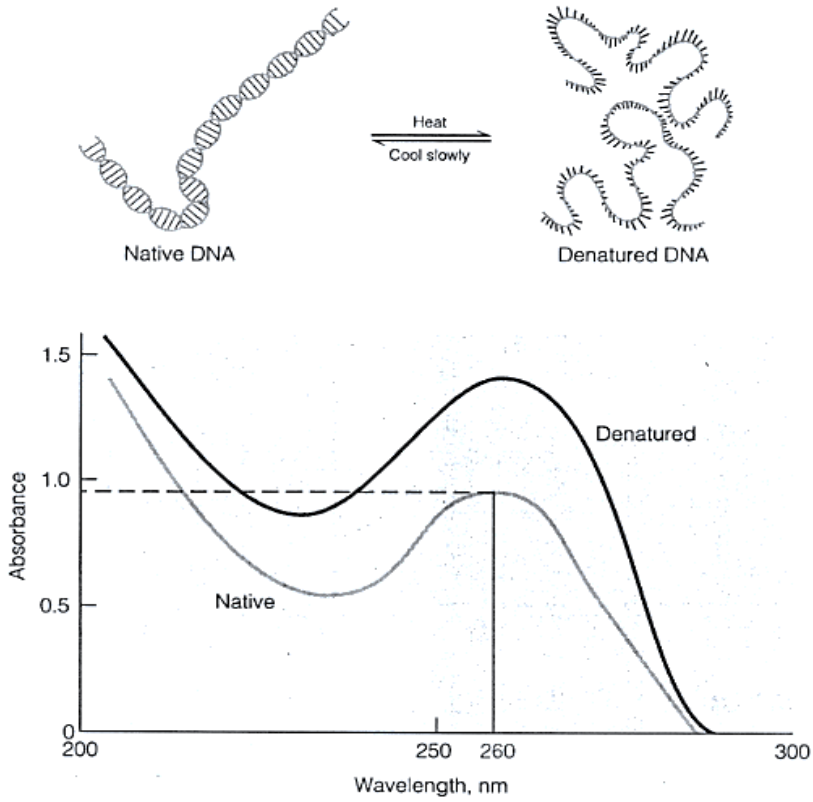

Figure 3.1.2.1.: Method of DNA thermal denaturation studies (Adapted from: Mathews and Van Holde, 1995).

The degree of DNA binding is determined by the Tm value (Melting Temperature): the higher the Tm value, the stronger the derivative binds to DNA.

To explore further the mode of action and DNA binding properties of novel BNIPs, a more selective diagnostic tool based on the competitive displacement of DNA bound EtBr, was used.

EtBr, is a well-known DNA intercalator, which binds to DNA resulting in an increase of emitted fluorescence at 600 nm (Dance *et al*., 2005). Derivatives with higher binding affinities than EtBr, displace EtBr bound to DNA, that results in fluorescence quenching which is proportional to the amount of displaced EtBr (Figure 3.1.2.2) (Vardevanyan *et al*, 2003).

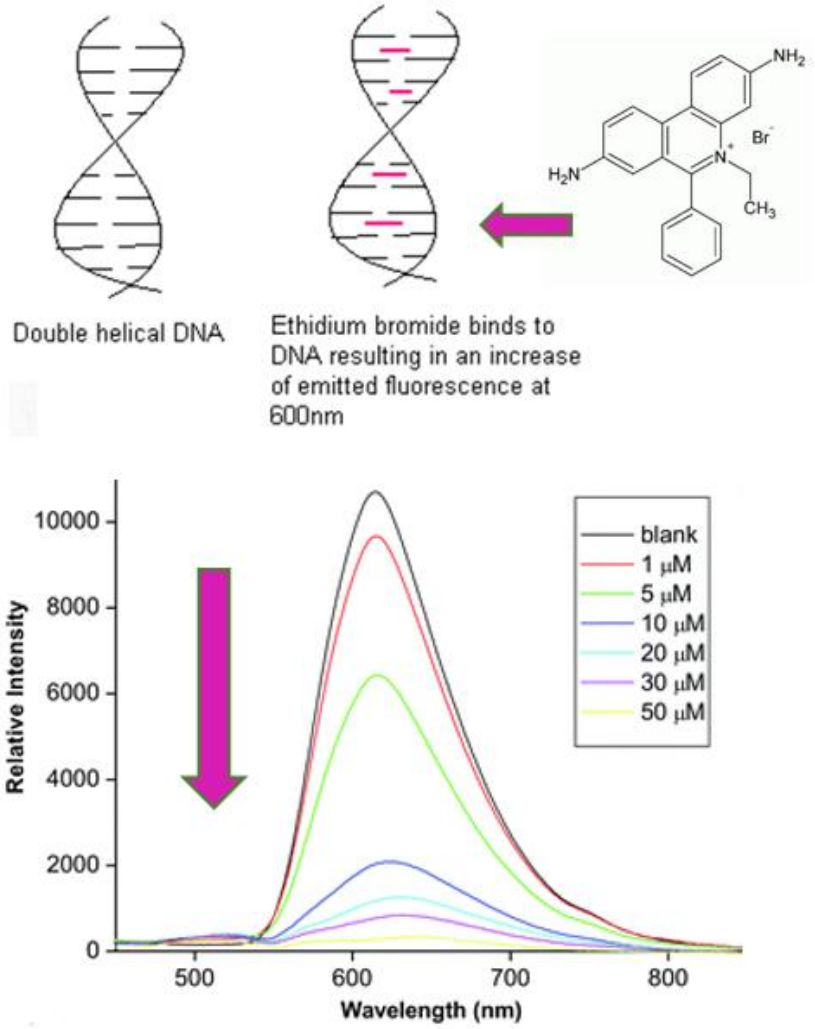

Figure 3.1.2.2.: Method of competitive displacement of DNA bound EtBr on Shimadzu RF-5301 spectrophotometer (Shimadzu, Japan). BNIPDaCHM in different concentrations (0-50 µM), resulting in fluorescence quenching after EtBr displacement from DNA.

In addition, UV absorption spectroscopy was used to examine the binding strength and binding mode of DNA with BNIPs (Figure 3.1.2.3). The degree of binding strength of the DNA-BNIP complex was quantitatively determined by calculating the K binding constants (see Appendix 2) (Zhi-Yong *et al*, 2014). The stronger the binding, the lower the UV absorption and the higher the K binding constant value.

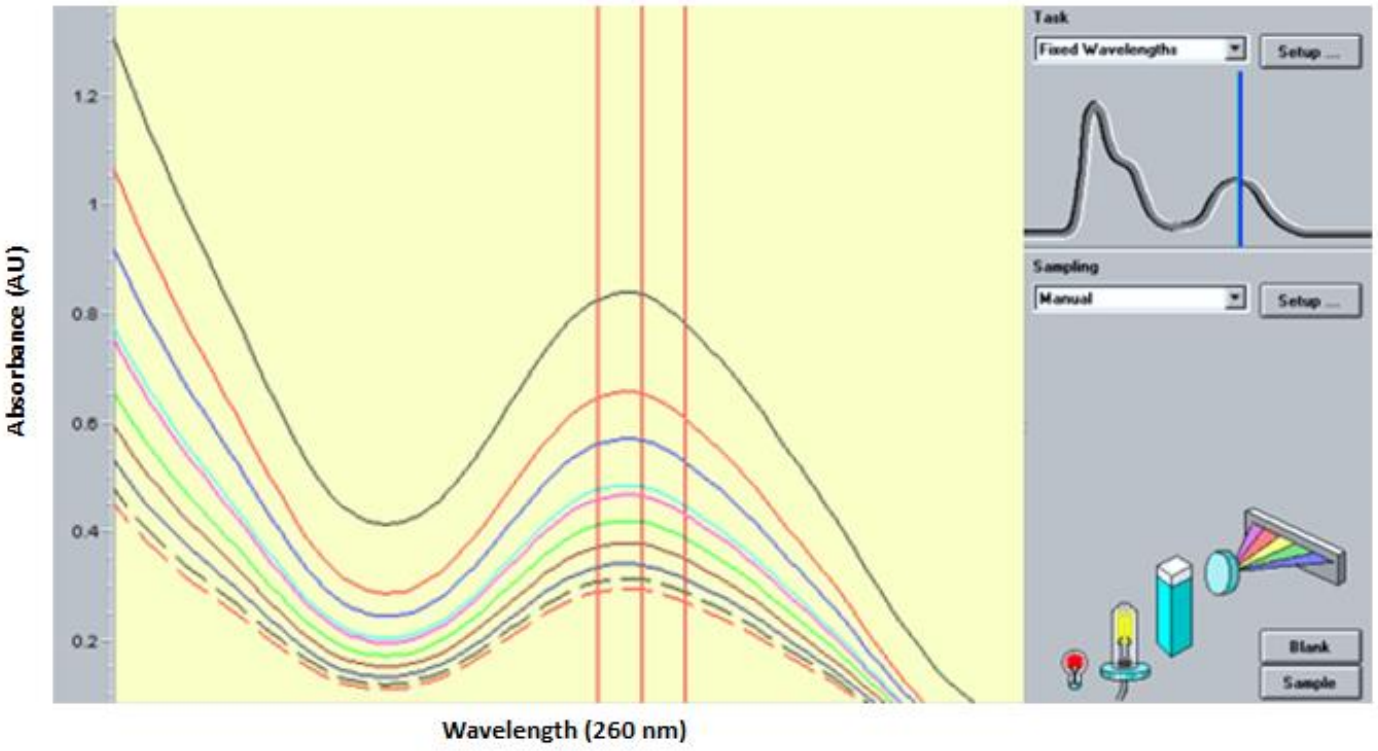

Figure 3.1.2.3.: Method of UV binding studies on Agilent 8453 UV-visible Spectroscopy System (GenTech, USA). A continuous decrease in UV absorption (from high to low peaks) was observed at 260 nm, within the range of BNIP concentrations (0–7 µM) investigated.

3.1.3 Aims

The aim of the work presented in Chapter 3 was to investigate the DNA binding properties of three novel BNIPs and their parental compound BNIPDaCHM, based on synthetic methods introduced by Kong Thoo Lin and Pavlov (2000) (see Chapter 2).

BNIPs were investigated for their DNA binding affinities by examination of DNA binding capacity and competitive displacement.

3.2 Materials and Instrumentation

3.2.1 Materials

A list of the reagents used during the DNA binding studies with BNIPs are presented below. All the reagents were handled according to the COSHH standards.

Calf Thymus DNA	Sigma-Aldrich, UK
Ethidium Bromide	Sigma-Aldrich, UK
Saline Sodium Citrate	Sigma-Aldrich, UK

3.2.2 Instrumentation

Thermal denaturation studies were carried out using a Shimadzu UV-1650 PC UV-Visible (Japan) spectrophotometer that was connected to a temperature controller and water supply. The samples were loaded in quartz glass flow cells (10 mm path length) (Hellma Analytics, UK).

Fluorescence-binding studies were performed in plastic cuvettes (1 cm path length) (Hellma Analytics, UK) using a Shimadzu RF-5301 spectrophotometer (Japan).

UV binding studies were carried out using an Agilent 8453 UV-visible Spectroscopy System (GenTech, USA) and a Diode array instrument. The samples were loaded in quartz glass flow cells (10 mm path length) (Hellma Analytics, UK).

3.3 Methods

3.3.1 Thermal denaturation studies of BNIP derivatives

BNIPDaCHM, BNIPPiProp and BNIPPiEth working solutions (100 μM) were prepared from their stock solutions (10 mM in 100% DMSO) and were further diluted to 10 μM final concentration in 0.01 M SSC buffer. For the DNA working solution, *Calf Thymus* DNA (0.5 g) was dissolved in 0.01 M saline-sodium citrate (SSC buffer) (100 mL). The final DNA-BNIP samples were prepared by adding *Calf Thymus* DNA (500 μL), 0.01 M SSC buffer (400 μL) and BNIP solution (100 μL) in the same Eppendorf tube.

After 12 hours incubation at room temperature, the DNA-test samples were analysed at 260 nm using a Shimadzu UV-1650 PC UV-Vis spectrophotometer (Section 3.2.2). The temperature was increased at a rate of 2 ^{o}C per minute between 40-100 ^{o}C and the thermal melting point (Tm (^{o}C)) was determined using a curve of absorbance against temperature.

3.3.2 EtBr Fluorescence studies

BNIPDaCHM, BNIPPiProp, BNIPPiEth and *trans,trans*-BNIPDaCHM working solutions (100 μM) were prepared from their stock solutions (10 mM in 100% DMSO), and were further diluted to 50 μM final concentration in 0.01xSSC buffer (Table 3.3.2). *Calf Thymus* DNA and 0.01 M SSC buffer were prepared as described in Section 3.3.1. EtBr solution (200 μM) was prepared by dissolving 3.94 mg of EtBr in distilled water (50 mL) and was further diluted in 0.01 M SSC buffer to give the final concentration of 20 μM (Figure 3.3.2).

Test solutions were prepared by adding varying volumes of SSC buffer (final volume 2000 μL), *Calf Thymus* DNA solution (200 μL), EtBr solution (20 μL) and

BNIP derivative solution (0-100 µL) in Eppendorf tubes (Table 3.3.2a). The final solutions were thoroughly mixed and analysed at 510 nm (excitation) and 520 nm (emission) using a Shimadzu RF-5301 spectrophotometer (Section 3.2.2). The C_{50} value was determined as the concentration (µM) required to decrease the fluorescence of DNA bound EtBr by 50%.

Table 3.3.2.: Preparation of test solutions with different BNIPs concentrations for EtBr Fluorescence studies.

Sample	A	B	C	D	E	F
Volume of SSC buffer (µL)	1780	1760	1740	1720	1700	1680
Volume of DNA solution (µL)	200	200	200	200	200	200
Volume of EtBr (µL)	20	20	20	20	20	20
Volume of compound (µL)	0	20	40	60	80	100
Final Volume (µL)	2000	2000	2000	2000	2000	2000
Final drug concentration (µM)	**0**	**0.5**	**1**	**1.5**	**2**	**2.5**

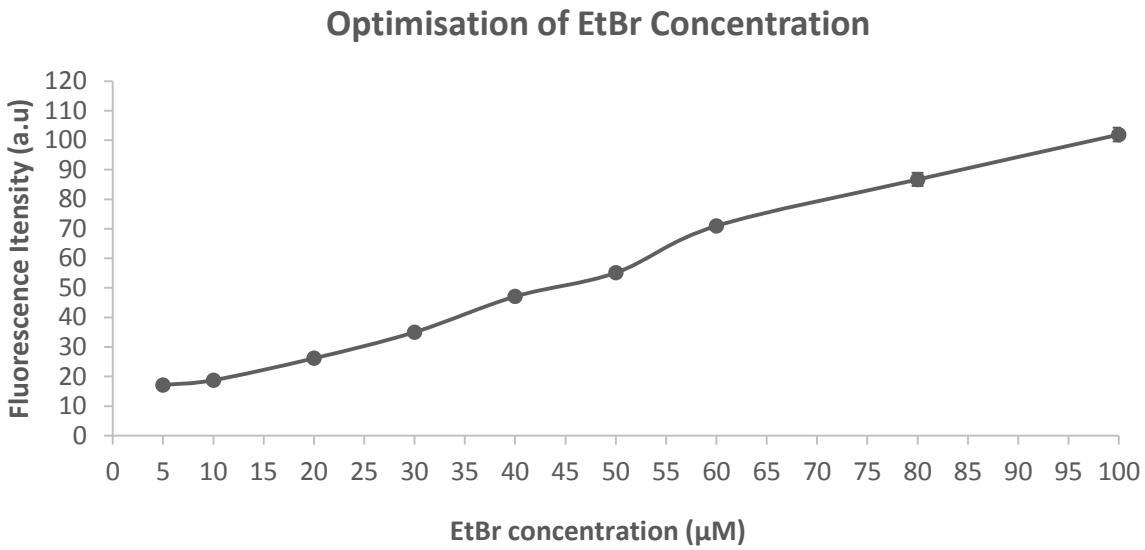

Figure 3.3.2.: Fluorescence emission of different EtBr concentrations in presence of *Calf Thymus* DNA. Data are presented as mean ± SEM, n=3.

3.3.3 UV binding studies

BNIPDaCHM, BNIPPiProp, BNIPPiEth and *trans,trans*-BNIPDaCHM working solutions (100 µM) were prepared from their stock solutions (10 mM in 50% DMSO/H_20), and were further diluted to 20 µM final concentration in 0.01 M SSC buffer. *Calf Thymus* DNA and 0.01 M SSC buffer were prepared as described in Section 3.3.2.

Test solutions were prepared by adding 1 mL of *Calf Thymus* DNA solution in a quartz glass flow cell and by adding on top 100 µL BNIP solution. The final solutions were thoroughly mixed and analysed at 260 nm using an Agilent 8453 UV-visible spectrophotometer (Section 3.2.2).

The values of apparent binding constants (K) were calculated from the intercept and slope by plotting $A_0/(A-A_0)$ against the BNIP derivative concentrations, where A_0 and A correspond to the absorbance values in the absence and presence of a compound.

3.3.4 Statistical analysis

Each data set contained a minimum of three independent experiments with two internal replicates, expressed as mean ± Standard Deviation (SD) or Standard Error of Mean (SEM). Statistical analysis was performed using GraphPad Prism 5.0 software (GraphPad Software, San Diego, CA, USA). Data sets (means ± SD or SEM) were compared using one-way analysis of variance (ANOVA) followed by a Tukey's post-test for pair-wise comparisons. Statistically significant data were detailed when *$p<0.05$, **$p<0.01$, ***$p<0.001$, ***$p<0.0001$.

3.4 Results and Discussion

3.4.1 Thermal denaturation studies and the effect of BNIPs on DNA binding

Thermal denaturation studies on *Calf Thymus* DNA were conducted to examine the DNA binding properties of the three novel BNIPs. The thermal denaturation profile of each derivative was represented by the thermal denaturation curves that corresponded to UV absorbance (260nm) for *Calf Thymus* DNA incubated in the absence and presence of 10 μM BNIPs. The Tm values of three independent experiments were averaged and presented as mean ± SD in Table 3.4.1.

According to Table 3.4.1, the melting point temperature of *Calf Thymus* DNA was 53.29^{o}C. The highest Tm value was observed with BNIPPiEth (91.05 ^{o}C), followed by BNIPPiProp (90.06 ^{o}C) and BNIPDaCHM (85.99 ^{o}C). The Tm value is defined as the temperature when half of the DNA has been dissociated. In presence of BNIPDaCHM, BNIPPiProp and BNIPPiEth, a significant increase by 32.70, 36.77, and 37.76 ^{o}C (DNA (ΔT)) in melting temperature was observed respectively ($p<0.0001$), as determined by one-way ANOVA analysis (Table 3.4.1). A ΔT value of 31.20 ^{o}C was previously reported for BNIPDaCHM by Barron *et al*. (2010), which was slightly lower than that observed in this study. However, discrepancies may have occurred due to purity differences among the synthesised compounds (Yurek *et al,* 2002).

BNIPPiEth was identified to be the most active DNA binding member of the BNIP family. BNIPPiEth, which is a structural analogue of BNIPPiProp, consists of a two-carbon linker sequence instead of a three-carbon linker sequence, as in BNIPPiProp.

Table 3.4.1.: Tm values of *Calf Thymus DNA* alone and in the presence of BNIPs.

Sample	Mean ± SD Tm (°C)	Mean ± SD ΔT (°C)
***Calf Thymus* DNA**	53.29±1.6	0.0
BNIPDaCHM	85.99±1.0 [a, c, d]	32.70±1.0
BNIPPiProp	90.06±0.9 [a, b]	36.77±0.9
BNIPPiEth	91.05±1.0 [a, b]	37.76±1.0

*ΔT is the difference between the mean Tm value of each compound and the mean Tm value of *Calf Thymus DNA*. Three independent experiments for each BNIP were performed (n=3). Statistical analysis was performed using one-way analysis of variance (ANOVA) (GraphPad Prism 5.0). A p-value of <0.05 was considered statistically significant and it is represent by different letters: a; compared to the control, b; compared to BNIPDaCHM, c; compared to BNIPPiProp and d; compared to BNIPPiEth.

Thus, the length of the linker sequence appears to affect a drug's binding potential to the DNA (O'Hare *et al*, 2001). Therefore, it would be appropriate to test BNIPs at different concentrations in order to determine the impact of linker sequence lengths in DNA intercalation in future work. The existence of electronegative amine groups that increase the stability of hydrogen bonds within the DNA and its structure that causes strong intercalation explain the high stabilising effect of BNIPDaCHM and BNIPPiProp, respectively (O'Hare *et al*, 2001).

3.4.2 Competitive displacement of EtBr by BNIPs

Competitive displacement of EtBr with BNIPs from *Calf Thymus* DNA was carried out to further investigate their DNA interactions. All three novel BNIPs competitively displaced EtBr from *Calf Thymus* DNA duplexes. For each derivative, a range of concentrations (0-7 μM) was tested and the corresponding C_{50} values calculated (see Appendix 1). All BNIPs displaced EtBr with C_{50} values ranging from 1.1 to 5.6 μM confirming their high DNA binding affinity (Table 3.4.2). BNIPDaCHM was included to evaluate and compare its binding properties to the three novel BNIPs.

Table 3.4.2.: Competitive displacement of EtBr from *Calf Thymus* DNA.

BNIP derivative	**Mean ± SD** **C_{50} value (μM)**
***Calf Thymus* DNA alone**	-
BNIPDaCHM	2.3±0.1 [a, c, d, e]
BNIPPiProp	3.9±0.3 [a, b, d, e]
BNIPPiEth	1.1±0.2 [a, b, c, e]
***trans,trans*-BNIPDaCHM**	5.6±0.2 [a, b, c, d]

*Effect of different BNIPs concentrations (0-7 μM) on % fluorescence intensity compared to *Calf Thymus* DNA alone. C_{50} value: concentration of each BNIP derivative required to cause a 50% decrease on fluorescence intensity of DNA-EtBr complex. Data are the mean ± SD of three independent experiments (n=3). Statistical analysis was performed using one-way analysis of variance (ANOVA) (GraphPad Prism 5.0). A p-value of <0.05 was considered statistically significant and it is represent by different letters: a; compared to the control, b; compared to BNIPDaCHM, c; compared to BNIPPiProp, d; compared to BNIPPiEth and e; compared to *trans,trans*-BNIPDaCHM.

The order of binding affinity to *Calf Thymus* DNA from highest to lowest was BNIPPiEth (1.1 ± 0.2 μM), BNIPDaCHM (2.3 ± 0.1 μM), BNIPPiProp (3.9 ± 0.3 μM) and *trans,trans*-BNIPDaCHM (5.6 ± 0.2 μM). BNIPPiEth with the shortest linker bearing two piperidine rings attached to an ethyl group, had the lowest C_{50} value. Therefore the shorter length of the linker chain, as well as the presence of a nitrogen atom within the cyclohexane ring, compared to BNIPDaCHM, resulted in increased binding affinity.

Moreover, the incorporation of the nitrogen atom within the cyclohexane ring was not found to improve the binding properties of BNIPPiProp (3.9 ± 0.3 μM), compared to BNIPDaCHM and BNIPPiEth, confirming that the length of the bridging alkyl linkers is crucial and affects significantly BNIP binding to DNA duplexes, which is in agreement with the findings of Liu *et al*. (2016).

The *trans,trans*-BNIPDaCHM, a stereoisomer of BNIPDaCHM, gave a C_{50} value of 5.6 ± 0.2 μM. BNIPDaCHM, consisting of three isomers, gave a C_{50} value of 2.3 ± 0.1 μM, suggested that in the absence of *cis,cis* or/and *cis,trans*, isomer *trans,trans*-BNIPDaCHM did not show as high DNA-binding interactions as with BNIPDaCHM. Based on the above results, the structure of BNIPDaCHM together with its mixture of three isomers was found to improve its interacting properties within the DNA base pairs, compared to *trans,trans*-BNIPDaCHM. This was further confirmed since *trans,trans*-BNIPDaCHM resulted in a higher C_{50} value compared to BNIPDaCHM, revealing that each of the three or more than one (*trans,trans/cis,trans* or *trans,trans/cis,cis*) isomers co-existing in BNIPDaCHM, are involved in the intramolecular complexes/interactions with DNA. By isolating one of its isomers (*trans,trans*-BNIPDaCHM), the DNA binding affinity was significantly decreased ($p<0.0001$). The above results revealed a similar DNA binding profile of all BNIPs, as for the thermal denaturation studies: the only

difference being that *trans,trans*-BNIPDaCHM had less DNA binding affinity to DNA, compared to BNIPDaCHM. The existence of three isomers on BNIPDaCHM structure seems to be crucial in inducing displacement of DNA bound EtBr and thus, enhancing the competition with EtBr in order to target more DNA intercalating sites.

3.4.3 UV binding studies and the effect of BNIPs on DNA binding

Along with the DNA thermal denaturation and EtBr displacement studies, the interaction of BNIPs with *Calf Thymus* DNA was also studied by UV-Vis spectroscopy. A continuous decrease in UV absorption was observed at 260 nm, within increasing BNIP concentration (0 - 7μM). The strength of the binding interaction between a single biomolecule (DNA) to its ligand/binding partner (BNIP) is measured quantitatively by the binding constant (K_B). The larger the K_B value, the greater the binding affinity of the ligand for its target. This is described by the equilibrium binding expression shown below:

$$DNA + BNIP \underset{}{\overset{K_B}{\rightleftarrows}} [DNA \bullet BNIP]$$

$$K_B = [DNA \bullet BNIP]/[DNA][BNIP]$$

The apparent K_B binding constants for the compounds under study were calculated from the intercept and the slope (K=intercept/slope) by plotting $A_0/(A-A_0)$ against the inverse BNIP concentrations (Zhi-Yong *et al*, 2014) (see Appendix 2), where A0 and A correspond to the absorbance values in the absence and presence of each BNIP compound (Figure 3.4.3a), respectively.

Binding constant values K_B for the BNIPs ranged between 3.25 x 10^4 M^{-1} - 12.23 x 10^4 M^{-1} (Figure 3.4.3b), and show that all BNIPs interact with the DNA helix. The highest binding constant was observed with BNIPDaCHM (12.23 x 10^4 M^{-1}), followed by *trans,trans*-BNIPDaCHM (11.38 x 10^4 M^{-1}) and BNIPPiEth (10.85 x 10^4 M^{-1}). The lowest K_B binding constant was observed for BNIPPiProp (3.25 x 10^4 M^{-1}). This result is in agreement with the competitive displacement of EtBr studies (Table 3.4.2), highlighting the importance of linker chain length in achieving strong DNA binding interactions.

In addition, the UV-Vis absorption studies revealed that *trans,trans*-BNIPDaCHM, to be the least effective BNIP, obtaining a binding constant of 11.38 x 10^4 M^{-1}, compared to BNIPDaCHM (12.23 x 10^4 M^{-1}: highest K_B binding constant). This suggests that *trans,trans*-BNIPDaCHM exhibits a lower intercalation capacity than when in combination with other two isomers present in BNIPDaCHM.

Previous molecular modelling studies have revealed that for the most stable conformation of bis-1,8-naphthalimide in presence of DNA, the naphthalimide rings obtain an antiparallel orientation and are detected in the major groove (Brana *et al*, 2004). Furthermore, naphthalimide rings have been reported to induce strand cleavage, allowing the electron transfer and formation of hydrogen bonding between the nitrogen atoms and the nucleobases (excluding guanine) of the minor groove (Bailly *et al*, 2003), suggesting that the relatively high K_B binding constant of *trans,trans*-BNIPDaCHM was obtained not only *via* intercalation, but also *via* binding on the major and/or minor groove of DNA.

a.

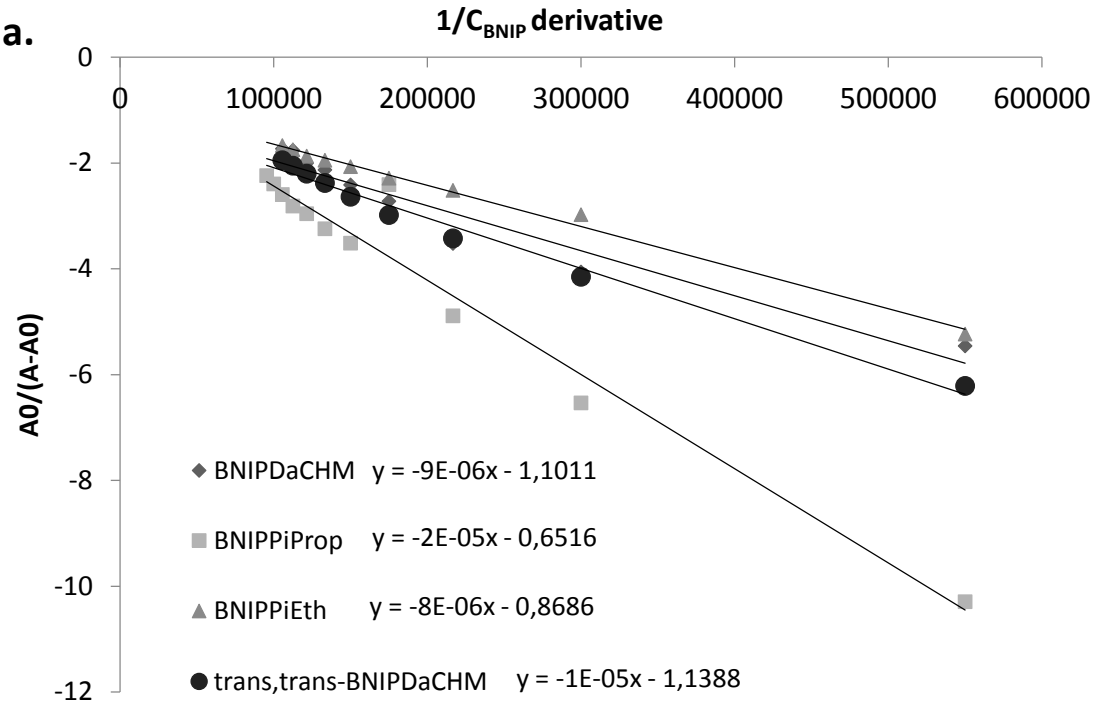

b.

BNIPs	**Corresponding value of K_B constant (M^{-1})**
BNIPDaCHM	12.23 x 10^4
BNIPPiProp	3.25 x 10^4
BNIPPiEth	10.85 x 10^4
***trans,trans*-BNIPDaCHM**	11.38 x 10^4

Figure 3.4.3.: a) Interaction between BNIPs and *Calf Thymus* DNA by UV spectroscopy. Plot of A0/ (A-A0) *versus* $1/C_{BNIP}$ of the interaction between BNIPs and *Calf Thymus* DNA. **b) K_B constant values of BNIPs after UV binding studies.**

3.5 Conclusion

In Chapter 3, physical properties of three novel BNIPs, BNIPPiProp, BNIPPiEth and *trans,trans* BNIPDaCHM were further investigated. Their DNA binding affinities were assessed by using different *in vitro* techniques, such as thermal denaturation studies, EtBr competitive displacement and UV binding studies. BNIPDaCHM, which is the parental BNIP, was tested alongside each of the other novel BNIPs.

Thermal denaturation studies have shown that BNIPPiProp and BNIPPiEth can intercalate and stabilize the double helix of *Calf Thymus* DNA that was confirmed by their increased T_m values compared to *Calf Thymus* DNA alone. BNIPPiEth was identified as the most active DNA binding member of the BNIPs.

Studies on competitive displacement of EtBr by BNIPs were performed to further evaluate their DNA binding affinity. Each novel BNIP can competitively displace EtBr from DNA in a dose dependent manner, confirming the hypothesis of DNA intercalation being responsible for their mode of action. BNIPs displaced EtBr with C_{50} values ranging among 1.1-5.6 μM, with BNIPPiEth showing the strongest binding affinity (1.1 μM). In parallel, by UV binding studies, strong K binding constants in the range of $3.25 \times 10^4\ M^{-1}$ - $12.23 \times 10^4\ M^{-1}$ were found for the three novel BNIPs.

This study confirmed that BNIPPiProp, BNIPPiEth and *trans,trans*-BNIPDaCHM have the ability to interact with DNA, by intercalating into its double helix and have been shown to exhibit strong *in vitro* DNA binding properties, suggesting that DNA is the main target for BNIPs (Figure 3.5).

Therefore, further DNA-associated processes and modes of cell death were investigated to determine the prospective of BNIPs as potential anti-cancer agents.

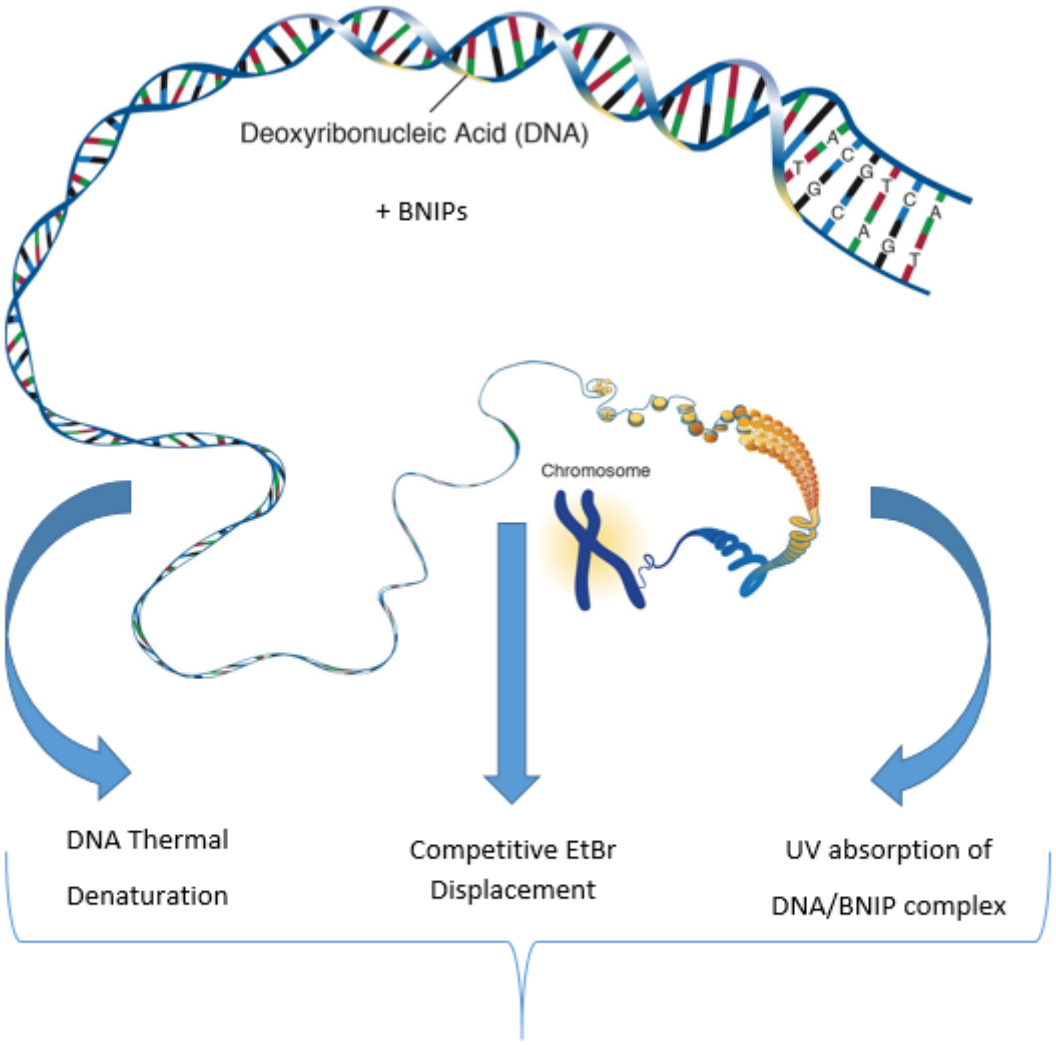

Figure 3.5.: Summary of DNA binding studies (Picture of DNA from: National Human Genome Research Institute, www.genome.gov).

CHAPTER 4

Cytotoxicity, reactive oxygen species and DNA damage studies

4.1 Introduction

4.1.1 Anti-cancer drugs and *in vitro* cytotoxicity

Drug-mediated inhibition of cell growth and proliferation is one of the first preclinical screenings to be carried out for potential anti-cancer drugs (Dobbelstein and Moll, 2014). Cytotoxic or antineoplastic drugs are a type of medicines that contain certain chemicals, which are toxic to the cells. More specifically, cytotoxic drugs have the ability to interfere with intracellular and extracellular regulatory processes such as cell division, replication or cell membrane integrity, induce DNA damage and cause cell death (Aydinlik *et al*, 2016).

Nowadays, various assays have been developed for *in vitro* cytotoxicity tests. Most of them are based on different cell functions such as cell adherence, cell membrane permeability, enzyme activity, adenosine Triphosphate (ATP) production or nucleotide uptake activity (Adan *et al*, 2016). As a result, the use of pre-treatment chemosensitivity assays (measurement of tumour cells that have been removed from the body and killed after chemotherapy treatment) promotes the selection of anti-cancer drugs with the greatest likelihood for clinical effectiveness and the exclusion of ineffective therapy.

The most common method to determine cytotoxicity is by assessing cell viability through the use of vital dyes (i.e. formazan dyes). The formazan dyes are chromogenic products formed by the reduction of tetrazolium salts by dehydrogenases (Figure 4.1.1.1) (McCluskey *et al*, 2005). Reductases and lactate dehydrogenase (LDH) are the main dehydrogenases that are released during cell death (Sobhani *et al*, 2016).

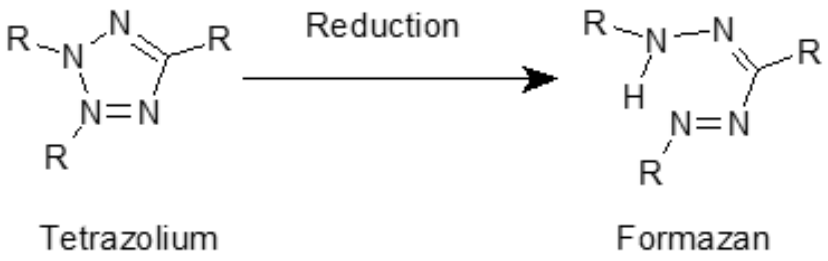

Figure 4.1.1.1.: Structure of tetrazolium and formazan salt.

Major tetrazolium salts that are commonly used in clinical biochemistry and cell biology include INT (2-(4-Iodophenyl)-3-(4-nitrophenyl)-5-phenyl-2H-tetrazolium chloride), MTT (3-(4, 5-dimethyl-2-thiazolyl)-2, 5-diphenyl-2H-tetrazolium bromide), MTS (3-(4,5-dimethylthiazol-2-yl)-5-(3-carboxymethoxyphenyl)-2-(4-sulfophenyl)-2H-tetrazolium), XTT (2,3-bis-(2-methoxy-4-nitro-5-sulfophenyl)-2H-tetrazolium-5-carboxanilide) and NBT (2,2′-bis(4-Nitrophenyl)-5,5′-diphenyl-3,3′-(3,3′-dimethoxy-4,4′-diphenylene)ditetrazolium chloride 3,3′-(3,3′-Dimethoxy-4,4′-biphenylene)bis[2-(4-nitrophenyl)-5-phenyl-2H-tetrazolium chloride]) (McCluskey *et al*, 2005).

In this study, cytotoxicity of BNIPs in two breast cancer cell lines, MDA-MB-231 and SKBR-3 cells, was determined by MTT assay. The MTT assay is a colourimetric assay that measures reduction in cell viability, when metabolic events lead to cell death (i.e. apoptosis or necrosis) and was first developed and introduced by Mosmann in 1983 (Mosmann, 1983). The main advantages of MTT assay compared to other methods, are its sensitivity and rapidity, excluding the use of radioisotopes (^{51}Cr) or radiolabelled biochemical ([^{3}H]-thymidine) that could be proved harmful for the working environment (Riss *et al*, 2016). The yellow, water-soluble, tetrazolium MTT (3-(4, 5-dimethylthiazolyl-2)-2, 5-diphenyltetrazolium

bromide) is reduced by metabolically active viable cells that activate several dehydrogenase enzymes (Figure 4.1.1.2) (Mosmann, 1983).

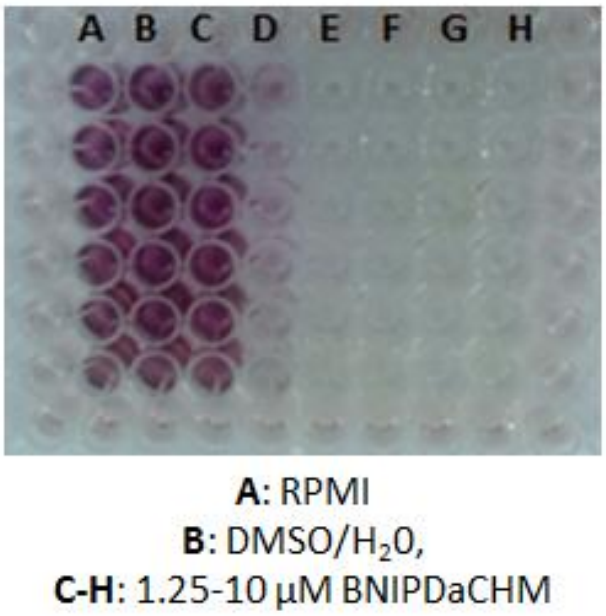

Figure 4.1.1.2.: A microtiter 96 well plate after an MTT assay. Yellow tetrazole was reduced to purple formazan (wells A-C) in living MDA-MB-231 cells. Wells C-H show MDA-MB-231 cells treated with 1.25-10 uM BNIPDaCHM for 24 hours. Dimethyl sulphoxide (DMSO) was added to dissolve the insoluble purple formazan product into a coloured solution.

This metabolic process forms reducing equivalents, such as NADH and NADPH that result in intracellular purple formazan. The formazan crystals are transported to the cell surface by exocytosis and after solubilisation with dimethyl sulfoxide or acidified ethanol solution, the absorbance of this coloured solution can be quantified at a specific wavelength (560 nm) by a spectrophotometer (Lü *et al*, 2012).

MDA-MB-231 and SKBR-3 cell lines have distinguishing features on gene expression profiling and also different responses to adjuvant therapy and different patterns of metastatic recurrence (Currey *et al*, 2006). More specifically, MDA-MB-231 cells are triple negative breast cancer cells (TNBC) (oestrogen receptor

negative (ER-), progesterone receptor negative (PR-), human epidermal growth factor receptor 2 negative (HER2-) with four gene mutations being reported (BRAF, CDKN2A, KRAS and TP53) and a fast-growing basal B tumour classification (49.5% proliferation index rate) (Kenny et al, 2007), which makes them less responsive to anti-cancer treatments, such as docetaxel or carboplatin, compared to cells that are hormone receptor positive, such as SKBR-3 cells (Kenny *et al*, 2007). SKBR-3 cells are double negative breast cancer cells (DNBC) (ER-, PR-, HER2+) without gene mutations and with a luminal tumour classification (35.2% proliferation index rate), resulting in a better response to anti-cancer treatments compared to TNBC, however, patients still have poor survival rates (Kenny *et al*, 2007). Both cells lines demonstrate invasive phenotype *in vitro*, without losing the complex inter-relationships that exist between cells *in vivo*, once the cell lines are cultured on plastic in two dimensions. In addition, MDA-MB-231 and SKBR-3 cells are not sensitive to culture conditions, such as the inclusion of growth factors, which has been found to alter the cell phenotype and cause inappropriate pathway activation or differentiation (Holliday and Speirs, 2011). By using two cell lines which are either unresponsive or partially responsive to currently available anti-cancer regimes, it is possible to extend the understanding on the cytotoxicity of BNIPs against different breast cancer cells types and to gain more information about their mode of action.

4.1.2 ROS levels in cancer cells

ROS are free radicals, molecules or ions that are derived from molecular oxygen (Bayr, 2005). Atomic oxygen has two unpaired electrons in separate orbits in its outer electron shell. This electron structure makes oxygen susceptible to radical formation (Apel and Hirt, 2004). On the other hand, ROS are highly reactive, as they have a single unpaired electron in their outermost shell of electrons (Figure 4.1.2.1) (Bayr, 2005). Thus, the addition of electrons leads to sequential reduction of oxygen and the formation of ROS.

ROS can be categorized into two groups: free oxygen radicals, such as superoxide ($O_2^{\bullet -}$), hydroxyl radical ($^{\bullet}OH$), nitric oxide ($NO^{\bullet}$), organic radicals ($R^{\bullet}$), peroxyl radicals ($ROO^{\bullet}$), alkoxyl radicals ($RO^{\bullet}$), thiyl radicals ($RS^{\bullet}$), sulfonyl radicals ($ROS^{\bullet}$), thiyl peroxyl radicals ($RSOO^{\bullet}$), disulfides (RSSR) and non-radical ROS, such as hydrogen peroxide (H_2O_2), singlet oxygen ($^1O_2$), ozone/trioxygen (O_3), organic hydroperoxides (ROOH), hypochloride (HOCl), peroxynitrite (ONO^-), nitrosoperoxycarbonate anion ($O{=}NOOCO_2^-$), nitrocarbonate anion ($O_2NOCO_2^-$), dinitrogen dioxide (N_2O_2), and nitronium (NO_2^+), respectively (Ray *et al*, 2012). The most well studied ROS in cancer are superoxide, hydrogen peroxide and hydroxyl radicals (Ray *et al*, 2012).

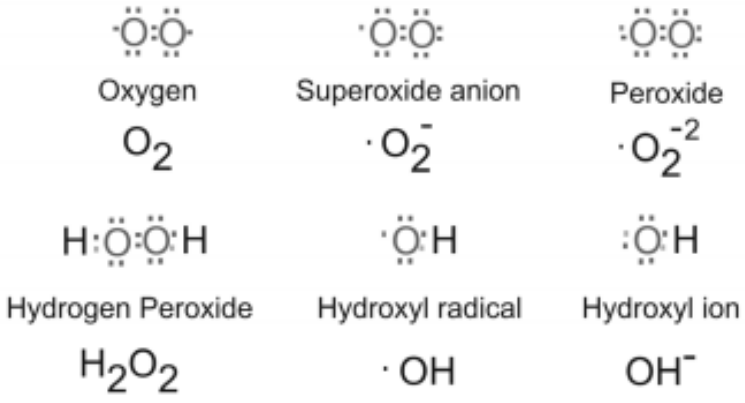

Figure 4.1.2.1.: Electron structures of common reactive oxygen species.

At the cellular level, specific ROS can be individually measured in tissue culture (Ameziane-El-Hassani and Dupuy, 2016). So far, several methods for the detection and quantification of ROS in aqueous solution have been developed. The most common methods are based on probes that react with ROS and produce detectable products. Chemiluminescent probes, such as luminol, 2-methyl-6-(p-methoxyphenyl)-3,7-dihydroimidazo[1,2-a]pyrazine-3-one (MCLA), and coelenterazine, fluorescent probes, such as dihydroethidium, mitoSOX, dichlorodihydrofluorescein diacetate or N-acetyl-3,7-dihydroxyphenoxazine and Ferricytochrome C reduction were the first, accurate methods for detecting ROS levels (Aitken *et al*, 2013). More recently, new, rapid and cost effective methods for the assessment of ROS levels were introduced: immune-spin trapping, boronate-based fluorescent probes, fluorescent protein-based redox probes and X- and L-Band ESR Spectroscopy are some of them (Wang, 2016). The development of novel tools for detecting, measuring and studying ROS in biological samples underlies their critical role in cell signalling and function, physiology and pathophysiology and nowadays, it is commonly accepted that free radicals are not strictly confined to the fields of chemistry and physics as in the past.

Assessment of ROS levels after treatment with BNIPs in the two breast cancer cell lines of interest, MDA-MB-231 and SKBR-3 cells, was determined by flow cytometry. Chloromethyl derivative of 2',7'-Dichlorodihydrofluorescein diacetate probe (CM-H_2DCFDA), was used as an indicator of ROS levels in breast cancer cells (Oparka *et al,* 2016). CM-H_2DCFDA diffuses into cells, where its acetate groups are cleaved by intracellular esterases and its thiol-reactive chloromethyl group reacts with intracellular glutathione and other thiols (Gomes *et al*, 2005) (Figure

4.1.2.2). Esterase cleavage of the lipophilic blocking groups yields a charged form of the dye that is retained by cells (Gomes *et al*, 2005).

Oxidation of the probes can be detected by monitoring the increase in fluorescence within each cells by using flow cytometry, using excitation sources and filters appropriate for fluorescein (FITC) (Excitation: 490 nm- Emission:525 nm) (Wang *et al,* 2016).

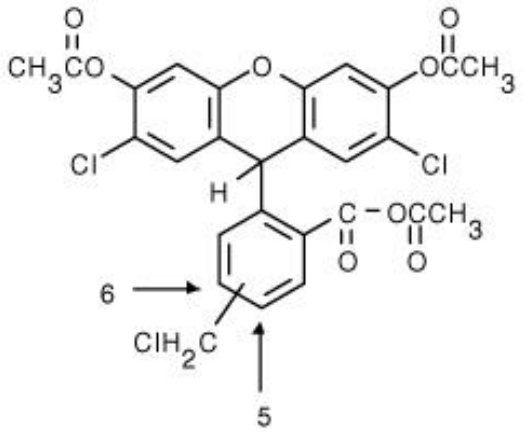

Figure 4.1.2.2.: Chemical structure of CM-H_2DCFDA probe.

4.1.3 DNA damage in cancer cells

Human cells are constantly subjected to external and internal stresses that cause damage to their DNA (Boveri, 2008). DNA damage can be harmful to the overall integrity of the cell as it can have a negative impact on vital cellular processes, like replication (Hoeijmakers, 2009). DNA damaging sources may be endogenous or environmental. Endogenous agents that promote DNA damage include ROS and nitrogen (N) OS that are produced by macrophages and neutrophils at sites of infection or inflammation (Trichopoulos and Petridou, 1994). ROS and NOS attack DNA and alter basepairing, block DNA replication/transcription or cause DNA single

strand breaks. These spontaneous alterations in DNA contribute to endogenous DNA damage. Environmental DNA-damaging agents, such as ultraviolet radiation (A and B), ionising radiation (X and γ) or chemical agents (alkylating anti-cancer drugs) can also generate various forms of DNA damage and double strand DNA breaks (DSBs) (Rastogi *et al*, 2010).

DNA strand breaks after exposure to environmental carcinogens occur once topoisomerase activity is aborted (Pourquier *et al*, 1997). Topoisomerase I and II are the two main enzymes that control the synthesis of proteins and facilitate replication by winding and unwinding of the DNA. Once this action is disrupted and cannot be repaired, cell cycle arrest and cell death occur (Pourquier *et al*, 1997).

Based on the importance of DNA integrity in maintaining cell viability and function, therapeutic strategies are focused on the synthesis of novel compounds that are able to inflict DNA damage and induce cell death in several groups of diseases/disorders, like cancer. One example of this is Etoposide, a chemotherapeutic agent (commercially available since 1983), which forms a complex with the Topoisomerase II enzyme in order to prevent the supercoiling of the DNA strands, causing errors in DNA (i.e. DNA mismatch) synthesis and apoptosis (Veuger and Curtin, 2014). Etoposide has been used as treatment against various types of cancer, including lung cancer, ovarian cancer, testicular cancer, leukaemia and lymphoma, proving that DNA is a viable target for cancer therapeutics also demonstrating the importance of drugs that are able to inflict its damage (Greco, 1998). Therefore, in breast cancer treatment, most currently used anti-cancer drugs, such as Camptothecin, Cisplatin, Doxorubicin and Etoposide were developed to induce DNA damage, by inflicting DNA double-strand break (DSB) (Li-Weber, 2013).

In the last decades, several methods for the assessment of DNA damage within mammalian cells have been developed, including immunological assays, high performance liquid or gas chromatography and neutral or alkali comet assays. In this study, DNA damage in MDA-MB-231 and SKBR-3 cells was assessed using alkali single cell gel electrophoresis, known as comet assay (Kumari *et al*, 2008).

Microgel electrophoresis was first introduced by Ostling and Johanson, in order to measure DNA single-strand breaks (SSBs) that were responsible for DNA supercoils relaxation (Ostling and Johanson, 1984). A few years later, Singh and colleagues (1988) published an improved protocol which used alkaline conditions that allowed DNA unwinding and maximum exposure of SSBs (Singh *et al*, 1988). This new method allowed visualising the migration of DNA strands from individual agarose-embedded cells by combining DNA gel electrophoresis with fluorescence microscopy.

In 1990, a new modification of the original method of Ostling and Johanson took place and was then introduced as the "comet assay", which is based on the quantification of DNA damage within an individual cell after staining with DNA binding fluorescent dye (4',6-diamidino-2-phenylindole (DAPI)) (Olive *et al*, 1990). The visualisation method was validated in 1998, by Duthie and Hawdon (1998) and has been broadly used in DNA damage studies since then. The high-molecular-weight DNA is located at the comet head and the leading ends of migrating fragments are located at the comet-tail, respectively (Duthie and Hawdon, 1998) (Figure 4.1.3). The relative fluorescence of the comet-head and the length of the comet-tail correspond to the exerted DNA damage, which is represented by DNA strands breaks (Duthie and Hawdon, 1998). The comet assay is versatile, relatively simple to perform and sensitive method that proved suitable

for studying DNA damage in MDA-MB-231 and SKBR-3 cells after treatment with novel BNIPs.

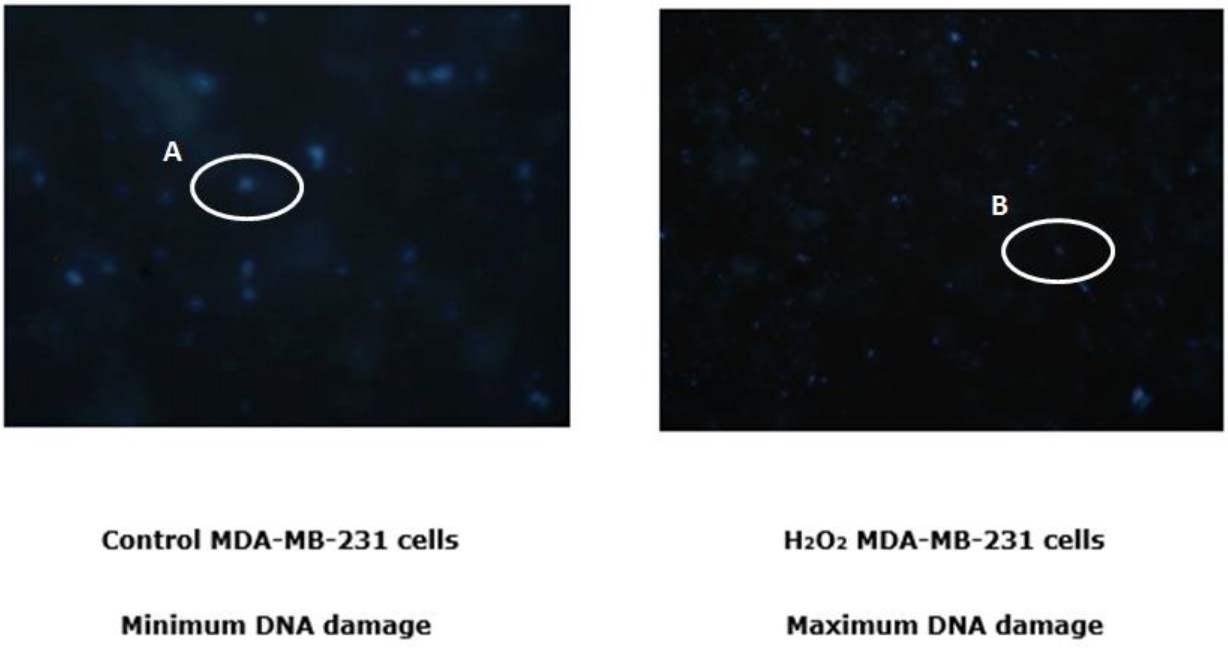

Figure 4.1.3.: DNA damage in MDA-MB-231 cells as determined by comet assay. Cells were visualised using a Leica DMRB fluorescence microscope with D filter (excitation bandpass (violet); 355 – 425 nm; emission longpass (green); 470 nm) following staining with DAPI (minimum (A: score 0) and maximum (B: score 4) DNA damage). Magnification x40.

4.1.4 Aims

In Chapter 4, the ability of BNIPDaCHM, BNIPPiProp, BNIPPiEth and *trans,trans*-BNIPDaCHM to affect metabolism in breast cancer MDA-MB-231 and SKBR-3 cells will be assessed to determine the cytotoxicity of the novel derivatives. Moreover, the effect of the four BNIPs on the levels of intracellular ROS and the extent of DNA damage induced by BNIPs in MDA-MB-231 and SKBR-3 cells treated with the above intercalating agents will be investigated.

4.2 Materials

A list of the reagents that were used for cell maintenance, cytotoxicity, ROS and DNA damage studies are presented below. All reagents were handled according to the COSHH standards and were used without purification.

4.2.1 Cell culture maintenance of MDA-MB-231 and SKBR-3 cells.

RPMI-1640 medium GlutaMAXTM-1 with 25Mm HEPES	Gibco, UK
Trypsin-EDTA	Sigma-Aldrich, UK
Phosphate buffered saline	Sigma-Aldrich, UK
Penicillin/Streptomycin	Invitrogen, UK
Fetal Bovine Serum	Sigma-Aldrich, UK

4.2.2 Colourimetric 3-(4, 5-Dimethylthiazol-2-yl)-2, 5 diphenyltetrazodium bromide (MTT) assay.

Methylthiazolyldiphenyl-tetrazolium bromide	Sigma-Aldrich, UK
Dimethyl Sulfoxide	Aldrich, UK

4.2.3 ROS Level Detection

CM-H_2DCFDA (General Oxidative Stress Indicator)	ThermoFisher, UK

4.2.4 COMET assay

Ethylenediaminetetraacetic acid (EDTA)	Sigma-Aldrich, UK
Sodium Hydroxide	Fisherbrand, UK
Tris Base	Fisherbrand, UK
Sodium Chloride	Fisherbrand, UK
Triton X-100	Sigma-Aldrich, UK
Agarose (1% w/v)	Sigma-Aldrich, UK
Low Melting Point Agarose (1% w/v)	Sigma-Aldrich, UK
Hydrogen Peroxide	Sigma, UK
4', 6-Diamidino-2-Phenylindole, Dihydrochloride	Sigma-Aldrich, UK

4.2.5 Instrumentation

HERASafe Class II Safety Cabinet	Thermo Electron Corporation, Germany
HERACell incubator	Heraeus, Germany
Centaur 2 centrifuge	MSE, UK
Neubauer Haemocytometer	Assitent, Germany
Leica DMIL light microscope	Leica Microsystems, UK
96-well plate reader	Synergy/HT, BIOTEK
Polymax 1040 Platform Shaker	Heidolph, USA
ALC Multispeed Refrigerated Centrifuge	Thomson Scientific,UK

Coulter Epics XL-MCL flow cytometer	Beckman Coulter, UK
Horizon 20.25 horizontal gel electrophoresis tank	Gibco, UK
Leica DMRB fluorescence microscope D filter	Leica Microsystems,UK

(excitation bandpass (colour violet): 355-425 nm, emission longpass (colour green):470 nm)

4.3 Methods

4.3.1 Cell culture maintenance of MDA-MB-231 and SKBR-3 cells.

MDA-MB-231 (ECACC, Public Health England, UK, 92020424) and SKBR-3 (ATCC, HTB-30) cells were maintained in Roswell Park Memorial Institute 1640 medium (RPMI-1640) (containing GlutaMAX™-1 with 25Mm HEPES), supplemented with 10% (v/v) Fetal Bovine Serum (FBS) and 1% Penicillin/(10,000 µg/mL) Streptomycin. Aseptic cell culture procedures were carried out within HERASafe Class II Safety Cabinet.

MDA-MB-231 and SKBR-3 cells were grown at 37 ^{o}C (5% CO_2) within a HERACell incubator, sub-cultured once they reached 80% confluence, washed twice with 5 mL of Phosphate Buffered Saline (PBS) and detached after incubating the flask at 37 ^{o}C (5% CO_2) for 2 minutes with 2 mL of Trypsin-EDTA (0.25%) solution. The cell mixture was transferred into a falcon tube and centrifuged at 1,000 *xg* for 5 minutes, using a Centaur 2 centrifuge. After pouring off the supernatant and re-suspending the cell pellet in 8 mL of fresh medium, cells were counted by using a Neubauer Haemocytometer. For routine cell maintenance, 1 x 10^6 cells/15 mL of RPMI-1640 were seeded into 75 cm^2 tissue culture flasks.

Ten µL of cell suspension were placed on the chamber and only the cells that were located in the four sections of the grid (A, B, C and D) were counted, under the microscope (Figure 4.3.1). The final concentration of cells in solution was calculated by the following equation: [(A+B+C+D)/4] x 10^4 = cells/mL.

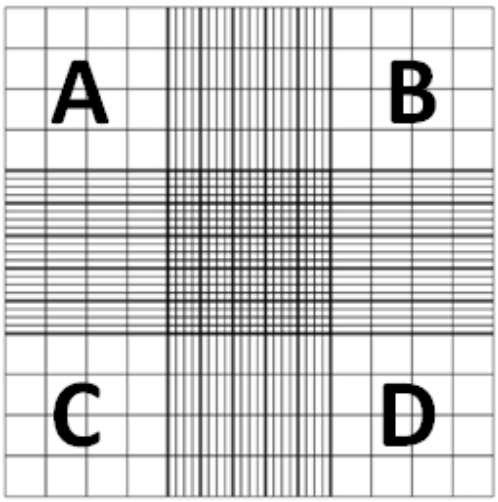

Figure 4.3.1.: Counting areas on Neubauer Haemocytometer.

4.3.2 Colourimetric 3-(4, 5-Dimethylthiazol-2-yl)-2, 5 diphenyltetrazodium bromide (MTT) assay.

Cytotoxicity testing of the novel BNIPs was performed by using a colourimetric MTT assay. MDA-MB-231 and SKBR-3 cells (7.5 x 10^3 cells/100 µL/well) were seeded in 96-well plates and after 24 hours were treated with different concentrations (0-10 µM) of BNIPDaCHM, BNIPPiProp, BNIPPiEth or *trans,trans*-BNIPDaCHM. Stock solutions (10 mM in 50% DMSO/H_20) of BNIP derivatives were diluted to the desired final concentrations with RPMI-1640 medium. In order to ensure that DMSO was not affecting MDA-MB-231 and SKBR-3 cells viability, a 50% DMSO/H_20 solution was added to one of the columns as a vehicle control. BNIPs were dissolved in RPMI before addition to the cells. After various treatment times (24 to 96 hours), the cell culture medium was removed and 100 µL of sterile-filtered MTT solution (1 mg/mL) was added to each well and the plate returned to the incubator. After 4 hour incubation at 37 ^oC (5% CO_2), in the dark, the MTT solution was removed and replaced by 200µL of DMSO. The 96-well plates were shaken for 20 minutes at room temperature, in the dark, and the absorbance was

measured at 560 nm on a 96-well plate reader. For each compound, three independent experiments were carried out and each treatment consisted of six replicates per plate. Curves were used for the representation of the percentage growth inhibition of MDA-MB-231 and SKBR-3 cells treated with BNIPs, with DMSO control representing 100% cell viability (see Appendix 3).

4.3.3 ROS Level Detection

MDA-MB-231 and SKBR-3 cells (1 x 10^6 cells/ T25 cm^2 flask) were incubated for 24 hours before treatment. Then, BNIPs (IC_{25} concentrations) were added and cells were incubated for 4 hours. After 4 hours of treatment, MDA-MB-321 and SKBR-3 cells were washed twice with PBS (2 mL), and fresh medium (5 mL) and ROS dye (5 µL) were added to each flask.

The cells were incubated for 45 minutes at 37 °C. After the desired incubation time, the cells were removed from the culture flasks by adding trypsin (1 mL) and centrifuged at 500 *xg* for 5 minutes at 4 °C. The supernatant of each sample was discarded and the pellet was resuspended in PBS (1 mL) and transferred to an Eppendorf tube. The cells were centrifuged at 500 *xg* for 5 minutes at 4 °C, the supernatant was discarded and the pellet was resuspended in fresh PBS (500 µL).

The samples were analysed by flow cytometry, on a Coulter Epics XL-MCL flow cytometer. EXPO-32 software was used to record and analyse 10,000 single events. The percentage of ROS production was calculated from FL-1 plots. An example of the gated region in control and BNIPDaCHM treated samples is provided in Figure 4.3.3. The markers are linked and represent the gated region where a shift of fluorescent is observed when ROS is produced. The markers were placed in the same position for all the ROS experiments undertaken.

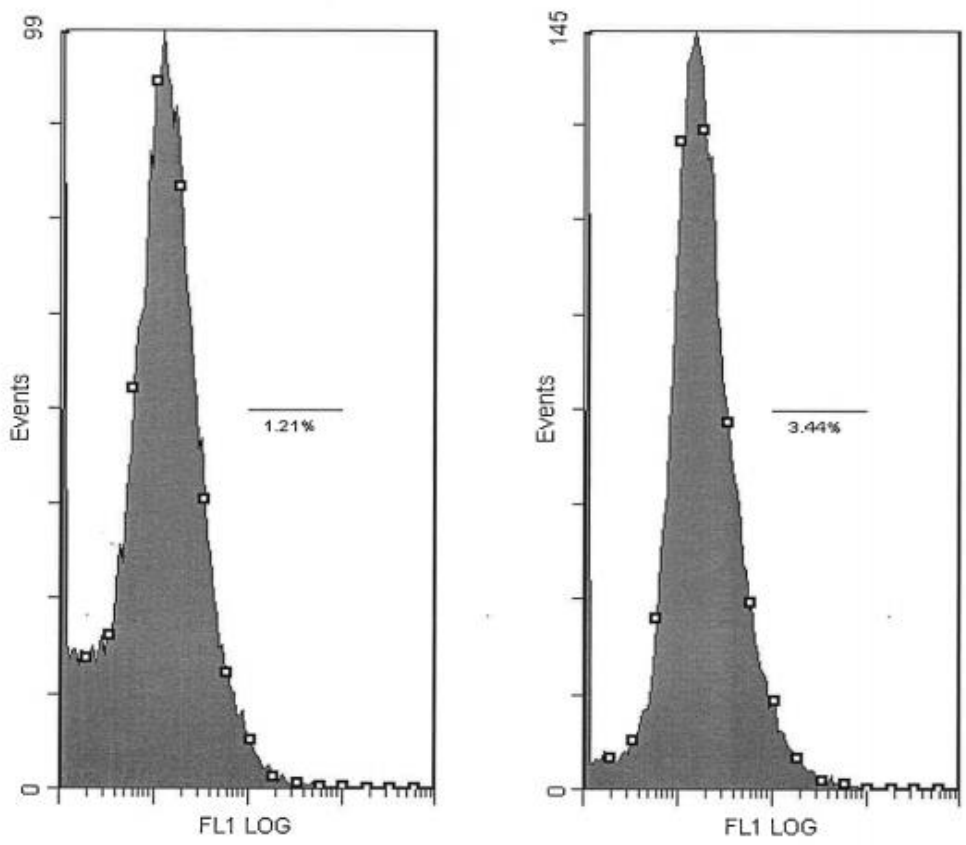

Figure 4.3.3.: ROS levels in MDA-MB-231 cells before (left) and after 8 hour treatment with BNIPDaCHM IC_{25} (right). For ROS studies, 10,000 events were recorded and images are representative of the results obtained using EXPO32 ADC analysis software.

4.3.4 COMET assay

MDA-MB-231 and SKBR-3 cells (16 x 10^4 cells/2 mL/well) were seeded in a 12 well plate and incubated for 24 hours before treatment. BNIPs (IC_{25} concentrations) were added and cells were incubated for 24 hours. After 24 hours of treatment, MDA-MB-231 and SKBR-3 cells were washed with PBS and 500 µL trypsin were added in each well. After trypsinisation, 500 µL of medium were added on top and the cell solution was collected in sterile Eppendorf tubes. The samples were centrifuged at 400 *xg* for 5 minutes at 10 °C and the supernatant was discarded. In each tube, 85 µL of 1% LMP agarose in PBS were added and

mixed with the cell pellet. In parallel, 85 μL of agarose were placed on fully frosted microscope slides, covered with 18 x 18 mm cover slips and left at 4 ^{o}C to set. The cells/LMP agarose mixture was placed on the pre-coated microscope slides, after removing the 18 x 18 mm cover slips. The gels were covered with new 18 x 18 mm cover slips and left for 10 minutes at 4 ^{o}C. Then the slides were placed in a black staining jar, filled with 200 mL of lysis solution (2.5 M NaCl, 0.1 M EDTA, 10 mM Tris Base, 1% (v/v) Triton X-100, NaOH pH=10) and incubated for 60 minutes at 4 ^{o}C. Slides were placed horizontally in an electrophoresis tank filled with 1.5 L of electrophoresis buffered (0.3 M NaOH, 1mM EDTA, pH 13) that was cooled before use. After 40 minutes incubation at 4 ^{o}C, electrophoresis was carried out at 25 V for 30 minutes at 4 ^{o}C. Then the slides were placed in black staining jars, adding 200 mL neutralising buffer (0.4 M Tris, HCl pH 7.8) on top of them. After three 5-minute washes, the slides were left at 4 ^{o}C until comet scoring.

The quantification of DNA damage was carried out by using DAPI. After removing the cover slips from each slide, 20 μL of DAPI were added on top of the gel and covered with 22 x 22 mm cover slips. One hundred comets per gel were scored using a fluorescence microscope, with scores between 0-4 (0: no damage, 4: maximum damage). The final score per sample ranged between 0 (no damaged cells) to 400 (totally damaged cells).

4.3.5 Statistical Analysis

Three independent experiments were conducted and each experiment was comprised of at least two internal replicates, unless otherwise stated. Data are presented as mean ± SD or ± SEM. Statistical analysis was performed using GraphPad Prism 5.0 software (GraphPad Software, San Diego, CA, USA). Data sets (means ± SD or SEM) were compared using one-way analysis of variance (ANOVA) followed by a Tukey's post-test for pair-wise comparisons. Statistically significant data were detailed when *$p<0.05$, **$p<0.01$, ***$p<0.001$, ***$p<0.0001$.

4.4 Results and Discussion

4.4.1 Cytotoxicity

The level of cytotoxicity induced by BNIPDaCHM, BNIPPiProp, BNIPPiEth and *trans,trans*-BNIPDaCHM in MDA-MB-231 and SKBR-3 cells was assessed by MTT assay (Mosmann, 1983).

Figure 4.4.1a represents the percentage of cell viability in MDA-MB-231 cells after treatment with BNIPDaCHM for 24, 48, 72 and 96 hours (Figure 4.4.1). Similar procedure was followed for all BNIPs in both MDA-MB-231 and SKBR-3 cells line and similar diagrams were obtained.

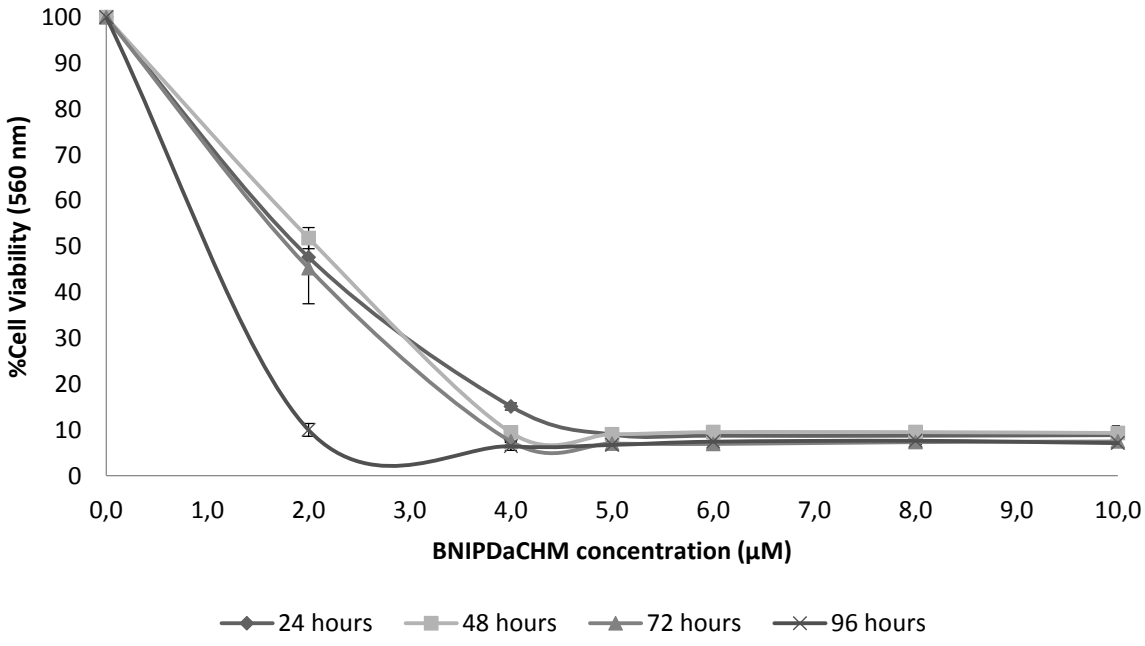

Figure 4.4.1.: The growth inhibition curve of BNIPDaCHM in MDA-MB-231 cells after 24, 48, 72 and 96 hours. Cytotoxicity was determined by MTT Assay. The curves are representative of all BNIP derivatives analysed within MDA-MB-231 and SKBR-3 cells. Data presented as mean ± SEM of 3 independent experiments (n=3).

In addition, the IC_{50} values of the newly synthesised BNIPs were calculated and compared with the previously synthesised parental compound, BNIPDaCHM (Barron *et al*, 2010). The IC_{50} value was defined as the BNIP concentration that causes 50% reduction in cell viability, compared to that of untreated cells. The IC_{50} was calculated according to the most widely used method of calculation as seen in the literature to date (Barron *et al*, 2010). Later, it was suggested that IC_{50} can also be analysed to fit a 4 parameter Hill equation instead of the polynomial analysis used. However, due to the limited range of concentrations tested, the first method of analysis was more applicable for the data observed. This was due to the fact that the 4 parameter Hill equation requires a much wider range of concentrations for a sufficiently accurate calculation of IC_{50} (see Appendix 4).

After 24 hours treatment, all novel BNIPs, exhibited strong cytotoxicity with IC_{50} values ranging from 1.4 μM to 3.3 μM in MDA-MB-231 cells (Table 4.4.1), compared to previously synthesised BNIPs or DNA intercalating drugs (Doxorubicin) that have been tested against the same cell line, with IC_{50} values ranging from 4.9 μM to 12.7 μM (Barron *et al*, 2010). In particular, *trans,trans*-BNIPDaCHM exhibited the lowest IC_{50} value of 1.4 μM, BNIPPiEth an IC_{50} of 1.8 μM and BNIPPiProp an IC_{50} of 3.3 μM, compared to the parental compound. A similar pattern of cytotoxicity was found for SKBR-3 cells, although the IC_{50} values were between 0.2 - 0.7 μM (Table 4.4.1).

trans,trans-BNIPDaCHM (1.4 μM) was more active ($p<0.01$) than BNIPDaCHM (2.3 μM) in MDA-MB-231 cells, showing that the existence of a single isomer in the linker sequence results in a more cytotoxic compound, compared to a compound which contains a mixture of isomers. BNIPPiEth was more cytotoxic ($p<0.05$) than BNIPDaCHM, suggesting that the shorter length of the linker chain,

as well as the incorporation of the nitrogen atom within the cyclohexane ring, not only improved the binding properties of BNIPPiEth, but enhanced significantly its *in vitro* cytotoxicity too. Regarding BNIPPiProp, the derivative with the longest linker sequence and the highest IC_{50} value, it was found that the linker chain length plays an important role in the functionality and effectiveness of a BNIP. In addition, all the derivatives followed a similar pattern of cytotoxicity in both cell lines, however, they appeared more cytotoxic against SKBR-3 cells. This may be due to the different mutational and tumorigenic statuses (Kao *et al*, 2009), as that have been discussed in detail in Section 4.1.2.

Moreover, compared to previously synthetised bisnaphthalimides, the three novel BNIPs exhibited low IC_{50} values in MDA-MB-231 and SKBR-3 cells. More specifically, Amonafide, which significantly inhibits the growth of HT-29, HeLa (cervical cancer cells), and PC3 (prostate cancer) cells, exhibited IC_{50} of 4.67 μM, 2.73 μM, and 6.38 μM, respectively (Brana *et al*, 2004). BNIPOSpm, which has been tested against CaCO-2 (human colon adenocarcinoma cells), HT-29 (human colon adenocarcinoma cells) and MCF-7 cells (human colon adenocarcinoma cells), exhibited IC_{50} values>50 μM (Ralton, 2006, Oliveira *et al,* 2007).

Thus, the structural modifications on the parental compound BNIPDaCHM, successfully improved the cytotoxicity of the three novel BNIPs, not only compared to previous BNIPs but also compared to anti-cancer drugs that are currently used in clinics (e.g. Doxorubicin), making BNIPPiProp, BNIPPiEth and *trans,trans*-BNIPDaCHM promising agents in breast cancer therapy.

Table 4.4.1.: MDA-MB-231 and SKBR-3 cells were treated with different BNIPs concentrations (0-10 µM) for 24 hours at 37 °C.

BNIPs	IC_{50} values (µM) (Mean ± SEM)	
	MDA-MB-231	SKBR-3
BNIPDaCHM	2.3± 0.1	0.4±0.1
BNIPPiProp	3.3± 0.1 **	0.7±0.1 *
BNIPPiEth	1.8±0.1 *	0.3±0.1 *
***trans,trans*-BNIPDaCHM**	1.4± 0.1 **	0.2±0.0 *

*IC_{50} values correspond to the concentration required to reduce cell growth by 50% compared to control cells. Data presented as mean ± SEM of 3 independent experiments (n=3). *p<0.05, **p<0.01, compared to BNIPDaCHM.

4.4.2 ROS levels

Intracellular ROS generation in MDA-MB-231 and SKBR-3 cells was detected using CM-H_2DCFDA dye and ROS positive cells were measured by flow cytometry.

Cells were treated with concentrations corresponding to IC_{25} values of BNIPs, in order to avoid loss of cell population during the assessment of ROS production (Table 4.4.2).

A time-course experiment with treatment times of 4, 8 and 12 hours in MDA-MB-231 (Figure 4.4.2.1a) and SKBR-3 cells (Figure 4.4.2.1b) with one novel compound, BNIPPiProp (higher IC_{25} value) were carried out and revealed that ROS levels in MDA-MB-231 cells were significantly increased after 4 hours treatment compared to untreated cells, but not in SKBR-3 cells ($p<0.01$). However, after 8 hours treatment, ROS production was significantly increased in both cell lines ($p<0.001$), while 12 hour treatment showed a significant increase in ROS levels ($p<0.001$) but to a lower extent, compared to 8 hour treatment. The decrease in ROS that was observed after 12 hours, could be attributed to antioxidant responses and cellular adjustments that BNIP treatment might have triggered in that specific timepoint.

Based on the time-course results, all the compounds were tested after 8 hour treatment in MDA-MB-231 and SKBR-3 cells, in order to compare the levels of intracellular ROS generation between the two different cell lines.

Table 4.4.2.: MDA-MB-231 and SKBR-3 cells were treated with BNIPs (IC_{25} concentrations) for 24 hours at 37 °C.

BNIPs	IC_{25} values (µM) (Mean ± SEM)	
	MDA-MB-231	SKBR-3
BNIPDaCHM	1.00± 0.06	0.2±0.00
BNIPPiProp	1.50± 0.06*	0.5±0.01 **
BNIPPiEth	0.80±0.03	0.15±0.00 **
***trans,trans*-BNIPDaCHM**	1.00± 0.03	0.11±0.01 **

*IC_{25} values correspond to the concentration required to reduce cell viability by 25% compared to control cells. Data presented as mean ± SEM of 3 independent experiments (n=3). *p<0.05, **p<0.01, compared to BNIPDaCHM.

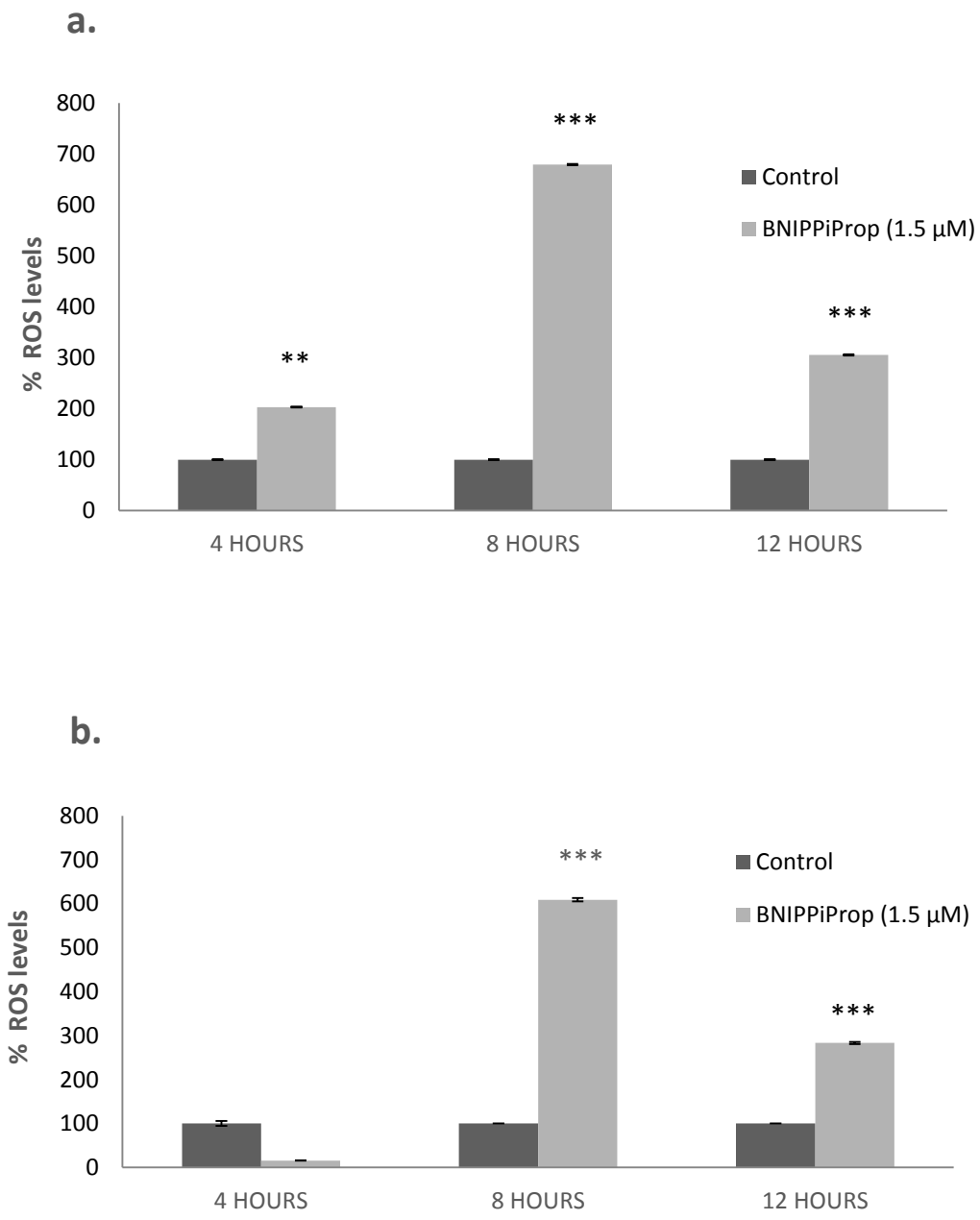

Figure 4.4.2.1.: Quantification of ROS levels by flow cytometry following ROS dye staining after 4, 8 and 12 hours treatment with BNIPPiProp (IC_{25}) in (a) MDA-MB-231 and (b) SKBR-3 cells. DMSO/H_2O was used as positive control. The percentage of ROS production was calculated from FL-1 plots (10,000 events). Data presented as mean ±SD (n=4). **p<0.01, ***p<0.001, compared to untreated MDA-MB-231 and SKBR-3 cells, respectively.

In MDA-MB-231 cells, after 8 hours treatment with BNIPDaCHM, ROS levels were significantly increased by 48.4% ($p<0.05$), compared to control cells (Figure 4.4.2.2a). After treatment with BNIPPiProp, ROS production was significantly increased by 35.1% ($p<0.05$). ROS levels after treatment with BNIPPiEth and *trans,trans*-BNIPDaCHM were increased by 43.2% and 25%, compared to untreated cells, respectively. The above results indicate that the three novel BNIPs and their parental compound BNIPDaCHM, induce the production of endogenous ROS. BNIPDaCHM is the derivative that caused the highest increase of ROS levels in MDA-MB-231 cells, followed by BNIPPiEth, BNIPPiProp and *trans,trans*-BNIPDaCHM was the derivative that cause the lowest increase of ROS levels. Moreover, according to statistical analysis, no significance difference was found in MDA-MB-231 cells after treatment with BNIPDaCHM, BNIPPiProp, BNIPPiEth and *trans,trans*-BNIPDaCHM, compared to each other.

In SKBR-3 cells, after 8 hours treatment with BNIPDaCHM, ROS levels were significantly increased by 362.4% ($p<0.05$) (Figure 4.4.2.2b). After treatment with BNIPPiProp, ROS production was significantly increased by 451.5% ($p<0.05$). ROS levels after treatment with BNIPPiEth and *trans,trans*-BNIPDaCHM were significantly increased by 355.5% ($p<0.05$) and 184.1% ($p<0.05$), compared to untreated cells, respectively. BNIPs were found to induce the production of endogenous ROS in SKBR-3 cells to a greater extend compared to MDA-MB-231 cells.

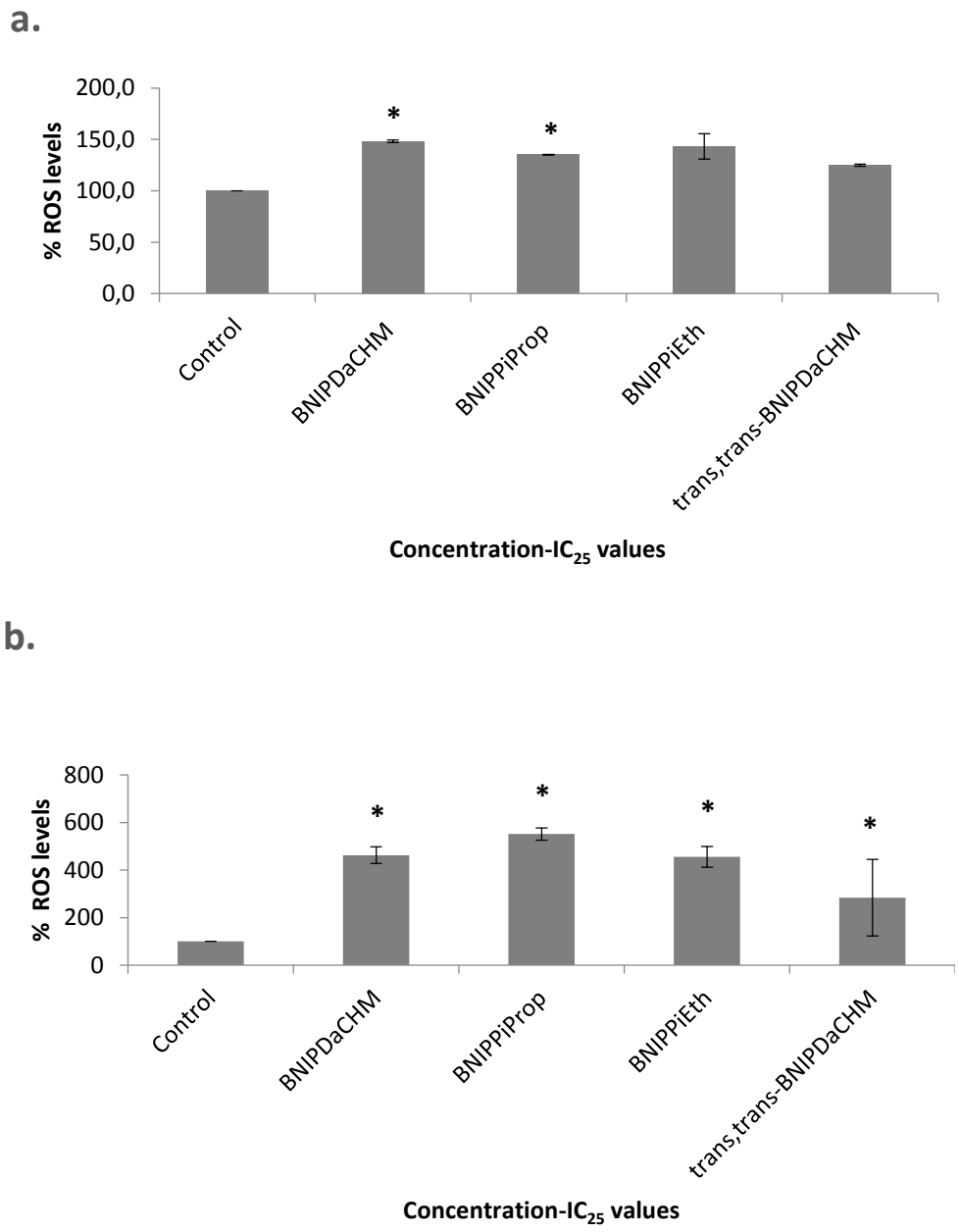

Figure 4.4.2.2.: Quantification of ROS levels by flow cytometry following ROS dye staining after 8 hours treatment with BNIPDaCHM, BNIPPiProp, BNIPPiEth and *trans,trans*-BNIPDaCHM in (a) MDA-MB-231 and (b) SKBR-3 cells, respectively. DMSO/H_2O was used as positive control. The percentage of ROS production was calculated from FL-1 plots (10,000 events). Data presented as mean ±SD (n=3). *p<0.05, compared to untreated MDA-MB-231 and SKBR-3 cells, respectively.

BNIPPiProp is the derivative that caused the highest increase of ROS levels in SKBR-3 cells, followed by BNIPDaCHM, BNIPPiEth, and *trans,trans*-BNIPDaCHM was the derivative that cause the lowest increase of ROS levels. According to statistical analysis, no significance difference was found in SKBR-3 cells after treatment with BNIPDaCHM, BNIPPiProp, BNIPPiEth and *trans,trans*-BNIPDaCHM, compared to each other.

A similar pattern of ROS production was found for MDA-MB-231 and SKBR-3 cells, in relation to treatment with individual BNIPs. However, the increase in ROS levels does not seem to parallel the cytotoxicity values determined by MTT assay after 24 hours (see Section 4.4.1) for each compound in the two cell lines. For example, although *trans,trans*-BNIPDaCHM was the most cytotoxic BNIP derivative in both MDA-MB-231 and SKBR-3 cells compared to BNIPDaCHM, it was not responsible for the highest increase of ROS levels. According to the above results, ROS levels were increased after treatment with BNIPs. Moreover, for less cytotoxic compounds, such as BNIPPiProp compared to *trans,trans*-BNIPDaCHM, higher concentration of compounds was used to achieve IC_{25}, resulting in higher levels of ROS being detected. Moreover, higher BNIP dose treatment in SKBR-3 cells resulted in higher levels of ROS compared to MDA-MB-231 cells. Thus, higher dose treatment seem to be linked with higher ROS level production, as it has been reported in a previous study, where Calu-6 lung cancer cells were treated with different doses of Antimycin A and ROS levels were only induced after treatment with the highest dose (100 μM) (Han and Park, 2009), which was a much higher concentration compared to BNIP treatments tested in this study. Similar studies have been undertaken for anti-cancer drugs that are currently used for breast cancer treatment in the clinic, such as Tamoxifen. Tamoxifen has been also found to promote ROS generation after 4 days treatment (10 μM) in MCF-7 breast cancer

cells (Lee et al, 2014). Thus, BNIPs seem to be promising candidates for breast cancer treatment, as they follow similar mode of action compared to current anti-cancer drugs (e.g. Tamoxifen) and their ability to induce ROS levels increase their potential of being clinically relevant.

The lower production of ROS after treatment with *trans,trans*-BNIPDaCHM compared to the other BNIPs, seem to be linked with the melting points and DNA binding studies that were presented in Chapter 3. The more stable the chemical structure (existence of one isomer) is, the more difficult for the agent to undergo oxidation by electron transfer hydrogen abstraction (Davasagaya *et al,* 2004). As a result, the possible sites of attack for free radical oxidants (Davasagaya *et al,* 2004) and *trans,trans*-BNIPDaCHM are decreased compared to BNIPDaCHM, which may be due to its structure and the existence of three stereoisomers retains its rotational freedom (see Chapter 3).

In addition, SKBR-3 cells (hormone receptor positive) have a better response to BNIP treatments compared to MDA-MB-231 cells, which is in agreement with the cytotoxicity findings. For example, after treatment with concentrations corresponding to IC_{25} values for BNIPs, in SKBR-3 cells an increase of 355.5% in ROS levels after treatment with BNIPPiEth was detected, when for MDA-MB-231 cells the increase was 43.2%. In both cases, it has to be investigated whether the elevated ROS levels after treatment with BNIPs in breast cancer cells induce DNA damage and intracellular DNA stability, as a mechanistic link between these two pathways has not been clearly elucidated.

4.4.3 DNA damage studies

In order to assess DNA damage induced by BNIPs within the two breast cancer cell lines, comet assay was used. Cells were treated with concentrations corresponding to IC_{25} values of BNIPs, in order to avoid loss of cell population during the assessment of DNA damage (similarly as in ROS levels detection in Section 4.4.2).

BNIPs induced a significant increase in DNA strand breaks compared to endogenous levels, after 24 hours treatment in MDA-MB-231 and SKBR-3 cells. In MDA-MB-231 cells (Figure 4.4.3a), significant change in the number of DNA strand breaks was observed for all BNIPs. In particular, BNIPDaCHM caused an increase of 221.9 ($p<0.0001$) strand breaks compared to untreated cells, BNIPPiProp an increase of 262.8 ($p<0.0001$) strand breaks, BNIPPiEth an increase of 250.8 ($p<0.0001$) strand breaks and *trans,trans*-BNIPDaCHM an increase of 205.0 ($p<0.0001$) strand breaks. H_2O_2 was used as a positive control and after 10 minutes treatment (200 μM concentration), significantly increased the DNA strand breaks by 326.7 ($p<0.0001$). Moreover, BNIPPiEth and *trans,trans*-BNIPDaCHM caused an increase in strand breaks compared to BNIPDaCHM. However, according to statistical analysis, no significance difference in the number of DNA strand breaks was found in MDA-MB-231 cells after treatment with BNIPPiEth and *trans,trans*-BNIPDaCHM, compared to BNIPDaCHM.

In SKBR-3 cells (Figure 4.4.3b), significant changes in the number of DNA strand breaks were observed for all BNIPs. In particular, BNIPDaCHM caused an increase of 98.4 ($p<0.0001$) strand breaks compared to untreated cells, BNIPPiProp an increase of 97.3 ($p<0.0001$) strand breaks, BNIPPiEth an increase of 176.1 ($p<0.0001$) strand breaks and *trans,trans*-BNIPDaCHM an increase of 130.0 ($p<0.0001$) strand breaks. Moreover, after 10 minutes treatment with 200 μM

H_2O_2 (used as a positive control), significantly increased the DNA strand breaks by 308.0 ($p<0.0001$). BNIPPiProp, BNIPPiEth and *trans,trans*-BNIPDaCHM caused a significant increase in strand breaks compared to BNIPDaCHM ($p<0.0001$) in SKBR-3 cells. According to statistical analysis, significance difference in the number of DNA strand breaks was found in SKBR-3 cells after treatment with BNIPPiProp, BNIPPiEth and *trans,trans*-BNIPDaCHM, compared to BNIPDaCHM ($p<0.0001$), similarly to MDA-MB-231 cells.

The above results indicate that all BNIPs induced DNA damage in MDA-MB-231 cells and with regard to BNIPDaCHM (parental compound), this study is in agreement with the findings of Barron *et al*. (2015). In MDA-MB-231 cells, BNIPPiProp induced a greater level of DNA strand breaks compared to endogenous levels, followed by BNIPPiEth, BNIPDaCHM and *trans,trans*-BNIPDaCHM. In SKBR-3 cells, BNIPPiEth induced a greater level of DNA strand breaks compared to endogenous levels and BNIPDaCHM, followed by *trans,trans*-BNIPDaCHM, BNIPDaCHM and BNIPPiProp.

Interestingly, a higher number of DNA strand breaks after treatment with BNIPs was observed in MDA-MB-231 cells, compared to SKBR-3 cells. MDA-MB-231 cells were found to be more susceptible to DNA instability after treatment with BNIPs, which appears to relate to different proliferation index rates between the two cells lines. As mentioned in Section 4.4.1, the proliferation index rate among the two cell lines differs: MDA-MB-231 cells proliferate at a 49.5% rate and SKBR-3 cells at 35.2% (Kenny *et al*, 2007). Thus, the faster the cells proliferate, the higher the DNA damage is caused over time. In this study, BNIPPiEth seem to be the best candidate out of the three novel compounds. BNIPPiEth was found to be the second most cytotoxic compound in MDA-MB-231 cells and SKBR-3 cells (after

trans,trans-BNIPDaCHM), a highly ROS-inducing compound (Section 4.4.2) and a strong intercalating BNIP (Chapter 3).

The above characteristics are in agreement with the findings observed in DNA damage studies. In addition, an important factor that may induce the DNA damage potential of BNIPPiEth is its structure. BNIPPiEth is the smallest molecule of all BNIPs and it seems that a short linker sequence enhances its activity (better cytotoxicity, more DNA strand breaks).

Similar studies have been undertaken for anti-cancer drugs that are currently used for breast cancer treatment in the clinic, such as Doxorubicin. The latter, a first-line chemotherapeutic for breast cancer, has been also found to induce DNA damage in triple-negative breast cancer cells (Staedler *et al*, 2011). However, Doxorubicin is associated with severe side effects to non-tumoral tissues, due to high dose treatments (10-50 mg per week) (Staedler *et al*, 2011). The induction of DNA damage is an additional similar mode of action between BNIPs and current anti-cancer drugs (e.g. Doxorubicin), suggesting their potential of being clinically relevant as novel breast cancer treatment. In Section 4.1.1, BNIPs were found to exhibit strong cytotoxicity (IC_{50} values ranging from 1.4 μM to 3.3 μM) compared to Doxorubicin (IC_{50} values ranging from 4.9 μM to 12.7 μM) in MDA-MB-231 cells, which suggests that lower dose treatments of BNIPs could be potentially more effective compared to Doxorubicin treatment within breast cancer patients, especially in case that BNIP treatment would not be accompanied by severe side effects as well.

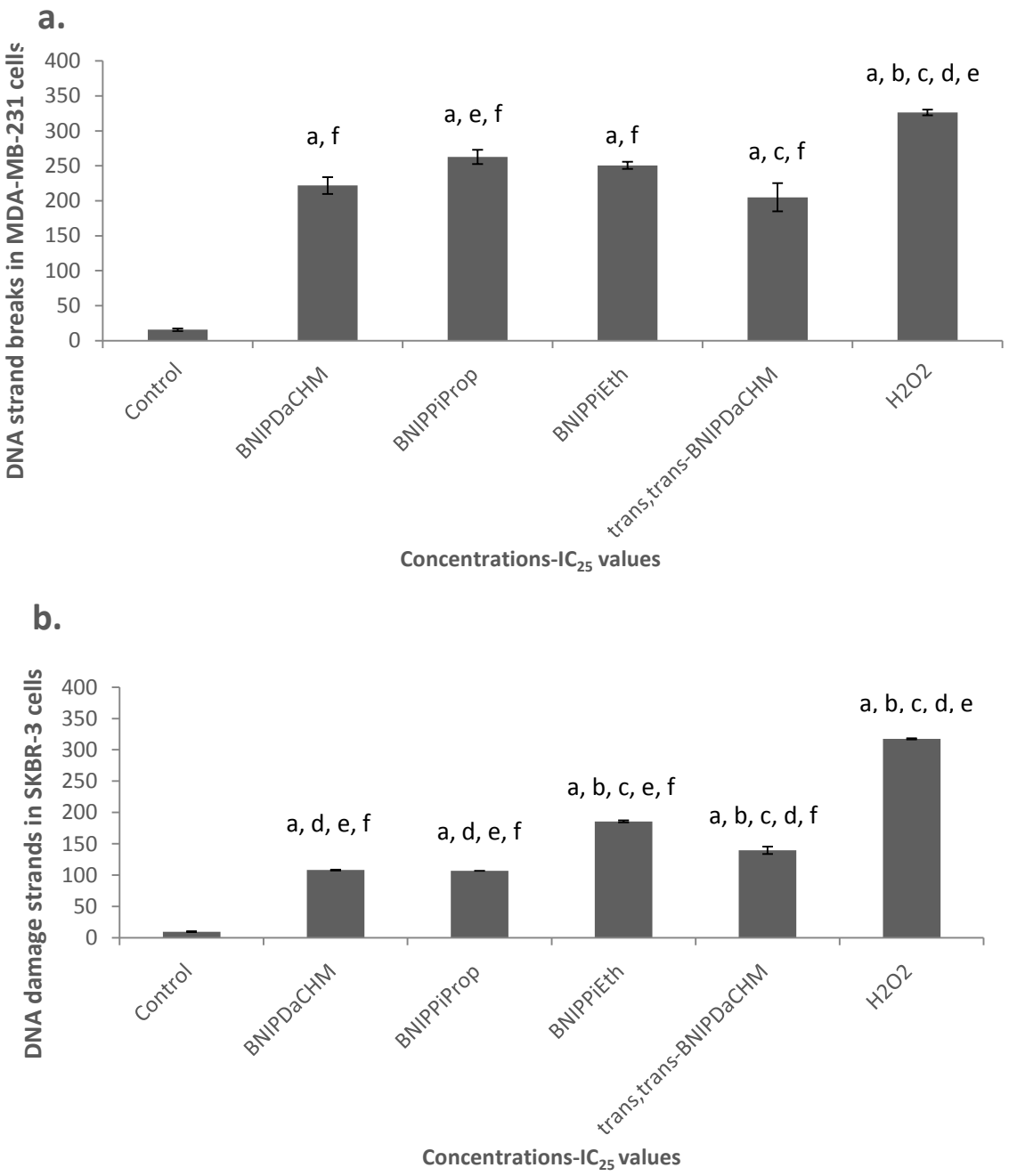

Figure 4.4.3.: DNA strand breaks in (a) MDA-MB-231 and (b) SKBR-3 cells after 24 hours treatment determined by comet assay. Data obtained after treating MDA-MB-231 and SKBR-3 cells with BNIPs (IC_{25}) for 24 hours. DNA damage in H_2O_2 (200 µM) treated cells were used as a positive control. Data are mean ± SEM of 8 replicates and two independent experiment (n = 2). A p-value of <0.05 was considered statistically significant and it is represent by different letters: a; compared to the control, b; compared to BNIPDaCHM, c; compared to BNIPPiProp, d; compared to BNIPPiEth, e; compared to *trans,trans*-BNIPDaCHM and f; compared to H_2O_2.

4.5 Conclusion

The three novel BNIPs, BNIPPiProp, BNIPPiEth and *trans,trans*-BNIPDaCHM and their parental compound, BNIPDaCHM, were screened for biological activity in breast cancer MDA-MB-231 and SKBR-3 cells (Figure 4.5). After 24 hours treatment, all novel BNIPs exhibited strong cytotoxicity with IC_{50} values ranging from 1.4 μM to 3.3 μM in MDA-MB-231 cells and 0.2 - 0.7 μM in SKBR-3 cells, confirming the importance of bisnaphthalimidopropyl functionality. More specifically, linker sequence modifications showed stronger cytotoxic effects against MDA-MB-231 and SKBR-3 cells, compared to the parental compound BNIPDaCHM. The lower IC_{50} value range shows that SKBR-3 cells are more susceptible to BNIP treatment, compared to MDA-MB-231 (triple negative breast cancer cells).

BNIPDaCHM was the derivative that caused the highest increase of ROS levels in MDA-MB-231 cells, followed by BNIPPiEth, BNIPPiProp and *trans,trans*-BNIPDaCHM was the derivative that caused the lowest increase of ROS levels. In SKBR-3 cells, BNIPPiProp caused the highest increase of ROS levels, followed by BNIPDaCHM, BNIPPiEth, and *trans,trans*-BNIPDaCHM was the derivative that caused the lowest increase of ROS levels, showing that BNIPs induce the production of endogenous ROS in SKBR-3 cells in a greater extent compared to MDA-MB-231 cells.

DNA damage studies revealed that BNIPs induced a significant increase in DNA strand breaks compared to endogenous levels, after 24 hours treatment in MDA-MB-231 and SKBR-3 cells. Higher number of DNA strand breaks after treatment with BNIPs was observed in MDA-MB-231 cells, compared to SKBR-3 cells. BNIPPiEth and BNIPPiProp were the BNIP candidates with the highest DNA damage potential in MDA-MB-231 and SKBR-3 cells lines, respectively.

The above findings suggest a potential of BNIPs being clinically relevant as novel breast cancer treatment, as they combine similar modes of action (e.g. ROS production, DNA damage) of current drugs used in clinics (such as Tamoxifen and Doxorubicin) in lower dose treatments that could potentially reduce the occurrence of severe side effects in patients.

In Chapter 5, BNIPs will be investigated further in order to assess their impact on cell cycle distribution and their mode of cell death.

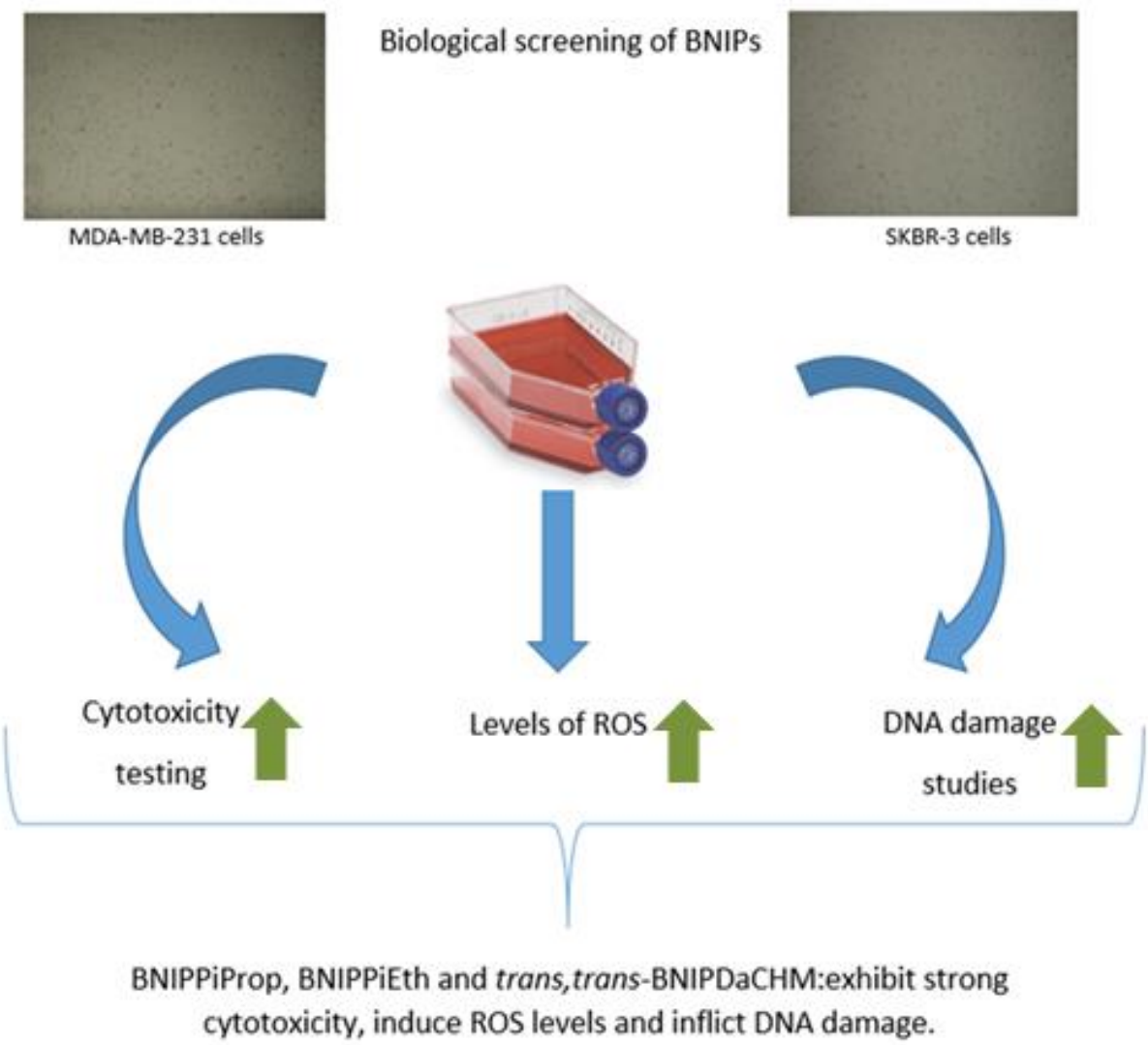

Figure 4.5.: Summary of cytotoxicity, ROS levels and DNA damage studies.

CHAPTER 5

Effect of novel bisnaphthalimidopropyl derivatives on cell cycle distribution and cell death

5.1 Introduction

5.1.1 Cell cycle and cancer

Cell cycle is a series of coordinated events that control DNA replication and division of a cell (Kastan and Bartek, 2004). Cell cycle progression consists of four phases: Gap phase 1 (G1), DNA synthesis (S), Gap 2 phase (G2 or interphase) and mitosis (M) (Figure 5.1.1) (Meeran and Katiyar, 2008). G1 and G2 phases are intervals of growth and reorganisation. Once cells stop cycling after their division, they enter a state of quiescence, also known as G0 (Dhawan and Laxman, 2015).

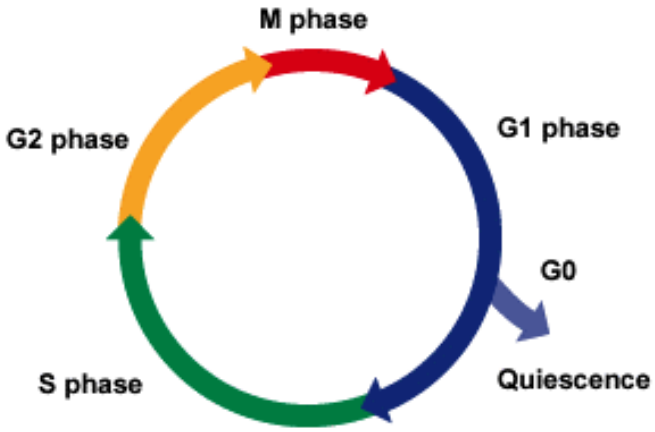

Figure 5.1.1.: Schematic representation of the cell cycle (Adapted from: The Biology Project- University of Arizona).

The above series of events are controlled by two types of cell cycle control mechanisms: (i) a set of checkpoints that monitors the successful completion of each phase and (ii) a cascade of proteins (cyclins) that regulate the cell transition from one stage to the next (Rao and Johnson, 1970, Murray, 1991, Murray, 1994). There are three main checkpoints that control cell cycle progression: the G1 checkpoint (between the G1-S transition), the G2 checkpoint (between the G2-M

transition) and the spindle checkpoint (during the anaphase where replicated chromosomes divide and daughter chromatids move to opposite poles) (Kastan and Bartek, 2004).

The second type of cell cycle control is regulation by cyclin/cyclin dependent kinase complexes (CDKs) (Grana and Reddy, 1995, Michalides, 1999). CDKs are formed and activated during the several stages of cell division and are mainly involved in DNA synthesis and mitosis (Hartwell and Kastan, 1994). CDKs consist of a catalytic domain that is not active when monomeric and unphosphorylated (Malumbres and Barbacid, 2001). Once CDKs are associated with a cyclin partner, they form heterodimeric complexes that are activated after phosphorylation/dephosphorylation of specific residues (for example, cyclins A1 and B2 interact and activate CDK1). However, CDK activity can be dysregulated by CDK inhibitors (CDKIs), leading to cell cycle arrest in response to cell cycle checkpoint machinery (Malumbres and Barbacid, 2004). Such an example is the dysregulation of the cyclin D1:CDK4/6 complex which is associated to different types of breast cancer, as according to Arnold *et al.* (2005), cyclin D1 is overexpressed in human tumours.

Alterations to the controlled and successful progression of the cell cycle can result in inappropriate cell proliferation and in an increase in genomic instability, leading to the development of diseases, such as cancer (Sherr and Roberts, 2004). Therefore, it is important to understand cell cycle in cancer research, as this would allow researchers to synthesise drugs that would attack cancer cells in particular phases (G1, S, G2) of the cell cycle and become more effective than radiotherapy, the latter targeting only cells that undergo cell division (M phase).

In this study, cell cycle distribution by quantitation of DNA content was assessed by flow cytometry following staining with propidium iodide (PI). PI is a DNA

intercalator and fluorescent molecule that binds to DNA, after the loss of plasma membrane integrity (Nicoletti *et al*, 1991). DNA content is proportional to the amount of PI bound to DNA thus, indicating the percentage of cells in each phase of the cell cycle. For example, in G1 phase the DNA content is 2n (diploid), DNA content doubles to 4n in S phase and remains at 4n during G2 phase (Crowley *et al*, 2016). When the DNA content is less than 2n, cells belong to the sub-G1 population, which is a hallmark of apoptotic cells (low DNA content) (Crowley *et al*, 2016).

5.1.2 Cell death and cancer

One of the most widely-studied area in cancer research is cell death, particularly apoptosis. The main reason is that better understanding of apoptotic mechanisms can give insights into the pathogenesis of cancer or clues about its treatment (Merkle, 2009).

Apoptosis is a biological phenomenon that was first discovered back in 70's, by Kerr *et al.* (1972). Apoptosis is derived from the Ancient Greek ἀπόπτωσις, which means "falling off" (Kerr *et al,* 1972). Nowadays, apoptosis is defined as a programmed sequence of events that eliminate cells that are a threat or no longer needed by a tightly regulated process of cell suicide process. At a morphological level apoptosis involves rounding-up of the cell, cell shrinkage, reduction of cellular volume (pyknosis), chromatin condensation, nuclear fragmentation, plasma membrane and cytoplasmic blebbing, and engulfment by resident phagocytes (Figure 5.1.2.1) (Krysco *et al*, 2008).

Apart from the morphological alterations that affect both the nucleus and cytoplasm, apoptosis is regulated by several pathways and biochemical mediators (Hacker, 2000). Caspases are central to the mechanism of apoptosis and can get

activated through the intrinsic (or mitochondrial) pathway (activation of pro-apoptotic proteins, such as Bax, Bak, Bad, Bcl-Xs, Bid, and anti-apoptotic proteins, such as Bcl-2, Bcl-XL, Bcl-W), the extrinsic (or death receptor) pathway (activation of death receptors, such as TNF, CD95 and DISC complex), or the intrinsic endoplasmic reticulum pathway (Youle and Strasser, 2008).

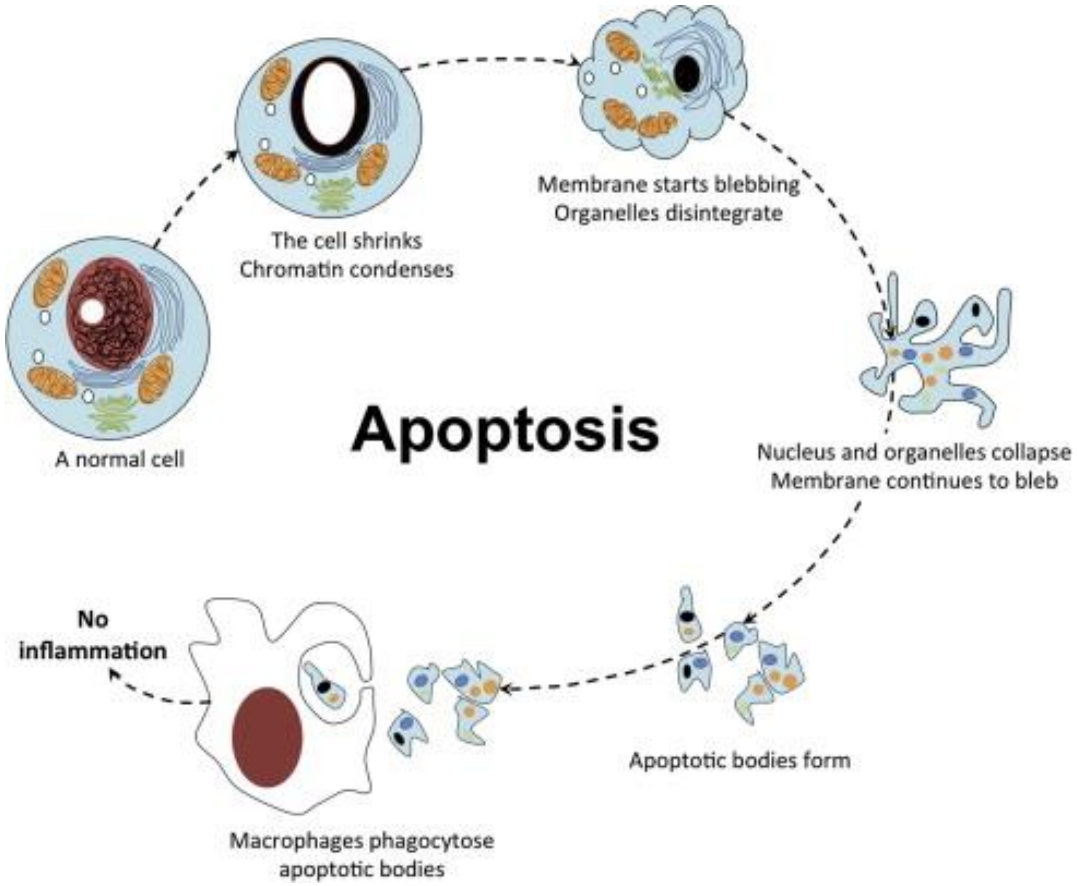

Figure 5.1.2.1.: Cytology of apoptosis (From: Abou-Ghali and Stiban, 2015).

Numerous methods have been developed in order to assess apoptotic cell death. These methods are based on major cell death parameters, such as morphology (time-lapse microscopy, flow cytometry and transmission electron microscopy), cell surface markers phosphatidylserine (PS) exposure *versus* membrane

permeability by flow cytometry), intracellular markers (oligonucleosomal DNA fragmentation, caspase activation, cytochrome c release or Bid cleavage) and extracellular markers in the supernatant (release of cytokeratin 18) (Krysco *et al*, 2008).

In this study, Annexin V-FITC/7-AAD staining, detected by flow cytometry, was used to study apoptosis in MDA-MB-231 and SKBR-3 breast cancer cells. Translocation of membrane PS from the inner side to the surface of the plasma membrane is one of the earliest events of apoptosis (Koopman *et al,* 1994). Annexin V, which is a Ca^{2+}-dependent phospholipid-binding protein conjugated to fluorescein isothiocyanate, binds to PS residues reversibly, serving as a sensitive probe for flow cytometry analysis of cells undergoing apoptosis (Figure 5.1.2.2). On the other hand, 7-AAD is a fluorescent dye that labels cells that have lost their plasma membrane integrity (necrotic cells) (Koopman *et al*, 1994, Van Engeland *et al*, 1998).

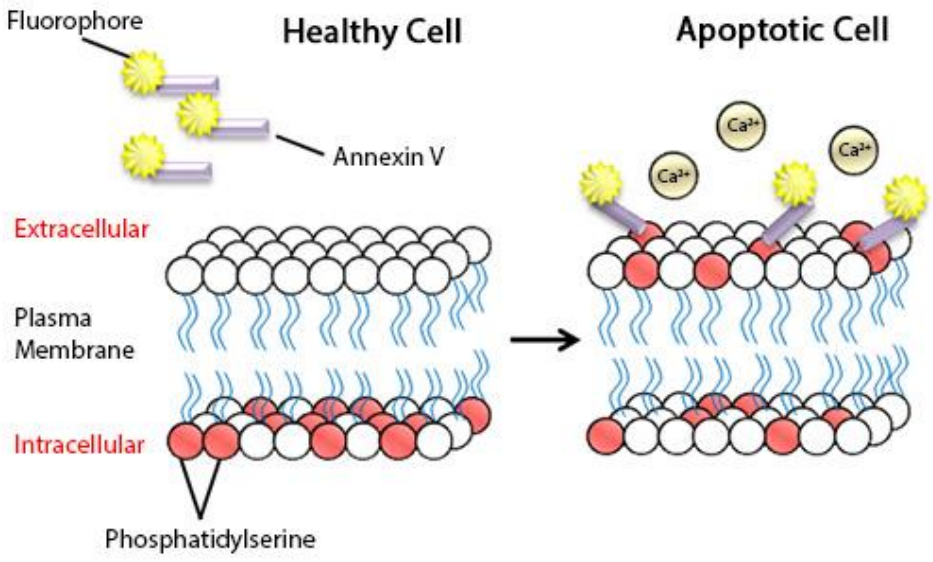

Figure 5.1.2.2.: Translocation of membrane PS from the inner side to the surface of the plasma membrane in apoptotic cell (BioLegend, www.biolegend.com)**.**

5.1.3 Crosstalk between cell death machineries

Several studies have shown that in some cases, apoptotic signalling pathways can trigger more than one mode of cell death (Fiers *et al*, 1999). More specifically, a functional relationship between apoptosis (self-killing) and autophagy has been reported (Nikoletopoulou *et al*, 2013), showing that the two machineries share common pathways and that crosstalk between them exists.

Autophagy (from the Ancient Greek αὐτόφαγος, meaning "self-devouring") is a cytoprotective process that allows the degradation and recycling of unnecessary or dysfunctional components (Suman *et al*, 2014). More specifically, autophagy is involved in removing misfolded proteins, damaged organelles, (mitochondria, peroxisomes, endoplasmic reticulum) and intracellular pathogens (Suman et al, 2014). Recent studies have also shown that autophagy promotes cancer cell survival, by protecting cancer cells from starvation, oxidative stress or hypoxia and causing tumour chemoresistance (Kroemer and Jaattela, 2005). For example, autophagy-mediated chemoresistance has been reported in colon and lung cancer cells after treatment with cisplatin and breast cancer cells after treatment with camptothecin (Li *et al*, 2010, Ren *et al*, 2010, Abedin *et al*, 2007). On the other hand, after treatment with temozolomide and dexamethasone anti-cancer agents autophagy is induced, promoting growth arrest in cancer cells (Kanzawa *et al*, 2004, Laane *et al*, 2009). However, although the role of autophagy in cancer seems to be pivotal, the mechanism that dictates autophagy-mediated cell death/survival and its interaction with other cell death machineries is unknown.

Recently, caspases were found to participate as crosstalk regulators between autophagy and apoptosis (Wu *et al,* 2014), acting either as initiators or effectors that are involved in apoptotic cascades (Figure 5.1.3). For example, several pro-apoptotic pathways induce caspases to trigger apoptosis, but in parallel, some of

the activated caspases break down or cleave critical autophagic proteins, like Beclin-1 and inactivate autophagic functions (Matsuzawa *et al*, 2015, Pagliarini *et al*, 2012).

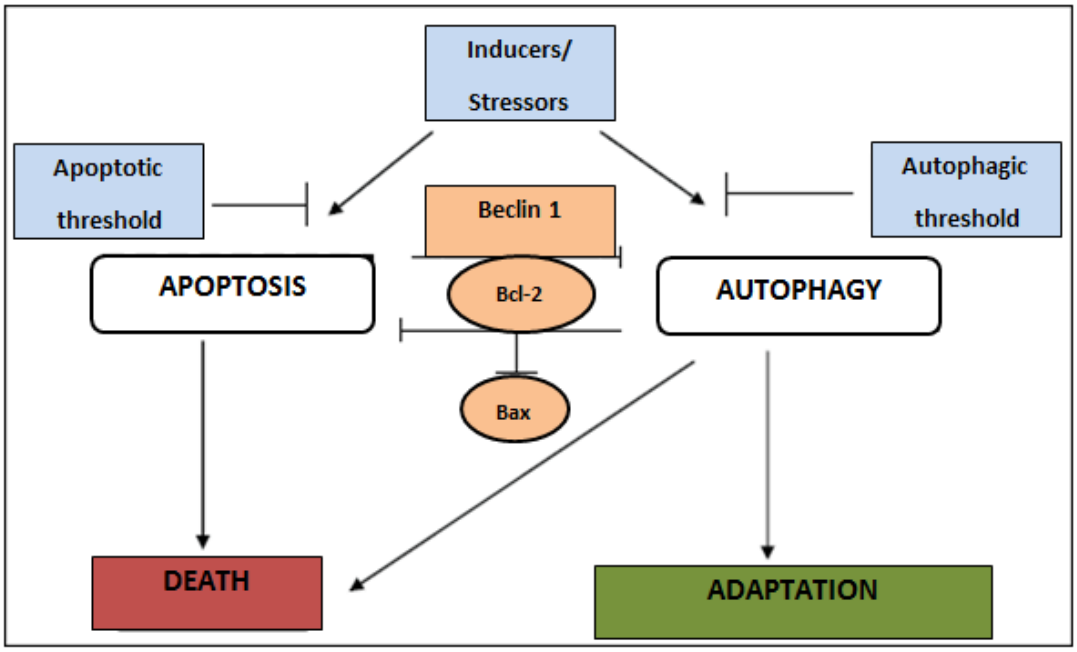

Figure 5.1.3.: The relationship between apoptosis and autophagy.

Recent findings have revealed that there is a differential activation of caspases among several types of cancer and they seem to trigger specific modes of cell death. For example, in the absence of Caspase-2 activity in mice neurons, apoptosis cannot occur, while autophagy is activated (Dorstyn and Kumar, 2009). In addition, Karna *et al* (2010) found the tubulin-binding noscapine analogue Red-Br-nos to induce autophagy followed by caspase-independent apoptotic cell death (CICD) in human prostate cancer PC-3 cells (Tait and Green, 2008).

The above findings suggest that further research on the multiple molecular mechanisms that coordinate autophagy and apoptosis or the role of proteins

involved in this crosstalk in cancer would be beneficial for the rational design of successful anti-cancer therapeutics.

In this study, induction of apoptosis was assessed *via* a Caspase-3 activity colourimetric assay. Caspase-3 is an effector caspase that is associated with the initiation of the "death cascade" (Porter and Janickle, 1999). Thus, Caspase-3 has been considered as an important marker of a cell's entry into the apoptotic signalling pathway. In addition, Caspase-3 is activated by the upstream Caspase-8 and Caspase-9 and is involved in different signalling pathways (Doonan *et al*, 2003). Therefore, measurement of its activity is well suited as a read-out in an apoptosis assay. Furthermore, autophagy as a potential mode of cell death was also investigated *via* an autophagy microplate assay.

5.1.4 Aims

In cancer research, drug discovery in the pharmaceutical industry has focused into targeting molecular mechanisms (linked to cell cycle and cell death) in order to disrupt their pathways. This approach has led to the development of cell cycle-based, mechanism-targeted cancer therapies that mimic the natural processes of the human organism in order to inhibit cancer cell proliferation, by inducing cell cycle arrest. Flavopiridol and Silibinin are two examples of anti-cancer drugs that target CDK activation and cause cell cycle arrest, resulting in growth inhibition and apoptosis in cancer cells (Deep and Agarwal, 2012). Therefore, as a consequence of their ability to intercalate with DNA and cause DNA strand breaks, it was crucial to investigate whether the novel BNIPs have the potential to induce cell cycle arrest and apoptotic cell death.

The aim of the work presented in Chapter 5 was to assess the ability of novel BNIPs to induce cell death. The objectives of the experimental work was to determine the effect of BNIPDaCHM, BNIPPiProp, BNIPPiEth and *trans,trans*-BNIPDaCHM on the cell cycle distribution and inducement of apoptosis (i.e. Caspase 3) or autophagy in breast cancer MDA-MB-231 and SKBR-3 cells.

5.2 Materials

A list of reagents that were used for cell cycle, Annexin V- FITC/7-AAD, Caspase 3 and autophagy studies are presented below. All reagents were handled according to the COSHH standards and were used without purification.

5.2.1 Cell cycle analysis/ propidium iodide (PI) staining

Disodium phosphate	Sigma-Aldrich, UK
Citric acid	Sigma-Aldrich, UK
Ribonuclease A	Sigma-Aldrich, UK
Propidium iodide	Sigma-Aldrich, UK

5.2.2 Annexin V-FITC/7-AAD Staining

Annexin V-FITC	
Kit System for Detection of Apoptosis	Beckman Coulter, UK

5.2.3 Caspase-3 colourimetric assay

Caspase 3 colourimetric assay kit	R&D Systems Inc., UK

5.2.4 Autophagy microplate assay

CYTO-ID Autophagy Detection Kit	Enzo, UK

5.2.5 Instrumentation

ALC Multispeed Refrigerated Centrifuge	Thomson Scientific, UK
Coulter Epics XL-MCL flow cytometer	Beckman Coulter, UK
96-well plate reader	Synergy/HT, BIOTEK

5.3 Methods

5.3.1 Cell cycle analysis

MDA-MB-231 and SKBR-3 cells (1 x 10^6 cells/T25 flask) were washed twice with PBS and serum free medium was added in order to achieve cell synchrony (Langan and Chou, 2011). The cells were incubated in serum free medium for 24 hours. BNIPs (IC_{25} concentrations) were then added and the cells were incubated for a further 24 hours, at 37 °C. The medium was removed and collected. The cells were washed twice with PBS (2 mL). Both washes were collected and the cells trypsinised, mixed with the collected washes and centrifuged at 500 x*g* for 5 minutes at 4 °C. The supernatant was discarded, the pellet resuspended in PBS (1 mL) and centrifuged as before, the supernatant was discarded again and the pellet resuspended in PBS (100 µL). To fix the cells, 70% (v/v) ice-cold ethanol (900 µL) was added and samples incubated for 2 hours at -20 °C. The cells were centrifuged at 3,000 *xg* for 5 minutes at 4 °C, the supernatant was discarded, the pellet resuspended in PBS (500 µL) and DNA extraction buffer (0.2 M Na_2HPO_4, 4 mM citric acid, pH 7.8, 500 µL) and incubated for 5 minutes at room temperature. The samples were centrifuged at 500 *xg* for 5 minutes at 4 °C, the supernatant removed and the pellets resuspended in DNA staining solution (0.2 mg/mL Ribonuclease A (DNAse-free) and 20 µg/mL PI in PBS). The samples were incubated for 30 minutes at 4°C in the dark and examined by flow cytometry. For cell cycle analysis, EXPO32 ADC analysis software was used to record and analyse 10,000 single events. The percentage of cells with DNA content in sub-G1, G1, S and G2/M phases was calculated from histograms of linear FL-2 plots (575 nm) in the gated region (Figure 5.3.1).

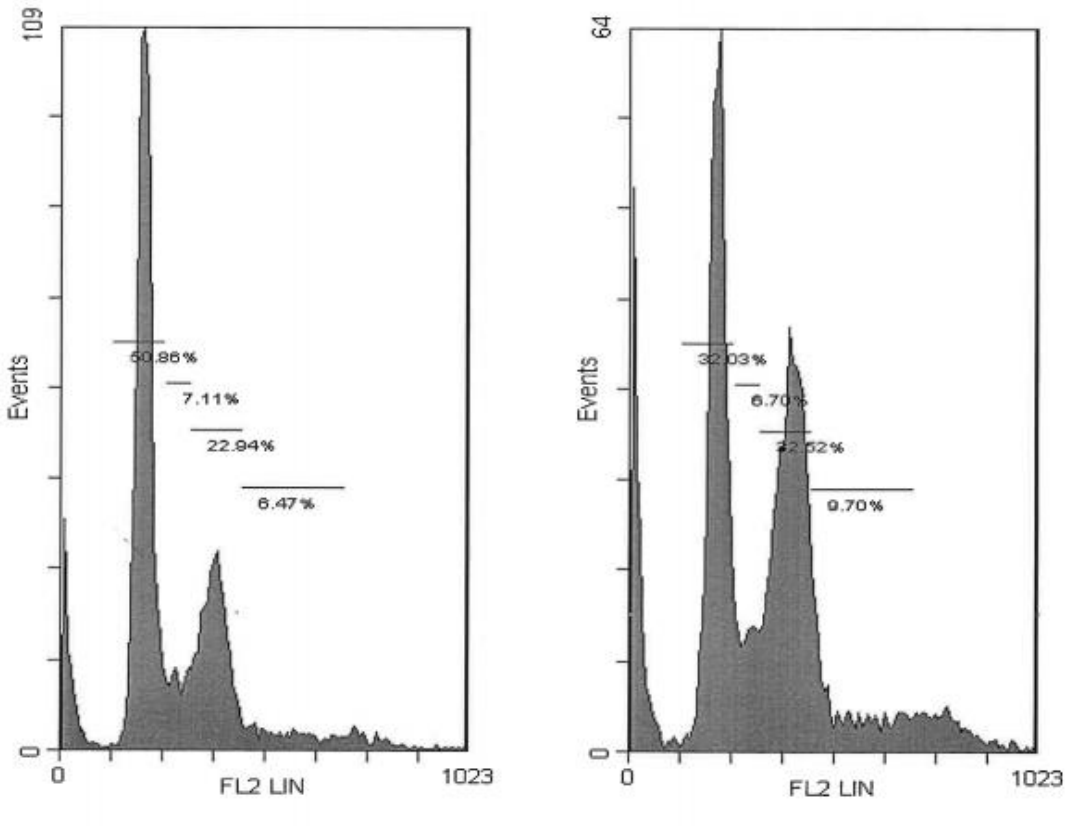

Figure 5.3.1.: Cell cycle distribution of MDA-MB-231 cells before (left) and after 24 hours treatment with BNIPDaCHM IC_{25} (right). Cells were stained with PI and analysed by flow cytometry (10,000 events were recorded). Line markers indicate the regions of the cell cycle: sub-G1, G1, S and G2/M phases (left-right). Images are representative of the results obtained using EXPO32 ADC analysis software.

In cell cycle analysis, doublet exclusion ensures the count of single cells and the exclusion of cell doublets. Doublets can be discriminated by using two parameter measurements plotting pulsed-height (FL-H) against pulsed-area (FL-A), which is not available in every instrument though (Coulter Epics XL-MCL flow cytometer).

Doublets form when cells in close proximity are identified by the flow cytometer as a single event (eg. cell coincidence or clumping during data acquisition). As a result, a doublet may be falsely identified as a single tetraploid cell in G2/M-phase (Nunez, 2001). If a sample contains many doublets, which could mistakenly increase the relative number of cells in the G2/M-phase of the cell cycle, yielding to an overestimation of G2/M population (Nunez, 2001). Thus, the above

statement confirms that there is no chance of having cell doublets in any other phase of the cell cycle apart from G2/M. In the cell cycle studies presented in this Chapter, there is no indication of increase in G2/M phase after treatment with BNIPs in MDA-MB-231 and SKBR-3 cells, after repeating 4 independent experiments.

5.3.2 Annexin V-FITC/7-AAD Staining

MDA-MB-231 and SKBR-3 cells (16 x 10^4 cells/2 mL/12-well plate) were seeded and incubated for 24 hours, at 37 °C. BNIPs (IC_{25} concentrations) were added and after the desired incubation time (0.5, 4 or 6 hours at 37 °C), medium containing BNIPs was removed and discarded. Cells were washed twice with ice-cold PBS, collected after trypsinisation and centrifuged at 300 *xg* for 5 minutes at 4 °C. The supernatant was discarded, pellet resuspended in 100 µL of ice-cold Binding Buffer (1x in dH_2O), containing 10 µL Annexin V-FITC solution and 20 µL 7-AAD viability dye. The solutions were mixed gently and incubated on ice for 15 minutes in the dark. After the required incubation time, 400 µL of ice-cold Binding Buffer (1x in dH_2O) was added. Annexin V-FITC and 7-AAD stained cell samples were analysed within 30 minutes by flow cytometry. For apoptosis analysis, 10,000 single events were recorded and analysed using the FL-1 (525 nm) channel for Annexin V-FITC detection and the FL-4 (675 nm) channel for detection of 7-AAD fluorescence. The percentage of apoptotic and necrotic cells was gated on the respective histogram plots LOG FL-1 and LOG FL-4 (Figure 5.3.2). Formaldehyde (3%) was used as positive control to achieve maximal apoptotic cell death after 30 minutes (Barron *et al*, 2015).

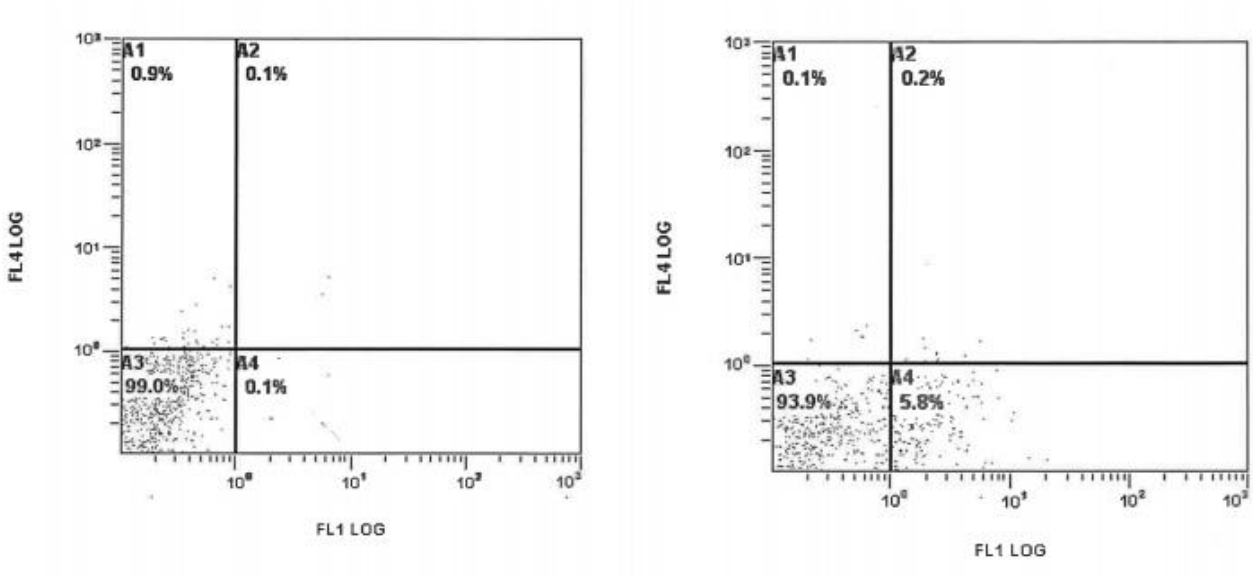

Figure 5.3.2.: Apoptotic (A4) and necrotic distribution (A2) of MDA-MB-231 cells before (left) and after 0.5 hour treatment with BNIPDaCHM IC_{25} (right). Cells were stained with annexin V-FITC/7-AAD and analysed by flow cytometry (10,000 events were recorded). Images are representative of the results obtained using EXPO32 ADC analysis software.

Caspase activity was measured using the manufacturer's protocol. The principle of the assay was to test the protease activity in the cell lysate by the addition of a Caspase 3-specific peptide that is conjugated to a colour reporter molecule (p nitroaniline) (pNA). The cleavage of the peptide by Caspase-3 releases the chromophore, which can be quantitated spectrophotometrically at a wavelength of 405 nm.

5.3.3 Caspase-3 Colourimetric assay

MDA-MB-231 and SKBR-3 cells (1 x 10^6 cells/T25 flask) were seeded and incubated for 24 hours, at 37°C. BNIPs (IC_{25} concentrations) were added. After 24 hour incubation time, medium containing BNIPs was removed and discarded. Cells were washed twice with ice-cold PBS, collected and centrifuged at 500 *xg* for 5 minutes at 4°C. The supernatant was discarded and the cell pellet was lysed by the addition of cold Lysis buffer (25 µL). The cell lysate was incubated on ice for 10 minutes and then centrifuged at 10,000 *xg* for 1 minute. The supernatants were transferred to Eppendorf tubes and kept on ice. The protein content was then quantified by protein assay (BCA Protein Assay).

In a 96-well flat bottom microplate, 50 µL of control or sample (i.e. BNIPs treated), 50 µL of 2X Reaction Buffer 3 and 5 µL of Caspase-3 colourimetric substrate (DEVD-pNA) was added per well. The plate was then incubated for 2 hours at 37 °C. Caspase-3 absorbance was measured with a microplate reader at 430 nm.

5.3.4 Autophagy microplate assay

Autophagy flux was determined using a Cyto-ID autophagy detection kit according to the manufacturer's instructions. The principle of the assay was to test the autophagic activity at the cellular level after treatment with BNIPs. The green fluorescent detection reagent supplied in the kit becomes brightly fluorescent in vesicles produced during autophagy and can be quantitated spectrophotometrically at a wavelength of 488 nm. An increase in the green autophagy signal is proportional to the accumulation of the probe within autophagic vesicles. Moreover, Rapamycin, an inducer of autophagy and Chloroquine, a lysosomal inhibitor, were also tested within the assay at concentrations suggested by the manufacturers.

MDA-MB-231 and SKBR-3 cells (7.5×10^3 cells/well) were seeded and incubated for 24 hours in a 96-well plate, at 37°C. BNIP derivatives (IC_{25} concentrations for 24 hours), Rapamycin (0.5 µM), Chloroquine (10 µM) and negative control were added. After treatment, the medium was carefully removed and discarded. Cells were washed with 1X Assay Buffer (100 µL) and dual colour detection solution was added in each well (100 µL). The plate was incubated in the dark for 30 minutes at 37°C. Cells were washed twice with 1X Assay Buffer (200 µL) to remove excess dye and then fresh 1X Assay Buffer (100 µL) was added in each well. The CYTO-ID Green detection reagent was read with a FITC filter (Excitation 480 nm, Emission 530 nm) and the Hoechst 33342 Nuclear Stain was read with a DAPI filter set (Excitation 340 nm, Emission 480 nm).

5.3.5 Statistical Analysis

Three independent experiments were conducted and each experiment was comprised of at least two internal replicates, unless otherwise stated. Data are presented as mean ± SD or ± SEM. Statistical analysis was performed by using an unpaired Student's t-test. Statistically significant data were detailed when *$p<0.05$, **$p<0.01$, ***$p<0.001$.

5.4 Results and Discussion

5.4.1 Cell cycle distribution in MDA-MB-231 and SKBR-3 cells

Cell cycle distribution of MDA-MB-231 and SKBR-3 cells was studied using flow cytometry following PI staining (Henry *et al*, 2013) with the most active compound *trans,trans*-BNIPDaCHM (Chapter 4), together with the parental compound BNIPDaCHM (mixture of isomers) that has been reported to induce cell cycle instability (Barron *et al*, 2015).

In order to accurately study the progression of cells through each phase of the cell cycle, MDA-MB-231 and SKBR-3 cells were synchronised by 24 hours serum deprivation (Figure 5.4.1). The elimination of serum resulted in the accumulation of cells in sub-G1 and G1 phase (Figures 5.4.1a and 5.4.1b) (see Appendix 5).

A significant increase in the proportion of MDA-MB-231 cells in sub-G1 phase after treatment with BNIPDaCHM (IC_{25}), *trans,trans*-BNIPDaCHM (IC_{25}) and camptothecin (21.9%, 25.5% and 20.1% increase) was exhibited relative to the control, whilst in G1 phase, the cell population was significantly decreased (by 16.2%, 15.1% and 9.36% respectively) (Figure 5.4.1.1a). The two BNIPs induced sub-G1 arrest in a similar way to camptothecin, which was used as a positive control. The proportion of MDA-MB-231 cells in S and G2 phase was not significantly different after treatment with the two BNIPs and camptothecin, compared to untreated cells.

These results indicate that both BNIPDaCHM and *trans,trans*-BNIPDaCHM induced sub-G1 cell cycle arrest in a similar way to camptothecin. Camptothecin is a well-known positive control for sub-G1 arrest (Chu *et al*, 2014, Doddapadeni *et al,* 2015) and for inducing apoptosis, even at low concentrations (e.g. 6 μM) (Kang *et al,* 2016, Hong *et al*, 2014).

Consequently, these findings suggest that BNIPDaCHM and *trans,trans*-BNIPDaCHM could use similar mechanisms of action compared to camptothecin and may trigger apoptotic cell death in MDA-MB-231 human breast cancer cells.

Similar experiments were carried out with synchronised SKBR-3 cells (Figure 5.4.1.1b), where the cell population was significantly increased in sub-G1 phase only after treatment with BNIPDaCHM (29.3%) and camptothecin (45.3%), but not for *trans,trans*-BNIPDaCHM compared to the control. This demonstrated that the effect of the two BNIPs investigated was different in each cell line and that the sole existence of one isomer (*trans,trans*-BNIPDaCHM) has a different effect on cell cycle distribution. Therefore, it is suggested that the mechanisms of cell death induced by *trans,trans*-BNIPDaCHM and BNIPDaCHM may differ among different cell lines, even though they belong to the same family of compounds.

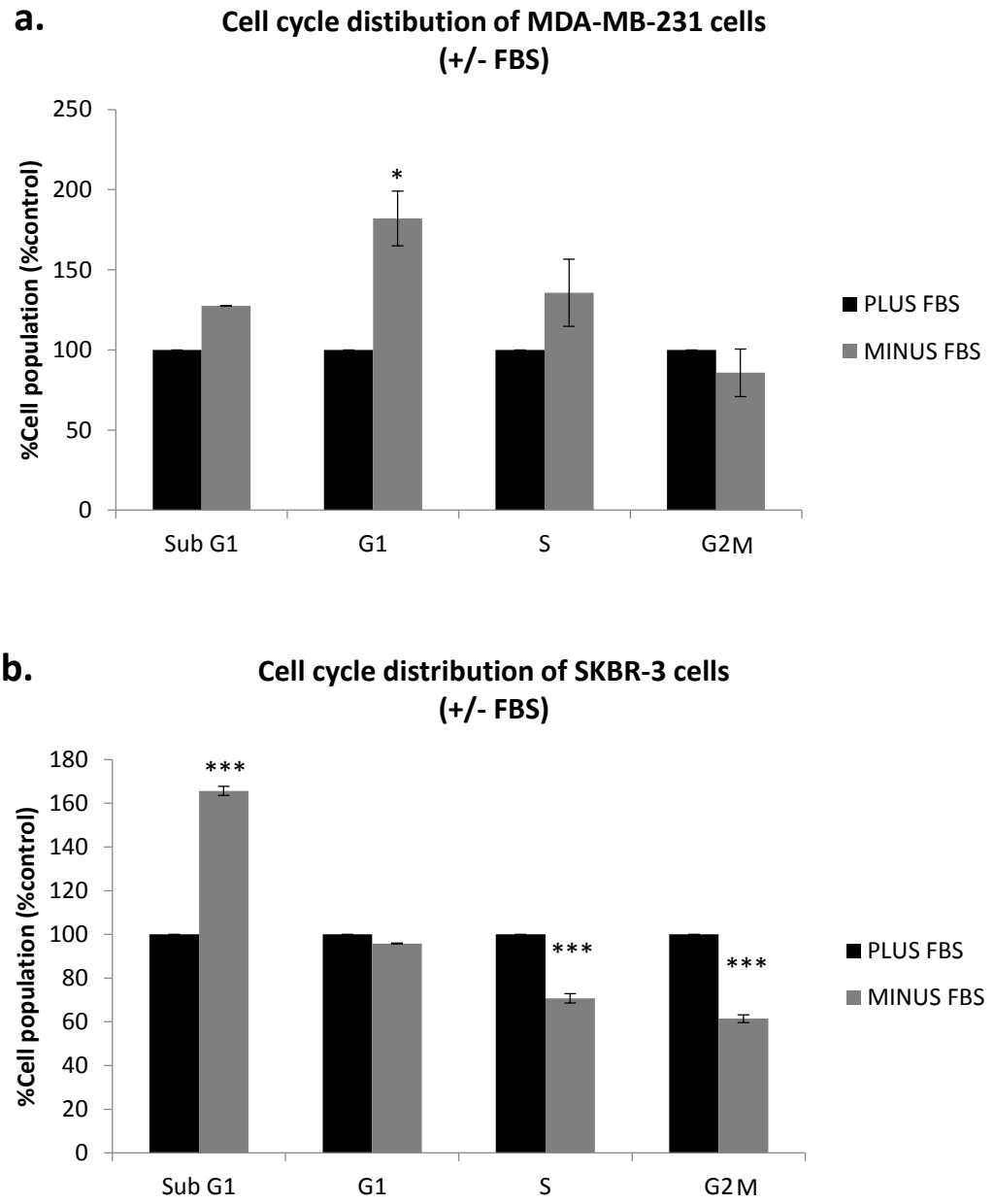

Figure 5.4.1.: a) Synchronisation of MDA-MB-231 and b) SKBR-3 cells after 24 hour serum deprivation. The percentage of the cell population in sub-G1, G1, S and G2/M were gated from histograms of linear FL-2 plots in the ungated regions (10,000 events). Data are mean ± SEM of three independent experiments (n = 3), conducted in duplicates. ***p< 0.001,*p< 0.05, compared to control.

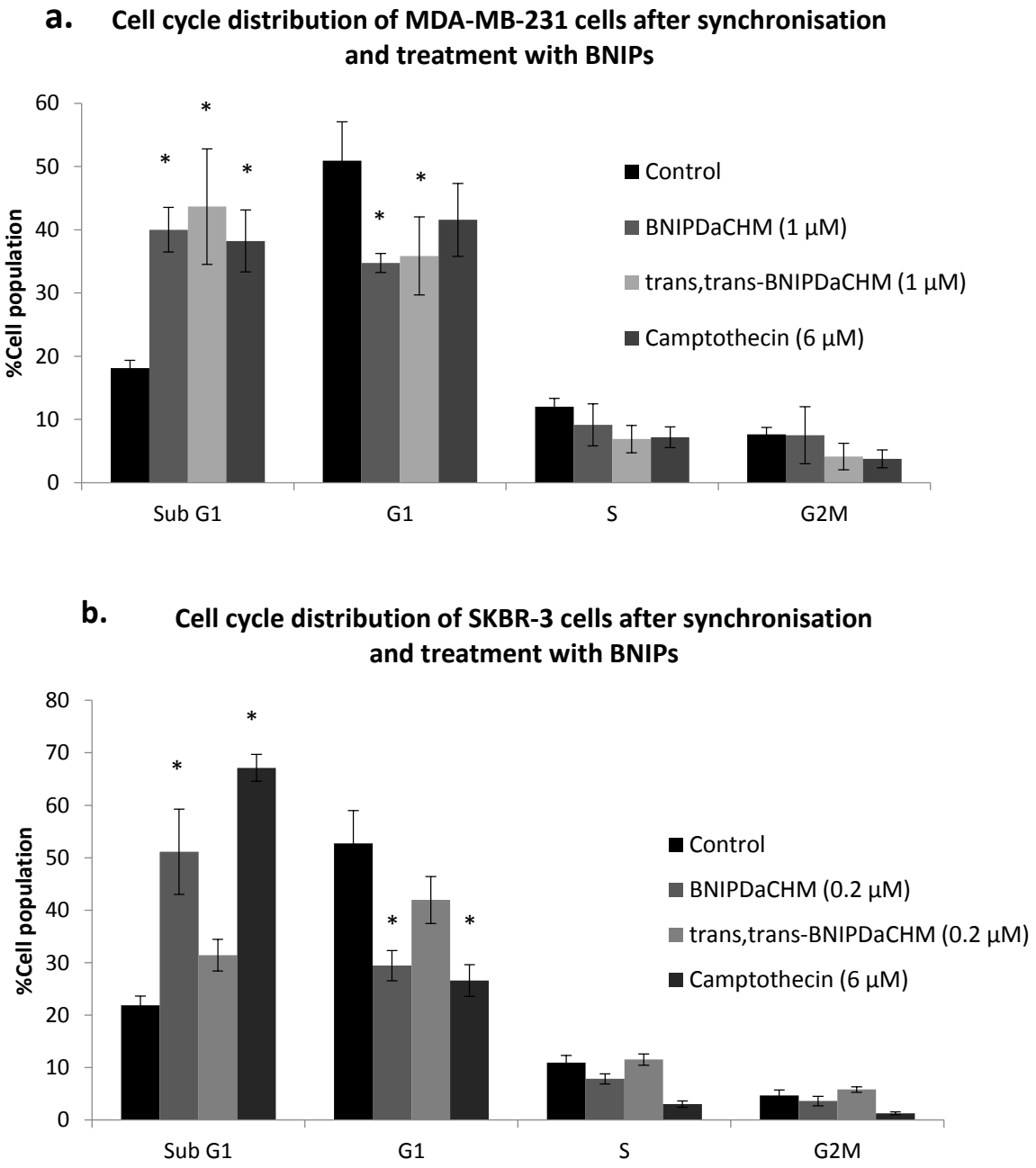

Figure 5.4.1.1.: a) Cell cycle distribution of MDA-MB-231 and b) SKBR-3 cells after BNIP treatment (IC_{25}). Quantification of MDA-MB-231 and SKBR-3 cell cycle profiles by flow cytometry following PI staining after 24 hour treatment with IC_{25} BNIPDaCHM, *trans,trans*-BNIPDaCHM and camptothecin. DMSO/dH_2O (50% v/v) was used as the solvent control. The percentage of the cell population in sub-G1, G1, S and G2/M were gated from histograms of linear FL-2 plots (10 000 events). Data are mean ± SEM of three independent experiments (n = 3), conducted in duplicates. *$p < 0.05$, compared to solvent control for each cell cycle phase.

5.4.2 Annexin V-FITC/7-AAD studies in MDA-MB-231 and SKBR-3 cells.

PS exposure and plasma membrane integrity in MDA-MB-231 and SKBR-3 cells after treatment with BNIPs were quantified using flow cytometry following Annexin V-FITC staining and 7-AAD labelling. Initially, cells were exposed to BNIPDaCHM for multiple timepoints (0.5, 2 and 4 hours) in order to capture the time frame by which the drug induce cell death in the above cell lines (Figure 5.4.2).

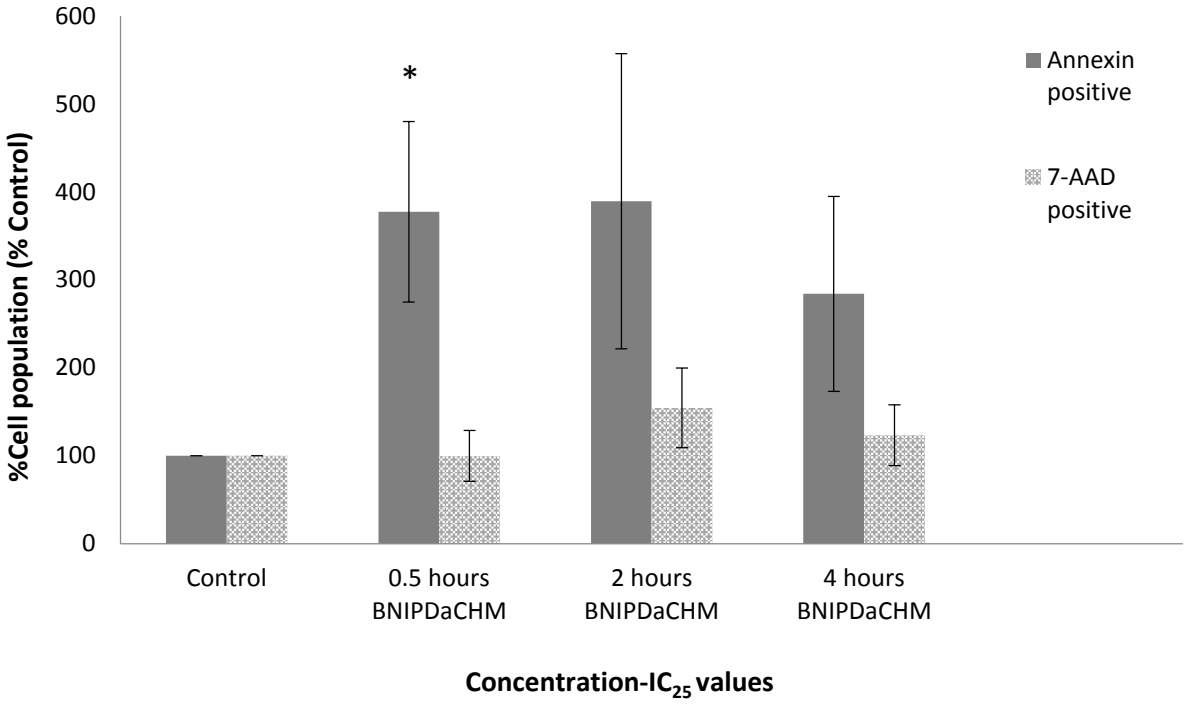

Figure 5.4.2.: PS exposure and membrane integrity profiles of MDA-MB-231 after 0.5, 2, and 4 hour treatment with IC_{25} BNIPDaCHM. Profiles were determined by flow cytometry following Annexin V-FITC staining and 7-AAD labelling. 10,000 single events were recorded, and cells labelled with Annexin V but not 7-AAD were considered Annexin positive. Cells labelled with 7-AAD were 7-AAD positive. DMSO/dH_2O (50% v/v) was used as the solvent control. Data are mean ± SEM of four independent experiments (n = 4), conducted in duplicates. *p< 0.05, compared to solvent control.

Apoptotic and necrotic histograms were obtained after 0.5, 2 and 4 hours treatment with BNIPDaCHM in MDA-MB-231 cells. Annexin V-FITC stains apoptotic cells, whilst 7-AAD viability dye stains necrotic cells. Cells labelled with Annexin V-FITC but not 7-AAD were Annexin positive and cells labelled with 7-AAD only, were 7-AAD positive. Cells labelled with both dyes were not considered in the study, as no change within the double positive population was observed after treatment with BNIPs (see Appendix 6).

Figure 5.4.2 shows that after 0.5 hour treatment with BNIPDaCHM (IC_{25}), a significant increase of 277.3% in Annexin V-FITC staining was observed, compared to the control. After 2 hours treatment with BNIPDaCHM, the Annexin V-FITC staining levels remained high (289.2%), but after 4 hours treatment, a decrease of 183.9% in Annexin V-FITC staining was observed, compared to the other two time points.

These results indicate that Annexin V-FITC can bind to PS residues, which are externalised to the outer layer of the MDA-MB-231 plasma membranes and this is linked to early apoptotic cell death. On the other hand, low levels of 7-AAD staining show that plasma membrane integrity of MDA-MB-231 cells is not affected (absence of necrotic cell population) compared to the control.

The decrease in Annexin V-FITC staining after 4 hour treatment with BNIPDaCHM confirms that PS exposure is an early apoptotic event. Therefore, it was crucial in this study to collect repeated measurements over time, in order to study the right time point for early apoptosis.

Based on the above results, PS exposure and plasma membrane integrity profiles after 0.5 hour treatment with all novel BNIPs were further studied. In the following experiments, Formaldehyde (3%) was used as positive control, as Formaldehyde

treatment has been found to significantly induce apoptotic cell death (Barron *et* al, 2015).

After 0.5 hour treatment with BNIPs (Figure 5.4.2.1a), significant differences in Annexin V-FITC staining compared to the control was observed in MDA-MB-231 cells. More specifically, after treatment with BNIPDaCHM Annexin V-FITC staining levels were increased by 593.8% ($p<0.05$). After treatment with BNIPPiProp, Annexin V-FITC levels were increased by 708.3% ($p<0.05$). Annexin V-FITC staining levels after treatment with BNIPPiEth and *trans,trans*-BNIPDaCHM were increased by 975.0% and 900.8%, compared to untreated cells, respectively. Formaldehyde treatment (positive control), increased the Annexin V-FITC staining levels by 1816.7%. Moreover, according to statistical analysis, no significance difference was found in MDA-MB-231 apoptotic cell populations after treatment with BNIPDaCHM, BNIPPiProp, BNIPPiEth and *trans,trans*-BNIPDaCHM, compared to each other.

According to these findings, the three novel BNIPs and their parental compound BNIPDaCHM, induced apoptotis in the cell population, as shown by an increase in Annexin V-FITC staining. BNIPPiEth caused the highest increase of Annexin V-FITC staining levels in MDA-MB-231 cells (975.0%), followed by *trans,trans*-NIPDaCHM (900.8%), BNIPPiProp (708.3%) and BNIPDaCHM had the lowest (593.8%). On the other hand, after treatment with BNIPs or Formaldehyde, 7-AAD viability dye staining levels were not increased compared to the control. 7-AAD can only label cells without membrane integrity. Therefore, the above results indicate that treatment with BNIPs did not compromise membrane integrity, which is associated to necrotic cell death.

Similar studies were performed in SKBR-3 cells (Figure 5.4.2.1b). After 0.5 hours treatment with BNIPs, a significant difference in Annexin V-FITC staining compared to the control was observed. More specifically, after treatment with BNIPDaCHM, Annexin V-FITC staining levels were increased by 41375.0% ($p<0.05$). After treatment with BNIPPiProp, Annexin V-FITC levels were increased by 32800.0% ($p<0.05$). Annexin V-FITC staining levels after treatment with BNIPPiEth and *trans,trans*-BNIPDaCHM were increased by 33883.3% and 42900.0%, compared to control cells, respectively. Formaldehyde treatment (positive control), increased Annexin V-FITC staining levels by 13466.7.7%, compared to the control. According to statistical analysis, no significance difference was found in SKBR-3 apoptotic cell populations after treatment with BNIPDaCHM, BNIPPiProp, BNIPPiEth and *trans,trans*-BNIPDaCHM, compared to each other.

Interestingly, BNIPs induce apoptosis not only in MDA-MB-231, but also in SKBR-3 cells and to a greater extent. *trans,trans*-BNIPDaCHM was the derivative that induced the highest increase of Annexin V-FITC staining levels in SKBR-3 cells (42900.0%), followed by BNIPDaCHM (41375.0%), BNIPPiEth (33883.3%) and BNIPPiProp was the derivative that caused the lowest increase of Annexin V-FITC staining levels (32800.0%).

Similarly to the previous findings in MDA-MB-231 cells, after treatment with BNIPs or Formaldehyde, necrotic cell population was virtually absent. Therefore, these results indicate that treatment with BNIPs also did not compromise plasma integrity in SKBR-3 cells. In addition, human epidermal growth factor receptor 2-overexpressing SK-BR-3 cells (hormone receptor positive) seem once more to have a better response to BNIP treatments with regards to induction of early apoptosis, compared to MDA-MB-231 cells.

After 0.5 hours, BNIPs elicit PS residues externalisation in both cell lines, preventing early plasma membrane damage. These findings suggest strongly that BNIPs induce early apoptosis, which could be the main mechanism in BNIP-induced cytotoxicity and cell cycle arrest. However, there are no similar finding in the literature that shows induction of early apoptosis after 0.5 hour treatment with anti-cancer drugs that are already in use, such as Capecitabine (Ershler, 2006).

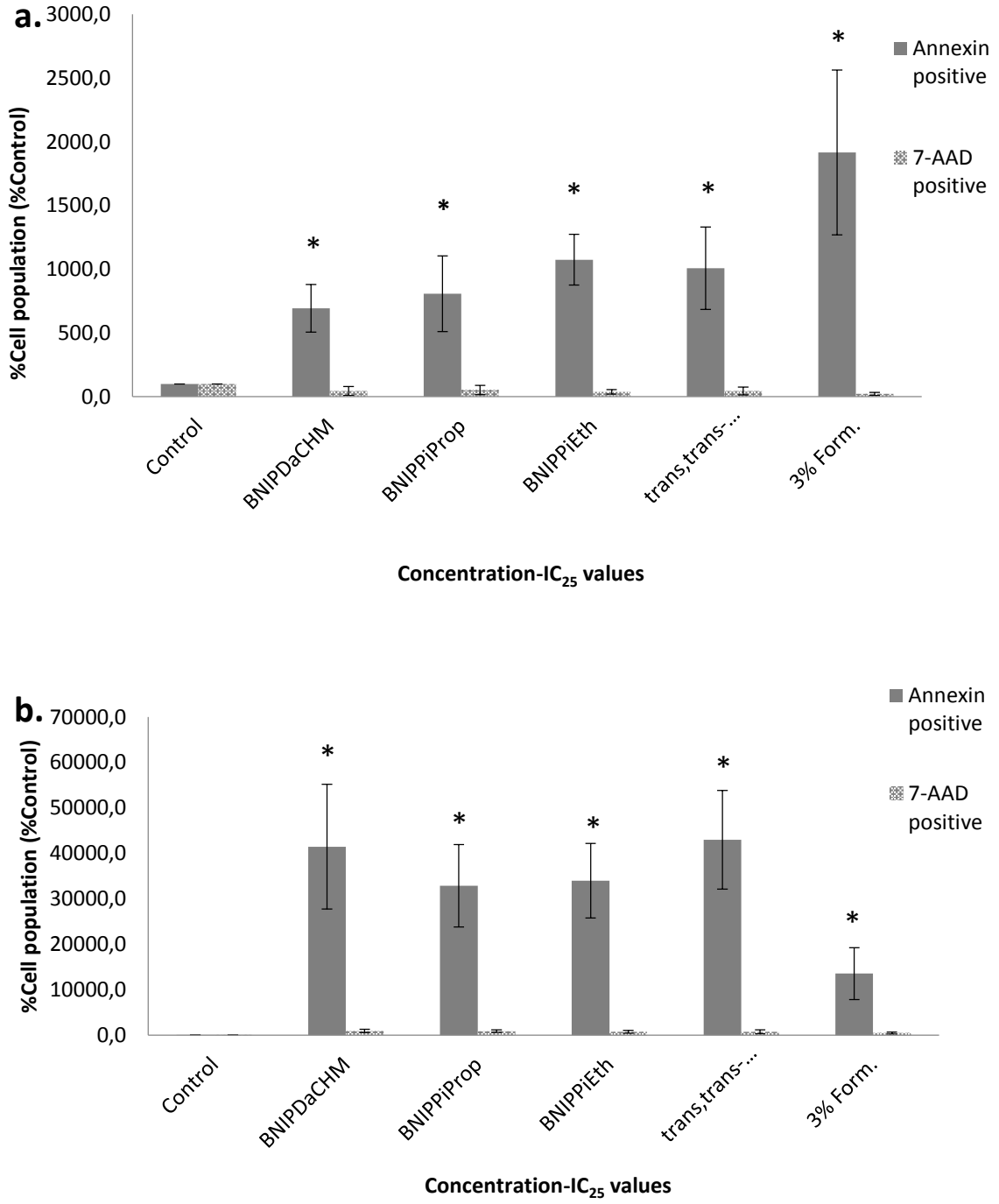

Figure 5.4.2.1.: a) PS exposure and membrane integrity profiles of MDA-MB-231 and b) SKBR-3 cells, after 0.5 hour treatment with IC_{25} BNIPs. Profiles were determined by flow cytometry following Annexin V-FITC staining and 7-AAD labelling. 10,000 single events were recorded, and cells labelled with Annexin V but not 7-AAD were Annexin positive. Cells labelled with 7-AAD were 7-AAD positive. DMSO/dH_2O (50% v/v) was used as the solvent control. Data are mean ± SEM of four independent experiments (n = 4), conducted in duplicates. *p< 0.05, compared to solvent control.

5.4.3 Caspase-3 studies in MDA-MB-231 and SKBR-3 cells

Caspase-3 is a mediator of programmed cell death and its activity was examined to determine the effect of BNIPs on apoptosis pathways in MDA-MB-231 and SKBR-3 cells.

After 24 hours treatment with BNIPs, a difference in Caspase-3 activity compared to untreated cells was observed in MDA-MB-231 cells (Figure 5.4.3a). More specifically, after treatment with BNIPDaCHM, Caspase-3 activity levels were significantly decreased by 81.5% ($p<0.01$). After treatment with BNIPPiProp, Caspase-3 activity was decreased by 81.7% ($p<0.05$). Similarly, Caspase-3 activity was not detected after treatment with BNIPPiEth and after treatment with *trans,trans*-BNIPDaCHM, Caspase-3 activity levels were similar to the control.

These results indicate that the three novel BNIPs investigated and their parental compound BNIPDaCHM did not activate Caspase-3 after 24 hour treatment in MDA-MB-231 cells, but rather decreased it. BNIPPiEth is the derivative that induced the highest decrease of Caspase-3 activity levels in MDA-MB-231 cells (100.0%), followed by BNIPPiProp (81.7%), BNIPPiEth (81.5.3%) and *trans,trans*-BNIPDaCHM had no change compared to the control. In contrast, after 24 hour treatment with BNIPs (IC_{25}), different findings with regards to Caspase-3 activity compared to the control was observed in SKBR-3 cells (Figure 5.4.3b). More specifically, after treatment with BNIPDaCHM, Caspase-3 activity levels were significantly increased by 771.5% ($p<0.001$). After treatment with BNIPPiProp and BNIPPiEth, Caspase-3 activity was not detected (0%, $p<0.001$). Moreover, *trans,trans*-BNIPDaCHM decreased Caspase-3 activity levels compared to the control by 71.9% ($p<0.001$).

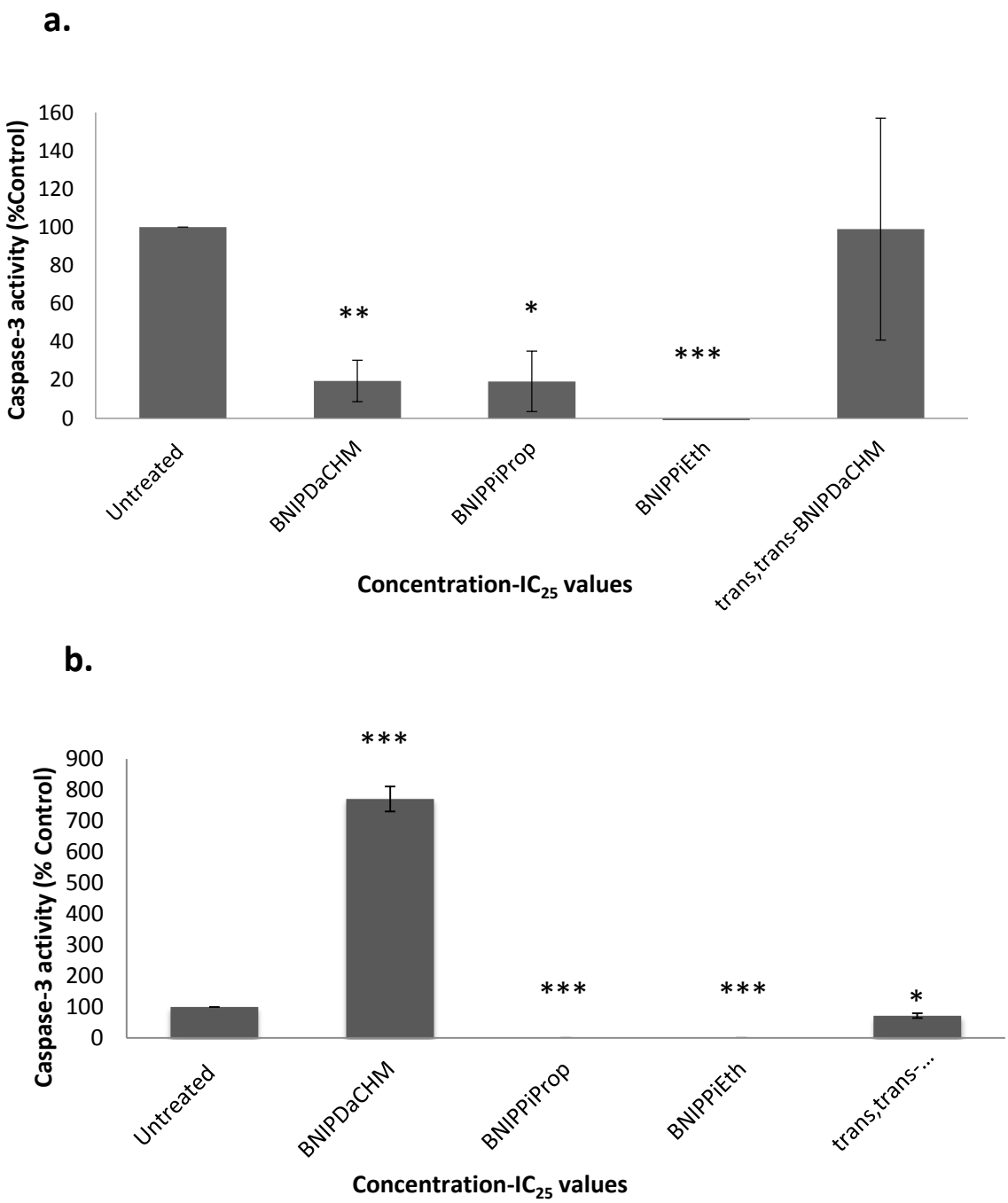

Figure 5.4.3.: a) Effect of BNIPs on Caspase-3 activity in MDA-MB-231 and b) SKBR-3 cells, after 24 hour treatment at 37 °C with BNIPDaCHM, BNIPPiProp, BNIPPiEth and *trans,trans*-BNIPDaCHM. DMSO/H_2O was used as solvent control. Data presented as mean ±SEM (n=3). ***p<0.001, **p<0.01, *p<0.05, compared to solvent control.

Results indicate that only the parental compound BNIPDaCHM, activated Caspase-3 activity after 24 hours treatment in SKBR-3cells. The other compounds either decreased Caspase-3 activity (*trans,trans*-BNIPDaCHM), or did not alter it at all (BNIPPiProp and BNIPPiEth). These findings show that Caspase-3 was not activated by any of the BNIPs after 24 hours in MDA-MB-231 cells and that only BNIPDaCHM activated Caspase-3 in SKBR-3 cells, which was the cell line that was more susceptible to BNIP treatments according to the previous results (Chapter 3). Consequently, further studies should be undertaken in order to determine the accurate time-point where Caspase-3 is potentially activated by BNIPPiProp, BNIPPiEth and *trans,trans*-BNIPDaCHM in MDA-MB-231 and SKBR-3 cells. However, according to the literature, there are types of cancer where Caspase-3 expression and activity can alter during carcinogenesis and not even exist once the cancer cells are terminally differentiated (Hague *et al,* 2006), or cases where early apoptosis interferes with autophagy, as both machineries share common pathways (Maiuri *et al,* 2007). Therefore, researchers are currently investigating whether specific mechanisms that involve Caspase-3 expression and activity could be used as potential targets for therapeutic benefit of cancer patients. Such an example is the study of Lee *et al*. (2016), where lambertianic acid treatment in prostate cancer cells was found to lead to apoptotic cell death due to induced sub-G1 arrest and cleaved Caspase-3 activity.

5.4.4 Autophagy studies in MDA-MB-231 and SKBR-3 cells

Autophagy flux in MDA-MB-231 and SKBR-3 cells was detected by CYTO ID fluorescence microplate assay.

After 24 hour treatment with BNIPs (IC_{25}), significant difference in autophagy flux compared to the control were observed in MDA-MB-231 cells (Figure 5.4.4a). More specifically, after treatment with BNIPDaCHM, autophagy was significantly increased by 26.4% ($p<0.001$). After treatment with BNIPPiProp, autophagy flux was increased by 25.7% ($p<0.001$). Autophagy levels after treatment with BNIPPiEth and *trans,trans*-BNIPDaCHM were elevated by 18.8% ($p<0.001$) and 17.9% ($p<0.001$), compared to the control, respectively. Rapamycin treatment increased the autophagy levels by 1.4% and Chloroquine by 13.4% ($p<0.05$). When Rapamycin and Chloroquine were combined, autophagy was induced, to a greater extent than a cumulative effect by 24.6% ($p<0.01$), suggesting a synergistic effect. According to these findings, the three novel BNIPs investigated and their parental compound BNIPDaCHM, induced autophagy in MDA-MB-231 cells after 24 hour treatment. BNIPDaCHM caused the highest increase of autophagy levels in MDA-MB-231 cells (26.4% ($p<0.001$)), followed by BNIPPiProp (25.7% ($p<0.001$)), BNIPPiEth (18.8% ($p<0.001$)) and *trans,trans*-BNIPDaCHM (17.9% ($p<0.001$)). Moreover, according to statistical analysis, no significance difference was found in MDA-MB-231 cell autophagy levels after treatment with BNIPDaCHM, BNIPPiProp, BNIPPiEth and *trans,trans*-BNIPDaCHM, compared to each other.

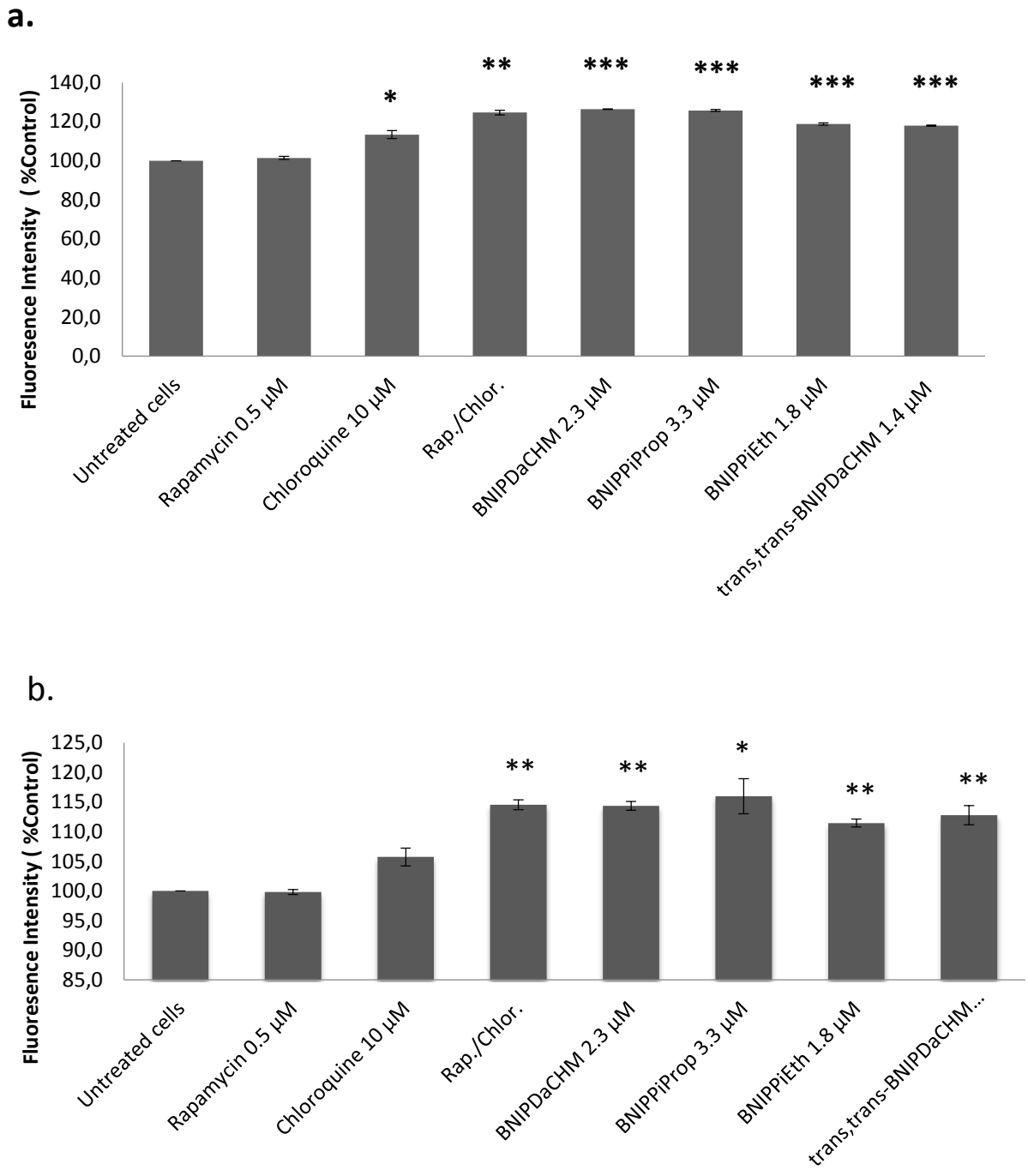

Figure 5.4.4.: a) Detection of autophagy by microplate reader in MDA-MB-231 and b) SKBR-3 cells. Cells were cultured with 0.5 µM rapamycin, 10 µM Chloroquine, 0.5 µM Rapamycin + 10 µM Chloroquine and BNIPs (IC_{25}), followed by staining with green detection reagent as described in the manual. Nuclei were counter stained with Hoechst 33342. The data indicate the relative green fluorescence intensity normalized by blue fluorescence intensity. DMSO/H_2O was used as solvent control. Data presented as mean ±SEM (n=3). ***p<0.001, **p<0.01, *p<0.05, compared to solvent control.

Interestingly, all the BNIPs were found to induce autophagy to a greater extent than the two positive controls, Rapamycin and Chloroquine, which strongly suggests the activation of autophagic response machineries after treatment with BNIPs. In addition, treatment with BNIPs may allow accumulation of the drugs in lysosomes and inhibit lysosomal function in the same way as Chloroquine (lysosomotropic compound).

With regards to SKBR-3 cells, BNIPs significantly induced differences in autophagy flux compared to the control, after 24 hour treatment with BNIPs (Figure 5.4.4b). More specifically, after treatment with BNIPDaCHM autophagy was significantly increased by 14.3% ($p<0.01$). After treatment with BNIPPiProp, autophagy flux was induced by 16.0% ($p<0.05$), compared to the control. When the cells were treated with BNIPPiEth and *trans,trans*-BNIPDaCHM, autophagy was elevated by 11.4% ($p<0.01$) and 12.8% ($p<0.01$), compared to control cells, respectively. For this cell type, Rapamycin treatment did not have any effect on autophagy and Chloroquine induced autophagy only by 5.7% ($p<0.05$). When Rapamycin and Chloroquine were combined, autophagy was induced by 14.5% ($p<0.01$), suggesting a synergistic effect, as shown in MDA-MB-231 cells.

The above results show that the three novel BNIPs and their parental compound BNIPDaCHM induced autophagy in SKBR-3 cells after 24 hour treatment. BNIPPiProp was the derivative that caused the highest increase of autophagy levels in SKBR-3 cells (16.0% ($p<0.05$)), followed by BNIPDaCHM (14.3% ($p<0.01$)), BNIPPiEth (12.8% ($p<0.01$)) and *trans,trans*-BNIPDaCHM (11.4% ($p<0.01$)). According to statistical analysis, no significant difference was found in SKBR-3 cell autophagy levels after treatment with BNIPDaCHM, BNIPPiProp, BNIPPiEth and *trans,trans*-BNIPDaCHM, compared to each other.

Caspase-3 activity was inhibited after 24 hour treatment with BNIPDaCHM, BNIPPiProp and BNIPPiEth in MDA-MB-231 and after treatment with BNIPPiProp, BNIPPiEth and *trans,trans*-BNIPDaCHM in SKBR-3 cells, despite the evidence of early apoptosis (after 0.5 hours) detected with Annexin V by flow cytometry (Section 5.4.2): investigating further the mode of cell death with BNIPs has brought to light complexity of the mechanisms involved. Interestingly, after 24 hour treatment with BNIPs in MDA-MB-231 and SKBR-3 cells, the formation of autophagosomes and autolysosomes (Sun *et al*, 2013) was triggered, suggesting BNIP-induced autophagy on the above human breast cancer cell lines. Therefore, this study demonstrates that, for the 1st time, BNIPs induce both early apoptosis and autophagy. The above findings are also supported by Karna *et al* (2010), where a tubulin-binding noscapine analogue, Red-Br-nos, was found to induce autophagy followed by caspase-independent apoptotic cell death (CICD) in human prostate cancer PC-3 cells, through the generation of ROS (Tait and Green, 2008). The findings of Karna *et al* (2010) are in agreement with the elevated ROS levels and inhibition of Caspase-3 activity after treatment with BNIPs (Chapters 4 and 5). Other studies also show a relationship between ROS levels and autophagy (Li *et al*, 2012). These results open up a new and exciting avenue for understanding into the cell death machinery after treatment with BNIPs that can potentially have implications for the treatment of cancer

5.5 Conclusion

In Chapter 5, the effect of BNIPs on cell cycle distribution and cell death was studied in MDA-MB-231 and SKBR-3 cells. An increase in the proportion of MDA-MB-231 cells in sub-G1 phase was exhibited compared to untreated cells, whilst in G1 phase, the cell population was significantly decreased after treatment with BNIPDaCHM and *trans,trans*-BNIPDaCHM. In SKBR-3 cells, the cell population was significantly increased in sub-G1 phase only after treatment with BNIPDaCHM, suggesting that the mechanisms of cell death amongst *trans,trans*-BNIPDaCHM and BNIPDaCHM may differ in different cell lines.

After 0.5 hour treatment with BNIPs, a significant difference in Annexin V-FITC staining compared to untreated cells was observed in MDA-MB-231 cells and SKBR-3 cells. BNIPPiEth caused the highest increase of Annexin V-FITC staining levels in MDA-MB-231 cells, and *trans,trans*-BNIPDaCHM in SKBR-3 cells, respectively, showing that BNIPs induced early apoptosis which could trigger cell cycle arrest. On the other hand, after 24 hour treatment, BNIPs were found to inhibit Caspase-3 activity in MDA-MB-231 and SKBR-3 cells. In addition, autophagy studies revealed that the formation of autophagosomes and autolysosomes was triggered after treatment with BNIPs, suggesting BNIP-induced autophagy on the tested human breast cancer cell lines seems to cross talk with caspase-independent apoptotic cell death (Figure 5.5). To further elucidate the mode of action of BNIPs, histone deacetylase (HDAC) activity and the expression of cell stress-related proteins were studied (Chapter 6).

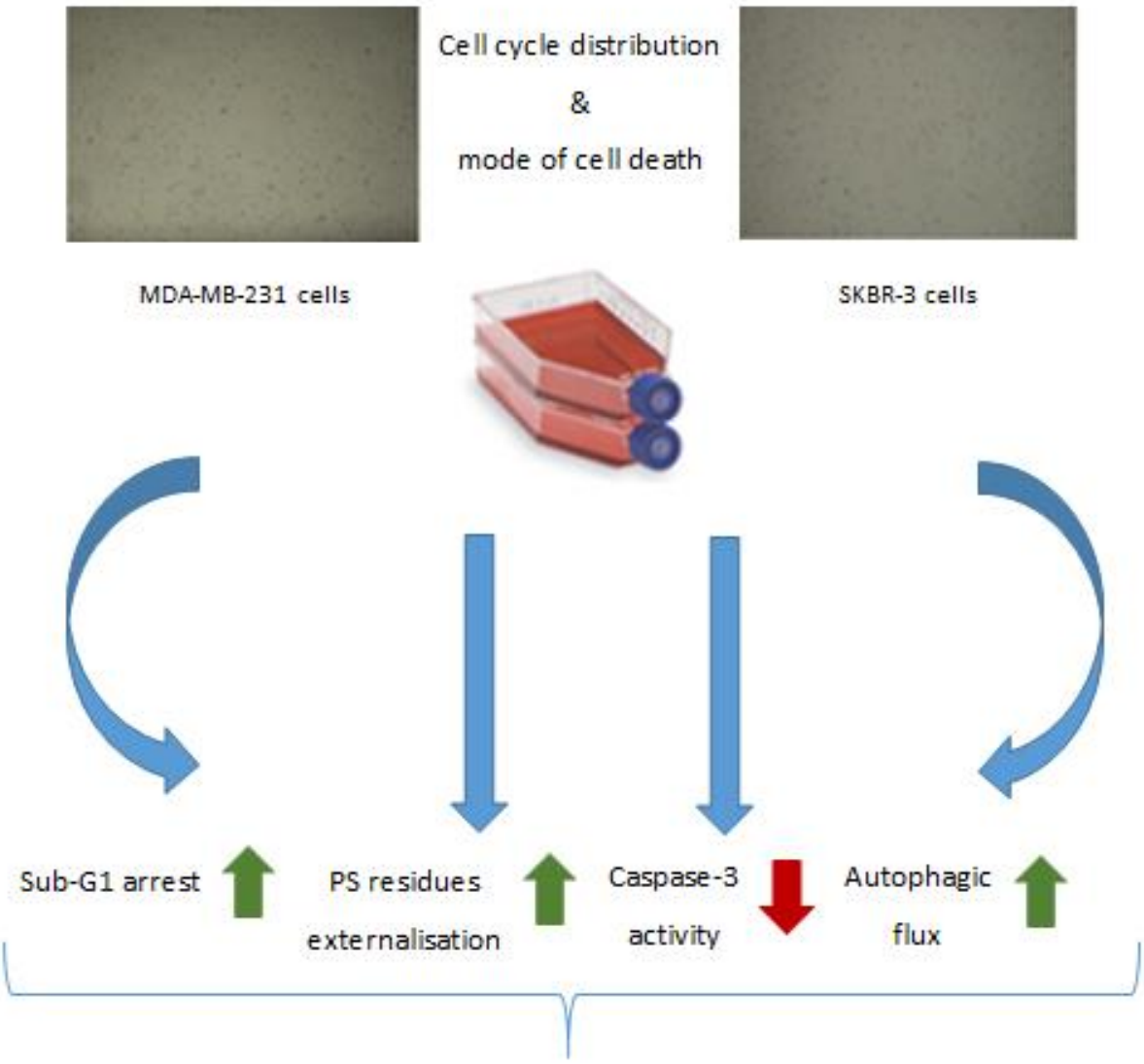

Figure 5.5.: Summary of cell cycle distribution and cell death studies.

CHAPTER 6

Effect of bisnaphthalimidopropyl derivatives on histone deacetylases and cell stress-related proteins

6.1 Introduction

The role of HDACs and HDACi have been previouslly covered in Chapter 1 (Sections 1.3 & 1.3.1). This chapter will focus on the role of specific Class III HDACs (sirtuins) and other cell stress proteins as key regulators in breast cancerogenesis.

6.1.2 Sirtuins and their role in tumourigenesis

Class III HDACs or sirtuins, are NAD^+-dependent protein modifying enzymes that produce nicotinamide and the by-product O-acetyl adenosine diphosphate (ADP) ribose (Jiang, 2008). Sirtuins have certain enzymatic activities, such as lysine deacetylation, ADP-ribosylation and ADP-deacylation (Roth and Chen, 2014). The mammalian sirtuins occupy three different subcellular compartments: nucleus, cytoplasm and mitochondria. Apart from their different subcellular localisation, the enzymatic activities differ among the seven members of the sirtuin family, known as SIRT1–7 (Roth and Chen, 2014, Yuan and Chen, 2013). SIRT1 is the most studied and best-characterised sirtuin and has been reported to have longevity-promoting effects (Roth and Chen, 2014, Yuan and Chen, 2013) as well as pivotal roles as regulator of cellular homeostasis and genomic stability (Yuan and Chen, 2013). After these findings, researchers started to explore further the roles of SIRT1 and other members of the sirtuins family, especially in cases where cellular homeostasis and genomic integrity has been lost, such as cancer (Haigis and Sinclair, 2010).

Members of this protein family have been shown to have diverse roles in several types of cancer, including breast carcinogenesis (Yuan and Chen, 2013). Apart from SIRT1, which is implicated in DNA repair pathways by deacetylating WRN (a

member of the RecQ DNA helicase family with functions in maintenance of genomic stability), evidence also suggests that SIRT2 has both tumour suppressor and promoter functions (Li *et al*, 2013, McGlynn *et al*, 2014). SIRT2 deacetylates a variety of proteins, implicated in inflammatory responses, such as NF-κB protein and activates proteins, like tumour suppressor p53 that are involved in DNA repair processed (Peck *et al*, 2010). Moreover, in several types of tumours, like gliomas, oesophageal or gastric adenocarcinomas, SIRT2 expression was shown to be reduced (Peters *et* al, 2010, Hiratsuka *et al*, 2003), whereas it is upregulated in breast cancer tissues (Igci *et al*, 2016). On the other hand, silencing SIRT2 in HeLa cells and in C6 glioma cells was shown to trigger apoptosis (He *et al*, 2012, Li *et al*, 2011). Expression of SIRT3, which is a tumour suppressor, is reduced in human breast and colon carcinoma (Finley *et al*, 2011), head and neck squamous cell carcinoma (Lai *et al,* 2013) and osteosarcoma (Zhang *et al,* 2012, Zhang and Zhou, 2012). On the other hand, the role of SIRT4 and SIRT6 in cancer formation is still unclear, as there are only few reports that show SIRT4 as a possible tumour suppressor (Jeong *et al,* 2013). SIRT6 is downregulated in pancreas malignancy (Csibi *et al,* 2013). SIRT5 has been found to facilitate cancer cell growth and drug resistance in non-small cell lung cancer (Lu *et al*, 2014). Lastly, in breast and thyroid cancers SIRT7 expression levels have been shown to be elevated (De Nigris *et al*, 2002).

The above findings indicate that HDACs and more specifically, sirtuins have a crucial role in the development of many tumours, including breast and provide potential targets for cancer therapy. Although it is still unclear how HDACs work in relation to cancer, researchers are investigating their role as therapeutic targets as well as any potential synergistic activity with other anti-cancer compounds.

Several methods have been developed for the assessment of cellular HDAC activity. Apart from antibody-based techniques, such as chromatin immunoprecipitation based analyses or western blotting, which are powerful tools for detecting histone acetylation levels, chemical tools and methods have been developed, to circumvent the issue of antibody quality (Egelhofer *et al,* 2011). Activity-based probes, such as suberoylanilide hydroxamic acid (SAHA), PET-active probes, such as fluorine-18, for *in vivo* imaging, and fluorogenic probes, such as Fluor De Lys, that switch their fluorescence properties upon enzymatic reaction, are the main methods for detecting HDAC activity (Minoshima and Kikuchi, 2015). Recently, HDAC cell-based assays have been developed, providing a useful tool for studying HDAC activity modulators in whole cells (Johnstone and Licht, 2003).

6.1.3 Aims

The aim of the work presented in Chapter 6 was to understand further the mode of action of the three novel BNIPs and their parental compound, with regards to HDACs and stress-related proteins. The objectives of the experimental work was to study the effect of BNIPs on HDAC activity in breast cancer cells, with emphasis on SIRT2 and cell stress-related proteins, based on our previous findings, where BNIPs were found to increase the intracellular levels of ROS and induce DNA damage in MDA-MB-231 and SKBR-3 cells. Moreover, a characterstic of many SIRT2 inhibitors is that they bear a naphthalene moiety, suggesting a possible link between BNIPs and HDAC inhibition. In addition, previous findings have already reported that BNIPDaCHM inhibits SIRT2 enzyme activity *in vitro* (Lima *et al*, 2013). Protein-protein interaction (PPI) network analysis was constructed to link the proteins of interest (based on the protein array) in breast cancer, applying Cytoscape V3.0 (Shannon *et al,* 2003) and STRING V10.0 (Szklarczyk *et al*, 2015) softwares, which will be discussed in this Chapter.

6.2 Materials

6.2.1 HDAC cell-based activity assay

HDAC cell-based activity assay	Cayman, UK

6.2.2 Total protein extraction

Phosphate buffered saline	Sigma-Aldrich, UK
Cell lysis buffer (10X)	Cell Signalling, UK
Proteinase Inhibitor Cocktail	Sigma-Aldrich, UK
Phenylmethanesulfonyl fluoride solution	Sigma-Aldrich, UK

6.2.3 Bradford protein concentration (BSA) assay

Bovine Serum Albumin (BSA) solution	Sigma-Aldrich, UK
DC™ Protein Assay Kit	Bio-Rad, UK
Triton X-100	Sigma-Aldrich, UK

6.2.4 Sodium dodecyl sulphate (SDS) Polyacrylamide gel electrophoresis (PAGE)

<u>Resolving gel 9% (10 mL):</u>

2.5 mL 1.5 M Tris pH 8.8	Fisherbrand, UK
100 µL 10% SDS	Fisherbrand, UK
2.25 mL 40% Acrylamide/Bisacrylamide	Bio-Rad, UK
5.1 mL H_2O	

50 µL 10% Ammonium Persulphate	Sigma-Aldrich, UK
5 µL Tetramethylethylenediamine (TEMED)	Sigma-Aldrich, UK

1.5 M Tris pH 8.8 (250 mL)

45.4 g Tris	Fisherbrand, UK
250 mL distilled H_2O	MilliQ, Millipore, UK

Stacking gel (5 mL):

0.625 mL 1M Tris pH 6.8	Fisherbrand, UK
50 µl 20% SDS	Fisherbrand, UK
0.750 mL 30% Acrylamide/Bisacrylamide	Bio-Rad, UK
3.525 mL H_2O	
25 µL 10% Ammonium Persulphate	Sigma-Aldrich, UK
5 µL TEMED	Sigma-Aldrich, UK

Loading buffer stock (10 ml):

5 mL 10% SDS	Sigma-Aldrich, UK
2.5 mL 100% Glycerol	Sigma-Aldrich, UK
2.5 mL 0.5 M Tris	Fisherbrand, UK
0.5% Bromophenol Blue (50 mg)	Sigma-Aldrich, UK

On the day, 7.5 µL β-mercaptoethanol (Sigma-Aldrich, UK), was added to 100 µL loading buffer stock.

Electrophoresis buffer x10 (500 mL):

15.125 g Tris	Fisherbrand, UK
93.75 g Glycine	Sigma-Aldrich, UK

5 g SDS	Fisherbrand, UK

Transfer Buffer x1 (1000 mL)

700 mL Electrophoresis Buffer x10	Prepared above
100 mL mL distilled H_2O	MilliQ, Millipore, UK
200 mL Methanol	Fisherbrand, UK

TBS/T x 10 (500 mL)

1.21 g Tris	Fisherbrand, UK
4 g NaCl	Fisherbrand, UK
0.5 mL Tween20	Sigma-Aldrich, UK
Precision Protein Kaleidoscope	Bio-Rad, UK

6.2.5 Western blotting and Detection

Methanol	Fisherbrand, UK
PVDF membrane Hybond™-P	Amersham Bioscience, UK
SuperSignal West Pico Substrate	Fisherbrand, UK
KODAK RP X-OMAT LO Developer and Fixer	Carestream, UK

6.2.6 Proteome Profiler Array

Proteome Profiler Human Cell Stress Array	R&D, USA

6.2.7 Instrumentation

Plate reader	Synergy/HT, BIOTEK
ALC PK 121R multispeed refrigerated centrifuge	Beckman Coulter, UK
WhirliMixerTM vortex mixer	Fisherbrand, UK
Bio-Rad Electrophoresis System	Bio-Rad, UK
Bio-Rad PowerPack Power Supply	Bio-Rad, UK
Bio-Rad Electrophoresis System	Bio-Rad, UK
Bio-Rad PowerPack Power Supply	Bio-Rad, UK
CL-XPosure X-ray film	Thermoscientific, UK
FUSION-FX7- SPECTRA	Vilber, Germany
BIO-1D™ imaging software	PeqLab, a VWR company, UK

6.3 Methods

6.3.1 HDAC cell-based activity assay

HDAC activity was determined using the HDAC Assay Kit according to the manufacturer's instructions. Briefly, MDA-MB-231 and SKBR-3 cells (7,500 cells/well) were seeded in culture medium (100 µL) in black, clear bottomed 96-well plates. Cells were incubated for 24 hours at 37 °C with BNIPs at IC_{25}. After 24 hours, the plate was centrifuged at 500×*g* for 5 minutes at 37 °C and the culture medium was aspirated. Assay Buffer (200 µL) was added to each well, the plate was centrifuged at 500×*g* for 5 minutes at 37 °C. The supernatant was aspirated and 90 µL of culture medium or positive control (recombinant HDAC1) was added to the non-inhibited samples, while 80 µL culture medium with 10 µL Trichostatin A (HDAC inhibitor) was added to the appropriate control wells. The HDAC reaction was initiated by adding 10 µL of the diluted HDAC substrate to each well. The plate was incubated for three hours at 37 °C. Cells were lysed with 50 µL Lysis/Developer Mixture and the plate was shaken for 2 minutes. After 15 minutes incubation at 37 °C, fluorescence was measured at an excitation wavelength of 360 nm and an emission wavelength of 440 nm on a 96-well plate reader.

6.3.2 Total protein extraction

MDA-MB-231 and SKBR-3 cells ($1x10^6$ cells/T25 flask) were treated with BNIPDaCHM IC_{25} concentration for 24 hours at 37 °C. After 24 hours incubation, the flasks were placed on ice and washed three times with ice cold PBS. Extraction buffer (200 µL) was added in each flask and incubated for 5 minutes on ice. The cells were harvested with a scraper and transferred to an Eppendorf tube. The samples were sonicated (2x 10 seconds) and then centrifuged at 2,000 *xg* for 10 minutes at 4 °C. The supernatant was collected in clean Eppendorf tube and stored at -20 °C until used.

6.3.3 Bradford protein concentration assay

The Bradford protein assay is a simple and colourimetric method commonly used to determine the total protein concentration of a sample, where the colour intensity is proportional to the protein concentration.

Briefly, 25 mg/mL solution of BSA was prepared and stored at -20 ^{o}C. For use, a 1:10 dilution of BSA stock solution was prepared, 1% (v/v) Triton X-100 was added and further dilutions of 0.5-1.25 mg/mL BSA were prepared. Into a 96-well plate, 5 µL of BSA standard protein sample and protein samples were added, in replicates of 8 and 4 respectively. Once all the standards and samples were plated, 25 µL of solution A (alkaline copper tartrate) and 200 µL of solution B (folin) were added in each well. The 96-well plate was incubated for 30 minutes at room temperature and the absorbance was measured at 650 nm on a 96-well plate reader.

6.3.4 Sodium dodecyl sulphate (SDS) Polyacrylamide gel electrophoresis (PAGE)

Total protein extracts (10, 15 and 20 µg) from MDA-MB-231 and SKBR-3 cells were subjected to SDS-PAGE. The gels were composed of a 9% resolving gel, which required 30 minutes polymerisation at room temperature and a stacking gel, which was left for 45 minutes at room temperature to polymerise. Alongside the protein samples, a protein marker ladder was loaded to enable the determination of the molecular weight of the detected protein bands. Electrophoresis was performed at 150 V for 50 minutes in 1x Electrophoresis Buffer. After electrophoresis, separated proteins were transferred to PVDF membrane. Each membrane was immersed in 100% Methanol for 10 minutes. On

the black side of the transfer cassette the stack was built as follows: one sponge, two filter papers, the activated PVDF membrane, the gel, two filters and one sponge on top. Sponges and filters were all soaked in 1x Transfer Buffer. Once the transfer cassette was placed in the tank with the black side of the cassette facing the black side of the tank, an ice block was added and the tank was filled with 1x Transfer Buffer. Transfer was performed at 360 mA for 45 minutes. After completion of the protein transfer, the PVDF membrane was washed with 1xTBS/T for 5 minutes at RT and blocked in 25 mL blocking buffer (1.25 g dried milk, 25 mL 1xTBS/T) for 1 hour at RT. The PVDF membrane was then washed three times with 15 mL TBS/T. Afterwards, 10 mL primary antibody solution was added and the membrane was left to be rolling for 2 hours at RT. The membrane was washed as before and the secondary antibody solution was added. Dilutions and incubation times for each primary and secondary antibody were optimised as detailed in Table 6.3.4.

Table 6.3.4.: Details of primary and secondary antibodies used for β-actin and SIRT2 protein detection.

Antibody	Dilution	Incubation Time
β-actin (Santa Cruz Biotechnology)	1/5000 Band size: 42 kDa	2 hours (Room temperature)
Anti-mouse secondary (Santa Cruz Biotechnology)	1/10000	1 hour (Room temperature)
SIRT2 (Abcam)	1/500 Band size: 43 kDa	Overnight (Cold room, 4 ^{o}C)
Anti-rabbit secondary (Santa Cruz Biotechnology)	1/1000	2 hours (Room temperature)

The antibodies were detected using SuperSignal WestPico chemiluminescent substrate. After washing the membrane as before, it was incubated with a 1:1 mixture of substrate A : substrate B in the dark. After 5 minutes at room temperature, the excess of detecting reagent was drained off and the membrane was placed in a development cassette between cling film sheet, avoiding bubbles. The detection was completed in the dark room, where a CL-XPosure X-ray film was placed on top of the PVDF membrane, the cassette was closed and left for 15 minutes.

The film was then soaked in developer solution for 1 minute, washed with water, soaked in fixer solution for 2 minutes and then washed with water. The dried film was then labelled and the bands from the molecular weight ladder were recorded (i.e. drawn) on the film.Once SIRT2 was detected, the membrane was incubated for 10 minutes at room temperature in stripping buffer to remove the antibody before undertaking the detection of the housekeeping protein, β-actin. The antibody incubation and the detection were performed as for SIRT2.

6.3.5 Cell stress-related Proteome Profiler Array

The Human Cell Stress Proteome Profiler Array kit was used to determine the expression profile of cell stress-related proteins, in MDA-MB-231 and SKBR-3 treated with BNIPs (Table 6.3.5). All steps were carried out according to the manufacturer's instructions. After 24hours, MDA-MB-231 and SKBR-3 cells were treated with the BNIPs of interest (BNIPDaCHM and BNIPPiEth) at IC_{25}.

After 24 hour incubation, the total protein content was extracted (Section 6.3.2) and the protein concentrations determined as previously described in Section 6.3.3 and 300 µg of protein lysate was used for each array membrane (maximum

amount of protein that was recommended by manufacturer). After a 1 hour membrane blocking step, the samples were pre-incubated with a cocktail of biotinylated detection antibodies (15 µL) and added to the membrane for an overnight incubation at 4 °C.

After three 10 minute washes, the membranes were incubated with streptavidin-horseradish peroxidase (HRP, 2 mL) for 30 minutes and the detection was performed by adding the chemiluminescence detection reagents in equal volumes to the membranes for 1 minute in the dark. The signal was detected by exposing the membrane to CL-XPosure X-ray film for 5 and 10 minutes and developed as previously described in Section 6.3.4.

The mean pixel density of the duplicate spots produced on each film was determined using a FUSION FX7™ imaging instrument with Fusion 1 and BIO-1D™ imaging software. Once the final pixel density was obtained after substracting the pixel density of the negative control, the control *versus* treatment ratio was calculated in order to assess the relative change in protein expression.

Two independent expreriments (two mebranes per sample) were carried out and values (mean ± SD, n = 2) were plotted using GraphPad Prism V7.0.

Table 6.3.5.: Cell stress-related proteins that were studied before and after treatment with BNIPDaCHM and BNIPPiEth in MDA-MB-231 and SKBR-3 cells.

ADAMTS1	HIF-2 alpha	Phospho-p38 alpha (T180/Y182)
Bcl-2	Phospho-HSP27 (S78/S82)	Phospho-p53 (S46)
Carbonic Anhydrase IX	HSP60	PON1
Cited-2	HSP70	PON2
COX-2	IDO	PON3
Cytochrome c	Phospho-JNK Pan (T183/Y185)	Thioredoxin-1
Dkk-4	NF-kappa-B1	SIRT2
FABP1/L-FABP	p21/CIP1	SOD2
HIF-1 alpha	p27/Kip1	

Abbreviations: ADAMTS1= ADAM Metallopeptidase with Thrombospondin Type 1 Motif 1, Bcl-2= B-cell lymphoma 2, Cited-2=Cbp/p300-interacting transactivator 2, COX-2= Cytochrome c Oxidase Subunit 2, Dkk-4= Dickkopf WNT Signaling Pathway Inhibitor 4, FABP1/L-FABP= Fatty Acid-Binding Protein 1, HIF-1 alpha= Hypoxia Inducible Factor 1 Alpha Subunit, HIF-2 alpha= Hypoxia Inducible Factor 2 Alpha Subunit, Phospho-HSP27 (S78/S82)= Phosphorylated Heat Shock Protein Family A (Hsp70) Member 1A, HSP60= Heat Shock Protein Family D (Hsp60), HSP70= Heat Shock Protein Family A (Hsp70) Member 1A, IDO= Indoleamine 2,3-Dioxygenase 1, Phospho-JNK Pan (T183/Y185)= Mitogen-Activated Protein Kinase 8, NF-kappa-B1= Nuclear factor NF-kappa-B, p21/CIP1= Cyclin-dependent kinase inhibitor 1, p27/Kip1= Cyclin-dependent kinase inhibitor 1B, Phospho-p38 alpha (T180/Y182)= P38 mitogen-activated protein kinase alpha, Phospho-p53 (S46)= Phosphoprotein 53, PON1=Paraoxonase 1, PON2=Paraoxonase 2, PON3=Paraoxonase 3, SIRT2= Sirtuin 2, SOD2= Superoxide dismutase 2.

6.3.6 Bioinformatic studies

From the results obtained with the cell stress-related protein arrays, proteins that demonstrated a level of expression that was 0.5 relative different between untreated and BNIP-treated MDA-MB-231 and SKBR-3 cells were recorded and used to construct a network where each protein, defined as a node, interacts with others (Zhang *et al*, 2016; Shannon *et al*, 2003).

The important topological parameters for the construction of a network are the degree (K), the betweenness centrality (BC) and the closeness centrality (CC) (Shannon *et al*, 2003). K represents the numbers of edges (i.e. links) that connect directly to a node. The BC of a node represents the degree (between 0 and 1) of which nodes stand between each other. Comparatively, CC is the inverse of the average length of the shortest paths going through a node (Shannon *et al,* 2003).

In this study, the PPI network construction and analysis was performed by Cytoscape V3.0 (Shannon *et al*, 2003), plus ClueGO V2.3.2 and CluePedia V1.3.2 (Bindea *et al*, 2009) and STRING V10.0 (Szklarczyk *et al,* 2015). The above softwares and their applications are powerful tools to provide useful data and information for the mapping of PPI networks. The used cut-off for interaction evidence was set at 0.05 (p-value threshold).

6.3.7 Statistical analysis

Three independent experiments were conducted and each experiment was comprised of at least two internal replicates, unless otherwise stated. Data are presented as mean ± SD or ± SEM. Statistical analysis was performed by using an unpaired Student's t-test. Statistically significant data were detailed when *$p<0.05$, **$p<0.01$, ***$p<0.001$.

6.4 Results and Discussion

6.4.1 Histone deacetylase activity of BNIPs

Targeting HDACs for breast cancer treatment has been a topic of debate, due to conflicting reports and lack of potent inhibitors. However, several studies have shown that HDACs are overexpressed in tumour cells and also under various environmental conditions, such as hypoxia or serum deprivation (Kim *et al*, 2001, Hu *et al*, 2003). Furthermore, HDAC inhibition is the primary cause of reduction of cancer cell proliferation and cell cycle inhibition (Ropero *et al,* 2006). Therefore, it is important to test novel anti-cancer drugs as potential HDAC inhibitors.

The effect of BNIPs on HDAC activity after 24 hour treatment in both cell lines was investigated to further explore the mechanism by which these derivatives inhibit cell growth and arrest the cell cycle, by performing the HDAC cell-based activity assay. The assay measured the activity of various protein lysine-specific deacetylases in intact cells, after incubation with a cell-permeable HDAC substrate. The fluorescence of the deacetylated reaction product was analysed using a plate reader.

As shown in Figure 6.4.1a, after 24 hour treatment with BNIPs, a difference in HDAC activity compared to untreated cells was observed in MDA-MB-231 cells. More specifically, after treatment with BNIPDaCHM, HDAC activity levels were decreased by 22.6%. After treatment with BNIPPiProp, HDAC activity was also decreased by 37.5%, while after treatment with BNIPPiEth, HDAC activity was significantly decreased by 50.9% ($p<0.05$). After treatment with *trans,trans*-BNIPDaCHM, HDAC activity levels were only slightly affected compared to untreated cells, with a decrease of 13.1%.

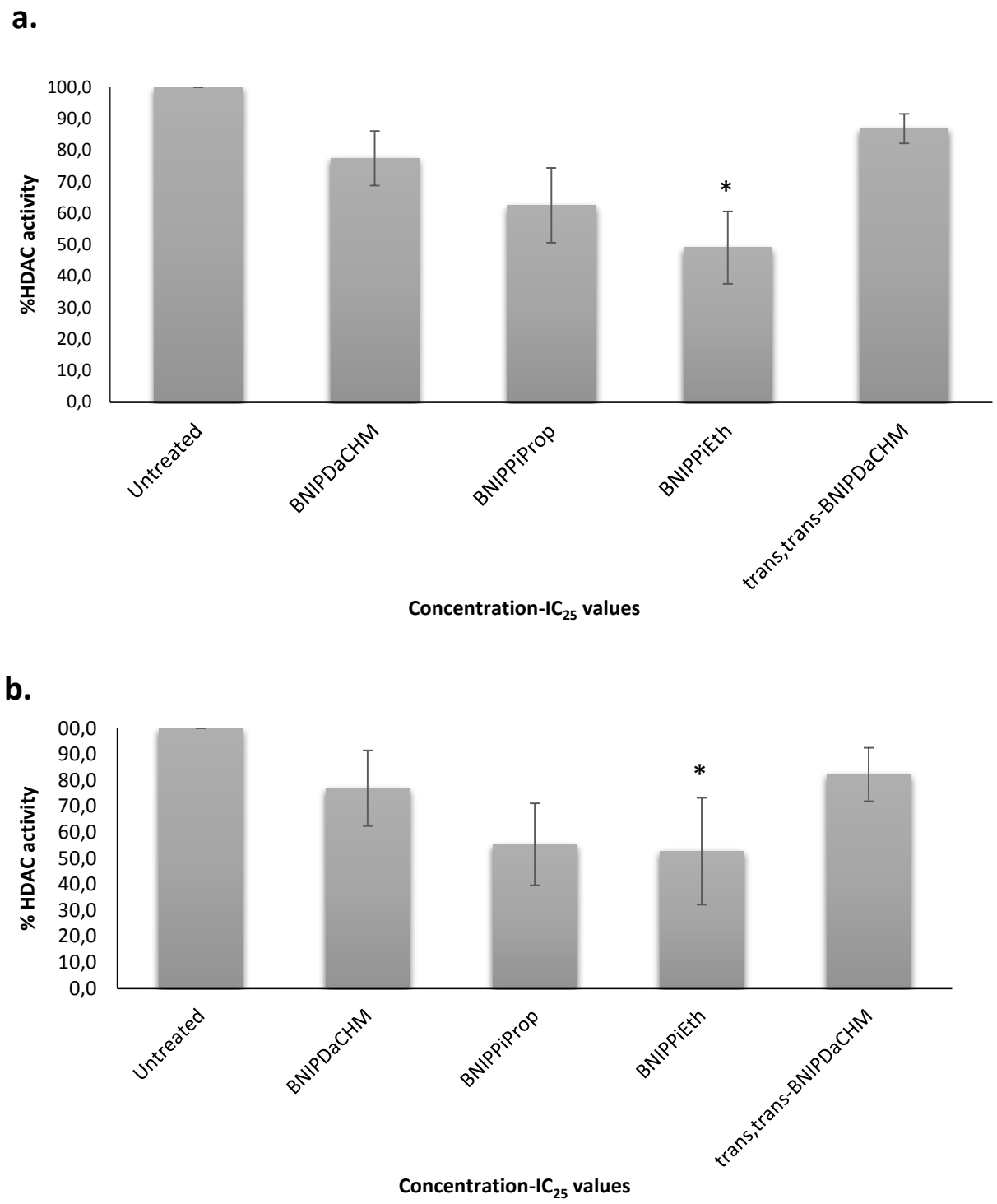

Figure 6.4.1.: Histone deacetylase (HDAC) activity of BNIPDaCHM, BNIPPiProp, BNIPPiEth and *trans,trans*-BNIPDaCHM in a) MDA-MB-231 and b) SKBR-3 cells. DMSO/dH_2O (50% v/v) was used as the solvent control. Data are mean ± SEM of three independent experiments (n = 3), conducted in duplicates. *$p<0.05$, compared to untreated cells.

These results indicate that the three novel BNIPs and their parental compound BNIPDaCHM reduced the HDAC activity after 24 hour treatment in MDA-MB-231 cells. However, BNIPPiEth was the only derivative that significantly reduced HDAC activity levels in MDA-MB-231 cells compared to the untreated cells.

A difference in HDAC activity after 24 hour treatment with BNIPs compared to untreated cells was also observed in SKBR-3 cells (Figure 6.4.1b). After treatment with BNIPDaCHM, HDAC activity levels were decreased by 24.1%, HDAC activity was decreased by 44.6% after treatment with BNIPPiProp, while after treatment with BNIPPiEth HDAC activity was decreased by 47.3% ($p<0.05$), compared to the untreated cells. After treatment with *trans,trans*-BNIPDaCHM, HDAC activity levels were slightly affected compared to untreated cells, with a decrease of 17.8%.

According to the above results, BNIPs have been shown to reduce HDAC activity after 24 hour treatment in SKBR-3 cells, in a similar pattern to that observed in MDA-MB-231 cells. As in MDA-MB-231 cells, BNIPPiEth was the derivative that significantly inhibited HDAC activity levels in SKBR-3 cells.

The HDAC activity in both cell lines was reduced after 24 hour treatment with BNIPs, implying that the inhibition of cell growth and cell cycle arrest that was found in this study can potentially be related to the inhibition of HDAC activity. In addition, BNIPs inhibited HDAC activity even after exposure to small BNIP doses, i.e. IC_{25} and not IC_{50}, in order to avoid extensive loss of the cell population.

Currently, there are four HDAC agents (Romidepsin, Belinostat, Panobinostat and Vorinostat) that inhibit HDAC enzymes and are commercially available for the treatment of cutaneous and peripheral T-cell lymphoma (Moskowitz and Horwitz, 2016). However, a recent study is introducing novel HDACi in breast cancer hormone therapy treatment as a tumour survival strategy, in order overcome

resistance to hormonal therapy, such as Tamoxifen (Munster *et al,* 2011). In addition, exposure to HDAC inhibitors seems to sensitise triple-negative breast cancer cells, according to preclinical research of Dr Bhalla and his group (35th San Antonio Breast Cancer Symposium, 2012).

6.4.2 SIRT2 expression in MDA-MB-231 and SKBR-3 cells

Based on the results presented in Section 6.4.1 where the HDAC activity in both cell types was inhibited after 24 hour treatment with BNIPs, and the fact that many SIRT2 inhibitors bear a naphthalene moiety, which seem to be responsible for their anti-cancer activity (Lima *et al*, 2013), the possible link between BNIPs and HDAC inhibition was further investigated.

The expression of SIRT2 was initially evaluated in MDA-MB-231 cells after 24 hour treatment with the parental compound, BNIPDaCHM at the IC_{25} concentration. Optimisation experiments were conducted with various amounts of total protein extracts (10, 15 and 20 µg) and subjected to SDS-PAGE and western-blot analysis to detect SIRT2 protein expression. After detection, samples containing 20 µg total protein were chosen. SIRT2 is not highly expressed in breast cancer tissues and therefore, the anti-SIRT2 antibody did not work for low protein amount (<20 µg). Beta-actin was used as the housekeeping protein to ensure equal protein loading.

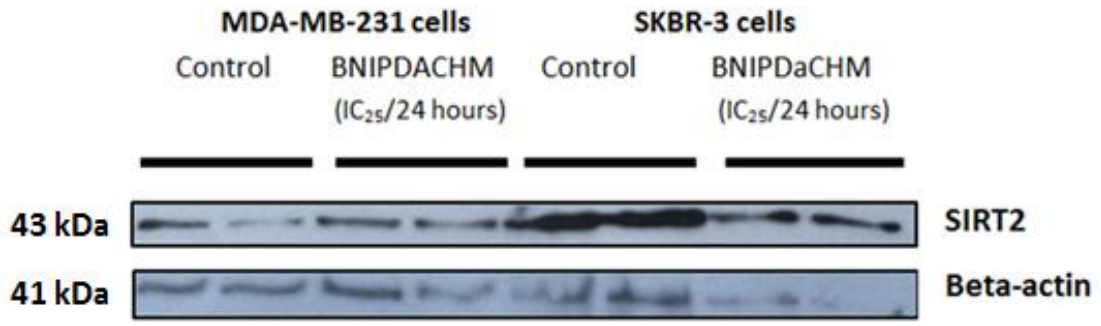

Figure 6.4.2.: Representative western blot showing the expression of SIRT2 and β-actin in MDA-MB-231 and SKBR-3 cells, after 24 hour treatment with BNIPDaCHM.

In MDA-MB-231 cells, no change was observed by visual assessment in SIRT2 expression after treatment with BNIPDaCHM. The band signal (43 kDa) was similar for both treated and control samples (Figure 6.4.2). Similar experiments were conducted in SKBR-3 cells, where SIRT2 expression was decreased after 24 hour treatment with BNIPDaCHM. In SKBR-3 cells, the band signal in treated samples was weaker compared to untreated cells.

However, the above results have to be validated by repeating confirmatory experiments, as it was not possible to repeat this experiment consistently. Different parameters such as decreasing the dilution factor of the primary antibody (1/500), modifying the antibody incubation time and/or the exposure time during detection, were tested to further optimise this experiment however the bands were either not detected or the signal was very weak.

However, these results indicate that SIRT2 expression differs among the two cell lines tested after treatment with BNIPDaCHM. Moreover, BNIPDaCHM could be a potential SIRT2 inhibitor, as in SKBR-3 cells SIRT2 expression was found to be visually decreased after 24 hours treatment with BNIPDaCHM.

Involvement of SIRT2 in tumourigenesis seems to be controversial. Indeed, recent genetic studies using SIRT2 knockout mice have revealed that SIRT2 may function as a tumour suppressor (Kim *et al,* 2011), whilst several reports show that SIRT2 promotes tumourigenesis (Chen *et al,* 2013, Sunami *et al,* 2013).

The reason for this discrepancy is still unknown, however, it may depend on cancer progression stage or cell type and this could explain why SIRT2 expression varies between the two cell types investigated in this study. It is also important to mention that currently there are no similar studies undertaken (making it difficult to draw conclusion), based on SIRT2 expression in MDA-MB-231 and SKBR-3

cancer cells, as according to the Human Protein Atlas data base (www.proteinatlas.org), SIRT2 expression in breast cancer tissues is low compared to glioma cancers (Table 6.4.2)

Table 6.4.2.: Levels of SIRT2 antibody staining/expression (high (dark blue), partially detected (light blue), not detected (white)) in breast cancer tissues. The Human Protein Atlas (www.proteinatlas.org).

Tissue	Cancer staining	Protein expression of normal tissue	Tissue	Cancer staining	Protein expression of normal tissue
Breast cancer			Melanoma		
Carcinoid			Ovarian cancer		
Cervical cancer			Pancreatic cancer		
Colorectal cancer			Prostate cancer		
Endometrial cancer			Renal cancer		
Glioma			Skin cancer		
Head and neck cancer			Stomach cancer		
Liver cancer			Testis cancer		
Lung cancer			Thyroid cancer		
Lymphoma			Urothelial cancer		
Staining summary	All gliomas displayed moderate to strong cytoplasmic positivity. Other cancer tissues were weakly stained or negative.				

6.4.3 Human cell stress-related protein expression after treatment with BNIPs in MDA-MB-231 and SKBR-3 cells

According to the results presented in Chapter 4, BNIPs increase the intracellular levels of ROS in MDA-MB-231 and SKBR-3 cells. Therefore, proteome profiler human cell stress arrays were used for the first time in this study to further explore and identify differences in cell stress-related protein expression that could be responsible for BNIP anti-cancer activity in both cell lines.

Levels of protein expression in control cells were compared to those in cells that were treated with BNIPDaCHM (parental compound) and BNIPPiEth (best BNIP candidate from the effects obtained on the parameters tested earlier). A cut-off of 0.5 ratio was used as considered threshold for meaningful changes in protein arrays studies.

In MDA-MB-231 cells (Figure 6.4.3.1), out of the 26 examined proteins, 7 proteins demonstrated a level of expression that was relatively different after treatment with BNIPPiEth and BNIPDaCHM. More specifically, Cytochrome c (382.0- relative change) showed an increased expression (ratio>0.5) compared to untreated cells, after treatment with BNIPPiEth. Increased expression was also noticed in SIRT2 (1.0- relative change) and SOD2 (0.9- relative change) (ratio>0.5). On the contrary, treatment with BNIPPiEth decreased the expression of PON1 (-1.0- relative change), PON2 (-1.0- relative change), HIF-1a (-0.7- relative change) and HSP60 (-0.7- relative change) (ratio<0.5). In parallel, SIRT2 (1.8- relative change) showed increased expression (ratio>0.5) compared to untreated cells, after treatment with BNIPDaCHM to a greater extent (0.8- relative change increase) than in BNIPPiEth-treated cells.

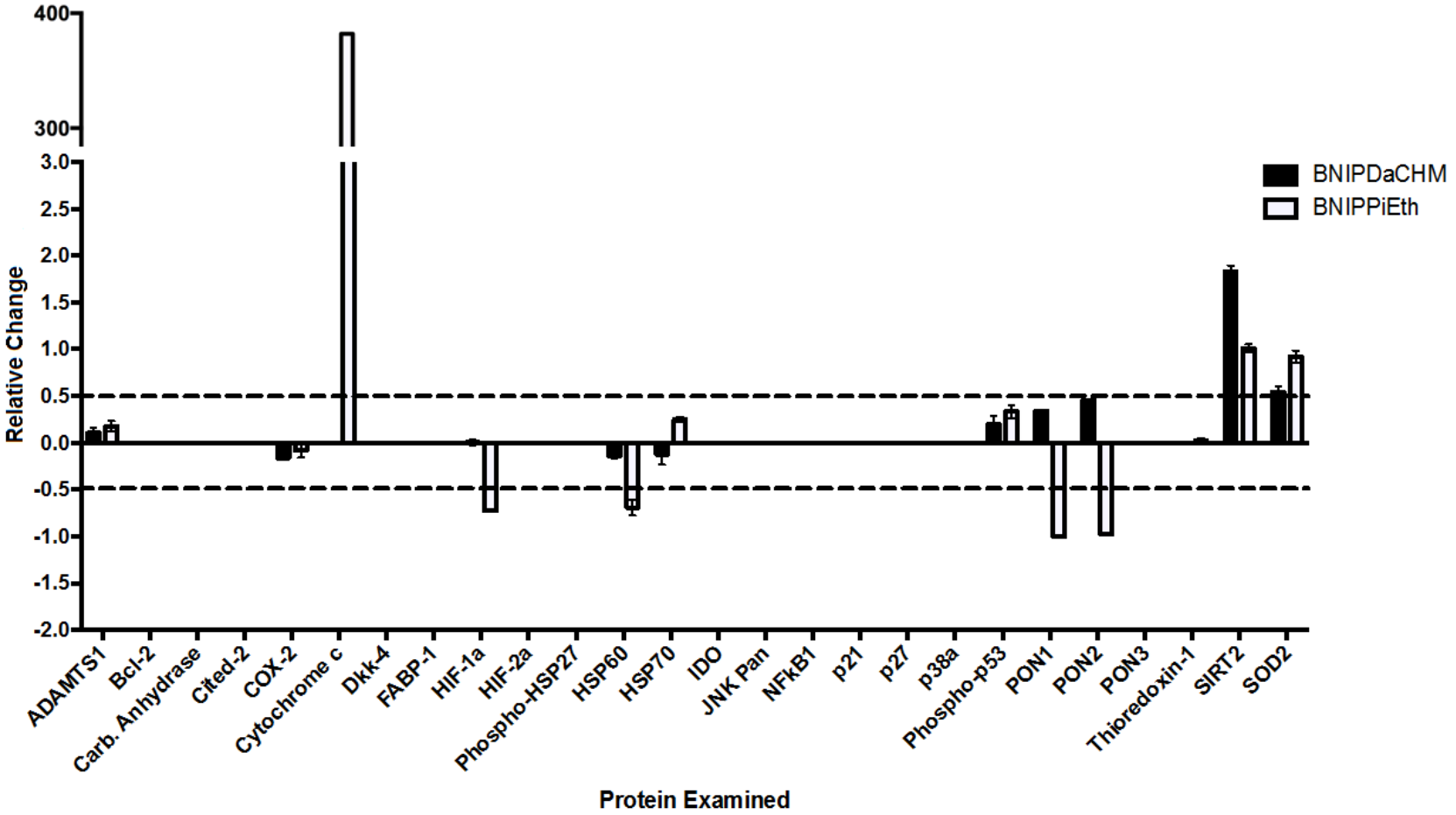

Figure 6.4.3.1.: Comparison of BNIPDaCHM and BNIPPiEth effects upon cell stress related proteins in MDA-MB-231 cells.

Data are mean ± SD of two independent experiments (n = 2), values were plotted using GraphPad Prism V7.

SOD2 (0.5 relative change) expression, however, was decreased (ratio<0.5) after treatment with BNIPDaCHM, compared to BNIPPiEth-treated cells.

Moreover, 19 proteins showed either no change or a relative change inferior to a 0.5 ratio in MDA-MB-231 cells (effects of BNIPs that do not lead to changes in protein abudance, such as post-translational modifications, can not be detected).

In SKBR-3 cells (Figure 6.4.3.2), out of the 26 examined proteins, 12 proteins demonstrated a level of expression that was relatively different after treatment with BNIPPiEth and BNIPDaCHM. More specifically, HIF-1a (0.9- relative change), HIF-2a (0.8- relative change), IDO (0.7- relative change), p21 (0.7- relative change), p27 (1.2- relative change), PON1 (1.0- relative change) and PON3 (1.0- relative change) showed increased expression (ratio>0.5) compared to untreated cells, after treatment with BNIPPiEth. In SKBR-3 cells, none of the examined proteins showed decreased expression after treatment with BNIPPiEth Moreover, ADAMTS1 (0.8- relative change), Bcl-2 (1.7- relative change), Carbonic Anhydrase IX (1.1- relative change), COX-2 (1.0- relative change), Dkk-4 (1.5- relative change), HIF-1a (1.0- relative change), IDO (0.9- relative change), p21 (1.0- relative change), p27 (1.2- relative change) and PON3 (89.0- relative change) showed an increased expression (ratio>0.5) after treatment with BNIPDaCHM and PON1 (-0.8- relative change) protein expression was the only protein to be decreased after treatment with BNIPDaCHM (ratio<0.5) compared to untreated cells.

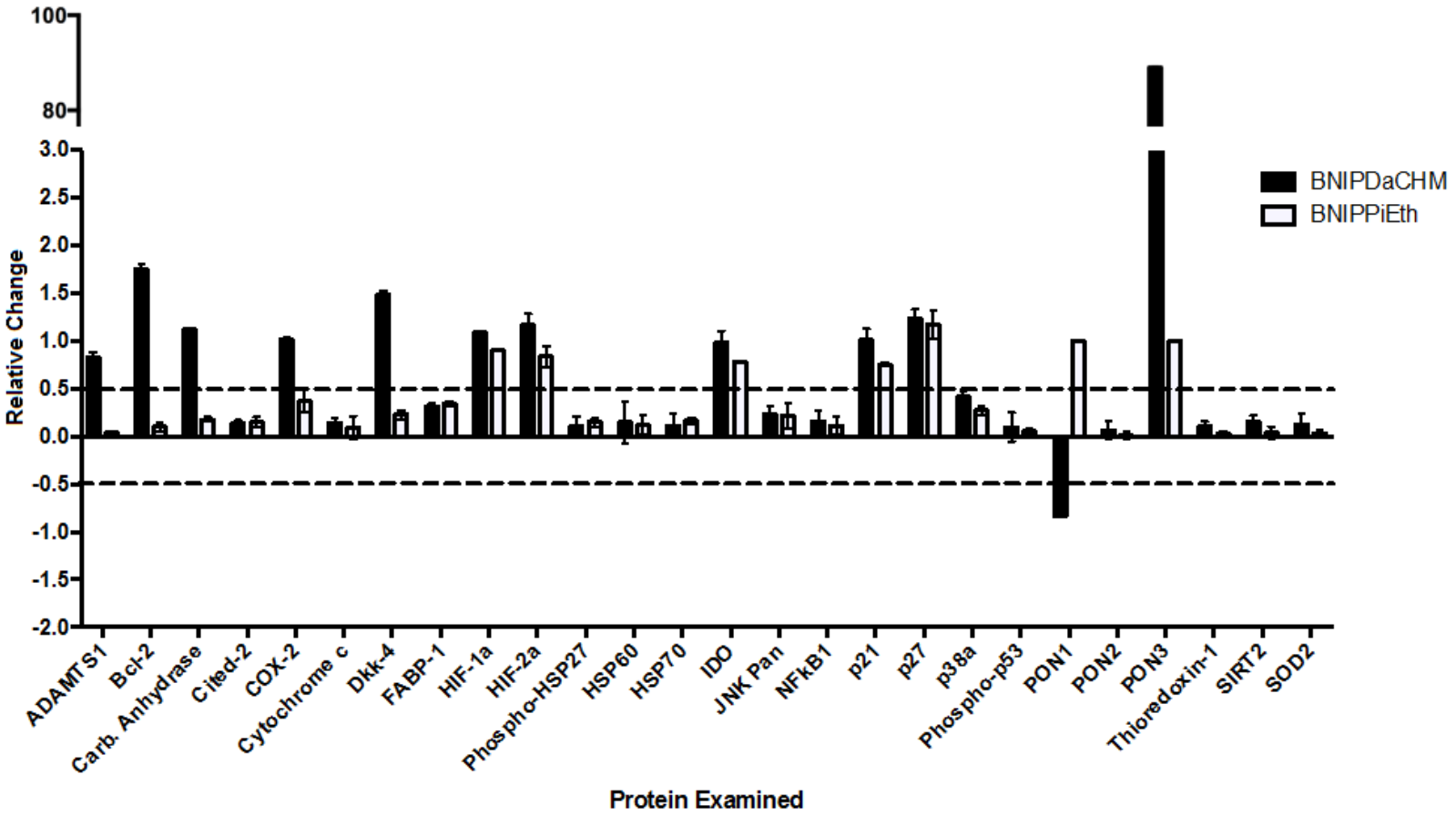

Figure 6.4.3.2.: Comparison of BNIPDaCHM and BNIPPiEth effects upon cell stress related proteins in SKBR-3 cells. Data are mean ± SD of two independent experiments (n = 2), values were plotted using GraphPad Prism V7.0.

Also, in SKBR-3 cells, 14 proteins showed either no change or a relative change inferior to 0.5 (effects of BNIPs that do not lead to changes in protein abudance, such as post-translational modifications, can not be detected).

In summary, the above results revealed that BNIPDaCHM and BNIPPiEth alter the expression (up- or downregulation) of cell stress-related proteins in a different pattern depending on the cell type, suggesting that the mechanism of action of BNIPs could be cell line dependent. To further validate the obtained experimental results and in order to reveal the biological processes involved, the cellular compartment localisation and the different pathways in which the above panel of proteins are involved (only cell stress-related proteins were examined, so more proteins could have been potentially affected after treatment treatment with BNIPs), bioinformatics studies were employed and findings are presented and discussed in the following section (Section 6.4.4).

6.4.4 Construction and analysis of Protein–Protein Interaction (PPI) Networks

Since interactome analysis can provide a candidate biomarker panel related to a disease, protein-protein interaction (PPI) network analysis was used to introduce the involved crucial proteins in breast cancer cells, based on the outcome of the protein array studies described in Section 6.4.3.

Proteins that demonstrated a level of expression 0.5 relatively different between untreated and BNIP-treated cells were determined and matched to construct the corresponding PPI networks. Three PPI networks were constructed and cellular compartment localisation of the examined proteins was predicted. The cut-off used for interaction evidence was set at 0.05 (p-value threshold).

The first step of the study was to construct a PPI network that included the 26 proteins examined *via* the Proteome Profiler Human Cell Stress Array, employing Cytoscape 3.4 (ClueGO V2.3.2. and CluePedia V1.3.2). The biological processes, in which these proteins (Table 6.4.4a) are involved (in both cell lines), are described in Figure 6.4.4.1.

The PPI network validated that the examined proteins were indeed cell stress related. Moreover, on Figure 6.4.4.1, their biological processes were determined and classified in four distinct categories:

- cellular response to oxidative stress (dark blue),
- response to oxygen levels (light blue),
- regulation of interlucin-12 production (dark green), and
- cellular oxidant detoxification (light green).

Protein names	Input names
ADAMTS1	ADAMTS1
Bcl-2	BCL2
Carb. Anhydrase	CAIX
Cited-2	MRG1
COX-2	COX2
Cytochrome c	COX1
Dkk-4	DKK4
FABP-1	FABP1
HIF-1a	HIF1A
HIF-2a	HIF2A/EPAS1
Phospho-HSP27	HSP27
HSP60	HSPD1
HSP70	HSP70
IDO	IDO1
JNK Pan	JNK1
NFkB1	NFKB1
p21	CDKN1
p27	CDKN1B
p38a	MAPK1
Phospho-p53	TP53
PON1	PON1
PON2	PON2
PON3	PON3
Thioredoxin-1	TXN
SIRT2	SIRT2
SOD2	SOD2

Table 6.4.4.: List of examined proteins/input names for bioinformatic studies.

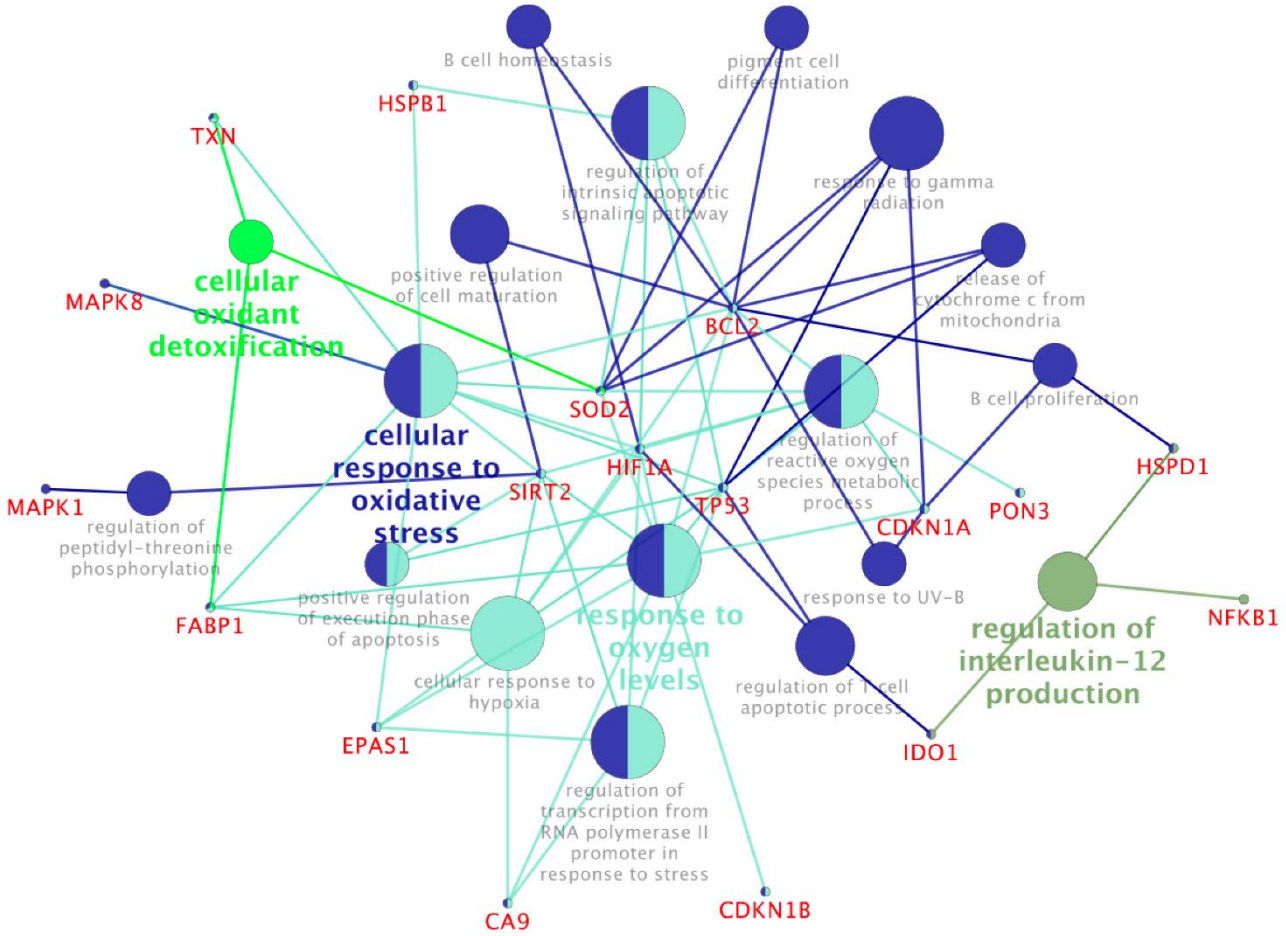

Figure 6.4.4.1.: Representation of the statistically significant (p-value threshold: 0.05) biological processes of proteins examined *via* the Proteome Profiler Human Cell Stress R&D Array, employing Cytoscape 3.4 (ClueGO V2.3.2 and CluePedia V1.3.2).

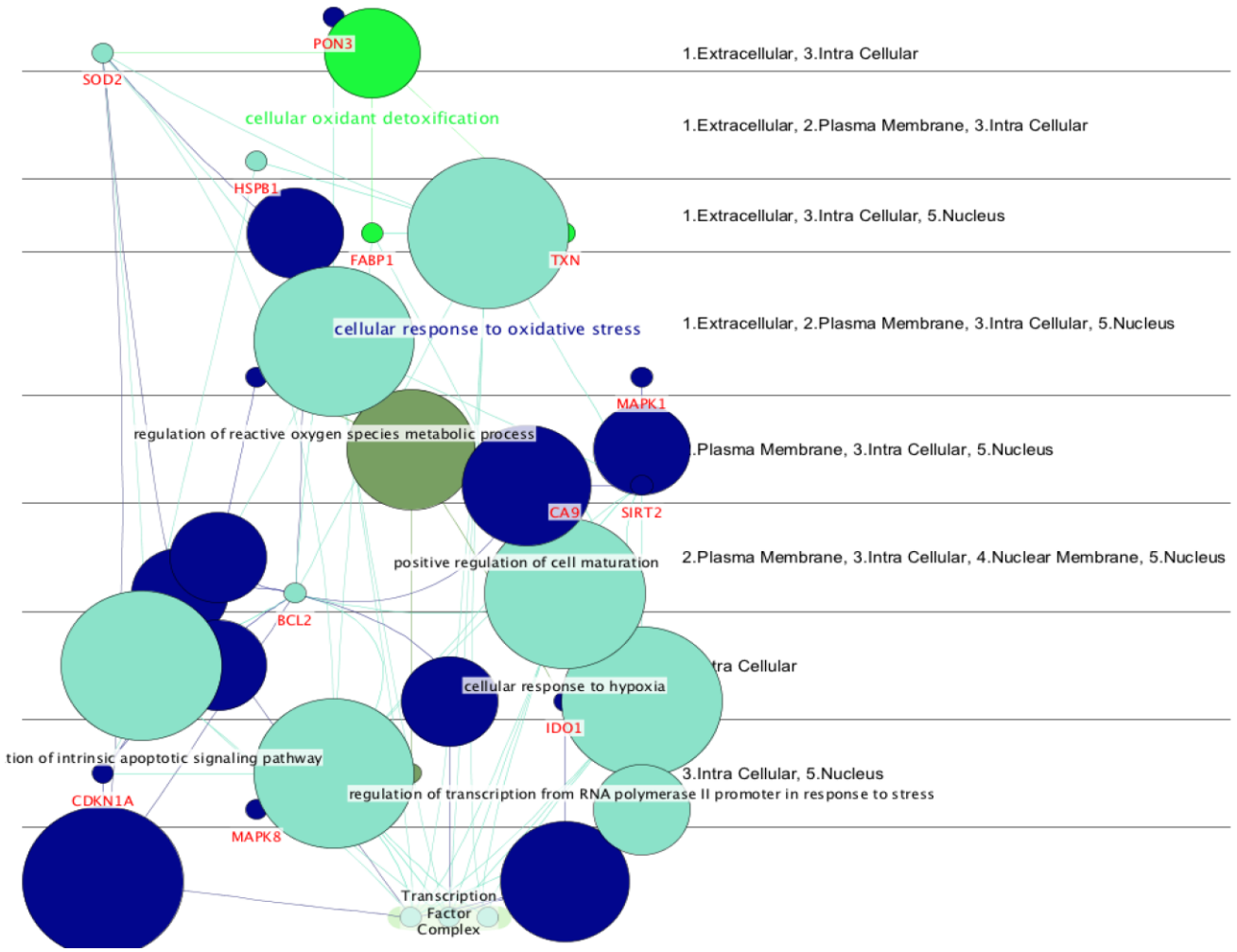

Figure 6.4.4.2.: Cellular compartment localisation prediction of the statistically significant (p-value threshold: 0.05) biological processes of proteins examined *via* the Proteome Profiler Human Cell Stress R&D Array, employing Cytoscape 3.4 (ClueGO V2.3.2 and CluePedia V1.3.2).

In addition, ClueGO V2.3.2 and CluePedia V1.3.2 were employed determining protein cellular compartment localisation, as seen in Figure 6.4.4.2. More specifically, the examined proteins are found in five cellular compartments: the nucleus, the nuclear membrane, the plasma membrane, intracellular and/or extracellular (Figure 6.4.4.2). Then, the 7 proteins (Cytochrome c, SIRT2, SOD2, PON1, PON2, HIF-1a and HSP60) that demonstrated a level of expression that was 0.5 relatively different between untreated and BNIP-treated MDA-MB-231 cells were grouped and used to construct the PPI network presented in Figure 6.4.4.3a. The PPI network consists of three connected nodes, SOD2, HIF-1A and SIRT2, while PON1 and HSP60 are represented as isolated nodes (which denotes no known interaction). Cytochrome c and PON2 did not meet the statistically significant cut-off of 0.05, and as a result, the corresponding nodes do not appear on the PPI network. The biological processes of the 7 examined proteins involve oxygen homeostasis, positive regulation of T cell mediated immune response to tumour cell and negative regulation of plasma lipoprotein particle oxidation (summarised in Figure 6.4.4.3b).

SOD2 is a well-known antioxidant protein highly involved in mitochondrial catabolic pathway, by binding to the superoxide byproducts of oxidative phosphorylation and converting them to hydrogen peroxide and/or diatomic oxygen (Fukai and Ushio-Fukai, 2011). On the other hand, HIF-1a (alpha subunit of transcription factor hypoxia-inducible factor-1 (HIF-1)) is a main regulator of cellular and systemic homeostatic response to hypoxia and activates the transcription of genes related to energy metabolism, angiogenesis, apoptosis or oxygen delivery (Ziello *et al*, 2007). The above network highlights a potential pathway, where the intracellular production of ROS after treatment with BNIPs

could alter the expression SOD2, which can interact with the transcription factor HIF-1a to regulate the expression of SIRT2 and therefore histone deacetylation.

Furthermore, cellular localisation of the proteins revealed that PON1 and HSP60 are located in more than one compartment (mainly extracellular/intracellular). However, there is no confirmed interaction with the rest of the examined proteins that could correlate with a mechanism of action of BNIPPiEth and BNIPDaCHM in MDA-MB-231 cells (Figure 6.4.4.4).

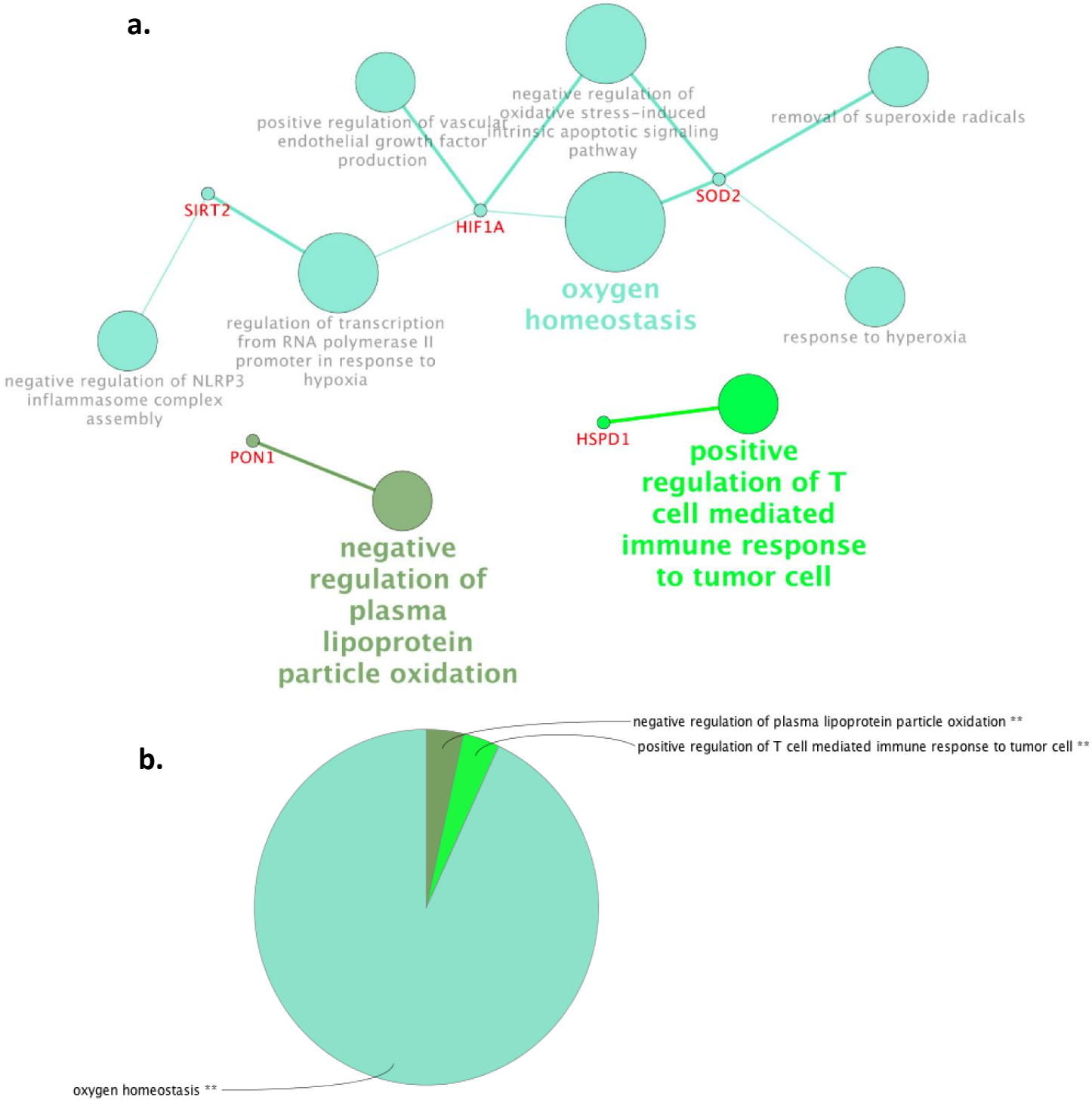

Figure 6.4.4.3.: Network (a) and pie chart (b) representation of the statistically significant (p-value threshold: 0.05) biological processes, of proteins that met the ± 0.5 relative change criteria (Figure 6.4.3.1) in MDA-MB-231 cells after treatment with BNIPs, employing Cytoscape 3.4 (ClueGO V2.3.2 and CluePedia V1.3.2).

Figure 6.4.4.4.: Cellular compartment localisation prediction of selected proteins that met the ± 0.5 relative change criteria (Figure 6.4.3.1) in MDA-MB-231 cells after treatment with BNIPs, employing Cytoscape 3.4 (ClueGO V2.3.2 and CluePedia V1.3.2).

Based on these findings, the 5 candidate proteins (SOD2, HIF-1a, SIRT2, PON1 and HSP60) were further examined *via* String functional protein association network analysis. This analysis performed both literature and proteomic/genomic database searches and represents putative or known associations between input proteins/genes.

As shown in Figure 6.4.4.5, the 5 proteins that met the cut-off criteria were found to be associated in a String network. The thin association lines between nodes indicate low confidence interactions (as derived from gene co-expression and literature searches) while thicker association lines indicate high confidence interactions (as derived from co-IPs, proteomic assays and multiple citations in the literature search).

PON1 (hydrolytic enzyme with antioxidant properties) (Mackness and Mackness, 2015) interacts with SOD2 and, in turn, SOD2 interacts with HSP60 which, while employing a linker protein, HSP90AA1 (heat shock protein, involved in hypoxic and oxygen homeostasis regulation of HIF-1a pathway) (Zuehlke *et al*, 2015), interacts with HIF-1a. HIF-1a, as previously mentioned, was found to interact directly with SIRT2. In addition, PON1, which was found to have an extracellular localisation (Figure 6.4.4.4), is suggested to be the upstream element of the proposed pathway, while HIF-1a and SIRT2 are suggested to be its downstream and terminal components, respectively. As a result, the construction of PPI networks indicated the crucial role of the highlighted proteins in MDA-MB-231 cells after treatment with BNIPs and, the possible mechanism of BNIP action, which seems to be related with the activation/regulation of a novel protein complex.

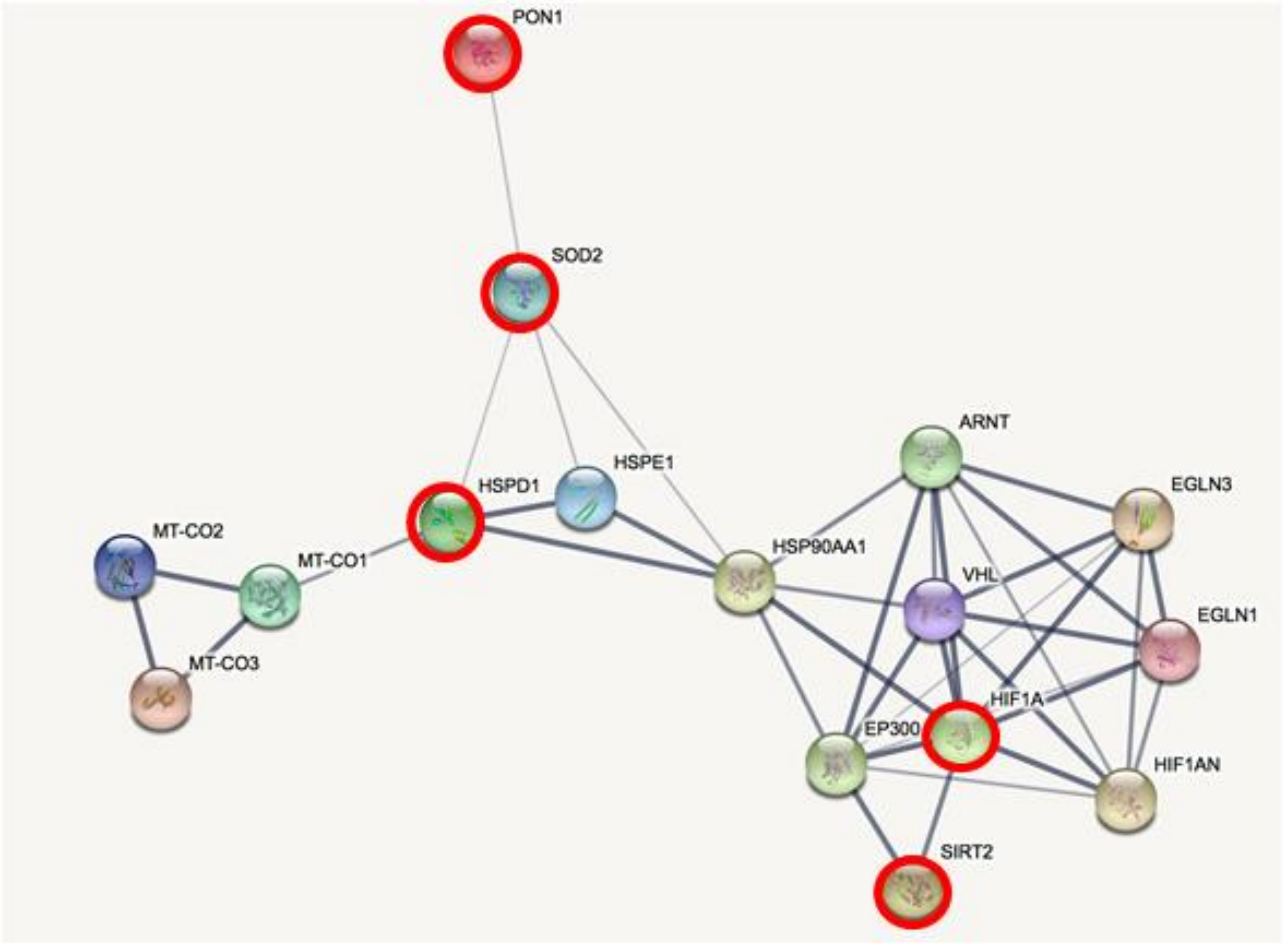

Figure 6.4.4.5.: Network with the statistically significant (p-value threshold: 0.05) proteins that met the ± 0.5 relative change criteria (Figure 6.4.3.1) in MDA-MB-231 cells after treatment with BNIPs (in red ring), and other non-examined proteins, after employing String V10.0.

The 12 proteins of interest which related to BNIP-treated SKBR-3 cells (i.e ADAMTS1, Bcl-2, Carbonic Anhydrase IX, COX-2, Cytochrome c, Dkk-4, HIF-1a, IDO, p21, p27, PON1 and PON3) have been studied, grouped and used for the construction of the PPI network presented in Figure 6.4.4.6a. The PPI network consists of several connected nodes (including ADAMTS1, Bcl-2, Carbonic Anhydrase IX, COX-2, Cytochrome c, HIF-1a, IDO, p21, p27 and PON3) with similar "linker" proteins and share similar biological processes; while only two proteins, PON1 and Dkk-4, are represented as isolated nodes (no known interaction). The interesting finding in the above network is that none of the 12 examined proteins interacts directly with each other. More specifically, the biological processes of the examined proteins involve negative regulation of the ROS metabolic process, intestinal epithelial cell maturation and regulation of transcription from RNA polymerase II promoter in response to hypoxia as presented in Figure 6.4.4.6b. Furthermore, cellular localisation of the above proteins revealed that PON1 and Dkk-4 are located in more than one compartment (mainly extracellular/intracellular) and there is no confirmed interaction with the rest of the examined proteins that could correlate with a mechanism of action of the BNIPPiEth and BNIPDaCHM studied in SKBR-3 (Figure 6.4.4.7).

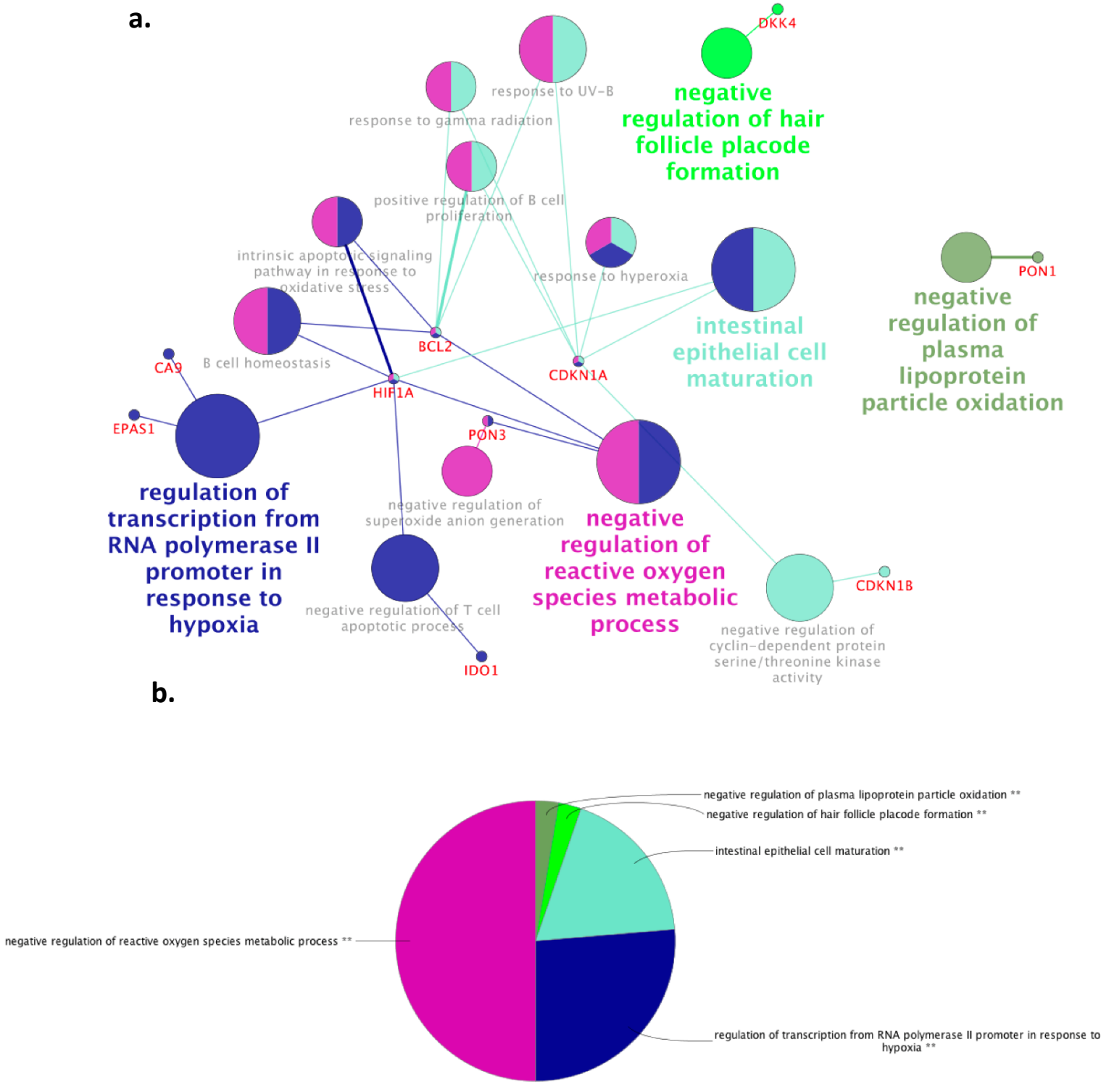

Figure 6.4.4.6.: Network (a) and pie chart (b) representation of the statistically significant (p-value threshold: 0.05) biological processes of proteins that met the ± 0.5 relative change criteria (Figure 6.4.3.2) in SKBR-3 cells after treatment with BNIPs, employing Cytoscape 3.4 (ClueGO V2.3.2 and CluePedia V1.3.2).

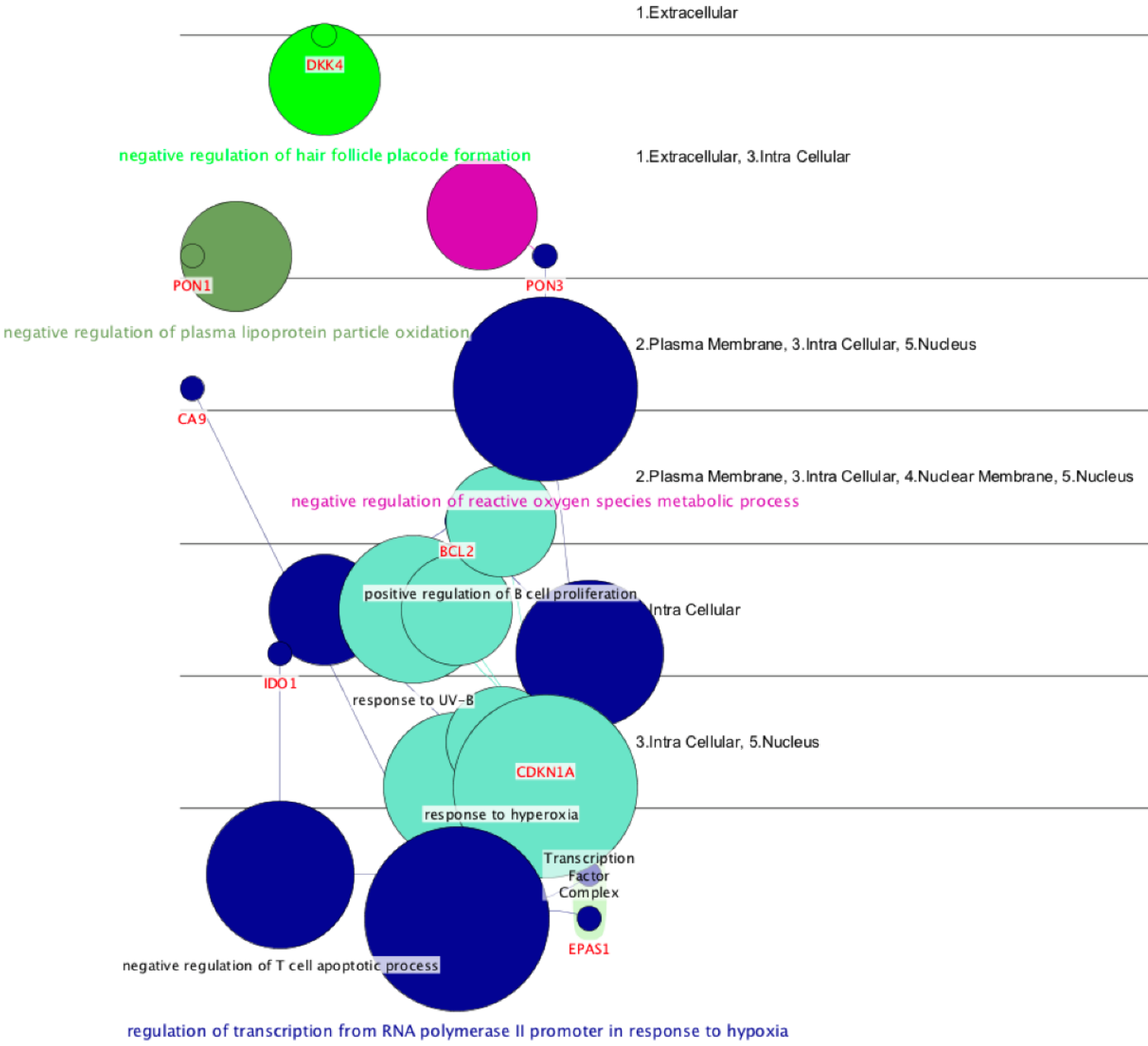

Figure 6.4.4.7.: Cellular compartment localisation prediction of selected proteins that met the ± 0.5 relative change criteria (Figure 6.4.3.2) in SKBR-3 cells after treatment with BNIPs, employing Cytoscape 3.4 (ClueGO V2.3.2 and CluePedia V1.3.2).

Similarly to the MDA-MB-231 cell line, string functional protein association network analysis was performed for proteins that met the cut-off criteria for SKBR-3 cells.

Carbonic Anhydrase IX (transmembrane protein and one of only two tumour-associated carbonic anhydrase isoenzymes known) interacts with Bcl-2 (apoptosis regulator, one out of the 154 genes involved in the Integrated Breast Cancer Pathway- Superpath (Belinky *et al*, 2015)) which then interacts with both p21 and p27 (cyclin dependent inhibitors and regulators of cell cycle progression) involved in G1 arrest (Belinky *et al,* 2015) (Figure 6.4.4.8). p21 interacts directly with HIF-1a which subsequently interacts with HIF-2a (transcription factor involved in the induction of genes regulated by oxygen and paralog of HIF-1a).

Carbonic Anhydrase IX, localized mainly in plasma membrane (Figure 6.4.4.4), is suggested to be the upstream element of the proposed pathway. However, even if there is not an established interaction with PON1 and PON3, a possible protein-protein interaction of the three should be studied, as PON1 and PON3 are localised on the extracellular compartment (Figure 6.4.4.7b) and could be potentially upstream elements of this pathway, as observed in MDA-MB-231 cells. HIF-1a and HIF-2a are suggested to be the downstream and terminal components, respectively.

As before, the construction of PPI networks indicated the crucial role of the highlighted proteins in BNIP-treated SKBR-3 cells and, the possible mechanism of BNIP action, which seems to be related with the activation/regulation of a novel protein complex, in which common protein elements compared to MDA-MB-231 cell/pathway are involved.

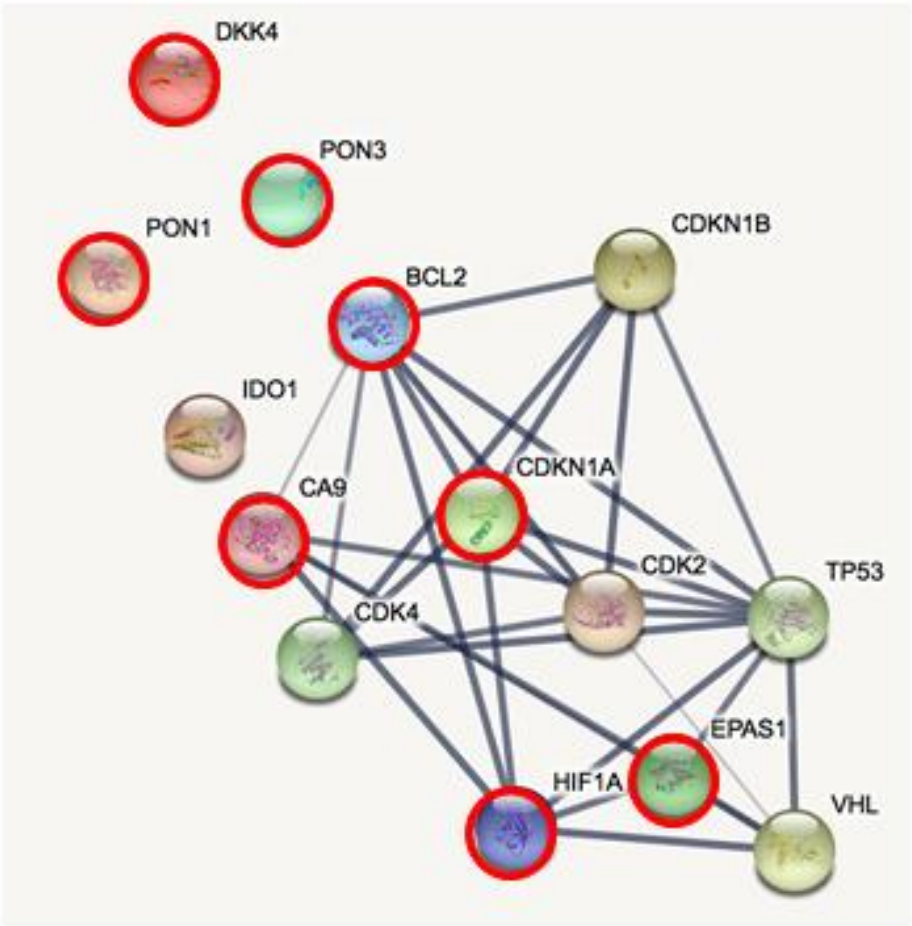

Figure 6.4.4.8.: Network with the statistically significant (p-value threshold: 0.05) proteins that met the ± 0.5 relative change criteria in SKBR-3 cells after treatment with BNIPs (in red ring), and other non-examined proteins, after employing String V10.0.

6.5 Conclusion

In Chapter 6, the effect of BNIPs on HDAC activity in breast cancer cells, with emphasis on SIRT2, and on cell stress-related proteins, was studied. The three novel BNIPs and their parental compound BNIPDaCHM (all at IC_{25} concentrations), decreased HDAC activity after 24 hours treatment in MDA-MB-231 cells. Similarly, BNIPs were found to decrease HDAC activity after 24 hour treatment in SKBR-3 cells, in a similar pattern to that observed in MDA-MB-231 cells. However, BNIPPiEth was the only derivative that significantly decreased HDAC activity levels in both MDA-MB-231 and SKBR-3 cells. Protein expression of SIRT2 only showed differences between the two different cell lines visually after 24 hour treatment with BNIPDaCHM. Moreover, BNIPDaCHM could be a potential SIRT2 inhibitor in SKBR-3 cells, where SIRT2 expression was found to decrease after 24 hours treatment with BNIPDaCHM. However, the above results have to be further validated by repeating confirmatory experiments to assess the optimum protein amount required and to define the most appropriate antibody concentration and incubation time. Proteome profiler arrays demonstrated that in BNIP-treated MDA-MB-231 cells, three proteins (Cytochrome c, SIRT2 and SOD2) had an increased expression and four (PON1, PON2, HIF-1a and HSP60) had a decreased expression. On the other hand, in BNIP-treated SKBR-3 cells, the protein expression of 12 proteins (ADAMTS1, Bcl-2, Carbonic Anhydrase IX, COX-2, Cytochrome c, Dkk-4, HIF-1a, IDO, p21, p27, PON1 and PON3) were increased and 1 (PON1) was decreased. Thus, BNIPDaCHM and BNIPPiEth altered the expression of cell stress-related proteins in a cell dependent manner. In addition, PPI network analysis was used to further validate the outcome of the protein array studies. Bioinformatic analysis revealed two novel, putative pathways for BNIP-induced oxidative stress-mediated cell death in MDA-MB-231 and SKBR-3 cells

(Figure 6.5). These findings create the stepping stone for further research and validation towards the delineation of the suggested pathways, as well as the mode/mechanisms of BNIP action in breast cancer.

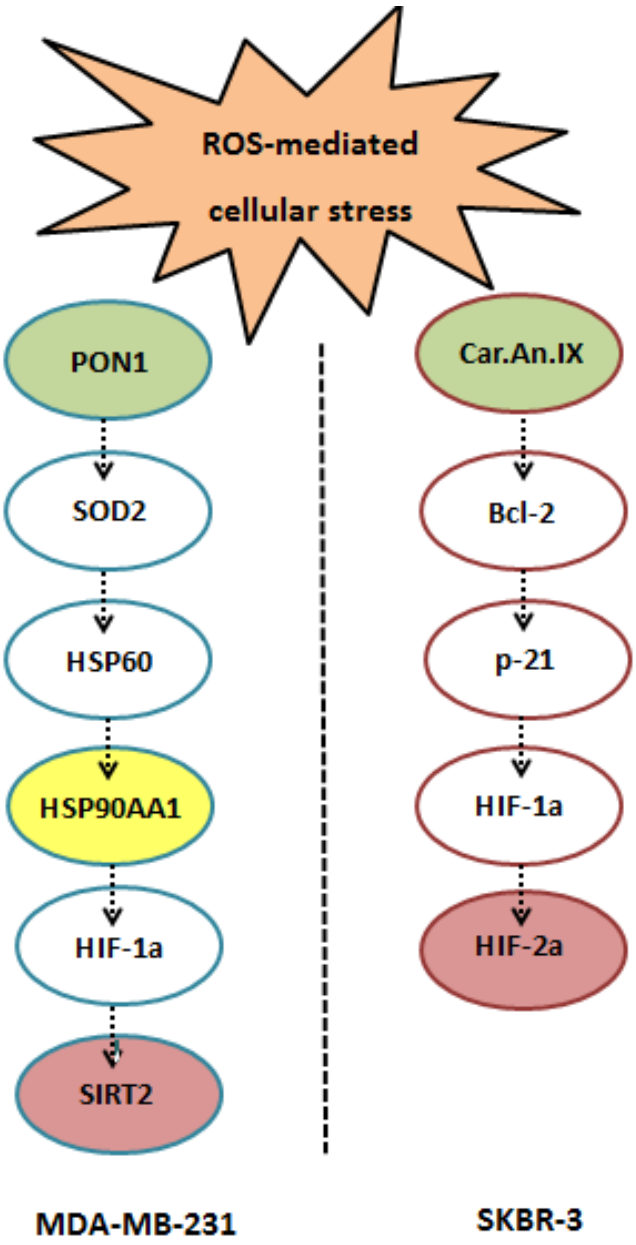

Figure 6.5.: Schematic representation of proposed mechanism for BNIP-induced oxidative stress-mediated cell death in MDA-MB-231 and SKBR-3 cells. Black arrows indicate pathways for cell death, green circles the upstream components, red circles the downstream components and yellow circles the linker proteins of the pathway.

CHAPTER 7.

Conclusion and future work.

This project focused on determining the role of novel compounds as anti-cancer drugs and to identify their mechanism(s) of action in breast cancer cells. The novel compounds were based on the parental compound BNIPDaCHM and were described to define the impact of the different types of isomers. The three novel BNIPs, BNIPPiProp, BNIPPiEth and *trans,trans*-BNIPDaCHM were successfully synthesised and characterised as presented in Chapter 2. The *N*-alkylation reaction that has been used previously for the synthesis of other BNIPs in the series has been proved a suitable synthetic process to produce the above compounds. Apart from high % yields, it resulted in formation of compounds without by-products (Lima *et al*, 2013, Barron *et al*, 2010, Kopsida *et al*, 2016).

The successful synthesis of the three novel BNIPs allowed further investigation on their DNA binding properties which is one of the main characteristics of certain cancer drugs. In Chapter 3, physical properties of three novel BNIPs, BNIPPiProp, BNIPPiEth and *trans,trans* BNIPDaCHM were further investigated. Their DNA binding affinities were assessed by using different *in vitro* techniques, such as thermal denaturation studies, EtBr competitive displacement and UV binding studies. Thermal denaturation studies have shown that BNIPPiProp and BNIPPiEth can intercalate and stabilise the double helix of *Calf Thymus* DNA that was confirmed by their increased T_m values compared to *Calf Thymus* DNA alone. BNIPPiEth was identified as the most active DNA binding member of the BNIPs. In addition, it was observed that the length of the linker sequence seems to affect a drug's binding potential to the DNA (O'Hare *et al*, 2001, Kopsida *et al*, 2016). Moreover, studies on competitive displacement of EtBr by BNIPs were performed to further evaluate their DNA binding affinity. Each BNIP competitively displaced EtBr from DNA in a dose dependent manner, confirming the hypothesis of DNA intercalation being responsible, at least in part, for their mode of action (Dance *et*

al, 2005). BNIPPiEth was identified as the BNIP with the strongest binding affinity. Moreover, the structure of BNIPDaCHM and its mixture of three isomers was found to improve its interacting properties within the DNA base pairs, compared to *trans,trans*-BNIPDaCHM. This was confirmed since *trans,trans*-BNIPDaCHM (1.1 ± 0.2 μM) resulted in a lower C_{50} value compared to BNIPDaCHM (2.3 ± 0.1 μM), revealing that each of the three or more than one (*trans,trans/cis,trans* or *trans,trans/cis,cis*) isomers co-existing in BNIPDaCHM, are involved in the intramolecular complexes/interactions with DNA. By isolating one of its isomers (*trans,trans*-BNIPDaCHM), the DNA binding affinity was significantly decreased. Thus, the structures of BNIPDaCHM with the presence of the aromatic naphthalimido rings allow them to fit between the base pairs (intercalation) and in parallel to the previous feature, the ability of possible rotational freedom within the plane of the aromatic rings, may allow their exposure of more than one intercalating sidechain to DNA (Kopsida *et al*, 2016). Strong K binding constants to reflect the binding potential of the compounds with DNA were determined for the three novel BNIPs, after carrying out UV binding studies, which is in agreement with the previous findings presented in Chapter 3. To further determine the DNA binding affinity of the three novel BNIPs and the molecular aspects of BNIP-DNA interactions, it would be important to verify their groove binding potential and sequence specificity *via* NMR.

Subsequently in Chapter 4, BNIPs were screened for biological activity in breast cancer MDA-MB-231 and SKBR-3 cells. After 24 hour treatment, all novel BNIPs exhibited strong cytotoxicity with IC_{50} values ranging from 1.4 μM to 3.3 μM in MDA-MB-231 cells and from 0.2 to 0.7 μM in SKBR-3 cells, confirming the importance of the bisnaphthalimidopropyl functionality for anticancer activity. More specifically, the current linker sequence modifications showed stronger

cytotoxic effects against MDA-MB-231 and SKBR-3 cells, when compared to the parental compound BNIPDaCHM. The lower IC_{50} value range shows that SKBR-3 cells are more sensitive to BNIP treatment, compared to MDA-MB-231 (triple negative breast cancer cells). *Trans,trans*-BNIPDaCHM exhibited stronger cytotoxicity compared to BNIPDaCHM in MDA-MB-231 cells, showing that the existence of a single isomer in the linker sequence results in a more cytotoxic compound, compared to a mixture of different isomers. BNIPPiEth was more cytotoxic than BNIPDaCHM, suggesting that the shorter length of the linker chain, as well as the incorporation of the nitrogen atom within the cyclohexane ring, not only improved the binding properties of BNIPPiEth, but enhanced significantly its *in vitro* cytotoxicity too. Regarding BNIPPiProp, the derivative with the longest linker sequence and the highest IC_{50} value, it was found that the linker chain length plays an important role in the functionality and effectiveness of the BNIPs. In addition, all the derivatives followed a similar pattern of cytotoxicity in both cell lines; however, they appeared more cytotoxic against SKBR-3 cells compared to MDA-MB-231 ones, which is probably due to the cells different mutational and tumourigenic statuses (Kao *et al*, 2009). Thus, it would be important to further investigate the cytotoxicity of the three novel BNIPs against different cell lines, as this would offer a valuable insight into their potential as anti-cancer agents not only in breast, but more types of cancer.

The effect of BNIPs in tuning the levels of intracellular ROS was also investigated in Chapter 4 as ROS production has been linked to cell death. BNIPDaCHM is the derivative that caused the highest increase of ROS levels in MDA-MB-231 cells, after 8 hour treatment, followed by BNIPPiEth, BNIPPiProp and *trans,trans*-BNIPDaCHM. In SKBR-3 cells, BNIPPiProp caused the highest increase of ROS levels, followed by BNIPDaCHM, BNIPPiEth, and *trans,trans*-BNIPDaCHM.

The above findings indicated that production of ROS was increased in both MDA-MB-231 and SKBR-3 cells, in relation to treatment with individual BNIPs. However, the increase in ROS levels does not seem to parallel the cytotoxicity values determined by MTT assay after 24 hour treatment (Chapter 3) for each compound in the two cell lines. For example, although *trans,trans*-BNIPDaCHM was the most cytotoxic BNIP derivative in both MDA-MB-231 and SKBR-3 cells, it was not responsible for the highest increase of ROS levels. ROS levels were increased in a dose dependent manner, as for less cytotoxic compounds, such as BNIPDaCHM, BNIPPiProp and BNIPPiEth, and in order to achieve IC_{25}, more of the compounds had to be used: this led to higher levels of ROS being detected. The lower ROS production induced by *trans,trans*-BNIPDaCHM compared to the other BNIPs, seem to be linked with the melting points and DNA binding studies results. The more stable the chemical structure (existence of one isomer) is, the more difficult for the agent to undergo oxidation by electron transfer hydrogen abstraction. As a result, the possible sites of attack for free radical oxidants (Davasagaya *et al.* 2004) and *trans,trans*-BNIPDaCHM are decreased compared to BNIPDaCHM, which retains its rotational freedom due to its structure and the existence of three stereoisomers (see Chapter 3). In addition, the above results revealed that SKBR-3 cells (hormone receptor positive) have a stronger response to BNIP treatments compared to MDA-MB-231 cells, which is in agreement with our cytotoxicity findings.

The effect of ROS in DNA damage after treatment with BNIPs was also investigated (Chapter 4). DNA damage studies revealed that BNIPs induced a significant increase in DNA strand breaks compared to endogenous levels, after 24 hour treatment in MDA-MB-231 and SKBR-3 cells. Interestingly, a higher number of DNA strand breaks after treatment with BNIPs was observed in MDA-MB-231 cells,

compared to SKBR-3 cells. MDA-MB-231 cells were found to be more susceptible to DNA instability after treatment with BNIPs, which appears to relate to different proliferation index rates between the two cells lines (Kenny *et al*, 2007). MDA-MB-231 cells proliferate at a 49.5% rate and SKBR-3 cells at 35.2% (Kenny *et al*, 2007). According to these observations, the faster the cells proliferate, the higher the DNA damage is caused over time. Moreover, BNIPPiEth (second most cytotoxic compound in MDA-MB-231 cells and SKBR-3 cells after *trans,trans*-BNIPDaCHM and highly ROS-inducing compound and strong intercalating BNIP) was the best candidate out of the three novel compounds in this study, suggesting that its short linker sequence may enhance its cellular uptake (better cytotoxicity, more DNA strand breaks). To further elucidate the mode of action of BNIPs, it would be interesting to study DNA repair and any potential DNA repair mechanisms that are activated after treatment with BNIPs.

In Chapter 5, the effect of BNIPs on cell cycle distribution and cell death was studied. An increase in the proportion of MDA-MB-231 cells in sub-G1 phase was exhibited relative to the control, whilst in G1 phase, the cell population was significantly decreased, after treatment with BNIPDaCHM (1μM) and *trans,trans*-BNIPDaCHM (1μM). In SKBR-3 cells, the cell population was significantly increased in sub-G1 phase only after treatment with BNIPDaCHM. In addition, the two BNIPs induced sub-G1 cell cycle arrest in both cell lines to a greater extent than camptothecin, which is a well-known positive control for sub-G1 arrest (Chu *et al*, 2014, Doddapadeni *et al,* 2015) and for inducing apoptosis (Hong *et al*, 2014, Kang *et al,* 2016). Moreover, the above findings demonstrated that the effect of the two BNIPs investigated was different in each cell line and that the sole existence of one isomer (*trans,trans*-BNIPDaCHM) has a different effect on cell cycle distribution. Supplementary studies into cell-cycle regulators, such as $p27_{Kip1}$

and cyclin E, alone and in combination, would be also beneficial, as they have been proved indicative of tumour behaviour in several types of cancer, including breast cancer (Porter *et al*, 2006).

The mode of cell death in MDA-MB-231 and SKBR-3 cells, several studies was investigated further. After 0.5 hour treatment with BNIPs, a significant difference in Annexin V-FITC staining compared to the control was observed in MDA-MB-231 and SKBR-3 cells. BNIPPiEth caused the highest increase of Annexin V-FITC staining levels in MDA-MB-231 cells, and *trans,trans*-BNIPDaCHM in SKBR-3 cells, suggesting that BNIPs induce early apoptosis, which could be the main mode of cell death in BNIP-induced cytotoxicity and cell cycle arrest. In addition, after 24 hour treatment, BNIPs were found to inhibit Caspase-3 activity in both cell lines and autophagy studies revealed for the very first time that the formation of autophagosomes and autolysosomes was triggered. This suggests that BNIP-induced autophagy on the tested human breast cancer cell lines seem to cross talk with caspase-independent apoptotic cell death. These findings should be further investigated in order to determine any other potential cross talk with other modes for cell death, such as necroptosis; a mode of cell death, which has been associated with a substantial decrease in Caspase-3 activity with increase in autophagic flux (Tait and Green, 2008).

In Chapter 6, the effect of BNIPs on HDAC activity in breast cancer cells, with emphasis on SIRT2, and on cell stress-related proteins, was studied. The three novel BNIPs and their parental compound BNIPDaCHM (all at IC_{25} concentrations), inhibited HDAC activity after 24 hour treatment in MDA-MB-231 cells. BNIPPiEth was the derivative that caused the highest decrease of HDAC activity, followed by BNIPPiProp, BNIPDaCHM and, finally, *trans,trans*-BNIPDaCHM. Similarly, BNIPs

were found to inhibit the HDAC activity after 24 hour treatment in SKBR-3 cells, in a similar pattern to that observed in MDA-MB-231 cells. This implies that the inhibition of cell growth and cell cycle arrest that was observed earlier can potentially be related to the inhibition of HDAC activity.

Protein expression of SIRT2 only showed differences between the two different cell lines after 24 hour treatment with the parental compound, BNIPDaCHM. It could therefore be a potential SIRT2 inhibitor in SKBR-3 cells, where SIRT2 expression was found to decrease after 24 hour treatment by visual observations. However, the above results have to be further validated by repeating confirmatory experiments to assess the optimum protein amount required, define the most appropriate antibody concentration and incubation time for detection by Western-blot analysis.

Finally, proteome profiler arrays demonstrated that after treatment with the parental compound, BNIPDaCHM, and BNIPPiEth (the best candidate, as defined by the previous experiments) in MDA-MB-231 cells, three cell stress-related proteins (Cytochrome c, SIRT2 and SOD2) had an increased expression while four (PON1, PON2, HIF-1a and HSP60) were decreased. On the other hand, in BNIP-treated SKBR-3 cells, the protein expression of 12 proteins (ADAMTS1, Bcl-2, Carbonic Anhydrase IX, COX-2, Cytochrome c, Dkk-4, HIF-1a, IDO, p21, p27, PON1 and PON3) were increased and only the expression of PON1 was decreased after treatment with BNIPDaCHM. The above results revealed that BNIPDaCHM and BNIPPiEth alter the expression of cell stress-related proteins in a different pattern depending on the cell type, suggesting that the mechanism of action of BNIPs could be cell line dependent, as it has been suggested in previous chapters. To further validate the obtained experimental results and in order to study the biological processes involved, bioinformatics studies were employed, where the

cellular compartment localisation and the different pathways in which the above panel of proteins are involved were explored. This study revealed two novel, putative pathways for BNIP-induced oxidative stress-mediated cell death in MDA-MB-231 and SKBR-3 cells, creating the stepping stone for further research and validation towards the delineation of the suggested pathways, as well as the mode/mechanisms of BNIP action in breast cancer in future studies.

In conclusion, the results obtained in this study highlight the importance of the three novel BNIPs, BNIPPiProp, BNIPPiEth and *trans,trans*-BNIPDaCHM and their parental compound, BNIPDaCHM, as potential anti-cancer agents and a summary of their proposed modes of action are presented in Figure 7.1. The work performed here could help with the design, synthesis of novel anti-cancer drugs, and also with the understanding and investigation of the cellular and molecular mechanisms relevant to future cancer treatment.

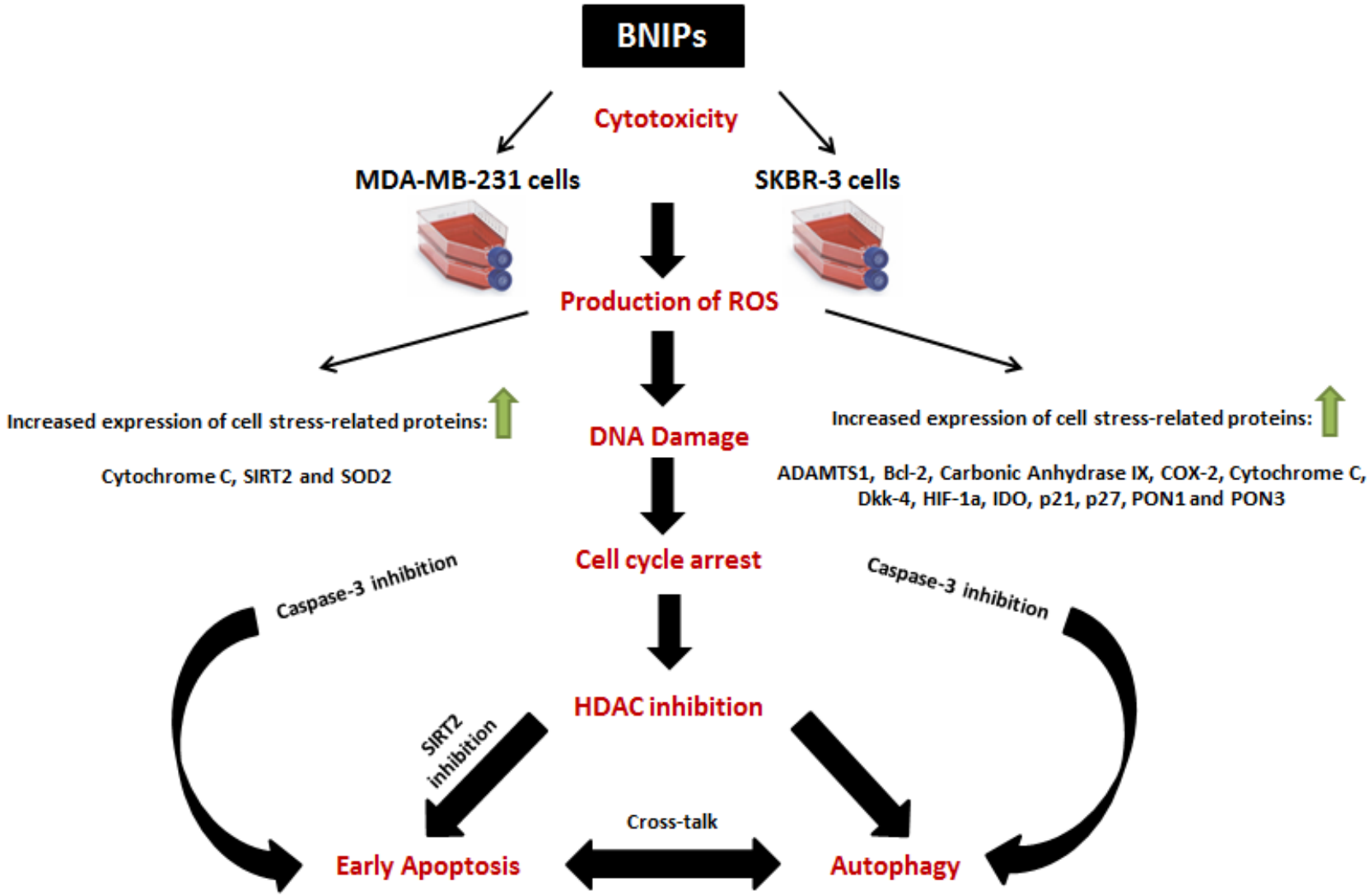

Figure 7.1.: Schematic representation of the proposed mode of action of BNIPs in MDA-MB-231 and SKBR-3 cells.

References

- Abedin, M., Wang, D., McDonnell, M. *et al.* (2007) Autophagy delays apoptotic death in breast cancer cells following DNA damage. *Cell Death and Differentiation*, **14**, 3, 500–510.
- Abdulkareem, I. (2013) Aetio-pathogenesis of breast cancer. *Nigerian Medical Journal: journal of the Nigeria Medical Association*, **54**, 6, 371-375.
- Abou-Ghali, M. and Stiban, J. (2015) Regulation of Ceramide Channel Formation and Disassembly: Insights on the Initiation of Apoptosis. *Saudi Journal of Biological Sciences*, **274**, 6, 760-772.
- Adan, A. Kiraz, Y. and Baran, Y. (2016) Cell Proliferation and Cytotoxicity Assays. *Current Pharmaceutical biotechnology*, PMID: 27604355.
- Aitken, R., Smith, T., Lord, T. *et al*. (2013) On methods for the detection of reactive oxygen species generation by human spermatozoa: analysis of the cellular responses to catechol oestrogen, lipid aldehyde, menadione and arachidonic acid. *Andrology*, **1**, 2, 192-205.
- Ali, A. and Bhattacharya, S. (2014) DNA binders in clinical trials and chemotherapy. *Bioorganic and Medicinal Chemistry*, **22**, 4506-4521.
- Ameziane-El-Hassani, R. and Dupuy, C. (2016) Detection of Reactive Oxygen Species in Cells Undergoing Oncogene-Induced Senescence. *Oncogene-Induced Senescence*, **1534**, 139-145.
- Antitumoral Drugs: What Worked and What Did Not Work. *Current Medicinal Chemistry*, **12**, 127 – 151.
- Apel, K. and Hirt, H. (2004) Reactive Oxygen Species: Metabolism, Oxidative Stress, and Signal Transduction. *Annual Review of Plant Biology*, **55**, 373-399.

- Arnold, A. and Papanikolaou, A. (2005) Cyclin D1 in Breast Cancer Pathogenesis. *Journal of Clinical Oncology*, **23**, 4215-4224.
- Aydinlik, S., Erkisa, M., Cevatemre, B., *et al.* (2016) Enhanced cytotoxic activity of doxorubicin through the inhibition of autophagy in triple negative breast cancer cell line. *Biochimica et Buophysica Acta*, doi: 10.1016/j.bbagen.2016.11.013.
- Banerjee, S., Veale, E., Phelan, C. *et al.* (2013) Recent advances in the development of 1,8-naphthalimide based DNA targeting binders, anti-cancer and fluorescent cellular imaging agents. *Chemical Society Reviews*, **42**, 1601-1618.
- Bannister, A. and Kouzarides, T. (2011) Regulation of chromatin by histone modifications. *Cell Research*, **21**, 381-395.
- Barron, G., Bermano, G., Gordon, A. *et al*. (2010) Synthesis, cytotoxicity and DNA-binding of novel bisnaphthalimidopropyl derivatives in breast cancer MDA-MB-231 cells. *European journal of medicinal chemistry*, **45**, 4, 1430-1437.
- Barron, G., Goua, M, Kuraoka, I. *et al*. (2015) Bisnaphthalimidopropyl diaminodicyclohexylmethane induces DNA damage and repair instability in triple negative breast cancer cells via p21 expression. *Chemico-Biological Interactions*, **242**, 307-315.
- Bayr, H. (2005) Reactive oxygen species. *Critical Care Medicine*, **33**, 12, 498-501.
- Becorpi, A., Sisti, G., Sorbi, F. *et al.* (2014) Management options of breast cancer related osteoporosis. *Clinical Cases in Mineral and Bone Metabolism*, **11**, 2, 110-113.

- Belinky, F., Nativ, N., Stelzer, G. *et al.* (2015) PathCards: multi-source consolidation of human biological pathways. *Database (Oxford)*, v.2015, PMC4343183.
- Benham, C. (1979) Torsional stress and local denaturation in supercoiled DNA, *Proceedings of the National Academy of Sciences of the United States of America*, **76**, 3870–3874.
- Benham, C. (1990) Theoretical analysis of heteropolymeric transitions in superhelical DNA at high temperature. *The Journal of Chemical Physics*, **92**, 6294–6305.
- Benham, C. (1996) Theoretical of the helix-coil transition in positively superhelical DNA at high temperature. *Physical Review E*, **53**, 2984–2987.
- Bergström, C., Norinder, U., Luthman, K. Artursson, P. (2003) Molecular Descriptors Influencing Melting Point and Their Role in Classification of Solid Drugs, *Journal of Chemical Information and Computing Science*, **43**, 4, 1177–1185.
- Bertoli, C., Skotheim, J. and de Bruin, R. (2013) Control of cell cycle transcription during G1 and S phases. *Nature Reviews Molecular Cell Biology*, **14**, 518–528.
- Bindea, G., Mlecnik, B., Hackl, H. *et al.* (2009) ClueGO: a Cytoscape plug-in to decipher functionally grouped gene ontology and pathway annotation networks. *Bioinformatics*, **25**, 8, 1091-1093.
- BioLegend: www.biolegend.com
- Biswas, S. and Rao, C. (2017) Epigenetics in cancer: Fundamentals and Beyond. *Pharmacology and Therapeutics*, pii: S0163-7258(17)30025-6. doi: 10.1016/j.pharmthera.2017.02.011.

- Boveri, T. (2008) Concerning the origin of malignant tumours by Theodor Boveri. Translated and annotated by Henry Harris. *Journal of Cell Science*, **121**, 1-2.
- Brana, M., Castellano, J., Moran, *et al*. (1993) Bis-naphthalimides: A New Class of Antitumour Agents. *Anti-cancer Drug Design*, **8**, 257-268.
- Brana, M., Cacho, M., Gradillas, A. *et al.* (2001) Intercalators as anti-cancer drugs. *Current Pharmaceutical Design*, **7**, 17, 1745-1780.
- Brana, M. and Ramos, A. (2001) Naphthalimides as Anti-cancer Agents: Synthesis and Biological Activity. *Current Medicinal Chemistry*, **1**, 3, 237-255.
- Brana, M., Cacho, M., Ramos, A. *et al.* (2003) Synthesis, Biological Evaluation and DNA Binding Properties of Novel Mono and Bisnaphthalimides. *Organic and Biomolecular Chemistry*, **1**, 648-654.
- Brana, M., Cacho, M., Garcia, M. *et al.* (2004) New Analogues of Amonafide and Elinafide, Containing Aromatic Heterocycles: Synthesis, Antitumor Activity, Molecular Modeling, and DNA Binding Properties. *Journal of Medicinal Chemistry*, **47**, 6, 1391-1399.
- Brana, M., Gradillas, A., Ovalles, B. *et al*. (2005) Synthesis and biological activity of N,N-dialkylaminoalkyl-substituted bisindolyl and diphenyl pyrazolone derivatives. *Bioorganic and Medicinal Chemistry*, **14**, 1, 9-16.
- Brinton, L., Felix, A., McMeekin, D. *et al.* (2013) Etiologic heterogeneity in endometrial cancer: Evidence from a Gynecologic Oncology Group trial. *Gynecologic Oncology*, **129**, 2, 277–284.
- Burcham, P. (2014) An introduction to toxicology. *Springer*, 221-256.

- Carey, L., Perou, C., Livasy, C. *et al.* (2006) Race, breast cancer subtypes, and survival in the Carolina Breast Cancer Study. *JAMA*, **295**, 21, 2492-2502.
- Cancer Research UK, 2011. Breast Cancer Statistics. London Cancer Research UK. Available from: http://www.cancerresearchuk.org/health-professional/cancer-statistics/statistics-by-cancer-type/breast-cancer. (Accessed 10 February 2015)
- Cancer Research UK, 2016. Breast Cancer Incidence (invasive) Statistics. London Cancer Research UK. Available from: http://www.cancerresearchuk.org/health-professional/cancer-statistics/statistics-by-cancer-type/breast-cancer/incidence-invasive. (Accessed 25 March 2016)
- Cazares-Marineiro, J., Buriez, O., Labbe, E. *et al.* (2013) Synthesis, Characterization, and Antiproliferative Activities of Novel Ferrocenophanic Suberamides against Human Triple-Negative MDA-MB-231 and Hormone-Dependent MCF-7 Breast Cancer Cells. *Organometallics*, **32**, 20, 5926-5934.
- Cazares-Marinero, J., Buriez, O., Labbe, E. *et al*. (2013) Efficient new constructs against triple negative breast cancer cells: synthesis and preliminary biological study of ferrocifen-SAHA hybrids and related species. *Dalton Trans*, **42**, 15489-15501.
- Ceccacci, E. and Minucci, S. (2016) Inhibition of histone deacetylases in cancer therapy: lessons from leukaemia. *British Journal of Cancer*, **114**, 605-611.
- Chen, F., Behrens, L., Behrens, S. *et al.* (1993) XB596, a promising bis-naphthalimide anti-cancer agent. *Anti-cancer drugs*, **4**, 4, 447-457.

- Chen, J., Chan, A., To, K. *et al.* (2013) SIRT2 Overexpression in Hepatocellular Carcinoma Mediates Epithelial to Mesenchymal Transition by Protein Kinase B/Glycogen Synthase Kinase-3b/bCatenin Signaling. *Hepatology*, **57**, 6, 1-12.
- Chinyama, C. (2014) The Normal female breast. Benign breast diseases, *Springer*, 1-7.
- Chu, C., Xu, J., Cheng, D. *et al. (*2014) Anti-Proliferative and Apoptosis-Inducing Effects of Camptothecin-20(s)-O-(2-pyrazolyl-1)acetic Ester in Human Breast Tumor MCF-7 Cells. *Molecules*, **19**, 4, 4941-4955.
- Crowley, L., Chojnowski, G. and Waterhouse, N. (2016) Measuring the DNA Content of Cells in Apoptosis and at Different Cell-Cycle Stages by Propidium Iodide Staining and Flow Cytometry. *Cold Spring Harbor Protocols*, doi:10.1101/pdb.prot087247.
- Csibi, A., Fendt, S., Poulogiannis, G. *et al.* (2013) The mTORC1 pathway stimulates glutamine metabolism and cell proliferation by repressing SIRT4. *Cell*, **153**, 4, 840-854.
- Dance, A., Ralton, L., Fuller, Z. *et al*. (2005) Synthesis and biological activities of bisnaphthalimido polyamines derivatives: cytotoxicity, DNA binding, DNA damage and drug localisation in breast cancer MCF 7 cells. *Biochemical Pharmacology*, **69**, 19-27.
- Dasmahapatra, G., Lembersky, D., Son, M. *et al*. (2011) Carfilzomib Interacts Synergistically with Histone Deacetylase Inhibitors in Mantle Cell Lymphoma Cells *In Vitro* and *In Vivo. Molecular Cancer Therapeutics*, **10**, 9, DOI: 10.1158/1535-7163.MCT-10-1108.

- Davasagaya, T., Tilak, J., Boloor, K., *et al*. (2004) Free Radicals and Antioxidants in Human Health: Current Status and Future Prospects. *Journal of Association of Physicians of India*, **52**, 794-804.
- Dawson, M. and Kouzarides, T. (2013) Cancer epigenetics: from mechanism to therapy. *Cell*, **150**, 12-27.
- De Nigris, F., Cerutti, J., Morelli, C. *et al.* (2002) Isolation of a SIR-like gene, SIR-T8, that is overexpressed in thyroid carcinoma cell lines and tissues. *British Journal of Cancer*, **86**, 6, 917-923.
- Denkert, C., Liedtke, C., Tutt, A. *et al.* (2016) Molecular alterations in triple-negative breast cancer-the road to new treatment strategies. *The Lancet*, **389**, 10087, 2430-2442.
- Dhawan, J. and Laxman, S. (2015) Decoding the stem cell quiescence cycle – lessons from yeast for regenerative biology. *Journal of Cell Science*, **128**, 4467-474.
- Dobbelstein, M. and Moll, U. (2014) Targeting tumour-supportive cellular machineries in anti-cancer drug development. *Nature Reviews Drug Discovery*, **13**, 179–196.
- Doddapaneni, R., Patel, K., and Singh, M. (2015) Synergistic anti-cancer effect of Noscapine and Camptothecin is mediated through apoptosis and cell cycle arrest in A549 lung cancer, *Cancer Research*, **75**, Supplement 15, 2619-2619.
- Doonan, F., Donovan, M. and Cotter, T. (2003) Caspase-independent photoreceptor apoptosis in mouse models of retinal degeneration. *Journal of Neuroscience*, **23**, 13, 5723-5731.
- Dorstyn, L. and Kumar, S. (2009) Putative functions of caspase-2. *F1000 Biology Reports*, **1**, 96, doi: 10.3410/B1-96.

- Duronio, R. and Xiong, Y. (2013) Signaling Pathways that Control Cell Proliferation. *Cold Spring Harbor Perspectives in Biology*, **5**, 3, doi: 10.1101/cshperspect.a008904.
- Duthie, S., and Hawdon, A., (1998) DNA Instability (Strand Breakage, Uracil Misincorporation, and Defective Repair) is Increased by Folic Acid Depletion in Human Lymphocytes *In Vitro*. *The Federation of American Societies for Experimental Biology Journal*, **12**, 1491 – 1497.
- Egelhofer, T., Minoda, A., Klugman, S. *et al*. (2011) An assessment of histone-modification antibody quality. *Nature structural and molecular Biology*, **18**, 91-93.
- Ershler, W. (2006) Capecitabine use in geriatric oncology: an analysis of current safety, efficacy, and quality of life data. *Critical Reviews in Oncology/Hematology*, **58**, 1, 68–78.
- Feinberg A. and Vogelstein, B. (1983) A technique for radiolabeling DNA restriction endonuclease fragments to high specific activity. *Analytical Biochemistry*, **132**, 6-13.
- Feldman, R., Ding, Q., Hussain, Y. *et al*. (2016) Aldosterone mediates metastatic spread of renal cancer via the G protein-coupled estrogen receptor (GPER). *FASEB journal: official publication of the Federation of American Societies for Experimental Biology*, **30**, 6, 2086-2096.
- Ferley, J., Steliarova-Foucher, E., Lorter-Tieulent, J. *et al.* (2013) Cancer incidence and mortality patterns in Europe: estimates for 40 countries in 2012. *European Journal of cancer*, **49**, 6, 1374-1403.
- Fernandez, S., Robertson, F., Pei, J. *et al.* (2013) Inflammatory breast cancer (IBC): clues for targeted therapies. *Breast Cancer Research and Treatment*, **140**, 1, 23-33.

- Fiers, W., Beyaert, R., Declercq, W. *et al.* (1999) More than one way to die: apoptosis, necrosis and reactive oxygen damage. *Oncogene*, **18**, 54, 7719-7730.
- Finley, L., Carracedo, A., Lee, J. *et al*. (2011) SIRT3 opposes reprogramming of cancer cell metabolism through HIF1α destabilization. *Cancer Cell*, **19**, 3, 416-428.
- Fouad, Y. and Aanei, C. (2017) Revisiting the hallmarks of cancer. *American Journal of Cancer Research*, **7**, 5, 1016-1036.
- Fukai, T. and Ushio-Fukai, M. (2011) Superoxide Dismutases: Role in Redox Signaling, Vascular Function, and Diseases. *Antioxidant Redox Signalling*, **15**, 6, 1583-1606.
- Geiss, H. (1987) *Fundamentals of thin layer chromatography planar chromatography. Heidelberg, Dr. A. Hüthig Verlag*, **482**.
- Gnerlich, J., Deshpande, A., Jeffe, D. *et al.* (2011) Poorer survival outcomes for male breast cancer compared with female breast cancer may be attributable to in-stage migration. *Annals of surgical oncology*, **18**, 7, 1837-1844.
- Gomes, A., Fernandes, E. and Lima, J. (2005) Fluorescence probes used for detection of reactive oxygen species. *Journal of Biochemical and Biophysical Methods*, **65**, 2-3, 45-80.
- Grana, X. and Reddy, E. (1995) Cell cycle control in mammalian cells: role of cyclins, cyclin dependent kinased (CDKs), growth suppressor genes and cyclin-dependent kinase inhibitors (CKIs). *Oncogene*, **1**, 211-219.
- Greco, A. (1998) Evolving Role of Oral Chemotherapy for the Treatment of Patients with Neoplasms. Oncology, **4**, 43-50.

- Hacker, G. (2000) The morphology of apoptosis. *Cell and Tissue Research*, **301**, 1, 5-17.
- Hague, A., Eveson, J., MacFarlane, M. *et al.* (2004) Caspase-3 expression is reduced, in the absence of cleavage, in terminally differentiated normal oral epithelium but is increased in oral squamous cell carcinomas and correlates with tumour stage. *The Journal of Pathology*, **204**, 2, 175-182.
- Haigis, M. and Snclair, D. (2010) Mammalian sirtuins: biological insights and disease relevance. *Annual Review of Pathology*, **5**, 253-295.
- Han, Y. and Park, W. (2009) Tiron, a ROS scavenger, protects human lung cancer Calu-6 cells against antimycin A-induced cell death. *Oncology Reports*, **21**, 1, 253-261.
- Hanahan, D. and Weinberg, R. (2000) The hallmarks of cancer. *Cell*, **100**, 1, 57-70.
- Hanahan, D. and Weinberg, R. (2011) Hallmarks of cancer: the next generation. *Cell*, **144**, 5, 646-676.
- Hartwell, L. and Kastan, M. (1994) Cell cycle control and cancer. *Science*, **266**, 1821–1828.
- He, W., Newman, J., Wang, M. *et al.* (2012) Mitochondrial sirtuins: regulators of protein acylation and metabolism. *Trends in Endocrinology and Metabolism*, **9**, 467-476.
- Henry, C., Hollville, E. and Martin, S. (2013) Measuring apoptosis by microscopy and flow cytometry. *Methods*, **61**, 2, 90-97.
- Hida, T., Yoneta, A., Nishizaka, T. *et al.* (2012) Pigmented mammary Paget's disease mimicking melanoma: report of three cases. *European Journal of Dermatology*, **22**, 121-124.

- Hiratsuka, M., Toshiaki, I., Tosifusa, T. *et al.* (2003) Proteomics-based identification of differentially expressed genes in human gliomas: down-regulation of SIRT2 gene. *Biochemical and Biophysical Research Communication*, **309**, 558-566.
- Hoeijmakers, J. (2009) DNA Damage, Aging, and Cancer. *The New England Journal of Medicine*, **361**, 1475-1485.
- Holliday, D. and Speirs, V. (2011) Choosing the right cell line for breast cancer research. *Breast Cancer Research*, **13**, 4, 215.
- Hong, J., Chung, H., Bae, S. *et al.* (2014) Induction of Cell Cycle Arrest and Apoptosis by Physcion, an Anthraquinone Isolated From Rhubarb (Rhizomes of Rheum tanguticum), in MDA-MB-231 Human Breast Cancer Cells. *Journal of cancer prevention*, **19**, 4, 273-278.
- Hu, E., Dul, E., Sung, C. *et al.* (2003) Identification of novel isoform-selective inhibitors within class I histone deacetylases. *Journal of Pharmacology and Experimental Therapeutics*, **307**, 720–728.
- Huang, F., Zhao, M., Zhang, *et al*. (2009) Synthesis, DNA Intercalation and 3D QSAR Analysis of cis-2,4,5-trisubstituted 1,3-dithiolanes as a Novel Class of Antitumour Agents. *Bioorganic and Medicinal Chemistry*, **17**, 6085 –6095.
- Huang, Y., Song, Y., Fan, Y., *et al*. (2016) Synthesis, DNA binding, and cytotoxicity activity of bis-naphalenyl compounds with different diamine linkers. *Research on Chemical Intermediates*, **42**, 7329-7344.
- Igci, M., Kalender, M., Borazan, E. *et al*. (2016) High-throughput screening of Sirtuin family of genes in breast cancer. *Gene*, **568**, 1, 123-128.
- Jeong, S., Xiao, C., Finley, L. *et al.* (2013) SIRT4 has tumor-suppressive activity and regulates the cellular metabolic response to DNA damage by

inhibiting mitochondrial glutamine metabolism. *Cancer Cell*, **23**, 4, 450-463.

- Jiang, W. (2008) Sirtuins: Novel targets for metabolic disease in drug development. *Biochemical and Biophysical Research Communications*, **373**, 341-344.
- João, P. (2013) How ageing processes influence cancer. *Nature Reviews Cancer*, **13**, 357-365.
- Johnstone, R. and Licht, J. (2003) Histone deacetylase inhibitors in cancer therapy: Is transcription the primary target? *Cancer Cell*, **4**, 13-18.
- Kaminska, M., Ciszewski, T., Lopacka-Szatan, K. *et al.* (2015) Breast cancer risk factors.*Przeglad menopauzalny: Menopause review*.
- Kang, M., Kook, H., Lee, S. *et al.* (2016) Theracurmin® efficiently inhibits the growth of human prostate and bladder cancer cells via induction of apoptotic cell death and cell cycle arrest. *Oncology reports*, **35**, 3, 1463-1472.
- Kanzawa, T., Germano, I., Komata, T. *et al.* (2004) Role of autophagy in temozolomide-induced cytotoxicity for malignant glioma cells. *Cell Death and Differentiation*, **11**, 4, 448–457.
- Karin, M. (2008) The IkappaB kinase - a bridge between inflammation and cancer. *Cell Research*, **18**, 3, 334–342.
- Karna, P., Zughaier, S., Pannu, R. *et al*. (2010) Induction of reactive oxygen species-mediated autophagy by a novel microtubule-modulating agent. *The Journal of Biological Chemistry*, **285**, 18737–18748.
- Kastan, M. and Bartek, J. (2004) Cell-cycle checkpoints and cancer. *Nature*, **432**, 316-323.

- Khavari, T. and Rinn, J. (2007) Ras/Erk MAPK signaling in epidermal homeostasis and neoplasia. *Cell Cycle*, **6**, 23, 2928–2931.
- Kenny, P., Lee, G., Myers, C., *et al*. (2007) The morphologies of breast cancer cell lines in three-dimensional assays correlate with their profiles of gene expression. *Molecular Oncology*, **1**, 1, 84–96.
- Kerr, J., Wyllie, A. and Currie, A. (1972) Apoptosis: a basic biological phenomenon with wide-ranging implications in tissue kinetics. *British Journal of Cancer*, **26**, 239-257.
- Kim, H., Vassilopoulos, A., Wang, R. *et al.* (2011) SIRT2 Maintains Genome Integrity and Suppresses Tumorigenesis through Regulating APC/C Activity. *Cancer Cell*, **20**, 4, 487-499.
- Kim, M., Blake, M., Baek, J. *et al.* (2003) Carrier Inhibition of histone deacetylase increase cytotoxicity to anti-cancer drugs targeting DNA. *Cancer Research*, **63**, 7291–7300.
- Koopman, G., Reutelingsperger, C., Kuijten, G., *et al.* (1994) Annexin V for flow cytometric detection of phosphatidylserine expression of B cells undergoing apoptosis. *Blood*, **84**, 1415–1420.
- Kopsida, M., Barron, G., Bermano, G., *et al.* (2016) Novel Bisnaphthalimidopropyl (BNIPs) derivatives as anti-cancer compounds targeting DNA in human breast cancer cells. *Organic and Biomolecular Chemistry*, **14**, 9780-9789.
- Koutcher, J. and Burt, C. (1984) Principles of Nuclear Magnetic Resonance. *The Journal of Nuclear Medicine*, **25**, 2, 101-111.
- Kouzarides, T. (2007) SnapShot: Histone-modifying enzymes. *Cell*, **131**, 822.

- Kroemer, G., El-Deiry, W., Golstein, P. *et al.* (2005) Classification of cell death: recommendations of the Nomenclature Committee on Cell Death. *Cell Death and Differentiation*, **12**, 1463-1467.
- Kroemer, G. and Jaattela, M. (2005) Lysosomes and autophagy in cell death control. *Nature Reviews Cancer*, **5**, 11, 886–897.
- Krysko, D., Berghe, T., D'Herde, K. *et al.* (2008) Apoptosis and necrosis: Detection, discrimination and phagocytosis. *Methods*, **44**, 3, 205-221.
- Kumari, S., Rastogi, R., Singh, K., *et al.* (2008) DNA damage: Detection strategies. *EXCLI Journal*, **7**, 44-62.
- Laane, E., Tamm, K., Buentke, E. *et al.* (2009) Cell death induced by dexamethasone in lymphoid leukemia is mediated through initiation of autophagy. *Cell Death and Differentiation*, **16**, 7, 1018–1029.
- Lai, C., Lin, P., Lin, S. *et al*. (2013) Altered expression of SIRT gene family in head and neck squamous cell carcinoma. *Tumour Biology*, **34**, 3, 1847-1854.
- Langan, T. and Chou, R. (2011) Synchronization of mammalian cell cultures by serum deprivation. *Methods in Molecular Biology*, **761**, 75-83.
- Lawrence, M., Stojanov, P., Mermel, C. *et al.* (2014) Discovery and saturation analysis of cancer genes across 21 tumour types. *Nature*, **505**, 495-501.
- Lazebnik, Y. (2000) What are the hallmarks of cancer? *Nature Reviews Cancer*, **10**, 1, 232-233.
- Lee, E., Pandey, N. and Popel, A. (2014) Pre-treatment of mice with tumor-conditioned media accelerates metastasis to lymph nodes and lungs: a new spontaneous breast cancer metastasis model. *Clinical and Experimental Metastasis*, **31**, 1, 67-79.

- Lee, M., Lee, S., Kim, S. *et al.* (2016) Anti-Cancer Effect of Lambertianic Acid by Inhibiting the AR in LNCaP Cells, *International Journal of Molecular Sciences*, **17**, 7, 1066.
- Lee, Y., Kang, B. and Bae, Y. (2014) Premature senescence in human breast cancer and colon cancer cells by tamoxifen-mediated reactive oxygen species generation. *Life Sciences*, **97**, 116-122.
- Lehmann, B. and Pietenpo, J. (2014) Identification and use of biomarkers in treatment strategies for triple-negative breast cancer subtypes. *The Journal of Pathology*, **232**, 142-150.
- Leong, L., Moey, T., and Sim, L. (2013) PB.06: Preliminary results in the performance comparison between the size ratio and colour scoring breast ultrasound elastographic techniques. *Breast Cancer Research*, **15**, 1, 1-6.
- Li, N. and Karin, M. (1999) Is NF-kappaB the sensor of oxidative stress? *Faseb Journal*, **13**, 10, 1137–1143.
- Li, J., Hou, N., Faried, A., *et al.* (2010) Inhibition of autophagy augments 5-fluorouracil chemotherapy in human colon cancer *in vitro* and *in vivo* model. *European Journal of Cancer*, **46**, 10, 1900–1909.
- Li, L., Ganchimeg, I. and Gibson, S. (2012) Reactive oxygen species regulation of autophagy in cancer: Implications for cancer treatment. *Free Radical Biology and Medicine*, **53**, 7, 1399-1410.
- Li-Weber, M. (2013) Targeting apoptosis pathways in cancer by Chinese medicine. *Cancer Letters*, **332**, 2, 304-312.
- Li, Y., Matsumori, H., Nakayama, Y. *et al.* (2011) SIRT2 down-regulation in HeLa can induce p53 accumulation via p38 MAPK activation-dependent p300 decrease, eventually leading to apoptosis. *Genes to Cells*, **16**, 1, 34-45.

- Li, Y., Wong, K., Giles, A. *et al.* (2013) Hepatic SIRT1 Attenuates Hepatic Steatosis and Controls Energy Balance in Mice by Inducing Fibroblast Growth Factor 21. *Gastroenterology*, **146**, 2, 539-549.
- Lima, R., Barron, G., Grabowska, J. *et al.* (2013) Cytotoxicity and Cell Death Mechanisms Induced by a Novel Bisnaphthalimidopropyl Derivative against the NCI-H460 non-small Lung Cancer Cell Line. *Anti-Cancer agents in Medicinal Chemistry*, **13**, 3, 414-421.
- Lin, Y. and Pasero, P. (2012) Interference Between DNA Replication and Transcription as a Cause of Genomic Instability. *Current Genomics*, **13**, 65-73.
- Liou, G. and Storz, P. (2014) Reactive oxygen species in cancer. *Free Radical Research*, **44**, 5, 479-496.
- Lipinski, C., Lombardo, F., Dominy, B., *et al.* (2012) Experimental and computational approaches to estimate solubility and permeability in drug discovery and development settings. *Advanced Drug Delivery Reviews*, **64**, 4-17.
- Liu, P., Wu, B., Liu, J. *et al*. (2016) DNA Binding and Photocleavage Properties, Cellular Uptake and Localisation, and *In Vitro* Cytotoxicity of Dinuclear Ruthenium(II) Complexes with Varying Lengths in Bridging Alkyl Linkers. *Inorganic Chemistry*, **55**, 1412-1422.
- Llombart, M., Poveda, A., Forner, E., *et al.* (1992) Phase I study of mitonafide in solid tumors. *Investigational new drugs*, **10**, 3, 177-181.
- Loi, S., Dafni, U., Karlis, D. *et al*. (2016) Effects of Estrogen Receptor and Human Epidermal Growth Factor Receptor-2 Levels on the Efficacy of Trastuzumab: A Secondary Analysis of the HERA Trial. *JAMA Oncology*, **2**, 8, 1040-1047.

- Lü, L., Zhang, L., Wai, M., *et al.* (2012) Exocytosis of MTT formazan could exacerbate cell injury. *Toxicology In Vitro*, **4**, 636-644.
- Lu, W., Zuo, Y., Feng, Y. *et al*. (2014) SIRT5 facilitates cancer cell growth and drug resistance in non-small cell lung cancer. *Tumor Biology*, **35**, 11, 10699-10705.
- Ma, J. and Ahmedin, J. (2013) Breast Cancer Metastasis and Drug Resistance. *Springer*, 1-18.
- Mackness, M. and Mackness, B. (2015) Human Paraoxonase-1 (PON1): Gene stucture and expression, promiscuous activities and multiple physiological roles. *Gene*, **567**, 1, 12-21.
- Malumbres, M. and Barbacid M. (2009) Cell cycle, CDKs and cancer: a changing paradigm. *Nature Reviews Cancer*, **9**, 153–166.
- Malumbres, M. and Barbacid, M. (2001) To cycle or not to cycle: a critical decision in cancer. *Nature Reviews Cancer*, **1**, 222–231.
- Mangham D. and Kindblom L. (2014) Rarely metastasizing soft tissue tumours, *Histopathology*, **64**, 88–100.
- Marks, P. (2010) Histone Deacetylase Inhibitors: A Chemical Genetics Approach to Understanding Cellular Functions. *Biochimica et Biophysica Acta*, **1799**, 717-725.
- Martinez, R, and Chacon-Garcia, L., (2005) The Search of DNA-Intercalators as antitumoral drugs: what it worked and what did not work. *Current Medicinal Chemistry*, **12**, 2, 127-151.
- Matsuzawa, Y., Oshima, S., Nibe, Y., *et al.* (2015) RIPK3 regulates p62-LC3 complex formation via the caspase-8-dependent cleavage of p62. *Biochemical and Biophysical Research Communication*, **456**, 298–304.

- McCluskey, C., Quinn, J. and McGrath, W. (2005) An Evaluation of Three New-Generation Tetrazolium Salts for the Measurement of Respiratory Activity in Activated Sludge Microorganisms. *Microbial Ecology*, **49**, 3, 379-387.
- McGlynn, L., Zinos, S., MacDonald, A. *et al.* (2014) SIRT2: tumour suppressor or tumour promoter in operable breast cancer? *European Journal of Cancer*, **50**, 2, 290-301.
- Meeran, S. and Katiyar S. (2008) Cell cycle control as a basis for cancer chemoprevention through dietary agents. *Frontiers in Bioscience*, **13**, 2191-2202.
- Merkle, C. (2009) Cellular adaptation, injury, and death. *Pathophysiology: concepts of altered health states*. Edited by: Porth, C. and Matfin, G. Philadelphia: Wolters Kluwer/Lippincott Williams and Wilkins, 94-111.
- Michalides, R. (1999) Cell cycle regulators: mechanisms and their role in aetiology, prognosis, and treatment of cancer. *Journal of Clinical Pathology*, **52**, 555–568.
- Minoshima, M. and Kikuchi, K. (2015) Chemical tools for probing histone deacetylase (HDAC) activity. *Anlytical Sciences: the international journal of the Japan Society for Analytical Chemistry*, **31**, 4, 287-292.
- Moskowitz, A. and Horwitz, S. (2017) Targeting histone deacetylases in T-cell lymphoma. *Leukemia and Lymphoma*, **58**, 6, 1306-1319.
- Mosmann, T. (1983) Rapid colourimetric assay for cellular growth and survival: application to proliferation and cytotoxicity assays. *Journal of immunological methods*, **65**, 1-2, 55-63.
- Munsell, M., Sprague, B., Berry, D. *et al.* (2014) Body Mass Index and Breast Cancer Risk According to Postmenopausal Estrogen-Progestin Use

and Hormone Receptor Status. *Oxford Journals: Medicine, Epidemiologic Reviews*, **36**, 1, 114-136.

- Munster, P., Thurn, K., Thomas, S. *et al.* (2011) A phase II study of the histone deacetylase inhibitor vorinostat combined with tamoxifen for the treatment of patients with hormone therapy-resistant breast cancer. *British Journal of Cance*r, **104**, 12, 1828-1835.
- Murray, A. (1991) Coordinating cell cycle events. *Cold Spring Harbor Symposia on Quantitative Biology*, **56**, 399–408.
- Murray, A. (1994) Cell cycle checkpoints. *Current Opinion of Cell Biology*, **6**, 872–876.
- Newbold, A., Falkenberg, K., Prince, M. et al. (2016) How do tumor cells respond to HDAC inhibition? *The FEBS Journal*, **283**, 22, 4032-4046.
- Nicoletti, I., Migliorati, G., Pagliacci, C. *et al*. (1991) A rapid and simple method for measuring thymocyte apoptosis by propidium iodide staining and flow cytometry. *Journal of Immunological Methods*, **139**, 3, 271-279.
- Nikoletopoulou, V., Markaki, M., Palikaras K. *et al.* (2013) Crosstalk between apoptosis, necrosis and autophagy. *Biochimica et Biophysica Acta (BBA)- Molecular Cell Research*, **1833**, 12, 3448-3459.
- Nunez, R. (2001) DNA Measurement and Cell Cycle Analysis by Flow Cytometry. Current issues in Molecular Biology, **3**, 3, 67-70.
- Olive, P., Banáth, J. and Durand, R. (1990) Heterogeneity in radiation-induced DNA damage and repair in tumor and normal cells measured using the "comet" assay. *Radiation Research*, **122**, 86–94.
- Oliveira, J., Ralton, L, Tavares, J. *et al*. (2007) The Synthesis and the *In Vitro* Cytotoxicity studies of Bisnaphthalimidopropyl Polyamne Derivatives

against Colon Cancer Cells and Parasite Leishmania infantum. *Bioorganic and Medicinal Chemistry*, **15**, 1, 541-545.

- Oparka, M., Walczak, J., Malinska, D., *et al*. (2016) Quantifying ROS levels using CM-H2DCFDA and HyPer. *Methods*, **109**, 3-11.
- Ostling, O. and Johanson, K. (1984) Microelectrophoretic study of radiation-induced DNA damages in individual mammalian cells. *Biochemical and Biophysical Research Communications*, **123**, 1, 291-298.
- Pagliarini, V., Wirawan, E., Romagnoli, A., *et al*. (2012) Proteolysis of Ambra1 during apoptosis has a role in the inhibition of the autophagic pro-survival response. *Cell Death Differentiation*, **19**, 1495–1504.
- Palchaudhuri, R. and Hergenrother, P. (2005) DNA as a target for anti-cancer compounds: methods to determine the mode of binding and the mechanism of action. *Current Opinion in Biotechnology*, **18**, 6, 497-503.
- Panieri, E. and Sentoro, M. (2016) ROS homeostasis and metabolism: a dangerous liason in cancer cells. *Cell death & disease*, **9**, 7(6): e2253.
- Park, S., Na, H., Kim, E. *et al*. (2009) 4-hydroxyestradiol induces anchorage-independent growth of human mammary epithelial cells *via* activation of IkappaB kinase: potential role of reactive oxygen species. *Cancer Research*, **69**, 6, 2416–2424.
- Pavlov, V., Kong Thoo Lin, P. and Rodilla, V. (2001) Cytotoxicity, DNA binding and localisation of novel bis-naphthalimidopropyl polyamine derivatives. *Chemico-biological interactions*, **137**, 15-24.
- Peck, B., Chen, C., Ho, K. *et al*. (2010) SIRT inhibitors induce cell death and p53 acetylation through targeting both SIRT1 and SIRT2. *Molecular Cancer Therapeutics*, **4**, 844-855.

- Peters, C., Rees, J., Hardwick, R. *et al.* (2010) A 4-gene signature predicts survival of patients with resected adenocarcinoma of the esophagus, junction, and gastric cardia. *Gastroenterology*, **139**, 6, 1995-2004.
- Phanstiel, O., Kaur, N. and Delcros. (2007) Structure-activity investigations of polyamine-anthracene conjugates and their uptake *via* the polyamine transporter. *Amino acids*, **33**, 2, 305-313.
- Popat, K., McQueen, K., Feelay, T. *et al*. (2013) The global burden of cancer. *Best Practice & Research Clinical Anaesthesiology*, **27**, 4, 399–408.
- Porter, A. and Janicle, R. (1999) Emerging roles of caspase-3 in apoptosis. *Cell death differentiation*, **6**, 2, 99-104.
- Porter, C., Cananaugh, P., Stolowich, N., *et al.* (1985) Biological properties of N4 and N1, N8-spermidine derivatives in cultured L1210 Leukaemia cells. *Cancer Research*, **45**, 5, 2050-2057.
- Pourquier, P., Pilon, A., Kohlhagen, G., *et al.* (1997) Trapping of Mammalian Topoisomerase I and Recombinations Induced by Damaged DNA Containing Nicks or Gaps. *The Journal of Biological Chemistry*, **272**, 26441-26447.
- Qi, X., Wildey, G. and Howe P. (2006) Evidence that Ser87 of BimEL is phosphorylated by Akt and regulates BimEL apoptotic function. *The Journal of Biological Chemistry*, **281**, 2, 813–823.
- Raha, p., Thomas, S., Thurn, K. *et al*. (2015) Combined histone deacetylase inhibition and tamoxifen induces apoptosis in tamoxifen-resistant breast cancer models, by reversing Bcl-2 overexpression. *Breast Cancer Research: BCR*, **17**, 26, 10.1186/s13058-015-0533-z.
- Rajesh, J., Rajasekaran, M., Rajagopal, G. *et al*. (2012) Analytical methods to determine the comparative DNA binding studies of curcumin–Cu(II)

complexes. *Spectrochimica Acta Part A: Molecular and Biomolecular Spectroscopy*, **97**, 223-230.

- Ralton, L. (2006) Novel polyamine based anti-cancer agents: Evaluation of the mode of action. Unpublished PhD thesis, The Robert Gordon University, Aberdeen.
- Ralton, L., Bestwick, C., Milne, L. *et al*. (2009) Bisnaphthalimidopropyl Spermidine induces Apoptosis within Colon Carcinoma Cells, *Chemico-Biological Interactions*, **177**, 1-6.
- Ramis, M., Esteban, S., Miralles, A. *et al.* (2015) Protective Effects of Melatonin and Mitochondria-targeted Antioxidants Against Oxidative Stress: A Review. *Current Medicinal Chemistry*, **22**, 2690-2711.
- Rao, P. and Johnson, R. (1970) Mammalian cell fusion: studies on the regulation of DNA synthesis and mitosis. *Nature*, **225**, 159–164.
- Rastogi, R., Richa, Kumar, A., *et al.* (2010) Molecular Mechanisms of Ultraviolet Radiation-Induced DNA Damage and Repair. *Journal of Nucleic Acids*, doi: 10.4061/2010/592980.
- Ray, P., Huang, B. and Tsuji, Y. (2012) Reactive oxygen species (ROS) homeostasis and redox regulation in cellular signalling. *Cellular Signalling*, **24**, 5, 981-990.
- Reddy, K. and Glaros, S. (2007) Inhibition of the MAP kinase activity suppresses estrogen-induced breast tumor growth both *in vitro* and *in vivo*. *International Journal of Oncology*, **30**, 4, 971–975.
- Redmond A., Byrne C., Bane F., Brown, G. *et al*. (2015) Genomic interaction between ER and HMGB2 identifies DDX18 as a novel driver of endocrine resistance in breast cancer cells. *Oncogene*, **34**, 3871-3880.

- Ren, J., He, W., Nong, L. *et al.* (2010) Acquired cisplatin resistance in human lung adenocarcinoma cells is associated with enhanced autophagy. *Cancer Biotherapy Radiopharmaceuticals*, **25**, 1, 75–80.
- Riss, T., Moravec, R., Niles, A., *et al.* (2013) Cell Viability Assays. Assay Guidance Manual [Internet], Last Update: July 1, 2016.
- River, R. and Bennett, L. (2010) Epigenetics in humans: an overview. *Current opinion in endocrinology, diabetes and obesity*, **17**, 493-499.
- Roberts, P. and Der, C. (2007) Targeting the Raf-MEK-ERK mitogen-activated protein kinase cascade for the treatment of cancer. *Oncogene*, **26**, 22, 3291–3310.
- Ropero, M., Fraga, E., Ballestar, R. *et al.* (2006) A truncating mutation of HDAC2 in human cancers confers resistance to histone deacetylase inhibition. *Nature Genetics*, **38**, 566–569.
- Roth, M. and Chen, W. (2014) Sorting out functions of sirtuins in cancer. *Oncogene*, **33**, 13, 1609-1620.
- Sandoval, L., Ober, K., Patrick M. *et al.* (2014) Commentary on "Gynecomastia: Etiologies, Clinical Presentations, Diagnosis, and Management". *Southern Medical Journal*, **107**, 1, 50-51.
- Schemies, J., Sippl, W. and Jung M. (2009) Histone deacetylase inhibitors that target tubulin. *Cancer Letters*, **280**, 22-32.
- Seidel, C., Schnekenburger, M., Zwergel, C. *et al*. (2014) Novel inhibitors of human histone deacetylases: design, synthesis and bioactivity of 3-alkenoylcoumarines. *Bioorganic and Medicinal Chemistry Letters*, **24**, 16, 3797-3801.
- Sena, L. and Chandel, N. (2012) Physiological Roles of Mitochondrial Reactive Oxygen Species. *Molecular Cell*, **48**, 2, 158-167.

- Shannon, P., Markiel, A., Ozier, O. *et al.* (2003) Cytoscape: a software environment for integrated models of biomolecular interaction networks. *Genome research*, **13**, 11, 2498-2504.
- Sherr, C. and Roberts, J. (2004) Living with or without cyclins and cyclin-dependent kinases. *Genes and Development*, **18**, 2699–2711.
- Siden, R. and Wolf, M. (2013) Disintegration of chemotherapy tablets for oral administration in patients with swallowing difficulties. *Journal of oncology pharmacy practice: official publication of the International Society of Oncology Pharmacy Practitioners*, **19**, 2, 145-150.
- Singh, N., McCoy, M., Tice, R., *et al*. (1988) A simple technique for quantitation of low levels of DNA damage in individual cells. *Experimental Cell Research*, **175**, 184–191.
- Smith, R., Loo, J., Loo, R. *et al.* (1991) Principles and practice of electrospray ionization—mass spectrometry for large polypeptides and proteins. *Mass Spectrometry Reviews*, **10**, 5, 359-452.
- Sobhani, M., Taheri, A., Jafarian, A. *et al.* (2016) The activity and tissue distribution of thioredoxin reductase in basal cell carcinoma. *Journal of Cancer Research and Clinical Oncology*, **142**, 11, 2303-2307.
- Stoddard, J., Nquyen, L., Mata-Chavez *et al*. (2007) TLC plates as convenient platform for solvent-free reactions. *Chemical communications*, **12**, 1240-1241.
- Staedler, D., Idrizi, E.,Kenzaoui, B. *et al.* (2011) Drug combinations with quercetin: doxorubicin plus quercetin in human breast cancer cells. *Cancer Chemotherapy and Pharmacology*, **68**, 5, 1161-1172.

- Strekowski, L. and Wilson, B. (2007) Noncovalent interactions with DNA: An overview. *Mutation Research/ Fundamental and Molecular Mechanisms of Mutagenesis*, **623**, 3-13.
- Suman, S., Das, T., Reddy, R. *et al.* (2014) The pro-apoptotic role of autophagy in breast cancer. *British Journal of Cancer*, **111**, 2, 309-317.
- Sun, Y., Zou, M., Hu, C. *et al.* (2013) Wogonoside induces autophagy in MDA-MB-231 cells by regulating MAPK-mTOR pathway. *Food and Chemical Toxicology*, **51**, 53-60.
- Sunami, Y., Araki, M., Hironaka, Y. *et al*. (2013) Inhibition of the NAD-Dependent Protein Deacetylase SIRT2 Induces Granulocytic Differentiation in Human Leukemia Cells. *PloS one*, **8**, 11: e57633.
- Szklarczyk, D., Franceschini, A., Wyder, S. *et al.* (2015) "STRING v10: Protein–protein Interaction Networks, Integrated over the Tree of Life." *Nucleic Acids Research*, **43**, 447–452.
- Tait, S. and Green, D. (2008) Caspase-independent cell death: leaving the set without the final cut. *Oncogene*, **27**, 6452-6461.
- Tang, B. (2016) Sirt1 and the Mitochondria. *Molecules and Cells*, **39**, 2, 87-95.
- The biology project- University of Arizona (Available from http://www.biology.arizona.edu/. Access date: May 1, 2017).
- Toh, T., Lim, J. and Chow, E. (2017) Epigenetics in cancer stem cells. *Molecular Cancer*, **1**, 16-29.
- Trachootham, D. Lu, W., Ogasawara, M., *et al*. (2008) Redox Regulation of Cell Survival. *Antioxidants & Redox Signalling*, **10**, 8, 1343-1374.
- Trichopoulos, D. and Petridou, E. (1994) Epidemiologic studies and cancer etiology in humans. *Medicine, Exercise, Nutrition and Health*, **3**, 206–225.

- UK Cancer Research, 2011. CancerStats: Cancer Statistics for the UK (Available from http://www.cancerresearchuk.org/cancer-info/cancerstats. Access date: May 1, 2017).
- Van Engeland, M., Nieland, L., Ramaekers, F. *et al.* (1998) Annexin V-affinity assay: a review on an apoptosis detection system based on phosphatidylserine exposure. *Cytometry*, **31**, 1–9.
- Vardevanyan, P., Antonyan, A. Parsadanyan, M. *et al*. (2003) The binding of ethidium bromide with DNA: interaction with single- and double-stranded structures. *Experimental and Molecular Medicine*, **35**, 527-533.
- Veuger, S. and Curtin, N. (2014) Inhibition of DNA Repair as a Therapeutic Target. *Cancer Drug Design and Discovery*, **1**, 2, 193-237.
- Vurusaner, B., Poli, G. and Basaga, H. (2012) Tumor suppressor genes and ROS: complex networks of interactions. *Free Radical Biology and Medicine*, **52**, 1, 7-18.
- Wang, H. (2016) Development of fluorescent and luminescent probes for reactive oxygen species. *TrAC Trends in Analytical Chemistry*, **85**, Part C, 181-202.
- Wang, X., Jiang, M., Wen, P., *et al*. (2016) Induction of apoptosis in human leukemia cells through an intrinsic pathway by cathachunine, a unique alkaloid isolated from *Catharanthus roseus*. *Phytomedicine*, **23**, 6, 641-653.
- Ward, E., DeSantis, C., Robbins, A. *et al*. (2014) Childhood and adolescent cancer statistics. *CA: a Cancer Journal for Clinicians*, **64**, 2, 83-103.
- Wilson, W. and Kool, E. (1998) DNA and RNA Intercalators: DNA and aspects of molecular biology. *Comprehensive Natural Products Chemistry*, **7**, Chapter 8.

- Woan, K., Sahakian, E., Sotomayor, E. *et al.* (2012) Modulation of antigen-presenting cells by HDAC inhibitors: implications in autoimmunity and cancer. *Immunology and Cell Biology*, **90**, 55-65.
- Xin, M. and Deng, X. (2005) Nicotine inactivation of the proapoptotic function of Bax through phosphorylation. *The Journal of Biological Chemistry*, **280**, 11, 10781–10789.
- Yang, Q., Yang, P., Qian, X. *et al.* (2008) Naphthalimide Intercalators with Chiral Amino Side Chains: Effects of chirality on DNA binding, photodamage, and antitumor cytotoxicity. *Bioorganic and Medicinal Chemistry*, **18**, 1, 6210-6213.
- Yang, X., Chang-Claude, J., Goode, E. *et al.* (2011) Associations of Breast Cancer Risk Factors With Tumour Subtypes: A Pooled Analysis From the Breast Cancer Association Consortium Studies. *Journal of the National Cancer Institute*, **103**, 3, 250-263.
- Youle, R. and Strasser, A. (2008) The BCL-2 protein family: opposing activities that mediate cell death. *Nature Reviews Molecular Cell Biology*, **9**, 47-59.
- Yuan, H. and Chen, W. (2013) The emerging and diverse roles of sirtuins in cancer: a clinical perspective. *OncoTargets and Therapy*, **6**, 1399-1416.
- Yurek, D., Branch, D., Kuo, M. *et al.* (2002) Development of a System to Evaluate Compound Identity, Purity, and Concentration in a Single Experiment and Its Application in Quality Assessment of Combinatorial Libraries and Screening Hits. *Journal of Combinatorial Chemistry*, **4**, 2, 138-148.

- Zhang, C., Cai, M., Pan, Y. *et al*. (2012) Low SIRT3 Expression Correlates with Poor Differentiation and Unfavorable Prognosis in Primary Hepatocellular Carcinoma, *PLoS ONE*, **7**, 12: e51703.
- Zhang, F., Ren, C., Lau, K. *et al.* (2016) A network medicine approach to build a comprehensive atlas for the prognosis of human cancer. *Brief Bioinformatics*, **17**, 1044–59.
- Zhang, Y. and Zhou, L. (2012) Sirt3 inhibits hepatocellular carcinoma cell growth through reducing Mdm2-mediated p53 degradation. *Biochemical and Biophysical Research Communications*, **423**, 26-31.
- Zhi-Yong, T., Jing-Hua, L., Qian, *et al*. (2014) Study on the Synthesis, Biological Activity and Spectroscopy of Naphthalimide-Diamine Conjugates. *Molecules*, **19**, 7646-7668.
- Ziello, J., Jovin, I., and Huang, Y. (2007) Hypoxia-Inducible Factor (HIF)-1 Regulatory Pathway and its Potential for Therapeutic Intervention in Malignancy and Ischemia. *Yale Journal of Biology and Medicine*, **80**, 2, 51-60.
- Zuehlke, A., Beebe, K., Neckers, L. *et al*. (2015) Regulation and function of the human HSP90AA1 gene. *Gene*, **570**, 1, 8-16.

Appendices

Appendix 1

trans,trans-BNIPDaCHM Concentration (μM)	Experiment 1	% fluorescence
0	589.342	100.0
0.5	566.257	96.1
1	549.91	93.3
2	487.946	82.8
3	422.133	71.6
4	356.918	60.6
5	302.358	53.4
6	266.254	48.4

Concentration	% fluorescence
0	100.0
0.5	96.1
1	93.3
2	82.8
3	71.6
4	60.6
5	53.4
6	48.4

trans,trans-BNIPDaCHM Concentration (μM)	Experiment 2	% fluorescence
0	581.51	100.0
0.5	569.461	97.9
1	549.844	94.6
2	500.322	86.0
3	426.082	73.3
4	360.507	62.0
5	306.607	53.8
6	270.358	49.2

Concentration	% fluorescence
0	100.0
0.5	97.9
1	94.6
2	86.0
3	73.3
4	62.0
5	53.8
6	49.2

trans,trans-BNIPDaCHM Concentration (μM)	Experiment 3	% fluorescence
0	591.903	100.0
0.5	583.303	98.5
1	562.423	95.0
2	526.673	89.0
3	471.601	79.7
4	411.016	69.4
5	361.016	61.9
6	279.793	49.7

Concentration	% fluorescence
0	100.00
0.5	98.55
1	95.02
2	88.98
3	
4	
5	
6	

Concentration (μM)	1	2	3	Average	StDev
0	100.000	100.000	100.000	100.000	0.000
0.5	96.083	97.928	98.547	97.519	1.282
1	93.309	94.555	95.019	94.294	0.884
2	82.795	86.038	88.980	85.938	3.094
3	71.628	73.272	79.675	74.858	4.252
4	60.562	61.995	69.440	63.999	4.766
5	53.396	53.842	61.892	56.376	4.782
6	48.418	49.170	49.748	49.112	0.667

Concentration (μM)	Average
0	100.0
0.5	97.5
1	94.3
2	85.9
3	74.9
4	64.0
5	56.4
6	49.1

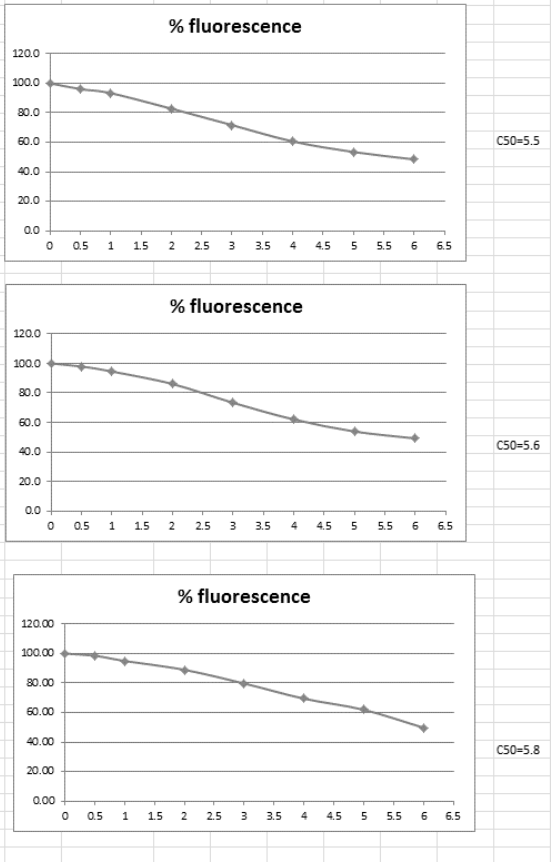

Figure A.1.: Example of C_{50} values calculation obtained by EtBr Fluorescence studies.

Appendix 2

BNIPPiEth

A0 = 0.558

	Total volume (mL)	Drug concentration	Mean Absorbance	A0/(A-A0)	1/[drug]
DNA only	1.0	0	0.55800		
1	1.1	1.81818E-06	0.45133	-5.23125	550000
2	1.2	3.33333E-06	0.37033	-2.973357	300000
3	1.3	4.61538E-06	0.33633	-2.5172932	216666.7
4	1.4	5.71429E-06	0.31367	-2.2837653	175000
5	1.5	6.66667E-06	0.28833	-2.0692213	150000
6	1.6	0.0000075	0.27100	-1.9442509	133333.3
7	1.7	8.23529E-06	0.25900	-1.8662207	121428.6
8	1.8	8.88889E-06	0.23900	-1.7492163	112500
9	1.9	9.47368E-06	0.22300	-1.6656716	105555.6

1/[drug]	A0/(A-A0)
550000	-5.23125
300000	-2.973357016
216666.6667	-2.517293233
175000	-2.283765348
150000	-2.069221261
133333.3333	-1.944250871
121428.5714	-1.866220736
112500	-1.749216301
105555.5556	-1.665671642

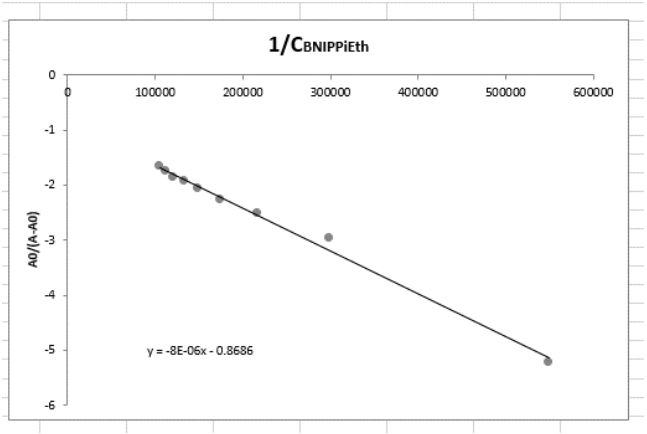

Figure A.2.: Example of K binding constants calculation with the formula A0/A-A0.

Appendix 3

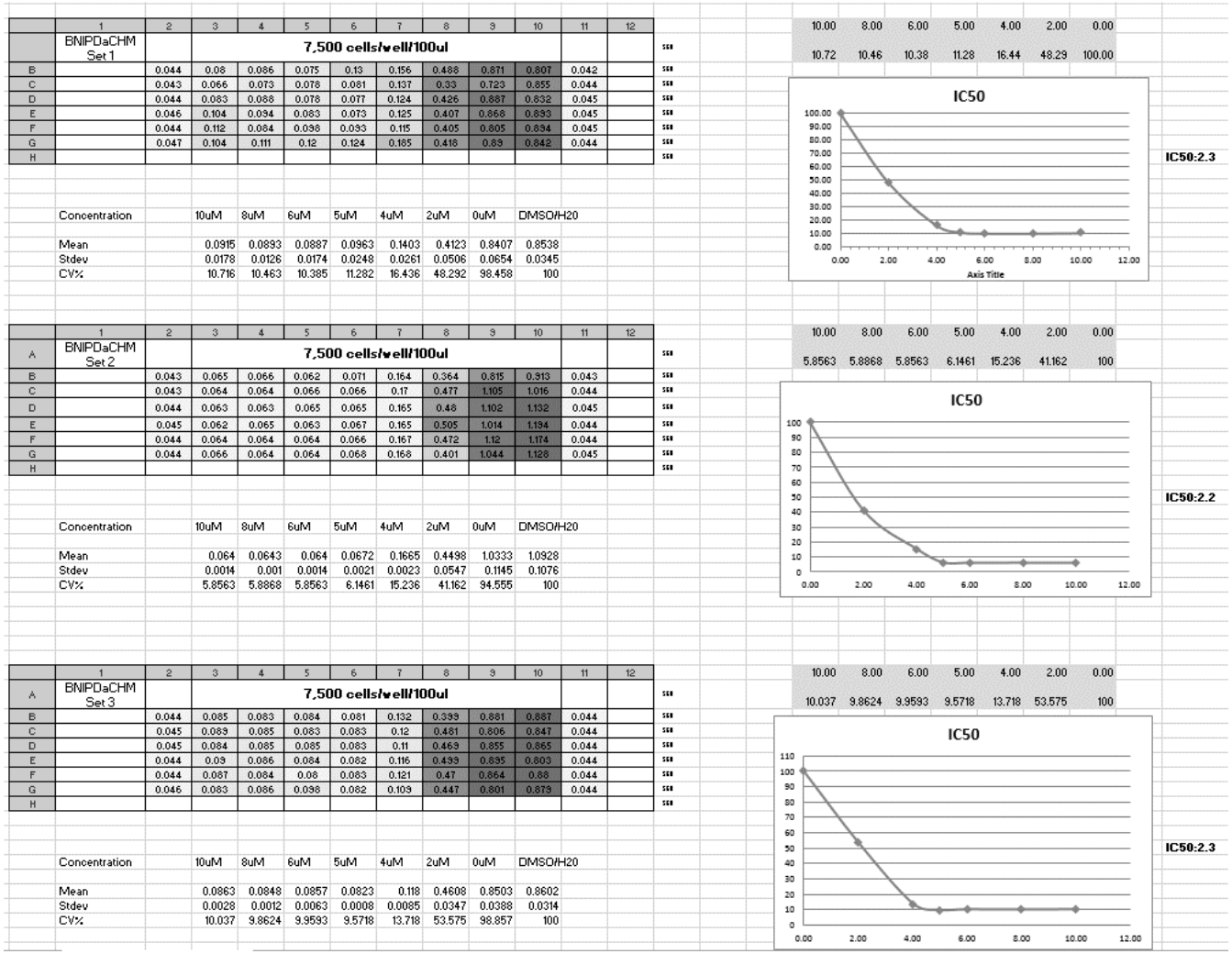

Figure A.3.: Example of IC_{50} values calculation obtained by cytotoxicity studies.

Appendix 4

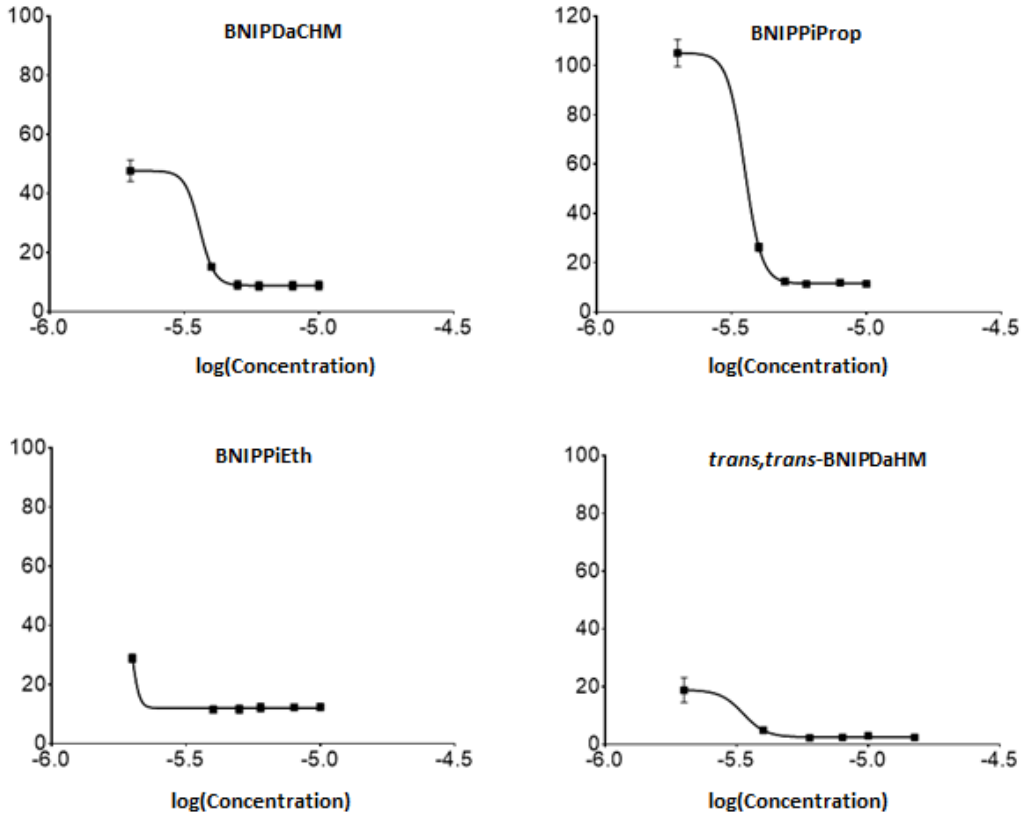

BNIPs	IC_{50} values (μM) MDA-MB-231
BNIPDaCHM	3.61
BNIPPiProp	3.54
BNIPPiEth	2.00
***trans,trans*-BNIPDaCHM**	3.35

Figure A.4.: Example of IC_{50} values calculation obtained by fitting the 4 parameter Hill equation to dose-response curve.

Appendix 5

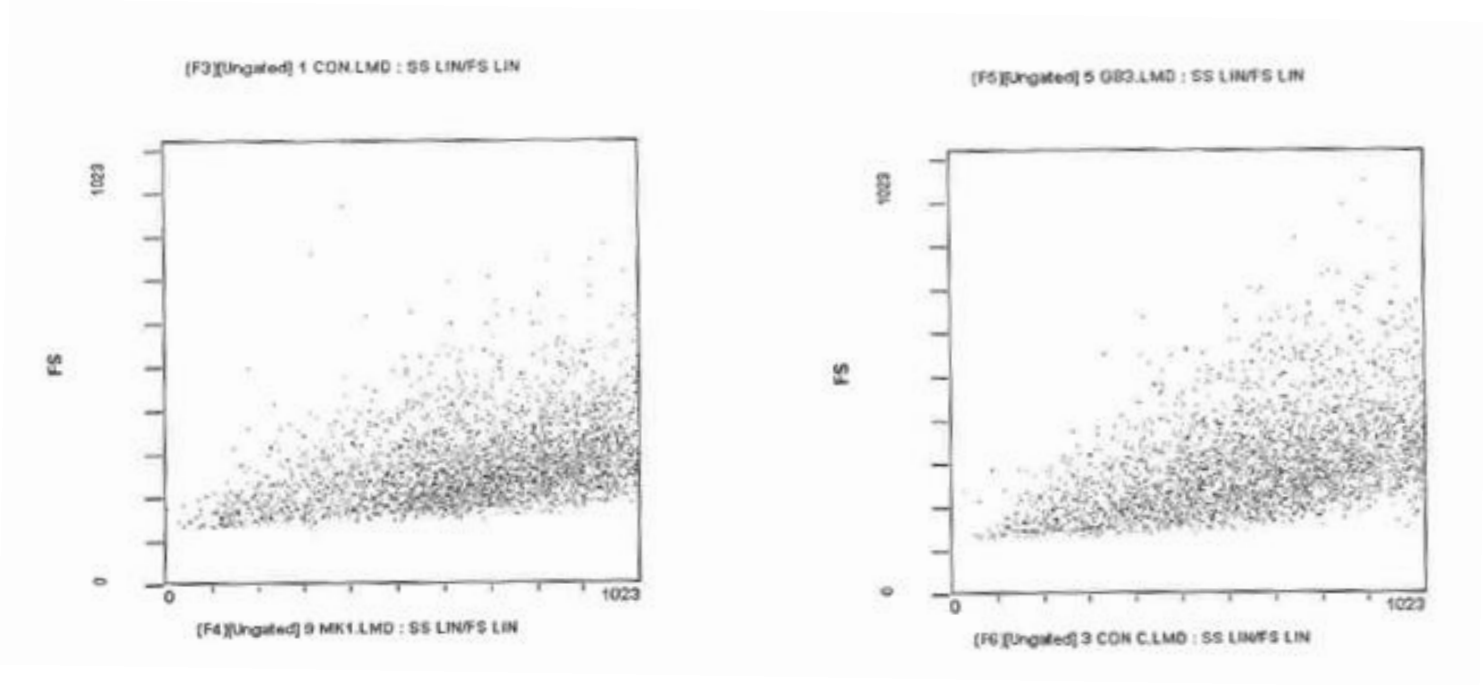

Figure A.5a.: Example of plotting forward scatter *versus* side scatter before and after treatment with BNIPDaCHM. No presence of cell doublets.

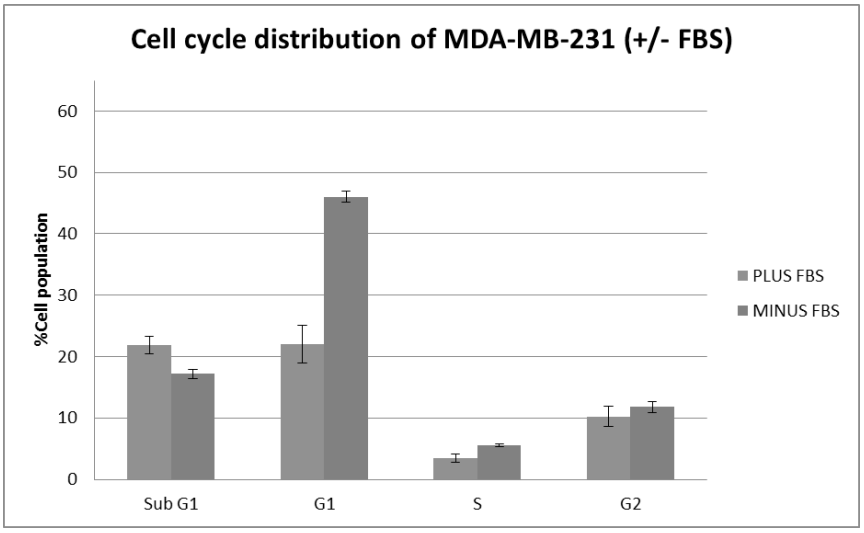

Figure A.5b.: Example of cell cycle distribution of MDA-MB-231 cells +/- FBS on a graph showing the % of the total population in each phase, without normalising it to the control. Serum starvation has caused synchronisation (more cells in G1, no increase in SubG1) - similar results as presenting the data after normalisation to the control.

Appendix 6

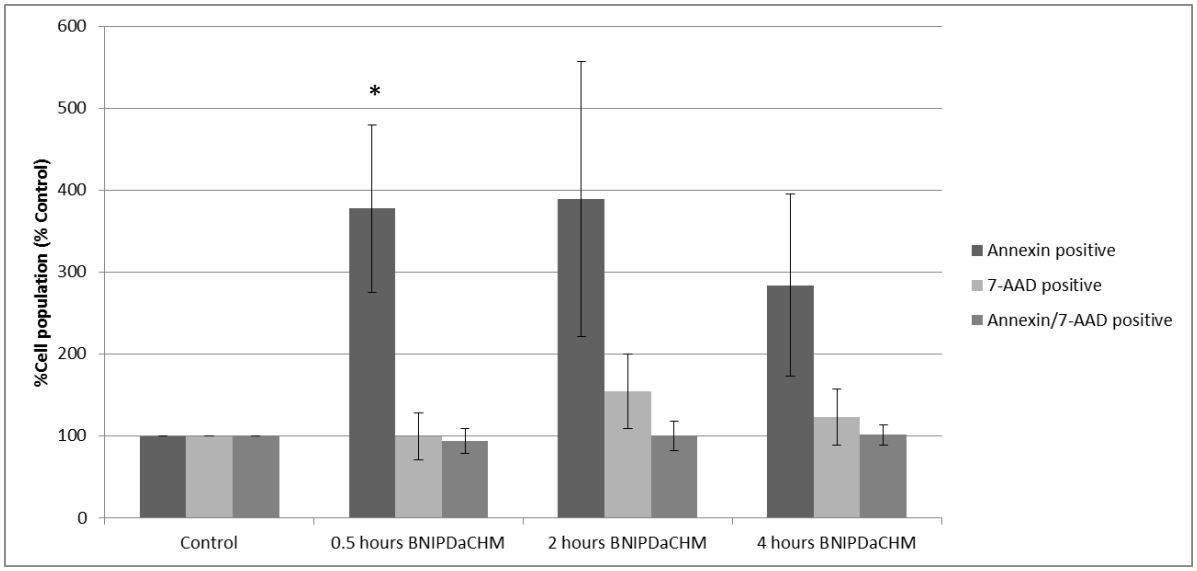

Figure A6.: PS exposure and membrane integrity profiles of MDA-MB-231 after 0.5, 2, and 4 hour treatment with IC_{25} BNIPDaCHM. Profiles were determined by flow cytometry following Annexin V-FITC staining and 7-AAD labelling. 10,000 single events were recorded, and cells labelled with Annexin V but not 7-AAD were considered Annexin positive. Cells labelled with 7-AAD were 7-AAD positive. Annexin/7-AAD labelled cells were considered double positive. However, no change was observed within Annexin/7-AAD population after treatment with BNIPs (see the example above, after treatment with BNIPDaCHM).

PUBLIC OUTPUT

Published paper:

- **Kopsida M**, Barron GA, Bermano G, Kong Thoo Lin P and Goua M-Novel Bisnaphthalimidopropyl (BNIPs) derivatives as anti-cancer compounds targeting DNA in human breast cancer cells. ***Org. Biomol. Chem.***, (2016), **14**, 9780-9789.

Oral presentations:

- Oral Presentation at the International Conference on Biochemistry and Molecular Biology (ICBMB) 2016, Venice, Italy, 27-29 April 2016
- Oral Presentation at the 4th Royal Society of Chemistry Early Career Symposium, Glasgow, United Kingdom, 23-34 June 2016

Poster presentations:

- Poster Presentation at the RGU FHSC Postgraduate Symposium 2016 (First Prize Winner), Aberdeen, United Kingdom, 26 May 2016.
- Poster Presentation at the Drug Discovery and Therapy World Congress 2016, Boston, MA, USA, 22-25 August 2016
- Poster at the 7th APS International PharmSci Conference, Glasgow, United Kingdom, 5-7 September 2016

Organic & Biomolecular Chemistry

PAPER

Cite this: *Org. Biomol. Chem.*, 2016, **14**, 9780

Novel bisnaphthalimidopropyl (BNIPs) derivatives as anticancer compounds targeting DNA in human breast cancer cells†

Maria Kopsida,[a] Gemma A. Barron,[a,b] Giovanna Bermano,[b] Paul Kong Thoo Lin[a] and Marie Goua*[a]

Received 23rd August 2016,
Accepted 21st September 2016

DOI: 10.1039/c6ob01850e

www.rsc.org/obc

Bisnaphthalimidopropyl (BNIP) derivatives are a family of compounds that exert anti-cancer activities *in vitro* and, according to previous studies, variations in the linker sequence have increased their DNA binding and cytotoxic activities. By modifying the linker sequence of bisnaphthalimidopropyl diaminodicyclohexylmethane (BNIPDaCHM), a previously synthesised BNIP derivative with anti-cancer properties, three novel BNIP derivatives were designed. Bisnaphthalimidopropyl-piperidylpropane (BNIPPiProp), a structural isomer of BNIPDaCHM, bisnaphthalimidopropyl ethylenedipiperidine dihydrobromide (BNIPPiEth), an isoform of BNIPDaCHM with a shorter linker chain, and (*trans*(*trans*))-bisnaphthalimidopropyl diaminodicyclohexylmethane (*trans*,*trans*-BNIPDaCHM), a stereoisomer of BNIPDaCHM, were successfully synthesised (72.3–29.5% yield) and characterised by nuclear magnetic resonance spectroscopy (NMR) and mass spectrometry (MS). Competitive displacement of ethidium bromide (EtBr) and UV binding studies were used to study the interactions of BNIP derivatives with *Calf Thymus* DNA. The cytotoxicity of these derivatives was assessed against human breast cancer MDA-MB-231 and SKBR-3 cells by MTT assay. Propidium iodide (PI) flow cytometry was conducted in order to evaluate the cellular DNA content in both breast cancer cell lines before and after treatment with BNIPs. The results showed that all novel BNIPs exhibit strong DNA binding properties *in vitro*, and strong cytotoxicity, with IC_{50} values in the range of 0.2–3.3 μM after 24 hours drug treatment. Two of the novel BNIP derivatives, BNIPPiEth and *trans*,*trans*-BNIPDaCHM, exhibited greater cytotoxicity against the two breast cancer cell lines studied, compared to BNIPDaCHM. By synthesising enantiopures and reducing the length of the linker sequence, the cytotoxicity of the BNIP derivatives was significantly improved compared to BNIPDaCHM, while maintaining DNA binding and bis-intercalating properties. In addition, cell cycle studies indicated that *trans*,*trans*-BNIPDaCHM, the most cytotoxic BNIP derivative, induced sub-G1 cell cycle arrest, indicative of apoptotic cell death. Based on these findings, further investigation is under way to assess the potential efficacy of *trans*,*trans*-BNIPDaCHM and BNIPPiEth in treating human breast cancer.

Introduction

Breast cancer is the most commonly occurring cancer in women, with incidence rates approaching 1.38 million cases per year worldwide.[1] Breast cancer, depending on whether it develops in response to the hormone oestrogen, is divided in two categories: oestrogen dependent (ER^+) and oestrogen independent (ER^-) cancer.[2] ER^+ breast cancers respond better to anti-oestrogen (endocrine) therapies, such as tamoxifen and exemestane, by inhibiting the effect of oestrogen and decreasing the uncontrolled proliferation of breast cancer cells.[2] On the other hand, ER-breast cancers are more invasive and less responsive to current standard-of-care treatment regimes, such as fluorouracil, epirubicin and doxorubicin, which do not selectively target breast cancer cells hence leading to severe side effects.[3] Over the last few decades, there have been numerous attempts to develop novel breast cancer-specific therapies that will act on specific molecular targets, increasing selectivity and potentially reducing treatment resistance and side effects.[4] DNA was one of the first biochemical targets identified in anti-cancer therapeutics,[5–7] which lead to a new

[a]*School of Pharmacy and Life Sciences, Robert Gordon University, Garthdee Road, Aberdeen, AB10 7GJ Scotland, UK. E-mail: m.goua@rgu.ac.uk*
[b]*Centre for Obesity Research and Education (CORE), Faculty of Health and Social Care, Robert Gordon University, Garthdee Road, Aberdeen, AB10 7GJ Scotland, UK*
†Electronic supplementary information (ESI) available. See DOI: 10.1039/c6ob01850e

generation of agents with improved efficacy and solubility. In the 1990s naphthalimido compounds, such as mitonafide, were found for the first time to be highly active against cervical cancer and leukaemia cells, however, a Phase I clinical trial revealed that mitonafide treatment at doses above 118 mg m^{-2} × 5 days lead to central nervous system toxicity.[8] Subsequently, bisnaphthalimido compounds were synthesised with improved therapeutic properties. They had also overcome the dose-limiting toxicity issues,[9] however, their aqueous insolubility limited their potential use as anti-cancer agents.[10] Kong Thoo Lin and Pavlov[10] designed and synthesised a number of bisnaphthalimidopropyl derivatives, by incorporating natural polyamines and, diamino or triamino alkyl chains into the bisnaphthalimide structure. This led to improved aqueous solubility, as well as anti-cancer activity.[11,12] Additional alterations to the linker were performed to confirm that BNIP moiety was crucial for *in vitro* anti-cancer activity. One such alteration was the introduction of a bicyclohexylmethane group (in the linker chain). This tended to reduce the flexibility of the linker but it enhanced its DNA binding properties, resulting in the synthesis of BNIPDaCHM (Fig. 1). BNIPDaCHM contained a pseudo-asymmetrical centre with a mixture of three isomers (*cis*,*cis*; *trans*,*trans* and *cis*,*trans*) (indicated by asterisks, Fig. 1).[13,14] This linker chain modification resulted in a more cytotoxic BNIP derivative against triple negative breast cancer cells MDA-MB-231 (IC_{50} value 6.8 μM), compared to chemotherapy drug doxorubicin (IC_{50} value 14.4 μM), after 24 hours treatment.[13] With regards to selectivity, non-tumourigenic breast epithelial MCF-10A cells were found to be less responsive to BNIPDaCHM (IC_{50} value 6.06 μM) than doxorubicin.[13]

In the present work, we describe for the first time, the synthesis and characterisation of three novel BNIP derivatives that were designed by considering several modifications to the structure of BNIPDaCHM (Fig. 1). The first BNIP derivative, bisnaphthalimidopropyl-piperidylpropane dihydrobromide (BNIPPiProp) is a structural isomer of BNIPDaCHM that consists of only one species (enantiopure). The aim of synthesising BNIPPiProp was to investigate whether cytotoxicity and DNA binding properties differ among structural isomers and how the position of the ring structure in the linker chain affects cytotoxicity. The second BNIP derivative, bisnaphthalimidopropyl-ethylenedipiperidine (BNIPPiEth), consists of one carbon less between the two piperidine ring structures, compared to BNIPPiProp and was synthesised in order to assess the effect of a shorter linker chain on cytotoxicity and DNA binding properties. In parallel, it is still unknown whether the cytotoxicity of BNIPDaCHM is associated with the existence of the three isomers in its structure, therefore (*trans*(*trans*))-4,4′-methylenebis (cyclohexylamine), the only commercially available stereoisomer precursor required to synthesise *trans*,*trans*-BNIPDaCHM the latter being, the third BNIP derivative used in this study. The synthesis of *trans*,*trans*-BNIPDaCHM lead to the investigation into the importance of this stereoisomer compared to the mixture of three stereoisomers present in BNIPDaCHM in relation to DNA binding affinities, cytotoxicity in MDA-MB-231 and SKBR-3 breast cancer cell lines and the possible mode of cell death *via* cell cycle analysis were studied for the three novel compounds. By using two cell lines which are unresponsive to currently available anti-cancer regimes, it is possible to extend our knowledge on BNIP derivative cytotoxicity against different breast cancer cells types and to gain more information about their mode of action.

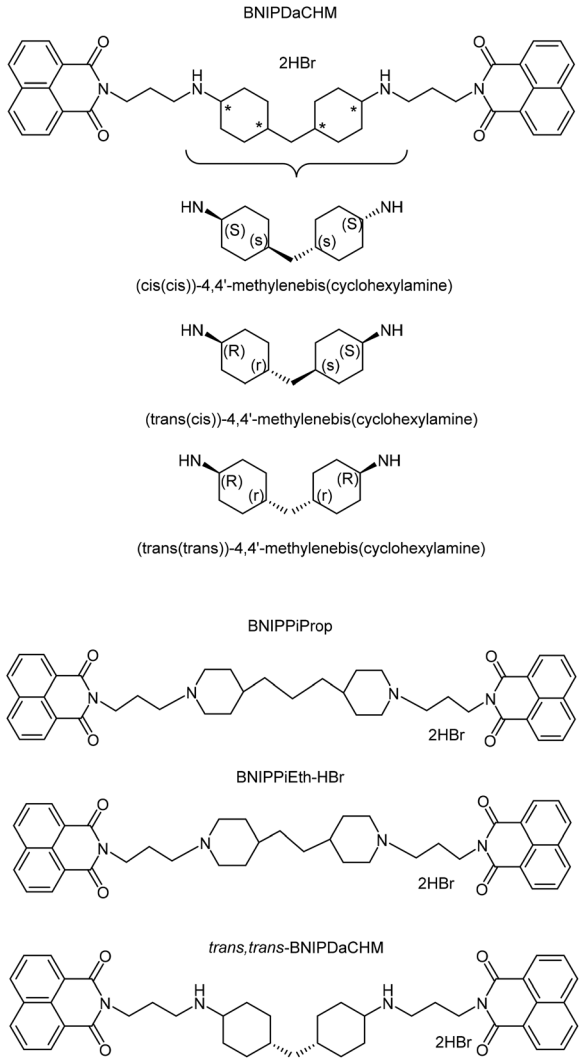

Fig. 1 Chemical structure of BNIP derivatives: BNIPDaCHM with its three stereo isomers, bisnaphthalimidopropyl-piperidylpropane (BNIPPiProp), bisnaphthalimidopropyl-ethylenedipiperidine (BNIPPiEth) and (*trans*(*trans*))-4,4′-methylenebis(cyclohexylamine) (*trans*,*trans*-BNIPDaCHM).

Results and discussion

Chemical synthesis

The synthesis of bisnaphthalimidopropyl-dipiperidyl-propane and ethane free bases was carried out by reacting 1,3-bis-(4-piperidyl) propane or 1,3-bis-(4-piperidyl)ethane and toluenesulfonyloxypropylnaphthalimide in tetrahydrofuran (THF) under reflux with subsequent addition of cesium car-

bonate (Scheme 1). The corresponding BNIPPiProp and BNIPPiEth dihydro chloride and bromide salts were prepared by their treatment with HBr/g·CH_3CO_2H and conc. HCl (72.3% and 29.5% yield), respectively.

The synthetic strategy of *trans*,*trans*-BNIPDaCHM (Scheme 2) was based on methods previously developed in our group for the synthesis of BNIPDaCHM.[13] Here the single isomer *trans*,*trans*-4,4′-methylenebiscyclohexylamine was used as the starting material. The synthesis of *trans*,*trans*-N^4,N^4-dimesityl-dicyclohexylmethane was carried out by reacting *trans*,*trans*-4,4′-methylenebis(cyclohexylamine), with 2-mesitylenesulfonyl chloride (Mts-Cl) in anhydrous pyridine (21.1% yield). *N*-Alkylation was performed by reacting *trans*,*trans*-N^4,N^4-dimesityl-dicyclohexylmethane with toluenesulfonyloxypropyl-naphthalimide in DMF (37.0% yield). For the final step, *trans*,*trans*-bisnaphthalimido-dimesityl-dicyclohexylmethane was dissolved in DCM, followed by treatment with hydrobromic acid/glacial acetic acid (HBr/g·CH_3CO_2H). All new compounds were fully characterised by NMR and high resolution mass spectrometry (see Experimental section). The melting point of *trans*,*trans*-BNIPDaCHM was found to be 120–125 °C indicating good purity. In contrast, BNIPDaCHM exhibited a

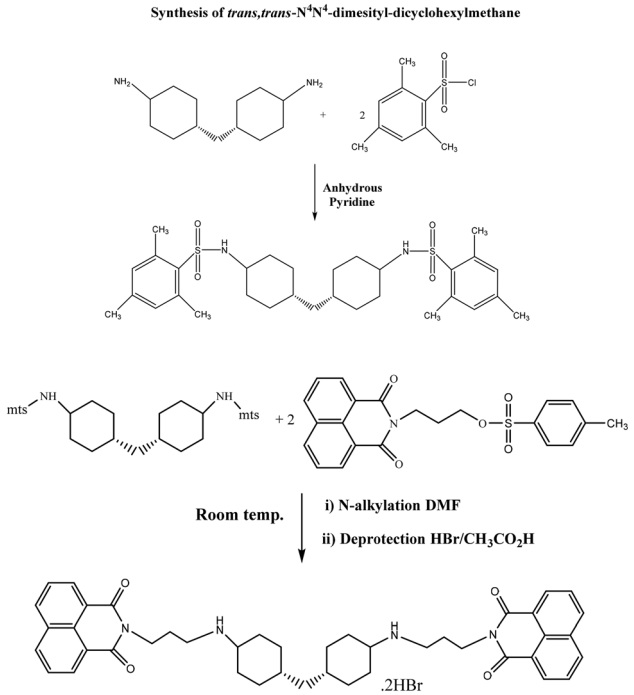

Scheme 2 Synthetic pathway of (*trans*(*trans*))-4,4′-methylenebis(cyclohexylamine) (*trans*,*trans*-BNIPDaCHM).

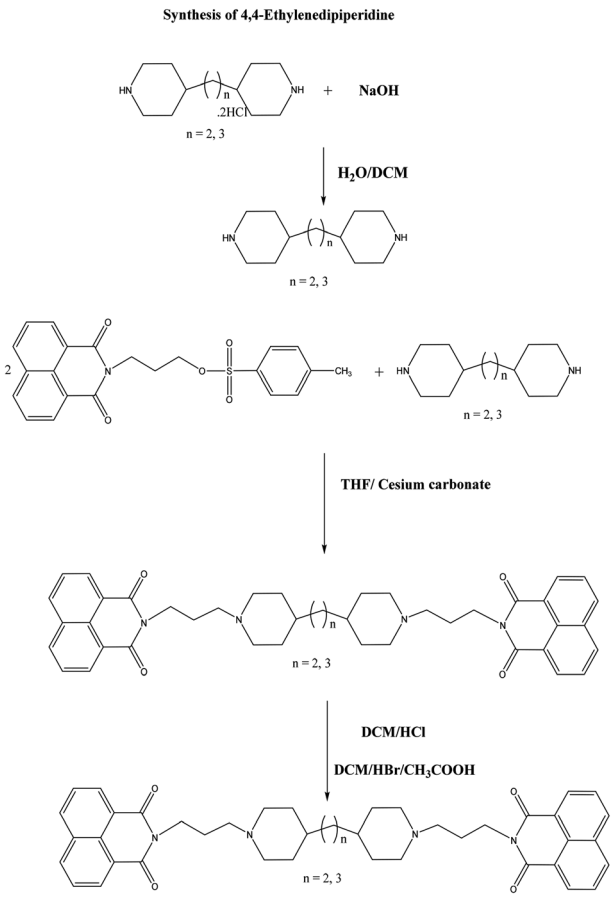

Scheme 1 Synthetic pathway of bisnaphthalimidopropyl-piperidylpropane (BNIPPiProp) and bisnaphthalimidopropyl-ethylenedipiperidine dihydrobromide (BNIPPiEth).

higher melting point range (105–130 °C) compared to *trans*,*trans*-BNIPDaCHM. BNIPPiProp and BNIPPiEth had melting points in the range of 160–170 °C and 120–125 °C, respectively, indicating their high purity.

According to matched molecular pair (MMP) analysis, which has been broadly used in the last few years to investigate the effects of hydrogen bond donors/acceptors and rotatable bonds on the melting point of drug-like compounds,[15–17] has shown that an increase in rotatable bonds leads to a decrease of the melting point.[18] Therefore, the existence of the three isomers on BNIPDaCHM increases its flexibility and leads to a low melting point, compared to the three novel compounds.

On the other hand, BNIPPiProp, with the longest linker sequence, has the highest melting point (160–170 °C), due to the increase of hydrogen bond donors/acceptors that stabilize the crystal lattice.[18]

DNA binding studies

Competitive displacement of ethidium bromide from *Calf Thymus* DNA. Competitive displacement of ethidium bromide (EtBr) with BNIPs from *Calf Thymus* DNA was carried out to investigate their DNA interactions. EtBr is a well known DNA structural probe and intercalating dye that exerts fluorescence once it binds to DNA.[19] A compound with higher DNA binding affinity than EtBr either displaces EtBr or breaks the DNA secondary structure, resulting in fluorescence quenching and a decrease in fluorescence intensity.[20] All three novel BNIP derivatives competitively displaced EtBr from *Calf Thymus* DNA duplexes. For each derivative, a range of concentrations

Table 1 Competitive displacement of EtBr from *Calf Thymus* DNA. Effect of different BNIP concentrations (0–7 μM) on % fluorescence intensity compared to *Calf Thymus* DNA alone. IC_{50} value: concentration of each BNIP derivative required to cause a 50% decrease on fluorescence intensity of DNA-EtBr complex. Data are the mean ± SD of three independent experiments (n = 3). *P < 0.05, **P < 0.01, compared to BNIPDaCHM

BNIP derivatives	Mean ± SD IC_{50} value (μM)
Calf Thymus DNA alone	–
BNIPDaCHM	2.3 ± 0.1
BNIPPiProp	3.9 ± 0.3*
BNIPPiEth	1.1 ± 0.2*
trans,*trans*-BNIPDaCHM	5.6 ± 0.2**

(0–7 μM) were tested and the corresponding IC_{50} values calculated. All BNIP derivatives displaced EtBr with IC_{50} values ranging from 1.1 to 5.6 μM confirming their high DNA binding affinity (Table 1). BNIPDaCHM was included in the following studies in order to evaluate and compare its binding properties to the novel BNIP derivatives.

The order of their binding affinity to *Calf Thymus* DNA from highest to lowest was BNIPPiEth (1.1 ± 0.2 μM), BNIPDaCHM (2.3 ± 0.1 μM), BNIPPiProp (3.9 ± 0.3 μM) and *trans*,*trans*-BNIPDaCHM (5.6 ± 0.2 μM).

BNIPPiEth, which has the shortest linker with two piperidine rings attached to an ethyl group, had the lowest IC_{50} value. The shorter length of the linker chain, as well as the incorporation of a nitrogen atom within the cyclohexane ring, compared to BNIPDaCHM, resulted in increased DNA binding. On the other hand, the incorporation of the nitrogen atom within the cyclohexane ring was not found to improve the binding properties of BNIPPiProp (3.9 ± 0.3 μM), compared to BNIPDaCHM and BNIPPiEth, confirming that the length of the bridging alkyl linkers is crucial and affects significantly BNIP binding to DNA duplexes.[21]

The *trans*,*trans*-BNIPDaCHM, a stereoisomer of BNIPDaCHM, gave a IC_{50} value of 5.6 ± 0.2 μM. BNIPDaCHM, which consists of three isomers, gave a IC_{50} value of 2.3 ± 0.1 μM, which indicated that in absence of *cis*,*cis* or/and *cis*, *trans*, *trans*,*trans*-BNIPDaCHM was not able to achieve as high DNA-binding interactions as BNIPDaCHM. Based on the above results, the planar structure of BNIPDaCHM and its mixture of three isomers was found to improve its interacting properties within the DNA base pairs, compared to *trans*,*trans*-BNIPDaCHM. This was confirmed since *trans*,*trans*-BNIPDaCHM resulted in a lower IC_{50} value compared to BNIPDaCHM, revealing that each of the three or more than one (*trans*,*trans*/*cis*,*trans* or *trans*,*trans*/*cis*,*cis*) isomers co-existing in BNIPDaCHM, are involved in the intramolecular complexes/interactions with DNA. By isolating one of its isomers (*trans*, *trans*-BNIPDaCHM), the DNA binding affinity was decreased (p < 0.01). The planar structure of BNIPDaCHM allows it to fit between the base pairs and in parallel, its rotational freedom within the plane of the aromatic rings, may allow the exposure of more than one intercalating sidechain to DNA.[22]

UV binding studies

The binding of the novel BNIP derivatives with *Calf Thymus* DNA was also studied by UV spectroscopy. A continuous decrease in UV absorption was observed at 260 nm, within the range of drug concentrations (0–7 μM) investigated. The apparent binding constants for the compounds under study, were calculated from the intercept and the slope by plotting $A_0/(A - A_0)$ against BNIP derivative concentrations,[23] where A_0 and A correspond to the absorbance values in the absence and presence of each BNIP compound (Fig. 2a), respectively. Binding constant values K for the BNIP derivatives range between 3.25×10^4–12.23×10^4 (Fig. 2b), and indicate that all BNIP derivatives interact with the DNA helix. The highest binding constant was observed with BNIPDaCHM (12.23×10^4), followed by *trans*,*trans*-BNIPDaCHM (11.38×10^4) and BNIPPiEth (10.85×10^4). The lowest K binding constant was observed for BNIPPiProp (3.25×10^4). This outcome is in agreement with the competitive displacement of EtBr studies (Table 1), highlighting the importance of linker chain length in achieving strong DNA binding interactions. In addition, the UV absorption studies revealed that *trans*,*trans*-BNIPDaCHM, the less effective derivative in displacing EtBr from DNA, obtained a high binding constant (11.38×10^4), compared to BNIPDaCHM (12.23×10^4: highest K binding constant). This suggests that *trans*,*trans*-BNIPDaCHM exhibits lower inter-

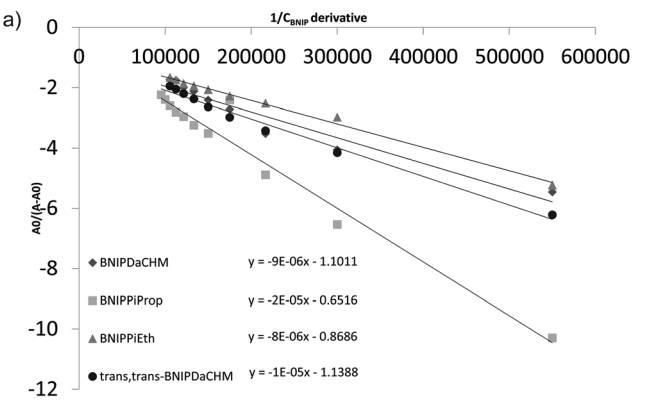

b)

BNIP derivatives	K constant
BNIPDaCHM	12.2×10^4
BNIPPiProp	3.3×10^4
BNIPPiEth	10.9×10^4
trans,trans-BNIPDaCHM	11.4×10^4

Fig. 2 (a) Competitive displacement of EtBr from *Calf Thymus* DNA. Plot of $A_0/(A - A_0)$ *versus* $1/C_{BNIP}$ of the interaction between BNIP derivatives and *Calf Thymus* DNA. (b) K constant values of BNIPP derivatives after UV binding studies.

calation capacity than the other two isomers present in the BNIPDaCHM. However, the *trans*,*trans* isomer has similar DNA affinity to the mixture of isomers present in BNIPDaCHM as demonstrated by their binding constant (Fig. 2b). Previous molecular modelling studies have revealed that for the most stable conformation of bis-1,8-naphthalimide in presence of DNA, the naphthalimide rings obtain an antiparallel orientation and are detected in the major groove.[24] Furthermore, they have been reported to induce strand cleavage, allowing the electron transfer and formation of hydrogen bonding between the nitrogen atoms and the nucleobases (excluding guanine) of the minor groove,[25] suggesting that the high *K* binding constant of *trans*,*trans*-BNIPDaCHM is obtained not only *via* intercalation, but also *via* binding on the major and minor groove of DNA.

Biological studies

Cytotoxicity. Cytotoxicity evaluation of BNIPDaCHM, BNIPPiProp, BNIPPiEth and *trans*,*trans*-BNIPDaCHM was performed by using MTT assay[26] against MDA-MB-231 and SKBR-3 cells (Table 2). After 24 hours treatment, all novel BNIP derivatives, exhibited strong cytotoxicity with IC_{50} values ranging from 1.4 μM to 3.3 μM in MDA-MB-231 cells (Table 2), compared to previously synthesised BNIPs or DNA intercalating drugs (doxorubicin) that have been tested against the same cell line, with IC_{50} values ranging from 4.9 μM to 12.7 μM.[13] In particular, *trans*,*trans*-BNIPDaCHM exhibited the lowest IC_{50} value of 1.4 μM, BNIPPiEth an IC_{50} of 1.8 μM and BNIPPiProp an IC_{50} of 3.3 μM. A similar pattern of cytotoxicity was found for SKBR-3 cells, although the IC_{50} values were between 0.2–0.7 μM (Table 2).

trans,*trans*-BNIPDaCHM (1.4 μM) was more active ($p < 0.01$) than BNIPDaCHM (2.3 μM) against MDA-MB-231 cells, showing that the existence of a single isomer in the linker sequence results in a more cytotoxic compound, compared to a compound which contains a mixture of isomers. BNIPPiEth was more cytotoxic ($p < 0.05$) than BNIPDaCHM, suggesting that the shorter length of the linker chain, as well as the incorporation of the nitrogen atom within the cyclohexane ring, not only improved the binding properties of BNIPPiEth, but enhanced significantly its *in vitro* cytotoxicity, too. Regarding BNIPPiProp, the derivative with the longest linker sequence and the highest IC_{50} value, it was found that the length of the linker chain length plays an important role in the functionality and effectiveness of a BNIP derivative. In addition, all the derivatives followed a similar pattern of cytotoxicity in both cell lines however, they appeared more cytotoxic against SKBR-3 cells. This may be due to the different mutational and tumorigenic statuses.

MDA-MB-231 cells are triple negative breast cancer cells (TNBC) (oestrogen receptor negative (ER^-), progesterone receptor negative (PR^-), human epidermal growth factor receptor 2 negative $HER2^-$) with four gene mutations being reported (BRAF, CDKN2A, KRAS and TP53) and a fast-growing basal B tumour classification (49.5% proliferation rate),[27] which makes them less responsive to anti-cancer treatments, such as docetaxel or carboplatin, compared to cells that are hormone receptor positive.[27] On the other hand, SKBR-3 cells are double negative breast cancer cells (DNBC) (ER^-, PR^-, $HER2^+$) without gene mutations and with a luminal tumour classification (35.2% proliferation rate),[27] resulting in a better response to anti-cancer treatments compared to TNBCs, which is in agreement with our findings.

Table 2 Cytotoxicity of BNIP derivatives against MDA-MB-231 and SKBR-3 cells. MDA-MB-231 and SKBR-3 cells were treated with different BNIP concentrations (0–10 μM) for 24 hours at 37 °C. IC_{50} values correspond to the concentration required to reduce cell growth by 50% compared to control cells. Data presented as mean ± SEM of 3 independent experiments ($n = 3$). *$P < 0.05$, **$P < 0.01$, compared to BNIPDaCHM

	IC_{50} values (μM)(Mean ± SEM)	
BNIP derivatives	MDA-MB-231	SKBR-3
BNIPDaCHM	2.3 ± 0.1	0.4 ± 0.1
BNIPPiProp	3.3 ± 0.1**	0.7 ± 0.1*
BNIPPiEth	1.8 ± 0.1*	0.3 ± 0.1*
trans,*trans*-BNIPDaCHM	1.4 ± 0.1**	0.2 ± 0.0*

Cell cycle analysis

Cell cycle distribution of MDA-MB-231 and SKBR-3 cells after cell synchronisation was studied using flow cytometry following PI staining[28] with the most active compound *trans*,*trans*-BNIPDaCHM (Table 2), together with BNIPDaCHM (mixture of isomers) that has been reported to induce cell cycle instability.[29]

An increase in the proportion of MDA-MB-231 cells in sub-G1 phase (122.3%, 139.3% and 142.2% increase, respectively) was exhibited relative to the control, whilst in G1 phase, the cell population was decreased after treatment with BNIPDaCHM (1 μM) and *trans*,*trans*-BNIPDaCHM (1 μM) (31.3% and 29.4% decrease, both $p < 0.05$) (Fig. 3a). The above results indicate that both BNIPDaCHM and *trans*,*trans*-BNIPDaCHM induced sub-G1 cell cycle arrest to a greater extent than camptothecin. Camptothecin is a well known positive control for sub-G1 arrest[30,31] and for inducing apoptosis.[32,33]

Therefore, this suggests that BNIPDaCHM and *trans*,*trans*-BNIPDaCHM could use similar mechanisms of action compared to camptothecin and may trigger apoptotic cell death in MDA-MB-231 and SKBR-3 human breast cancer cells.

Similar experiments were carried out with synchronised SKBR-3 cells (Fig. 3b), where the cell population was significantly increased in sub-G1 phase only after treatment with BNIPDaCHM (136.4%) and camptothecin (210.2%), but not for *trans*,*trans*-BNIPDaCHM, demonstrating that the effect of the two BNIP derivatives was different in each cell line and that the existence of one isomer has a different effect on cell cycle distribution. Therefore, it is suggested that the mechanisms of cell death among *trans*,*trans*-BNIPDaCHM and BNIPDaCHM may differ, even though they belong to the same family of compounds.

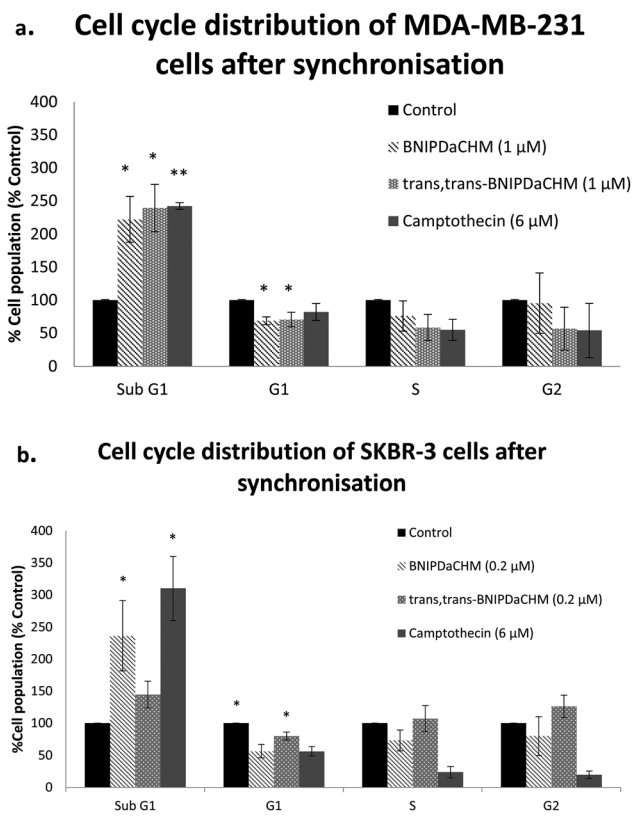

Fig. 3 Cell cycle distribution of MDA-MB-231 and SKBR-3 cells after BNIP treatment. (a) Quantification of MDA-MB-231 and (b) SKBR-3 cell cycle profiles by flow cytometry following PI staining after 24 hours treatment with BNIPDaCHM, *trans*,*trans*-BNIPDaCHM and camptothecin. DMSO/dH_2O (50% v/v) was used as the solvent control. The percentage of the cell population in sub-G1, G1, S and G2/M were calculated from histograms of linear FL-2 plots in the ungated regions (10 000 events). Data are mean ± SEM of three independent experiments (n = 3), conducted in duplicates. *P < 0.05, compared to solvent control.

Conclusions

In this study, we have shown that three BNIP derivatives, BNIPPiProp, BNIPPiEth and *trans*,*trans*-BNIPDaCHM could have potential as anti-cancer agents. DNA binding affinity was confirmed as each BNIP derivative had the ability to competitively displace EtBr from DNA and quenched UV absorption in presence of DNA in a dose dependent manner. Linker sequence modifications showed stronger cytotoxic effects against MDA-MB-231 and SKBR-3 cells, compared to the parental compound BNIPDaCHM. In addition, cell cycle analysis showed that *trans*,*trans*-BNIPDaCHM induced sub-G1 arrest in MDA-MB-231 cells, but not in SKBR-3 cells, suggesting that its mode of action could be cell line dependent, in contrast to BNIPDaCHM that shows a similar trend in cell cycle arrest in both cell lines. This study has confirmed that BNIPPiProp, BNIPPiEth and *trans*,*trans*-BNIPDaCHM have the ability to interact with DNA, intercalate and stabilise the double helix, and exhibit better cytotoxic activities, compared to previously synthesised BNIP derivatives. Further research is ongoing into the mode of DNA damage, cell death or pathway deregulations in human breast cancer cell lines.

Experimental

Chemical synthesis

BNIPPiProp, BNIPPiEth and *trans*,*trans*-BNIPDaCHM were synthesised according to the methods (with some modifications) previously described by Kong Thoo Lin and Pavlov.[10] The chemical structure, purity and stability of the derivatives were confirmed by TLC, NMR, MS and melting point determination. All reagents were purchased from Fisher Scientific or Sigma-Aldrich, unless otherwise stated. TLC was performed on silica gel 60 F254 aluminium plates (EMD/Merck) in chloroform/methanol (95 : 5). NMR was recorded on a Bruker 400 Ultrashield spectrometer operating at 400.1 MHz for ^{1}H and 100.6 MHz for ^{13}C. Accurate mass spectra were obtained by were obtained on Thermo Scientific LTQ Orbitrap XL or Waters Xevo G2-S analytical instruments (EPSRC National Mass Spectrometry Service Centre at Swansea University, Swansea).

Synthesis of bisnaphthalimidopropyl-dipiperidyl-propane base

1,3-Bis-(4-piperidyl)propane (1.19×10^{-3} mol, 0.25 g) and toluenesulfonyloxypropylnaphtalamide (2.39×10^{-3} mol, 0.98 g) were dissolved in tetrahydrofuran (THF) (6 mL). Using a reflux condenser, the reaction was stirred at 50 °C for 15 minutes and after the addition of caesium carbonate (3.069×10^{-3} mol, 1 g), the reaction was left to stir overnight at 50 °C. The reaction was monitored with TLC and once complete, the solution was poured into icy water (100 mL). A precipitate was formed and after vacuum filtration, the product was dried in a vacuum oven at 45 °C overnight. The crude product (base of BNIPPiProp) was recrystallized from ethanol and the pure product was characterised by ^{1}H-NMR (64.8% yield).

^{1}H-NMR ($CDCl_3$): δ_H 8.53–8.51 (2H, CH aromatic protons), 8.14–8.12 (2H, CH aromatic protons), 7.70–7.66 (2H, CH aromatic protons), 4.17–4.14 (2, CH_2 protons), 2.84–2.82 (2H, CH_2 protons), 2.41–2.37 (2H, CH_2 protons), 1.91–1.83 (2H, CH_2 protons), 1.79–1.74 (2H, CH_2 protons), 1.51–1.48 (2H, CH_2 protons), 1.71–1.09 (H, CH proton) ppm (parts per million).

Synthesis of BNIPPiProp salt

The base of BNIPPiProp (1.459×10^{-3} mol, 1 g) was dissolved in DCM (20 mL) and HBr/CH_3CO_2H (2 mL) was added slowly. The reaction was stirred for 2 hours at room temperature and reaction completion was monitored by TLC yielding a precipitate. The precipitate was filtered by vacuum filtration and washed with DCM (30 mL) and ether (10 mL). The BNIPPiProp salt was dried under negative pressure in a vacuum oven set at 45 °C for 2 hours (72.3% yield).

^{1}H-NMR ($CDCl_3$): δ_H 8.53–8.51 (2H, CH aromatic protons), 8.14–8.12 (2H, CH aromatic protons), 7.70–7.66 (2H, CH aromatic protons), 4.69 (2H, CH_2 protons), 4.17–4.14 (2H, CH_2 protons), 2.84–2.82 (2H, CH_2 protons), 2.41–2.37 (2H, CH_2

protons), 1.91–1.83 (2H, CH_2 protons), 1.79–1.74 (2H, CH_2 protons), 1.51–1.48 (2H, CH_2 protons), 1.71–1.09 (H, CH proton) ppm.

^{13}C-NMR ($CDCl_3$): δ_H 164.24 (C═O), 131.87 (CH aromatic), 131.60 (C aromatic), 131.24 (CH aromatic), 127.75 (C aromatic), 126.94 (CH aromatic), 122.80 (C aromatic), 56.58 (CH_2), 54.03 (CH_2), 39.10 (CH_2 aromatic), 36.77–35.69 (CH), 32.34 (CH2), 25.33 (CH_2) and 23.76 (CH_2) ppm.

Mass spectrum (HRMS), m/z = 685.3739 $(M + H)^+$ $C_{43}H_{48}N_4O_4$ requires 685.3748 $(M + H)^+$.

Synthesis of 4,4-ethylenedipiperidine

4,4-Ethylenedipiperidine dihydrochloride (7.428×10^{-4} mol, 0.2 g) was dissolved in distilled water (2 mL), sodium hydroxide (2 M, 1 mL) was added, which resulted in the formation of a precipitate. The pH was 14. The resulting was transferred into a separating funnel (100 mL) followed by extraction with DCM (300 mL). The organic layer was collected, dried with sodium sulfate and filtered. The solvent was evaporated by a rotary film evaporator. The final white solid product was left to dry under negative pressure in a vacuum oven at 45 °C for 30 minutes (90.6% yield). The synthesis of the free base was confirmed by ^{1}H-NMR.

^{1}H-NMR ($CDCl_3$): δ 2.98–2.95 (2H, CH_2 protons), 2.52–2.45 (2H, CH_2 protons), 1.8 (NH), 1.60–1.57 (2H, CH_2 protons), 1.25–1.21 (H, CH protons) and 1.19–1.16 (2H, CH_2 protons) ppm.

Synthesis of BNIPPiEth base

4,4-Ethylenedipiperidine (5.044×10^{-4} mol, 0.1 g) was reacted with toluenesulfonyloxypropyl-naphthalamide (1.001×10^{-3} mol, 0.41 g, 2.01 excess). Caesium carbonate (3.069×10^{-3} mol, 1 g) was added in the reaction. All the reagents were dissolved in THF (6 mL) and the solution refluxed overnight at 60 °C. The reaction was monitored using TLC. Once the reaction was complete, the solution was poured into icy water (100 mL), which resulting in the formation of a precipitate. The precipitate was filtered using a Buchner funnel and the product was left to dry under negative pressure in a vacuum oven at 45 °C for 60 minutes (72.3% yield). The crude product was recrystallised from ethanol and the pure product was characterised by ^{1}H-NMR.

^{1}H-NMR ($CDCl_3$): δ_H 8.52–8.50 (2H, CH aromatic protons), 8.13–8.11 (2H, CH aromatic protons), 7.69–7.65 (2H, CH aromatic protons), 4.18–4.14 (2H, CH_2 protons), 2.83–2.80 (2H, CH_2 protons), 2.40–2.36 (2H, CH_2 protons), 1.90–1.83 (2H, CH_2 protons), 1.79–1.71 (2H, CH_2 protons), 1.48 (2H, CH_2 protons), 1.2 (H, CH protons) and 1.00–0.80 (2H, CH_2 protons) ppm.

Synthesis of BNIPPiEth

BNIPPiEth (0.1 g) was dissolved in DCM (20 mL). Then, conc. HCl (1.5 mL) was added dropwise and the solution stirred at room temperature for 60 minutes, which resulted in the formation of a pale, blue precipitate. The latter was filtered and washed with ether (50 mL) and afterwards with ethanol (50 mL). The product was left under negative pressure in a vacuum oven at 45 °C for 60 minutes (29.5% yield).

^{1}H-NMR ($CDCl_3$): δ_H 8.42–8.38 (2H, CH aromatic protons), 7.82–7.78 (2H, CH aromatic protons), 4.05–4.01 (2H, CH_2 protons), 2.7 (2H, CH_2 protons), 2.44–2.43 (2H, CH_2 protons), 2.05 (2H, CH_2 protons), 1.70–1.67 (2H, CH_2 protons), 1.35–1.32 (H, CH protons) and 1.090 (2H, CH_2 protons) ppm.

^{13}C-NMR ($CDCl_3$): δ_H 164.10 (C═O), 134.81 (CH aromatic), 131.76 (C aromatic), 131.18 (CH aromatic), 127.92 (C aromatic), 127.68 (CH aromatic), 122.59 (C aromatic), 55.40 (CH_2), 52.27 (CH_2), 37.79 (CH), 29.43 (CH_2) 23.04 (CH_2) and 22.54 (CH_2) ppm.

Mass spectrum (HRMS), m/z = 671.5372 $(M + H)^+$ $C_{42}H_{46}N_4O_4$ requires 671.3592 $(M + H)^+$.

Synthesis of *N*-(3-hydroxypropyl)naphthalimide

1,8-Naphthalic anhydride (0.050 mol, 10 g) was dissolved in dimethylformamide (DMF) (140 mL). Once the 1,8-naphthalic anhydride was totally dissolved, 3-amino-1-propanol (0.050 mol, 3.75 g) and 1,8-diazabicylo[5.4.0]undec-7-ene (DBU) (13 mL) were added. The reaction was left to stir for 5 hours at 85 °C. Reaction completion was monitored with TLC and once completed; the solution was poured into icy water (200 mL) while stirring with a glass rod to form a precipitate. The precipitate was filtered and washed with water. The pure product was characterised using ^{1}H-NMR. Yield was calculated as: 53.9%.

^{1}H-NMR ($CDCl_3$): δ_H 8.66–8.63 (2H, aromatic H, doublet, J = 7.2 Hz), 8.29–8.25 (2H, aromatic H, doublet, J = 8.4 Hz), 7.83–7.78 (2H, aromatic H, doublet, J = 8.0 Hz), 4.41–4.38 (3H, triplet, J = 5.6 Hz), 3.64–3.59 (2H, CH_2, multiplet) 3.23 (OH, singlet) and 2.06–2.00 (2H, CH_2 multiplet) ppm.

Synthesis of toluenesulfonyloxypropylnaphthalimide

N-(3-Hydropropyl)naphthalimide (0.0196 mol, 5.0 g) was dissolved in anhydrous pyridine (70 mL), whilst stirring on ice. Once the *N*-(3-hydroxypropyl)naphthalimide was completely dissolved, *p*-toluenesulfonyl chloride (Ts-Cl) (0.0394 mol, 7.51 g, 2.01 excess) was slowly added to the reaction. The reaction was left at 4 °C overnight. The reaction was monitored using TLC and once it was complete, the solution was poured into icy water (200 mL) to form a precipitate which was filtered and washed thoroughly with water. The crude product was recrystallised from ethanol (68.2% yield).

^{1}H-NMR ($CDCl_3$): δ_H 8.59–8.57 (2H, aromatic H, doublet, 8.2 Hz), 8.25–8.23 (2H, aromatic H, triplet, 7.2 Hz), 7.81–7.76 (2H, multiplet), 7.30 (2H, aromatic H, doublet, 1.2 Hz), 4.27–4.20 (2H, CH_2, multiplet), 2.44 (3H, CH_3, singlet) and 2.19–2.12 (2H, CH_2, multiplet) ppm.

Synthesis of N^4,N^4-dimesityl-dicyclohexylmethane

4,4′-Methylenebis(cyclohexylamine) (4.75×10^{-3} mol, 1.0 g) was dissolved in anhydrous pyridine (10 mL) and left to stir for 15 minutes. 2-Mesitylenesulfonyl chloride (Mts-Cl) (9.56 × 10–3 mol; 2.1 g) was added. The reaction was left to stir overnight at room temperature and TLC confirmed completion of

reaction. The solution was poured into icy water (150 mL) with the formation of a precipitate. The latter was filtered by vacuum filtration, left to dry in a vacuum oven set at 45 °C for 24 hours (43.3% yield).

^{1}H-NMR ($CDCl_3$): δ_H 7.30 (NH), 6.97 (4H, CH aromatic protons), 2.99 (4H, CH protons), 2.67–2.66 (6H, CH_3-Mts protons) and 1.73–1.49 (CH_2 and cyclohexane protons) ppm.

Synthesis of protected bisnaphthalimido-dimesityl-dicyclohexylmethane

N^4,N^4-Dimesityl-dicyclohexylmethane (6.968×10^{-4} mol, 0.4 g) and toluenesulfonyloxypropylnaphthalimide (1.400×10^{-3} mol, 2.01 excess) were dissolved in DMF (8 mL). Afterwards, excess of caesium carbonate (1.13 g, 3.5×10^{-3} mol, 2.5 g excess) was added slowly. The reaction was left to stir for 48 hours at 60 °C. After TLC confirmed the reaction was complete, the solution was poured into icy water (150 mL) to form a precipitate. After vacuum filtration and several washes with water, the product was left to dry under negative filtration in a vacuum oven at 45 °C for 3 hours (92.2% yield). The product was recrystallised from ethanol and characterised by NMR.

^{1}H-NMR ($CDCl_3$): δ_H 8.50–8.47 (2H, aromatic H), 8.18–8.15 (2H, aromatic H), 7.72–7.67 (2H, aromatic H), 6.87 (2H, CH-Mts H), 6.55–6.53 (2H, CH-Mts H), 3.94–3.92 (2H, CH_2), 3.12–3.10 (2H, CH_2), 2.87–2.80 (2H, CH_2), 2.35–2.32 (3H, CH_3), 2.05–2.04 (3H, CH_3), 1.61–1.58 (H, CH), 1.61 (2H, CH_2) 1.49–1.37 (2H, CH) and 1.04 (2H, CH_2) ppm.

^{13}C-NMR ($CDCl_3$): δ_H 163.87–162.76 (C═O), 134.36 (C aromatic), 131.40–130.74 (C aromatic), 127.75 (C aromatic), 35.75 (CH_2), 30.41 (CH_2), 21.97 (CH_3) and 20.32 (CH_3) ppm.

Synthesis of bisnaphthalimidopropyl-diamino-dicyclohexylmethane dihydro-bromide salt

Bisnaphthalimido-dimesityl-dicyclohexylmethane (3.813×10^{-4} mol, 0.4 g) was dissolved in dichloromethane (DCM) (8 mL). Afterwards, hydrobromic acid/glacial acetic acid (HBr/CH_3CO_2H) (1 mL) was added drop wise. The reaction was stirred overnight at room temperature. TLC was used to confirm that the reaction was complete. The precipitate formed, was filtered by vacuum filtration and washed with DCM (15 mL) and ether (5 mL). The final product was dried under negative pressure in a vacuum oven set at 45 °C for 3 hours (37.5% yield).

^{1}H-NMR ($CDCl_3$): δ_H 8.32–8.25 (2H, aromatic Hs), 7.73–7.65 (2H, aromatic Hs), 3.70–3.64 (2H, CH_2 protons), 3.13 (2H, CH_2 protons), 2.90–2.30 (3H, CH_3 protons), 2.09–2.02 (3H, CH_3 protons), 1.83–1.80 (H, CH proton), 1.43–1.33 (2H, CH_2 protons) ppm.

^{13}C-NMR($CDCl_3$): δ 163.87–162.76 (C═O), 134.36 (C aromatic), 131.40–130.74 (C aromatic), 127.75 (C aromatic), 35.75 (CH_2) and 30.41 (CH_2) ppm.

Mass spectrum (HRMS), m/z = 685.3764 $(M + H)^+$ $C_{43}H_{48}N_4O_4$ requires 685.3748 $(M + H)^+$.

Synthesis of *trans*,*trans*-N^4,N^4-dimesityl-dicyclohexylmethane

trans,*trans*-4,4′-Methylenebis(cyclohexylamine) (2.38×10^{-4} mol, 0.05 g) was added in anhydrous pyridine (1.5 mL) and left to stir for 15 minutes with warming. After dissolution, 2-mesitylenesulfonyl chloride (Mts) (4.76×10^{-4} mol; 0.10 g) was added. The reaction was left to stir overnight at room temperature and TLC confirmed reaction completion. The solution was poured into icy water (10 mL) and stirred with a glass rod until the formation of a precipitate. The suspension was centrifuged and was washed 3 times with distilled water and the precipitate was left to dry under negative pressure in a vacuum oven set at 45 °C for overnight (21% yield). The product was afterwards characterised by 1H-NMR.

^{1}H-NMR ($CDCl_3$): δ_H 7.31 (NH), 6.98 (4H, CH aromatic protons), 3.87 (4H, CH protons), 2.67 (6H, CH_3-Mts protons), 2.33 (3H, CH_3-Mts protons), 1.84–1.82 (CH_2-cyclohexane ring), 1.65–1.62 (CH_2-cyclohexane ring), 1.16–1.10 (CH-cyclohexane ring) and 0.99–0.95 (CH_2 cyclohexane protons) ppm.

Synthesis of protected *trans*,*trans*-bisnaphthalimidopropyl-dimesityl-dicyclohexylmethane

trans,*trans*-N^4,N^4-Dimesityl-dicyclohexylmethane (6.44×10^{-5} mol, 0.037 g) and toluenesulfonyloxypropylnaphthalimide (1.29×10^{-4} mol, 0.053 g, 2.01 excess) were dissolved in DMF (1 mL). Afterwards, excess of caesium carbonate ($n = 3.07 \times 10^{-4}$ mol, 0.1 g, 5.0 excess) was added slowly. The reaction was left to stir for 48 hours at 60 °C. After TLC confirmed the reaction was complete, the solution was poured into icy water (10 mL) to form a precipitate. The suspension was centrifuged and was washed twice with distilled water. The product was left to dry under negative pressure in a vacuum oven at 45 °C for 24 hours. The crude product (59 mg, 88% yield) was purified using column chromatography and the final product (25 mg, 37% yield) was characterised by ^{1}H-NMR.

^{1}H-NMR ($CDCl_3$): δ_H 8.65–8.59 (2H, CH aromatic protons), 8.30–8.25 (2H, CH aromatic protons), 7.84–7.78 (2H, CH aromatic protons), 6.65 (4H, CH-Mts protons), 4.41–4.38 (2H, CH_2 protons), 4.06–4.04 (2H, CH_2 protons), 3.71–3.68 (2H, CH_2 protons), 2.68 (3H, CH_3 protons), 2.46–2.44 (3H, CH_3 protons), 2.34 (H, CH protons), 2.16–2.15 (2H, CH_2 protons) 1.84 (2H, CH protons) and 1.73–1.71 (2H, CH_2 protons) ppm.

^{13}C-NMR ($CDCl_3$): δ_H 141.93 (C═O), 138.76 (C aromatic), 135.17 (C aromatic), 131.95 (C aromatic), 43.72 (CH_2), 33.93–31.99 (CH_2), 23.02 (CH_3) and 20.97 (CH_3) ppm.

Synthesis of *trans*,*trans*-bisnaphthalimidopropyl-diamino-dicyclohexylmethane dihydro-bromide salt

trans,*trans*-Bisnaphthalimido-dimesityl-dicyclohexylmethane (2.38×10^{-5} mol, 25 mg) was dissolved in dichloromethane (DCM) (1.0 mL). Afterwards, hydrobromic acid/glacial acetic acid (HBr/CH_3CO_2H) (0.2 mL) was added slowly. The reaction was stirred overnight at room temperature. TLC was used to confirm that the reaction was complete. The suspension formed was transferred to Eppendorf tubes and centrifuged, was with DCM (1.0 mL) and ether (1.0 mL). The final product

was dried under negative pressure in a vacuum oven set at 45 °C for 3 hours to give the product as a white solid (8.3 mg, 41% yield).

^{1}H-NMR ($CDCl_3$): δ 8.53–8.49 (2H, CH aromatic protons), 4.16–4.12 (2H, CH aromatic protons), 3.42 (2H, CH aromatic protons) 3.04 (2H, CH_2 protons), 2.94 (2H, CH_2 protons), 2.51–2.49 (3H, CH_3 protons), 2.09–1.99 (3H, CH_3 protons), 1.75–1.72 (H, CH proton), 1.31–1.28 (2H, CH_2 protons) ppm.

^{13}C-NMR($CDCl_3$): δ 164.26 (C═O), 131.82–131.23 (C aromatic), 127.99–127.75 (C aromatic), 122.66 (C aromatic), 42.45 (CH_2) and 40.61–37.61 (CH_2) ppm.

Mass spectrum (HRMS), m/z = 685.3732 $(M + H)^+$ $C_{43}H_{48}N_4O_4$ requires 685.3748 $(M + H)^+$.

Ethidium bromide (EtBr) fluorescence displacement studies

BNIPDaCHM, BNIPPiProp, BNIPPiEth and *trans*,*trans*-BNIPDaCHM working solutions (100 μM) were prepared from stock solutions (10 mM in 50% DMSO/H_20) and were further diluted to a final concentration of 50 μM in 0.01 M saline sodium citrate (SSC) buffer. *Calf Thymus* DNA (0.5 g) was dissolved in 0.01 M SSC buffer (100 mL). EtBr solution (200 μM) was prepared by dissolving 3.94 mg of EtBr in distilled water (50 mL) and was further diluted in 0.01 SSC buffer to give the final concentration of 20 μM. Test solutions were prepared by adding varying volumes of SSC buffer, *Calf Thymus* DNA solution, EtBr solution and BNIP derivative solution. The final solutions were thoroughly mixed and analysed at 510 nm (excitation) and 520 nm (emission) using a Shimadzu RF-5301 spectrophotometer. The IC_{50} values were determined as the concentration (μM) required to decrease the fluorescence of DNA bound EtBr by 50%.

UV binding studies

BNIPDaCHM, BNIPPiProp, BNIPPiEth and BNIPDaCHM working solutions (100 μM) were prepared from their stock solutions (10 mM) as before, and were further diluted to 20 μM final concentration in 0.01 M SSC buffer. *Calf Thymus* DNA and 0.01 SSC buffer were prepared as described before (EtBr Fluorescence Displacement studies). Test solutions were prepared by adding *Calf Thymus* DNA solution (1 mL) in a quartz cuvette and BNIP derivative solution (100 μL) was added. The final solutions were thoroughly mixed and analysed at 260 nm using an Agilent 8453 UV-visible spectrophotometer. The values of apparent binding constants (K) were calculated from the intercept and slope by plotting $A_0/(A - A_0)$ against the BNIP derivative concentrations, where A_0 and A correspond to the absorbance values in absence and presence of a compound.

Cell culture maintenance

MDA-MB-231 (ECACC, Public Health England, UK, 92020424) and SKBR-3 (ATCC, HTB-30) cells were maintained in Roswell Park Memorial Institute 1640 medium (RPMI-1640) (containing GlutaMAX-1 with 25 mM HEPES), supplemented with 10% (v/v) Fetal Bovine Serum (FBS) and 1% penicillin/streptomycin (10 000 μg mL^{-1}). Cells were grown at 37 °C (5% CO_2).

Cytotoxicity

Colourimetric 3-(4,5-dimethylthiazol-2-yl)-2,5-diphenyltetrazodium bromide (MTT) assay was performed to access the growth/inhibitory effects of each BNIP compound. MDA-MB-231 and SKBR-3 cells (7.5×10^3 cells per 100 μL) were treated with different concentrations (0–10 μM) of BNIP derivatives. After 24 hours treatment, sterile-filtered MTT solution (1 mg mL^{-1}) was added to each well. After 4 hours incubation at 37 °C, the MTT solution was removed and formazan crystals solubilised in DMSO. The plates were shaken for 20 minutes at room temperature and absorbance measured at 560 nm (Synergy/HT, BIOTEK, UK). For each compound, three independent experiments were carried out and each treatment consisted of six replicates per plate. Curves were used to represent the percentage growth inhibition of MDA-MB-231 and SKBR-3 cells treated with BNIP derivatives, compared to DMSO/H_2O control that represented 100% cell viability. IC_{50} values were defined as the drug concentration that reduces absorbance compared to control values by 50%.

Cell cycle analysis

MDA-MB-231 and SKBR-3 cells (1×10^6 cells per T75 flask) cells were washed with PBS and serum free medium added in the flasks in order to achieve cell synchrony. The cells were incubated in serum free medium for 24 hours. BNIP derivatives (IC_{25} concentrations) were added and incubated for 24 hours, at 37 °C. After 24 hours treatment, the medium was removed and collected. The cells were washed twice with PBS. Both washes were collected and the cells trypsinised, mixed with the collected washes and centrifuged at 2500 rpm for 5 minutes at 4 °C. The supernatant of each sample was discarded, the pellet was resuspended in PBS (1 mL) and centrifuged at 2500 rpm for 5 minutes at 4 °C, the supernatant was discarded and the pellet resuspended in PBS (100 μL). Then, 70% (v/v) ice-cold ethanol (900 μL) was added and samples incubated for 2 hours at −20 °C. The cells were centrifuged at 5000 rpm for 5 minutes at 4 °C, the supernatant was discarded and the pellet resuspended in PBS (1 mL), followed by re-centrifugation at 5000 rpm for 5 minutes at 4 °C. The supernatant was discarded once more and the pellet resuspended in PBS (500 μL) and DNA extraction buffer (0.2 M Na_2HPO_4, 4 mM citric acid, pH 7.8, 500 μL) and incubated for 5 minutes at room temperature. The extracts were centrifuged at 5000 rpm for 5 minutes at 4 °C, the supernatant was removed and the pellets were resuspended in DNA staining solution (0.2 mg mL^{-1} Ribonuclease A (DNAse-free) and 20 μg mL^{-1} propidium iodide (PI) in PBS). The samples were incubated for 30 minutes at 4 °C in the dark and PI nuclei were examined by flow cytometry (EXPO32 ADC XL 4 color, Beckman Coulter, UK). For cell cycle analysis, EXPO32 ADC analysis software (Beckman Coulter, UK) was used to record and analyse 10 000 single events. The percentage of cells with DNA content in sub-G_1, G_1, S and G_2/M phases was calculated from histograms of linear FL-2 plots (575 nm) in the gated region.

Statistics

Three independent experiments were conducted and each experiment was comprised of at least two internal replicates. Data are presented as mean ± SD or mean ± SEM. Statistical analysis was performed by using an unpaired Student's *t*-test. Statistically significant data were detailed when $P < 0.05$).

Acknowledgements

The authors acknowledge the Robert Gordon University for financial support, and the EPSRC National Mass Spectrometry Service Centre at Swansea University, Swansea for mass spectral analysis.

References

1 R. Siegel, D. Naishadham and A. Jemal, *CA-Cancer J. Clin.*, 2013, **63**, 11–30.
2 A. Redmond, C. Byrne, F. Bane, G. Brown, P. Tibbitts, K. O'Brien, A. Hill, J. Carroll and L. Young, *Oncogene*, 2015, **34**, 3871–3880.
3 A. Becorpi, G. Sisti, F. Sorbi, E. Malosso and S. Guaschino, *Clin. Cases Miner. Bone Metab.*, 2014, **11**, 110–113.
4 B. Lehmann and J. Pietenpol, *J. Pathol.*, 2013, **232**, 142–150.
5 S. F. Chen, D. L. Behrens, C. H. Behrens, P. M. Czerniak, D. L. Dexter, B. L. Dusak, J. R. Fredericks, K. C. Gale, J. L. Gross, J. B. Jiang, M. Kirshenbau, R. J. McRipley, L. M. Papp, A. D. Patten, F. W. Perrella, S. P. Seitz, M. P. Stafford, J. H. Sun, T. Sun, M. A. Wuonola and D. D. Von Hoff, *Anti-Cancer Drugs*, 1993, **4**, 4.
6 M. F. Braña, M. Cacho, A. Gradillas, B. de Pascual-Teresa and A. Ramos, *Curr. Pharm. Des.*, 2001, **7**, 1745–1780.
7 V. Pavlov, P. Kong Thoo Lin and V. Rodilla, *Chem.-Biol. Interact.*, 2001, **137**, 15–24.
8 M. Llombart, A. Poveda, E. Forner, C. Fernández Martos, C. Gaspar, M. Muñoz, T. Olmos, A. Ruiz, V. Soriano, A. Benavides, M. Martin, E. Schlick and V. Guillem, *Invest. New Drugs*, 1992, **10**, 177–181.
9 M. F. Braña and A. Ramos, *Curr. Med. Chem.: Anti-Cancer Agents*, 2001, **1**, 237–255.
10 P. Kong Thoo Lin and V. Pavlov, *Bioorg. Med. Chem. Lett.*, 2000, **10**, 1609–1612.
11 V. Pavlov, P. Kong Thoo Lin and V. Rodilla, *Chem.-Biol. Interact.*, 2001, **137**, 15–24.
12 J. Oliveira, L. Ralton, J. Tavares, A. Codeiro-Da-Silva, C. S. Bestwick, A. MacPherson and P. Kong Thoo Lin, *Bioorg. Med. Chem.*, 2007, **15**, 541–545.
13 G. A. Barron, G. Bermano, A. Gordon and P. Kong Thoo Lin, *Eur. J. Med. Chem.*, 2010, **45**, 1430–1437.
14 R. Lima, G. A. Barron, J. Grabowska, G. Bermano, S. Kaur, N. Roy, M. Vasconcelos and P. Kong Thoo Lin, *Anti-Cancer Agents Med. Chem.*, 2013, **3**, 414–421.
15 A. Birch, P. Kenny, I. Simpson and P. Whittamore, *Bioorg. Med. Chem. Lett.*, 2009, **19**, 850–853.
16 P. Gleeson, G. Bravi, S. Modi and D. Lowe, *Bioorg. Med. Chem.*, 2009, **17**, 5906–5919.
17 P. Hajduk and D. Sauer, *J. Med. Chem.*, 2008, **51**, 553–564.
18 S. Scultes, C. de Graaf, H. Berger, M. Mayer, A. Steffen, E. Haaksma, I. de Esch, R. Leurs and O. Kramer, *MedChemComm*, 2012, **3**, 584–591.
19 P. Scaria and R. J. Shafer, *J. Biol. Chem.*, 1991, **266**, 5417–5423.
20 W. Chen, J. Turro and D. Tomalia, *Langmuir*, 2000, **16**, 15–19.
21 P. Liu, B. Wu, J. Liu, Y. Dai, Y. Wang and K. Wang, *Inorg. Chem.*, 2016, **55**, 1412–1422.
22 M. F. Braña, M. Cacho, A. Ramos, M. Dominguez, J. Pozuelo, C. Abradelo, M. Rey-Stolle, M. Yuste, C. Carrasco and C. Bailly, *Org. Biomol. Chem.*, 2003, **1**, 648–654.
23 T. Zhi-Yong, L. Jing-Hua, L. Qian, Z. Feng-Lei, Z. Zhong-Hua and W. Chao-Jie, *Molecules*, 2014, **19**, 7646–7668.
24 M. F. Braña, M. Cacho, M. Garcia, B. de Pascual-Teresa, A. Ramos, M. Dominguez, J. Pozuelo, C. Abradelo, M. Rey-Stolle, M. Yuste, M. Banez-Coronel and J. Lacal, *J. Med. Chem.*, 2004, **47**, 1391–1399.
25 C. Bailly, C. Carrasco, A. Joubert, C. Bal, N. Wattez, M. Hildebrand, A. Lansiaux, P. Colson, C. Houssier, M. Cacho, A. Ramos and M. F. Braña, *Biochemistry*, 2003, **42**, 4136–4150.
26 T. Mosmann, *J. Immunol. Methods*, 1983, **16**, 55–63.
27 P. Kenny, G. Lee, C. Myers, R. Neve, J. Semeiks, P. Spellman, K. Lorenz, E. Lee, M. Barcellos-Hoff, O. Petersen, J. Greay and M. Bissell, *Mol. Oncol.*, 2007, **1**, 84–96.
28 C. M. Henry, E. Hollville and S. J. Martin, *Methods*, 2013, **61**(2), 90–97.
29 G. A. Barron, M. Goua, I. Kuraoka, G. Bermano, S. Iwai and P. Kong Thoo Lin, *Chem.-Biol. Interact.*, 2015, **242**, 307–315.
30 C. Chu, J. Xu, D. Cheng, X. Li, S. Tong, J. Yan and Q. Li, *Mol.*, 2014, **19**(4), 4941–4955.
31 R. Doddapaneni, K. Patel and M. Singh, *Cancer Res.*, 2015, **75**(15), 2619.
32 M. Kang, J. N. Ho, H. R. Kook, S. Lee, J. J. Oh, S. K. Hong, S. E. Lee and S. S. Byun, *Oncol. Rep.*, 2016, **35**(3), 1463–1472.
33 J. U. Hong, H. J. Chung, S. Y. Bae, T. N. Trung, K. Bae and S. K. Lee, *J. Cancer Prev.*, 2004, **19**(4), 273–278.

Oral Presentation at ICBMB 2016, International Conference on Biochemistry and Molecular Biology,
Venice, Italy, 27-29 April 2016

The influence of novel Bisnaphthalimidopropyl derivatives (BNIPs) on proliferation, DNA damage, cell cycle progression and apoptosis in triple negative breast cancer cells *in vitro*.

M. Kopsida[*1], G. A. Barron[1, 2], G. Bermano[2], P. Kong Thoo Lin[1] and M. Goua[1]

[1]*School of Pharmacy and Life Sciences, Robert Gordon University, Garthdee Road, Aberdeen, AB10 7GJ, Scotland, UK*
[2]*Centre for Obesity Research and Education (CORE), Faculty of Health and Social Care, Robert Gordon University, Garthdee Road, Aberdeen, AB10 7GJ, Scotland, UK*

Bisnaphthalimidopropyl (BNIP) derivatives are a family of DNA intercalating compounds that exert anti-cancer activity against a variety of cancer cell lines *in vitro* [1,2]. Variations in the linker sequence have been found to improve the aqueous solubility and cytotoxic activity of BNIP derivatives, thus enhancing their potential application as anticancer drugs [3,4]. The aim of this study was to investigate the effect of three novel BNIP derivatives against triple negative human breast carcinoma cells and their mode of action, with regards to cell death. Bisnaphthalimidopropyl-piperidylpropane (BNIPPiProp), bisnaphthalimidopropyl- ethylenedipiperidine dihydrobromide (BNIPPiEth) and (*trans(trans)*)-4,4'-methylenebis-cyclohexylamine *(trans,trans*-bisnaphthalimidopropyl diaminodicyclohexylmethane or *trans,trans*-BNIPDaCHM) were synthesised and characterised for the first time. The chemical structure of the BNIP derivatives was confirmed by Thin Layer Chromatography (TLC), Nuclear Magnetic Resonance (NMR), Mass Spectrometry (MS) while their DNA binding properties were determined by UV and fluorescence spectroscopy. Cytotoxicity of BNIP derivatives was assessed against human breast cancer MDA-MB-231 cells by MTT assay [5], resulting in IC_{50} values between 1.4-3.3 μM after 24 hours treatment. In addition, using the single cell gel electrophoresis (COMET) assay [6], it was found that BNIPPiProp, BNIPPiEth and *trans,trans*-BNIPDaCHM, showed significant DNA damage to treated MDA-MB-231 cells after 24 hours treatment. Intracellular reactive oxygen species (ROS) accumulation was studied by flow cytometry, showing that the generation of ROS levels was induced after 4, 8 and 12 hours treatment with BNIP derivatives. After cell synchronisation, cell cycle distribution was conducted

using propidium iodide (PI) staining of MDA-MB-231 cells and indicated that *trans,trans*-BNIPDaCHM induces sub-G1 cell cycle arrest, which has been previously associated with apoptotic cell death [7]. In particular, an increase of 139% and 142% in sub-G1 cell population after 24 hours treatment was observed with 1 μM *trans,trans*-BNIPDaCHM and 6 μM Camptothecin (positive control for sub-G1 arrest), respectively, compared to untreated cells. The above findings indicate that BNIPPiProp, BNIPPiEth and *trans,trans*-BNIPDaCHM exhibit dose-dependent cytotoxic effects *in vitro* (*trans,trans*-BNIPDaCHM>BNIPPiEth>BNIPPiProp), induce DNA damage and enhance ROS accumulation. Further investigation to confirm apoptotic cell death is on-going and this could define the potential use of BNIP derivatives as anti-cancer agents in the future.

[1]Brana, M.F., Cacho, M., Gradillas, A., de Pascual-Teresa, B. and Ramos, A., Curr. Pharm. Des., 2001, 7, 1745-1780.

[2]Brana, M.F and Ramos, A., Curr. Med. Chem. Anti-Canc. Agents, 2001, 1, 237-255.

[3]Pavlov, V., Kong Thoo Lin, P. and Rodilla, V., Chem Biol Interact, 2001, 137, 15-24.

[4]Barron, G., Bermano, G., Gordon, A. and Kong Thoo Lin, P., Eur. J. Med. Chem., 2010, 45 (4), 1430-1437.

[5]Mosmann, T., J. Immunol. Methods, 1983, 16;65 (1-2), 55-63.

[6]Barron, G., Goua, M., Kuraoka, I., Bermano, G., Iwai, S., Kong Thoo Lin, P., Chem Biol Interact, 2015, 307-315.

[7]Pucci, B., Kasten, M., Giordano, A., Neoplasia, 2000, 291-299.

Poster at the RGU FHSC Graduate School Symposium 2016 (First Prize Winner)

Aberdeen, United Kingdom, 26 May 2016

Effect of Novel Bisnaphthalimidopropyl derivatives (BNIPs) designed for targeting DNA in a human breast cancer cell system.

M. Kopsida*1, G. A. Barron1, 2, G. Bermano2, P. Kong Thoo Lin1 and M. Goua1

1School of Pharmacy and Life Sciences, Robert Gordon University, Garthdee Road, Aberdeen, AB10 7GJ, Scotland, UK

2Centre for Obesity Research and Education (CORE), Faculty of Health and Social Care, Robert Gordon University, Garthdee Road, Aberdeen, AB10 7GJ, Scotland, UK

Bisnaphthalimidopropyl (BNIP) derivatives are a family of DNA intercalating compounds that exert anti-cancer activity against a variety of cancer cell lines in vitro 1,2. Variations in the linker sequence have been found to improve the aqueous solubility and cytotoxic activity of BNIP derivatives, thus enhancing their potential application as anticancer drugs 3,4. The aim of this study was to investigate the effect of three novel BNIP derivatives against triple negative human breast carcinoma cells and their mode of action, with regards to cell death. Bisnaphthalimidopropyl-piperidylpropane (BNIPPiProp), bisnaphthalimidopropyl- ethylenedipiperidine dihydrobromide (BNIPPiEth) and (trans(trans))-4,4'-methylenebis-cyclohexylamine (trans,trans-bisnaphthalimidopropyl diaminodicyclohexylmethane or trans,trans-BNIPDaCHM) were synthesised and characterised for the first time. The chemical structure of the BNIP derivatives was confirmed by Thin Layer Chromatography (TLC), Nuclear Magnetic Resonance (NMR), Mass Spectrometry (MS) while their DNA binding properties were determined by UV and fluorescence spectroscopy. Cytotoxicity of BNIP derivatives was assessed against human breast cancer MDA-MB-231 cells by MTT assay5, resulting in IC50 values between 1.4-3.3 μM after 24 hours treatment. In addition, using the single cell gel electrophoresis (COMET) assay6, it was found that BNIPPiProp, BNIPPiEth and trans,trans-BNIPDaCHM, showed significant DNA damage to treated MDA-MB-231 cells after 24 hours treatment. Intracellular reactive oxygen species (ROS) accumulation was studied by flow cytometry, showing that the generation of ROS levels was induced after 4, 8 and 12 hours treatment with BNIP derivatives. After cell synchronisation, cell cycle distribution was conducted

using propidium iodide (PI) staining of MDA-MB-231 cells and indicated that trans,trans-BNIPDaCHM induces sub-G1 cell cycle arrest, which has been previously associated with apoptotic cell death7. In particular, an increase of 139% and 142% in sub-G1 cell population after 24 hours treatment was observed with 1 μM trans,trans-BNIPDaCHM and 6 μM Camptothecin (positive control for sub-G1 arrest), respectively, compared to untreated cells. The above findings indicate that BNIPPiProp, BNIPPiEth and *trans,trans*-BNIPDaCHM exhibit dose-dependent cytotoxic effects in vitro (trans,trans-BNIPDaCHM>BNIPPiEth>BNIPPiProp), induce DNA damage and enhance ROS accumulation. Further investigation to confirm apoptotic cell death is on-going and this could define the potential use of BNIP derivatives as anti-cancer agents in the future.

[1]Brana, M.F., Cacho, M., Gradillas, A., de Pascual-Teresa, B. and Ramos, A., Curr. Pharm. Des., 2001, 7, 1745-1780

[2]Brana, M.F and Ramos, A., Curr. Med. Chem. Anti-Canc. Agents, 2001, 1, 237-255

[3]Pavlov, V., Kong Thoo Lin, P. and Rodilla, V., Chem Biol Interact, 2001, 137, 15-24

[4]Barron, G., Bermano, G., Gordon, A. and Kong Thoo Lin, P., Eur. J. Med. Chem., 2010, 45 (4), 1430-1437

[5]Mosmann, T., J. Immunol. Methods, 1983, 16;65 (1-2), 55-63

[6]Barron, G., Goua, M., Kuraoka, I., Bermano, G., Iwai, S., Kong Thoo Lin, P., Chem Biol Interact, 2015, 307-315

[7]Pucci, B., Kasten, M., Giordano, A., Neoplasia, 2000, 291-299

Effect of Novel Bisnaphthalimidopropyl derivatives (BNIPs) designed for targeting DNA in a human breast cancer cell system

Maria Kopsida[a], Gemma A. Barron[a,b], Giovanna Bermano[b], Paul Kong Thoo Lin[a] and Marie Goua[a]

[a]School of Pharmacy and Life Sciences, Robert Gordon University, Garthdee Road, Aberdeen, AB10 7GJ, Scotland, UK

[b]Centre of Obesity Research and Education (CORE), Faculty of Health and Social Care, Robert Gordon University, Garthdee Road, Aberdeen, AB10 7GJ, Scotland, UK

Introduction

Breast cancer is the most commonly occurring cancer in women, with incidence rates approaching 1.38 million cases per year worldwide[1]. Bisnaphthalimidopropyl (BNIP) derivatives are a family of compounds that were initially designed and synthesised in our laboratories in 2000 and were found to exert anti-cancer activities[2,3]. According to previous studies[4,5], variations in the linker sequence seem to improve the aqueous solubility, DNA binding and cytotoxic activity of BNIP derivatives, enhancing their potential application as anticancer drugs[5].

Aims

- Synthesis and characterisation of three novel BNIP derivatives: BNIPPiProp, BNIPPiEth-HBr and trans,trans-BNIPDaCHM (Figure 1) and compared with BNIPDaCHM (parental compound).
- Investigation of their DNA binding affinities via intercalation.
- Determination of in vitro cytotoxicity of BNIP derivatives against MDA-MB-231 cells.
- Cell cycle analysis after 24 hours treatment with BNIPs.

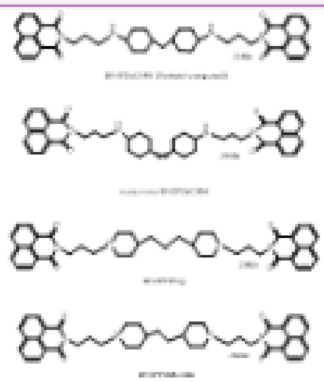

Figure 1: Structures of bisnaphthalimidopropyl diaminodicyclohexylmethane (BNIPDaCHM) (Parental compound), trans,trans-bisnaphthalimidopropyl diaminodicyclohexylmethane (trans,trans-BNIPDaCHM), bisnaphthalimidopropylpiperidylpropane (BNIPPiProp) and bisnaphthalimidopropylethylenedipiperidine dihydrobromide (BNIPPiEth-HBr).

Methods

- Thermal melting points were defined by using the standard operating procedure of Griffin Melting Point Apparatus (Fisher Scientific, UK).
- Fluorescence-binding studies were performed in plastic cuvettes (1 cm path length) (Hellma Analytics, UK) using a Shimadzu RF-5301 spectrophotometer (Japan).
- UV binding studies were carried out using an Agilent 8453 UV-visible Spectroscopy System (GenTech, USA) and a Diode array instrument. The samples were loaded in quartz glass flow cells (10 mm path length) (Hellma Analytics, UK) and measured at 260 nm.
- Cytotoxicity was determined by using the 3-(4, 5-Dimethylthiazol-2-yl)-2, 5-diphenyltetrazolium bromide (MTT) assay and absorbance was measured at 560 nm on a 96-well plate reader (Synergy/HT, BIOTEK).
- Propidium iodide stained nuclei were examined by flow cytometry on an Coulter Epics XL-MCL flow cytometer (Beckman Coulter, UK). For cells cycle analysis, EXPO-32 software (Applied Cytometry Systems, Sheffield, UK) was used to record and analyse 10,000 single events.

Results

1. Determination of melting points

BNIP derivatives	Melting Point (°C)
BNIPDaCHM	105-110
BNIPPiProp	160-170
BNIPPiEth	125-130
trans,trans-BNIPDaCHM	120-125

Table 1. Melting points of BNIPDaCHM, BNIPPiProp, BNIPPiEth and trans,trans-BNIPDaCHM (use of variable heat 7). A compatible capillary (10 cm length, 1.0 mm internal diameter and 0.2 mm wall thickness) for testing each compound was used.

2. EtBr displacement from *Calf Thymus* DNA

BNIP derivatives	C_{50} value (µM) Mean ± SD
Calf Thymus DNA alone	-
BNIPDaCHM	2.3±0.1
BNIPPiProp	3.9±0.3*
BNIPPiEth	1.1±0.2*
trans,trans-BNIPDaCHM	5.6±0.2**

Table 2. The effect of BNIP derivatives on EtBr displacement from *Calf Thymus* DNA. Samples were analysed at 510 nm (excitation) 600 nm (emission) using a Shimadzu RF-5301 spectrophotometer. C_{50} values correspond to concentrations that a derivative generates a 50% decrease on fluorescence intensity of bound EtBr. Data presented as mean ±SD (n=3). **P<0.01, *P<0.05, compared to BNIPDaCHM.

3. UV binding studies

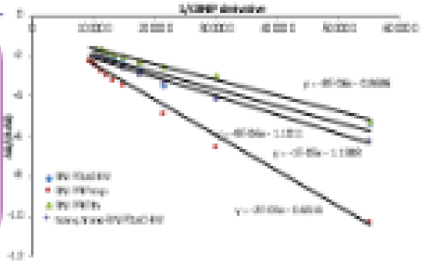

Figure 2. Plot of A0/(A-A0) versus 1/Concentration of the interaction between BNIP derivatives and *Calf Thymus* DNA. Samples were analysed at 260 nm using an Agilent 8453 UV-visible spectrophotometer. Data presented as mean ±SD (n=3).

4. Determination of K binding constants

BNIP derivatives	Corresponding value of K constant
BNIPDaCHM	12.23 x 10[5]
BNIPPiProp	3.25 x 10[5]
BNIPPiEth	10.85 x 10[5]
trans,trans-BNIPDaCHM	11.38 x 10[5]

Table 4. K constant values of BNIP derivatives after UV binding studies were calculated from the intercept and slope by plotting A0/(A-A0) versus 1/Concentration. Data presented as mean ±SD (n=3).

5. Cytotoxicity studies

BNIP derivatives	IC_{50} values (µM) (Mean ± SEM)
BNIPDaCHM	2.30±0.03
BNIPPiProp	3.30±0.06 **
BNIPPiEth	1.80±0.07 *
trans,trans-BNIPDaCHM	1.40±0.07 **

Table 5. BNIP derivatives IC_{50} values (µM) after 24 hours, at 37°C. MDA-MB-231 cells (7.5×10^4 cells/100 µL) were seeded in 96-well plates and after 24 hours were treated with different concentrations (0-15 µM) of BNIP derivatives. DMSO/H2O was used as positive control and absorbance was measured at 560 nm. IC_{50} values correspond to concentrations that cause 50% growth inhibition of the cell population compared to control cells. Data presented as mean ±SEM (n=3). **P<0.01, *P<0.05, compared to BNIPDaCHM.

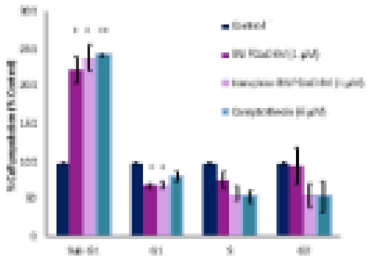

Figure 3. Quantification of cell cycle profiles by flow cytometry following PI staining after 24 hours treatment with BNIPDaCHM, trans,trans-BNIPDaCHM and Camptothecin. DMSO/H2O was used as positive control. The percentage of cells with DNA content in each cell cycle phase was calculated from histograms of linear FL-3 plots in the or gated region (10,000 events). Data presented as mean ±SD (n=3). **P<0.01, *P<0.05, compared to untreated MDA-MB-231 cells.

Conclusions

- ✓ Low melting point ranges confirmed the purity of the three novel BNIP derivatives.
- ✓ BNIPs competitively displace EtBr from DNA, with C_{50} values between 1.1-5.6 µM (binding capacity to *Calf Thymus* DNA from highest to lowest: BNIPPiEth, BNIPDaCHM, BNIPPiProp and *trans,trans*-BNIPDaCHM).
- ✓ Corresponding values for K binding constants from highest to lowest: BNIPDaCHM (12.23 x 10[5]), followed by *trans,trans*-BNIPDaCHM (11.38 x 10[5]), BNIPPiEth (10.85 x 10[5]) and BNIPPiProp (3.25 x 10[5]).
- ✓ BNIPs exhibit strong cytotoxic activity against MDA-MB-231 cells, with IC_{50} values ranging between 1.9-3.3 µM after 24 hours treatment.
- ✓ BNIPDaCHM and *trans,trans*-BNIPDaCHM induce a sub-G1 cell cycle arrest which is associated with apoptotic cell death.

➢ Further work:

Novel BNIP derivatives exhibit strong cytotoxic and DNA binding properties *in vitro* and further investigation in mode of cell death, in relation to apoptosis, would be beneficial for their development as potential anticancer agents.

References: [illegible]

Acknowledgements: Robert Gordon University for funding the above project.

Oral Presentation at 4th Royal Society of Chemistry Early Career Symposium, Glasgow, United Kingdom, 23-34 June 2016

trans,trans-BNIPDaCHM: a Novel Bisnaphthalimidopropyl (BNIP) derivative designed for targeting DNA in a human breast cancer cell line

M. Kopsida*[1], G. A. Barron[1, 2], G. Bermano[2], P. Kong Thoo Lin[1] and M. Goua[1]

[1]*School of Pharmacy and Life Sciences, Robert Gordon University, Garthdee Road, Aberdeen, AB10 7GJ, Scotland, UK*

[2]*Centre for Obesity Research and Education (CORE), Faculty of Health and Social Care, Robert Gordon University, Garthdee Road, Aberdeen, AB10 7GJ, Scotland, UK*

Breast cancer is the most commonly occurring cancer in women, with incidence rates approaching 1.38 million cases per year worldwide. Over the last few decades, there have been numerous attempts to develop, synthesise and advance into the clinic, novel and selective breast cancer therapies. As previously reported[1], bisnaphthalimidopropyl diaminodicyclohexylmethane (BNIPDaCHM) (Figure 1) exerted potent *in vitro* anti-cancer activities and strong DNA binding properties. Here we report for the first time the synthesis, characterisation and biological activity of the *trans,trans*-BNIPDaCHM isomer. ^{1}H-NMR, ^{13}C-NMR, MS and melting point determination were used to confirm the structural identity of *trans,trans*-BNIPDaCHM derivative. The cytotoxicity of *trans,trans*-BNIPDaCHM was assessed against a human breast cancer cell line (MDA-MB-231) by MTT assay. In parallel, DNA binding properties of *trans,trans*-BNIPDaCHM were determined using Fluorescence and UV quenching experiments. This novel compound exhibited strong cytotoxic activity against MDA-MB-231 cells, with an IC_{50} value of 1.4 μM after 24 hours treatment. *trans,trans*-BNIPDaCHM competitively displaced EtBr from DNA, with a C_{50} value of 5.6 μM and the DNA binding K constant of *trans,trans*-BNIPDaCHM was 11.38 x 10^4. In conclusion, the above findings signify that *trans,trans*-BNIPDaCHM exhibits strong cytotoxic and DNA binding properties *in vitro*. Future work will study the potential molecular targets of *trans,trans*-BNIPDaCHM in breast cancer cells.

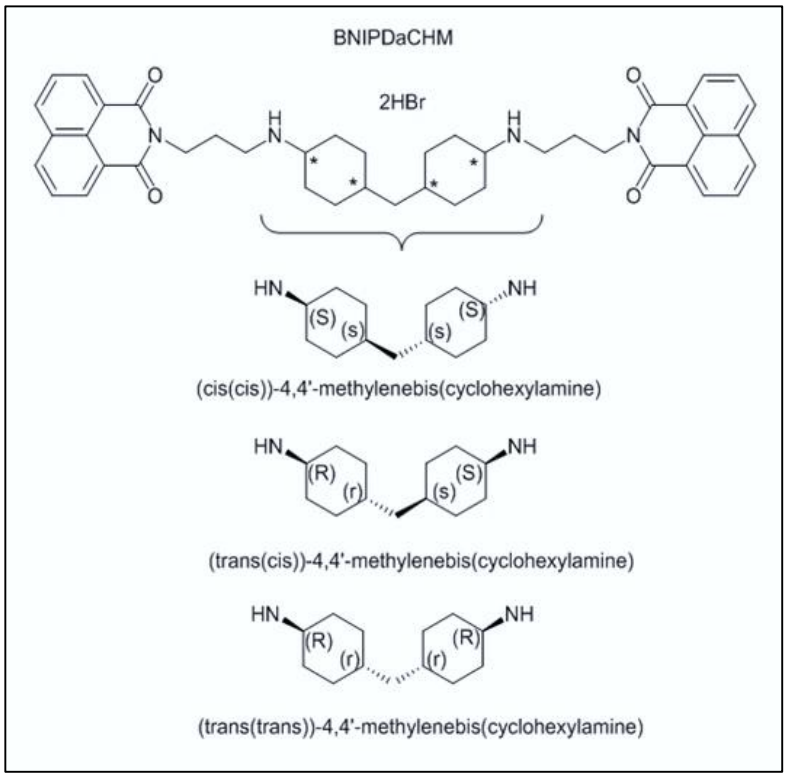

Figure 1. Structure of the parental compound, BNIPDaCHM, with its three stereo isomers including *trans,trans*-BNIPDaCHM.

[1]Barron, G., Bermano, G., Gordon, A. and Kong Thoo Lin, P., Eur. J. Med. Chem., 2010, 45 (4), 1430-1437.

Poster Presentation at Drug Discovery and Therapy World Congress 2016, Boston, MA, USA, 22-25 August 2016

Novel Bisnaphthalimidopropyl (BNIP) derivatives induce oxidative stress that trigger DNA damage in triple negative human breast cancer cells.

M. Kopsida[*1], G. A. Barron[1, 2], G. Bermano[2], P. Kong Thoo Lin[1] and M. Goua[1]

[1]School of Pharmacy and Life Sciences, Robert Gordon University, Garthdee Road, Aberdeen, AB10 7GJ, Scotland, UK

[2]Centre for Obesity Research and Education (CORE), Faculty of Health and Social Care, Robert Gordon University, Garthdee Road, Aberdeen, AB10 7GJ, Scotland, UK

Advances in the development and applications of novel DNA intercalators in drug design have created new opportunities for anticancer compound development. A series of novel bisnaphthalimidopropyl (BNIP) derivatives, bisnaphthalimidopropyl-piperidylpropane (BNIPPiProp), bisnaphthalimidopropyl- ethylenedipiperidine (BNIPPiEth) and (*trans(trans*))-4,4'-methylenebis-cyclohexylamine *(trans,trans*-BNIPDaCHM) were synthesised, characterised and studies for their DNA binding and anticancer activities against human breast cancer MDA-MB-231 cells. Fluorescence binding/UV binding studies were used to determine their DNA binding properties. Cytotoxicity evaluation was performed by 3-(4, 5-Dimethylthiazol-2-yl)-2, 5-diphenyltetrazodium bromide (MTT) assay. All compounds induced cell death (1.4-2.3 μM) after 24 hours treatment, with *trans,trans*-BNIPDaCHM being the most promising candidate. Further evaluation of the cellular DNA content after 24 hours treatment with BNIPs showed induction of sub-G1 cell cycle arrest, indicative of apoptotic cell death and confirmed by studies on the externalization of phosphatidylserine residues in MDA-MB-231 cells. In addition, intracellular reactive oxygen species levels were increased after 4, 8 and 12 hours treatment with BNIP derivatives, while DNA damage studies showed a significant upturn in the number of DNA strand breaks in MDA-MB-231 cells. The above findings, relating to oxidative stress, form the basis to explore further BNIPs as potential treatment for triple negative breast cancer cells.

Novel Bisnaphthalimidopropyl (BNIP) derivatives induce oxidative stress that trigger DNA damage in triple negative human breast cancer cells.

Maria Kopsida[a], Gemma A. Barron[a,b], Giovanna Bermano[b], Paul Kong Thoo Lin[a] and Marie Goua[a]

[a]School of Pharmacy and Life Sciences, Robert Gordon University, Garthdee Road, Aberdeen, AB10 7GJ, Scotland, UK

[b]Centre for Obesity Research and Education (CORE), Faculty of Health and Social Care, Robert Gordon University, Garthdee Road, Aberdeen, AB10 7GJ, Scotland, UK

Drug Discovery & Therapy World Congress 2016
August 22 - 25, 2016, Boston, MA, USA

Introduction

Advances in the development and applications of novel DNA intercalators in drug design have created new opportunities for anticancer compound development. Bisnaphthalimidopropyl (BNIP) derivatives are a family of compounds that exert anti-cancer activities in a wide range of human cancer cell lines[1-3] and variations in their linker sequence seem to improve the aqueous solubility[4], DNA binding and cytotoxic activity of BNIP derivatives[3], enhancing their potential application as anticancer drugs[4].

Aims

- Synthesis and characterisation of three novel BNIP derivatives: BNIPPProp, BNIPPEth-HBr and *trans,trans*-BNIPDaCHM.
- Investigation of their DNA binding affinities, *in vitro* cytotoxicity and cell cycle analysis after 24 hours treatment with BNIPs in triple negative MDA-MB-231 cells.
- Studies on reactive oxygen species (ROS) levels and DNA damage.

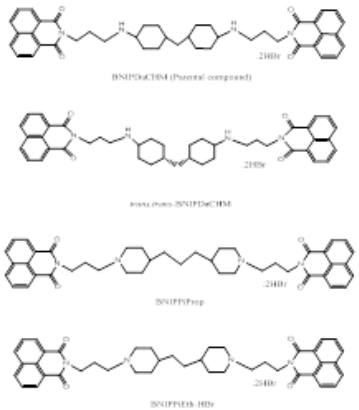

Figure 1: Structures of bisnaphthalimidopropyl diamino diacyl chasorimachane (BNIPDaCHM) (Parental compound), *trans,trans*-bisnaphthalimidopropyl diamino diacyl chasorima chane (*trans,trans*-BNIPDaCHM), bisnaphthalimidopropyl-1-oberidinbrocane (BNIPPProp) and bisnaphthalimidopropyl- ethylenediaberidine dihydrobromide (BNIPPEth-HBr).

Methods

- Fluorescence-binding studies with EtBr were performed in plastic cuvettes (1 cm path length) (Hellma Analytics, UK) using a Shimadzu RF-5301 spectrophotometer (Japan). Samples were analysed at 510 nm (excitation)-520 nm (emission).
- UV binding studies were carried out using an Agilent 8453 UV-visible Spectroscopy System (GenTech, USA) and a Diode array instrument. The samples were loaded in quartz glass flow cells (10 mm path length) (Hellma Analytics, UK) and measured at 260 nm .
- Cytotoxicity was determined by using the 3-(4, 5-Dimethylthiazol-2-yl)-2, 5-diphenyltetrazodium bromide (MTT) assay and absorbance was measured at 560 nm on a 96-well plate reader (Synergy/HT, BIOTEK).
- Propidium Iodide stained nuclei and ROS dye stained MDA-MB-231 cells were examined by flow cytometry, on an Coulter Epics XL-MCL flow cytometer (Beckman Coulter, UK). EXPO-32 software (Applied Cytometry Systems, Sheffield, UK) was used to record and analyse 10,000 single events. The percentage of cells with DNA content in each cell cycle phase was calculated from histograms of linear FL-2 plots and the percentage of ROS production was calculated from FL-1 plots in ungated regions, respectively.
- The quantification of the comet assay was carried out by using 4',6-Diamidino-2-Phenylindole, Dihydrochloride (DAPI). One hundred comets per gel were scored under fluorescence microscope (Leica DMRB, Leica Microsystems UK), with scores between 0-4 (0:no damage, 4:cmaximum damage).

Results

EtBr displacement from *Calf Thymus* DNA

BNIP derivatives	C_{50} value (μM) Mean ±SD
Calf Thymus DNA alone	-
BNIPDaCHM	2.2±0.1
BNIPPProp	2.9±0.2*
BNIPPEth	1.1±0.2*
trans,trans-BNIPDaCHM	5.6±0.2**

Table 1. The effect of BNIP derivatives on EtBr displacement from *Calf Thymus* DNA. C_{50} values correspond to concentrations that a derivative zone raises a 50% decrease on fluorescence intensity of bound EtBr. Data presented as mean ±SD (n=2). *$P<0.01$, **$P<0.05$, compared to BNIPDaCHM.

UV binding studies

BNIP derivatives	Corresponding value of K constant
BNIPDaCHM	12.23×10^4
BNIPPProp	3.25×10^4
BNIPPEth	10.95×10^4
trans,trans-BNIPDaCHM	11.39×10^4

Table 2. K constant values of BNIP derivatives after UV binding studies were calculated from the intercept and slope by plotting A0/(A-A0) versus 1/Concentration. Data presented as mean ±SD (n=2).

Cytotoxicity studies

BNIP derivatives	IC_{50} values (μM) (Mean ±SEM)
BNIPDaCHM	2.30± 0.03
BNIPPProp	2.30± 0.06 **
BNIPPEth	1.80±0.07 *
trans,trans-BNIPDaCHM	1.40± 0.07 **

Table 3. BNIP derivative IC_{50} values (μM) after 24 hours, at 37°C. MDA-MB-231 cells (7.5×10^5 cells/100 μL) were seeded in 96-well plates and after 24 hours were treated with different concentrations (0-10 μM) of BNIP derivatives. DMSO:H_2O was used as positive control and absorbance was measured at 560 nm. IC_{50} values correspond to concentrations that cause 50% growth inhibition of the cell population compared to control cells. Data presented as mean ±SEM(n=2). **$P<0.01$, *$P<0.05$, compared to BNIPDaCHM.

Cell cycle analysis

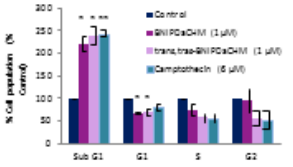

Figure 2. Quantification of cell cycle profiles by flow cytometry following PI staining after 24 hours treatment with BNIPDaCHM, *trans,trans*-BNIPDaCHM and Camptothecin. DMSO:H_2O was used as positive control. The percentage of cells with DNA content in each cell cycle phase was calculated from histograms of linear FL-2 plots in the ungated region: (10,000 events). Data presented as mean ±SD (n=2). **$P<0.01$, *$P<0.05$, compared to untreated MDA-MB-231 cells.

DNA damage studies

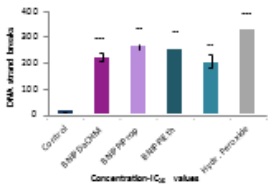

Figure 3. DNA strand breaks in MDA-MB-231 cells determined by comet assay. Data obtained after treating MDA-MB-231 cells with BNIPs for 24 hours. DNA damage in H_2O_2 (200 μM) treated cells were used as a positive control. Data are mean ± SEM of 2 replicates, (n = 2). **$P<0.01$, *$P<0.05$, compared to untreated MDA-MB-231 cells.

ROS levels

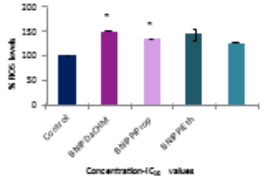

Figure 4. Quantification of ROS levels by flow cytometry following PI staining after 2 hours treatment with BNIPDaCHM, BNIPPProp, BNIPPEth and *trans,trans*-BNIPDaCHM. DMSO:H_2O was used as positive control. The percentages of ROS production was calculated from FL-1 plots in ungated regions (10,000 events). Data presented as mean ±SD (n=2). *$P<0.05$, compared to untreated MDA-MB-231 cells.

Conclusion

BNIPs competitively displace EtBr from DNA, with C_{50} values between 1.1-5.6 μM and bind to DNA with K constants between 12.23×10^4-3.25×10^4.

BNIPs exhibit strong cytotoxic activity against MDA-MB-231 cells, with IC_{50} values ranging between 1.9-3.3 μM after 24 hours treatment.

BNIPDaCHM and *trans,trans*-BNIPDaCHM induce a sub-G1 cell cycle arrest which is associated with apoptotic cell death.

DNA damage studies showed a significant upturn in the number of DNA strand breaks in MDA-MB-231 cells, while intracellular reactive oxygen species levels were increased after treatment with BNIP derivatives.

Novel BNIP derivatives exhibit strong cytotoxic and DNA binding properties *in vitro* and further investigation in mode of cell death, in relation to apoptosis, would be beneficial for their development as potential anticancer agents.

References: [1]Siegal, R., MA, N. and Jamal, A. (2013) Canc. J. Clin., 2013, 63, (1), 1-11, [2]Brana, M.F., Cacho, M., Gradillas, A., de Pascual-Teresa, B. and Ramos, A., Curr. Pharm. Des., 2001, 7, 1745-1780, [3]Brana, M.F and Ramos, A., Curr. Med. Chem. Anti-Canc. Agents, 2001, 1, 237-255, [4]Pavlov, V., Kong Thoo Lin, P. and Rodilla, V., Chem. Biol. Interact, 2001, 137, 15-24, [5]Barron, G., Bermano, G., Gordon, A. and Kong Thoo Lin, P., J. Med. Chem., 2010, 45 (4), 1430-1437, [6]Barron, G., Goua, M., Kuraoka, I., Bermano, G., Iwai, S., Kong Thoo Lin, P., Chem Biol Interact, 2015, 307-315.

Travel awards:

AMGEN®

BIOCHEMICAL SOCIETY

Poster at the 7th APS International PharmSci Conference, Glasgow, United Kingdom, 5-7 September 2016

Effect of Novel Bisnaphthalimidopropyl derivatives (BNIPs) designed for targeting DNA in a human breast cancer cell system.

M. Kopsida[*1], G. A. Barron[1, 2], G. Bermano[2], P. Kong Thoo Lin[1] and M. Goua[1]

[1]School of Pharmacy and Life Sciences, Robert Gordon University, Garthdee Road, Aberdeen, AB10 7GJ, Scotland, UK

[2]Centre for Obesity Research and Education (CORE), Faculty of Health and Social Care, Robert Gordon University, Garthdee Road, Aberdeen, AB10 7GJ, Scotland, UK

Bisnaphthalimidopropyl (BNIP) derivatives are a family of compounds that were initially synthesised with natural polyamines incorporated into their linker chain and were found to exert anti-cancer activities[1, 2]. According to previous studies[3, 4], variations in the linker sequence seem to improve the aqueous solubility and cytotoxic activity of BNIP derivatives, enhancing their potential application as anticancer drugs. The aim of this project was to synthesise and characterise three novel BNIP derivatives, bisnaphthalimidopropyl-piperidylpropane (BNIPPiProp), bisnaphthalimidopropyl-ethylenedipiperidine dihydrobromide (BNIPPiEth-HBr) and (*trans(trans)*)-4,4'-methylenebis-cyclohexylamine *(trans,trans*-BNIPDaCHM). ^{1}H-NMR, ^{13}C-NMR, MS and melting point determination confirmed the structural identity of derivative. The cytotoxicity of novel BNIP derivatives was assessed against human breast cancer MDA-MB-231 cells by MTT assay[5]. In parallel, DNA binding studies investigated whether the BNIP derivatives can successfully target DNA. Fluorescence-binding experiments and UV binding studies were used to determine their DNA binding properties[6]. Propidium Iodide (PI) flow cytometry was conducted in order to evaluate the cellular DNA content in breast cancer cells and assess the induction of apoptotic cell death by BNIP derivatives. All the derivatives exhibited strong cytotoxic activity against MDA-MB-231 cells, with IC_{50} values ranging between 1.4-2.3 μM after 24 hours treatment. Competitive ethidium bromide displacement experiments revealed that BNIPPiProp, BNIPPiEth-HBr and *trans,trans*-BNIPDaCHM competitively displace EtBr from DNA, with C_{50} values in a range of 1.1-5.6 μM. Corresponding values for K binding constants varied from 3.25×10^4 to 12.23×10^4, according to UV spectroscopy studies. Furthermore, cell cycle distribution of MDA-MB-231 cells after cell synchronisation indicated that *trans,trans*-BNIPDaCHM induces a sub-G1 cell cycle arrest which is associated with apoptotic cell death. In particular, an increase of

139.3% and 142.2% in sub-G1 cell population after 24 hours treatment with 1μM trans,trans-BNIPDaCHM and 6μM Camptothecin (a known control for sub-G1 arrest), respectively was observed compared to untreated cells. In conclusion, the above findings signify that novel BNIP derivatives exhibit strong cytotoxic and DNA binding properties *in vitro* and further investigation in mode of cell death, in relation to apoptosis, would be beneficial for their development as potential anticancer agents.

[1]Brana, M.F., Cacho, M., Gradillas, A., de Pascual-Teresa, B. and Ramos, A., Curr. Pharm. Des., 2001, 7, 1745-1780

[2]Brana, M.F and Ramos, A., Curr. Med. Chem. Anti-Canc. Agents, 2001, 1, 237-255

[3]Pavlov, V., Kong Thoo Lin, P. and Rodilla, V., Chem Biol Interact, 2001, 137, 15-24

[4]Barron, G., Bermano, G., Gordon, A. and Kong Thoo Lin, P., J. Med. Chem., 2010, 45 (4), 1430-1437

[5]Mosmann, T., J. Immunol. Methods, 1983, 16;65 (1-2), 55-63

[6]Zhi-Yong, T., Jing-Hua, L., Qian, L., Feng-Lei, Z., Zhong-Hua, Z. and Chao-Jie, W., Molecules, 2014, 19, 7646-7668

Effect of Novel Bisnaphthalimidopropyl (BNIPs) derivatives designed for targeting DNA in a human breast cancer cell system

Marie Kopsida[a], Gemma A. Barron[a,b], Giovanna Bermano[b], Paul Kong Thoo Lin[a] and Marie Goua[a]

ROBERT GORDON UNIVERSITY ABERDEEN

[a]School of Pharmacy and Life Sciences, Robert Gordon University, Garthdee Road, Aberdeen, AB10 7GJ, Scotland, UK

[b]Centre for Obesity Research and Education (CORE), Faculty of Health and Social Care, Robert Gordon University, Garthdee Road, Aberdeen, AB10 7GJ, Scotland, UK

Introduction

Advances in the development and applications of novel DNA intercalators in drug design have created new opportunities for anticancer compound development. Bisnaphthalimidopropyl (BNIP) derivatives are a family of compounds that exert anti-cancer activities in a wide range of human cancer cell lines[1,2] and variations in their linker sequence seem to improve the aqueous solubility[3]. DNA binding and cytotoxic activity of BNIP derivatives[4], enhancing their potential application as anticancer drugs[5].

Aims

- To synthesise and characterise three novel BNIP derivatives: BNIPPiProp, BNIPPiEth-HBr and trans,trans-BNIPDaCHM (Figure 1).
- To investigate their DNA binding affinities, in vitro cytotoxicity and their effect on cell cycle in triple negative MDA-MB-231 cells.
- To study their effect on reactive oxygen species (ROS) levels and DNA damage.

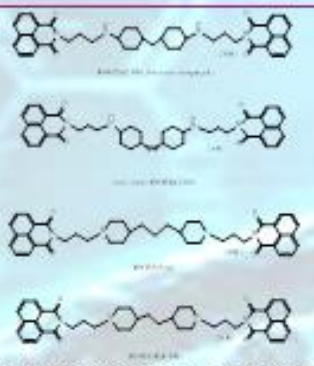

Figure 1. [illegible] (BNIPDaCHM) [illegible] (trans,trans-BNIPDaCHM), [illegible] (BNIPPiProp) and [illegible] (BNIPPiEth-HBr).

Methods

- Thermal melting points were defined by using the standard operating procedure of Griffin Melting Point Apparatus (Fisher Scientific, UK).
- Fluorescence-binding studies were performed in plastic cuvettes (1 cm path length) (Hellma Analytics, UK) using a Shimadzu RF-5301 spectrophotometer (Japan).
- UV binding studies were carried out using an Agilent 8453 UV-visible Spectroscopy System (GenTech, USA) and a Diode array instrument. The samples were loaded in quartz glass flow cells (10 mm path length) (Hellma Analytics, UK) and measured at 260 nm.
- Cytotoxicity was determined by using the 3-(4, 5-Dimethylthiazol-2-yl)-2, 5-diphenyltetrazolium bromide (MTT) assay and absorbance was measured at 560 nm on a 96-well plate reader (Synergy/HT, BIOTEK).
- Propidium iodide stained nuclei and ROS dye stained MDA-MB-231 cells were examined by flow cytometry on an Coulter Epics XL-MCL flow cytometer (Beckman Coulter, UK). EXPO-32 software (Applied Cytometry Systems, Sheffield, UK) was used to record and analyse 10,000 single events. The percentage of cells with DNA content in each cell cycle phase was calculated from histograms of linear FL-2 plots (575 nm band-pass) and the percentage of ROS production was calculated from FL-1 plots (525 nm band-pass) in ungated regions, respectively.
- The quantification of the comet assay was carried out by using 4',6-Diamidino-2-Phenylindole, Dihydrochloride (DAPI). One hundred comets per gel were scored under fluorescence microscope (Leica DMRB, Leica Microsystems UK), with scores between 0-4 (0: no damage, 4: maximum damage).

Results

1. Determination of melting points

BNIP derivatives	Melting Point (°C)
BNIPDaCHM	103-130
BNIPPiProp	160-170
BNIPPiEth	133-150
trans,trans-BNIPDaCHM	130-133

Table 1. Melting points of BNIPDaCHM, BNIPPiProp, BNIPPiEth and trans,trans-BNIPDaCHM [illegible]

2. EtBr displacement from *Calf Thymus* DNA

BNIP derivatives	C50 value (μM) Mean ± SD
Calf Thymus DNA alone	-
BNIPDaCHM	3.3±0.1
BNIPPiProp	3.9±0.3*
BNIPPiEth	1.1±0.3*
trans,trans-BNIPDaCHM	2.0±0.3**

Table 2. The effect of BNIP derivatives on EtBr displacement from *Calf Thymus* DNA. [illegible]

3. UV binding studies

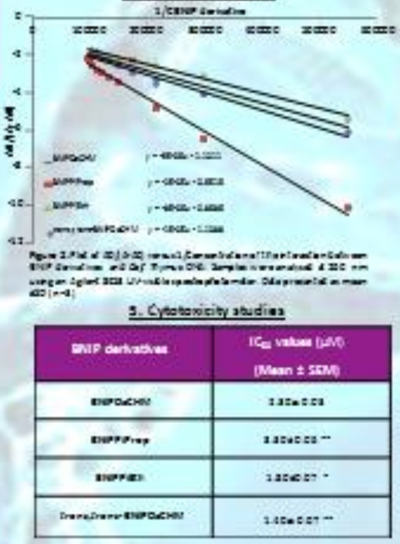

Figure 2. Plot of [illegible] versus 1/Concentration [illegible] BNIP derivatives and *Calf Thymus* DNA. [illegible]

4. Determination of K binding constants

BNIP derivatives	Corresponding value of K constant
BNIPDaCHM	13.33 ×10⁴
BNIPPiProp	3.33 ×10⁴
BNIPPiEth	10.83 ×10⁴
trans,trans-BNIPDaCHM	11.88 ×10⁴

Table 3. K constant values of BNIP derivatives after UV binding studies were calculated from the intercept and slope by plotting [illegible] versus 1/Concentration. Data presented as mean ±SD (n=3).

5. Cytotoxicity studies

BNIP derivatives	IC_{50} values (μM) (Mean ± SEM)
BNIPDaCHM	3.30±0.03
BNIPPiProp	3.30±0.03 **
BNIPPiEth	1.30±0.07 *
trans,trans-BNIPDaCHM	1.40±0.07 **

Table 4. BNIP derivative IC50 values (μM) after [illegible] MDA-MB-231 cells [illegible]

6. Cell cycle analysis

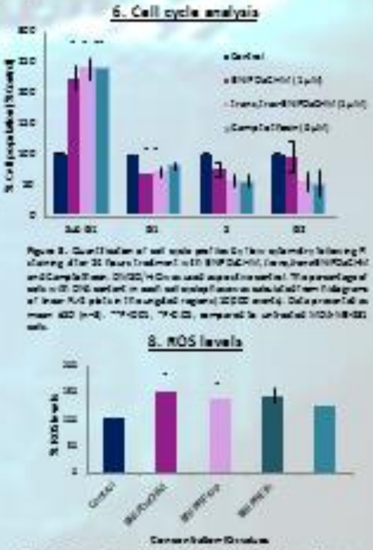

Figure 3. Quantification of cell cycle profiles by flow cytometry following PI staining [illegible] BNIPDaCHM, trans,trans-BNIPDaCHM and Camptothecin. [illegible] compared to untreated MDA-MB-231 cells.

7. DNA damage studies

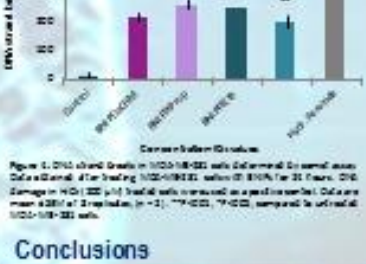

Figure 4. DNA strand breaks in MDA-MB-231 cells determined by comet assay. [illegible] compared to untreated MDA-MB-231 cells.

8. ROS levels

Figure 5. Quantification of ROS levels by flow cytometry following [illegible] BNIPDaCHM, BNIPPiProp, BNIPPiEth and trans,trans-BNIPDaCHM. [illegible] compared to untreated MDA-MB-231 cells.

Conclusions

Novel BNIP derivatives exhibit strong cytotoxic and DNA binding properties *in vitro* and further investigation in mode of cell death, in relation to apoptosis, would be beneficial for their development as potential anticancer agents.

References [illegible]

Acknowledgements: Robert Gordon University for funding this project.